Universität Basel

Morphologic, biogeographic and ontogenetic investigation of Mid-Pliocene menardellids (planktonic foraminifera)

Inauguraldissertation

zur
Erlangung der Würde eines Doktors der Philosophie
vorgelegt der
Philosophisch-Naturwissenschaftlichen Fakultät
der Universität Basel

von

Yannick MARY

aus Frankreich

Basel, 2013

Genehmigt von der Philosophisch-Naturwissenschaftlichen Fakultät
auf Antrag von:

Prof. Dr. Andreas Wetzel	Universität Basel
PD Dr. Michael Knappertsbusch	Naturhistorisches Museum Basel
PD Dr. Frédérique Eynaud	Université de Bordeaux 1

Basel, den 24 Mai 2013
(Datum der Fakultätssitzung)

Prof. Dr. Jörg Schibler
Dekan

« Nous ne parlerons pas des animaux de grande taille. Quoique leur surface individuelle soit souvent très étendue, leur proportion numérique et l'espace qu'ils occupent sur la Terre ne sont réèllement rien dans la balance. Voulons-nous voir quel rôle peuvent jouer, dans la nautre, les petits corps qui nous entourent, et dont beaucoup n'atteignent que la moitié, le quart, ou le sixième d'un millimètre ? Nous n'aurons pas moins lieu de nous étonner. L'étude que nous avons faite du sable de toutes les parties du monde nous a démontré que les restes de Foraminifères forment, en grande partie, des bancs qui gênent la navigation, viennent obstruer les golfes et les détroits, combler les ports, et former, avec les coraux, ces îles qui surgissent tout les jours au sein des regions chaudes de l'océan. »

Alcide d'Orbigny, 1839. *Foraminifères de l'ile de Cuba*

Content

List of tables

List of plates

List of figures

List of figures in Appendix

Acknowledgements

I wish to acknowledge my research supervisor, Dr Michael Knappertsbusch, for his patient direction during the planning and development of this research work, and for making this four year "mind experiment" unforgivable in all means. I would also like to convey thanks to Prof. Andreas Wetzel for standing as my university referee, and to acknowledge Prof. Christian Meyer for kindly accepting to examinate my PhD defense. I wish to express my very great appreciation to Dr. Frédérique Eynaud, for accepting to stand as my co-referee.

I also acknowledge the generous support of Swiss National Foundation, through which this research was funded (*Evolutionary prospection in Neogene planktonic foraminifera* SNF-Grant No. 200021-121599 / 1 and No. 200020-137486 / 1), and the continuous support of the Natural History Museum Basel. Also I wish to thank IODP and its curators and technical staff for providing all the sample materials (ODP requests#21438A, B, and C). And, without the competent assistance of Daniel Mathys and Marcel Düggelin from the Zentrum für Mikroskopie Basel (ZMB) the ontogenetic studies would not have been possible.

Deepest gratitude is also due to Dr. Loïc Costeur for being, even if he doesn't want to admit it, my second informal supervisor during these four years of thesis. Thank you for being abundantly helpful and offering invaluable assistance and guidance, and for supporting all my scientific production.

My acknowledgments naturally go then to the so-called "*Sarcastic Sir Costeur's Lab*", my everyday co-workers and colleagues. Huge thanks to Celia, without whose knowledge and assistance this study would not have been successful. Immense thanks to Vanesa, the first "*Costeurette*" among all, for mutual support, precious advices, and manuscript reviews. Thanks to Pietro, *le seigneur des chameaux*, and Lilia, the new recruit from Wild White Russia. A german *danke* to my german teacher Olivier (despite 80's music). Huge thanks for my true friend Antoine, the best Alsatian in the world and my great technical adviser.

I am also grateful to all my other colleagues of the Nature History Museum Basel for support and assistance, Walter, Antoinette, André, Marcus, Martin and Basil, with a special thank to Carmelo, for our Spanish coffee and philosophic discussions.

Dedicated a few lines of my thesis will never be enough to show gratitude to all my fantastic friends, particularly my old mates Thomas, Amandine, Cyril and Cecile (without forgetting my sweet little Elias), for the numerous night spent together, in every corner of the world. I can't thank you enough for this tremendous support and help. A special thanks to my amazing friend Perrine, for daily attentions and enthusiastic encouragements, from the beginning to the end of my Swiss journey. I felt motivated and encouraged every time I attended our Parisian meetings. My special thanks are extended to Steven, alias *Le Beau*, and Stephanie, lost in the U.S, for their marvelous and inflexible support. That was truly appreciated.

I take an immense pleasure in thanking all my friends from Bordeaux, Gael and Estelle, Nicolas and Aya, Flo and Sophie, Guillaume, Pef, Gniarf, Raphael, Cesar, Drake, and my virtual co-author Bruno "*Dieu*" (we will make this Mary and Mery paper !). I thank the support from the Atlas-Polaris team, especially Cap'tain Derg and his second man Bigfoot. A special mention to Isthun for the appearance of menardellids and foraminifers in its awesome MP3 fiction *Kingdom Paf*. A great thanks to my professors and friends, back in Bordeaux, Frédérique (again!), Sebastien, Bruno and Linda (and their adorable Marion), for your kind help, reviews, comments and support. I sincerely thank Nicolas and Jürg, my comrades and guides in the discovery of Basel.

The last acknowledgments are addressed to my entire family, and specially my father and his wife, for their understanding and their endless love, through the duration of my never-ending education. A special one for Bassam, my brother more than in law, and Marie, which has often swallowed the kilometers between France and Switzerland to rescue me. A huge thank to my sweet Nina-lou, who had always the little attention that cheer me up.

And finally, I am forever indebted to my beloved Sana, the co-author of my life, which has always been on my side, fighting with me against all odds, providing me any kind of support I could think of. Thank you so much for everything, as always. My heartfelt thanks to Nelly, over the oceans and so far away. Thanks you for pushing me forward to follow my dreams, half a world away, and giving me the strength to arrive this far. I dedicate this thesis to you.

Abstract

The universal definition of planktonic foraminifera species remains a major challenge, despite their central place in biostratigraphy and paleoceanography. During the last decade, combined outcomes of molecular and morphometric studies have brought to the light challenging aspects of their classification: within the formerly and traditionally defined morpho-species exists a considerable degree of genotypic variation that defines biogeographically and ecologically distinct sibling "cryptic" species. The recognition of sibling species requires techniques, which are based on other properties than the sole shell morphology.

The present work investigates the morphological variability in planktonic foraminifera of the sub-genus *Menardella*, a subset within the genus *Globorotalia*, in a time slice at 3.2Ma (Mid-Pliocene). This time was selected because it includes a major diversification of menardellids, during which 6 homeomorphic species evolved, leading to an intricate taxonomy. Here, a new population-based taxonomical approach is proposed, which relies on the combination of size frequency distributions (SFDs), geometric morphometry of the shells and sequential ontogenetic reconstructions of populations. A total of 7700 specimens collected from 19 localities in the tropical Atlantic, Pacific and Indian Oceans were investigated in great detail. The collection of morphometric data was achieved with the help of an automated device, the robot AMOR.

The analysis of Mid-Pliocene menardellid SFDs allowed the identification of 6 different sedimentary populations, which on the basis of morphometric and other properties - allowed the recognition of 8 distinct morphotypes.These morphotypes are differentiated by their size distribution, the shape of their test (given by the ratio of axial diameter (δY)/spiral height (δX)), their wall structure and reflectivity and their number of chambers in the final whorl. The relative abundance of these morphotypes permits the establishment of 5 distinct menardellid provinces at 3.2 Ma: morphotypes MA and MB are cosmopolitans, whereas the morphotypes MC3, SH1 and SH2 are restricted to the Atlantic Ocean, and the morphotype ME to the Pacific Warm Pool. These morphotypes are compared with the formally established menardellid morpho-species.

Both morphotypes MA and ME are interpreted as *Globorotalia menardii*. SFDs of these forms suggest the occurrence of two separated populations with distinct biogeographic ranges. Size is the most important parameter to distinguish these two morphotypes. Specific growth patterns derived from

ontogenetic studies confirm that small specimens (<200µm) of morphotype MA are adult individuals that have undergone reproduced with a specific growth pattern.

The morphotype MB corresponds to the established species *G. (M.) limbata*. This morphotype shows an extended neanic stage with a high intra-specific variability, leading to larger shells. In comparison with morphotype MA, the morphotype MB show an early onset of chamber morphological evolution during growth, which can be explained by a delay of the reproduction age of the individual (hypermorphosis).

The traditional morpho-species *G. (M.) multicamerata* was found to split into the 3 morphotypes MC1, MC2 and MC3. Morphotypes MC1 and MC2 belong to the same population, and their biogeographies overlap significantly. Dominance of MC2 was found to be restricted to the West Atlantic and the Pacific Warm pool. In contrast, morphotype MC1 was typically observed to occur in the Indian Ocean and it also dominates the menardiform faunas in the eastern Atlantic locations. Morphotypes MC1 and MC2 are interpreted as two eco-variants of the same species. Investigation of ontogenetic sequence of these morphotypes revealed a strong extension of the adult stage in comparison to the entire ontogenetic life span of an individual, which is interpreted as a K-stragtegy behavior, possibly as a result of adaptation to their shallower adult habitat.

The morphotypes SH1 and SH2 are attributed to *G. (M.) exilis* and *G. (M.) pertenuis*, respectively. They are separated from each other by their densely perforated wall aspect and by a distinct allometric direction during growth.

The applied protocol of SFD analysis proved to be one possible way to describe and investigate diversity patterns in a complex morphological plexus of planktonic foraminiferal species. The identification of foraminiferal populations with the help of size frequency analysis could be confirmed by ontogenetic studies, *i.e.* the correspondence of a specific growth pattern within a population to the size SFD of that population.

Keywords: morphometry; biogeography, ontogeny, planktonic foraminifera, morphotypes, menardellids, evolution, diversity, heterochrony, Pliocene, taxonomy.

Résumé

La recherche d'une définition adéquate des espèces de foraminifères planctoniques reste un défi majeur de la micropaléontologie, malgré la place centrale des foraminifères en biostratigraphie et en paleocéanographie. Au cours de la dernière décennie, des études combinant analyses génétiques et morphologiques ont mis en évidence certains problèmes critiques dans la classification des foraminifères : les morpho-espèces planctoniques, telles qu'elles sont traditionnellement définies, seraient composées de plusieurs espèces sibyllines "cryptiques", montrant des différences génétiques, biogéographiques et écologiques fondamentales. La reconnaissance de ces espèces sibyllines nécessite de nouvelles approches prenant en compte des paramètres extérieurs à la morphologie du test.

Par la présente étude, la variabilité morphologique est examinée chez les foraminifères planctoniques du sous-genre *Menardella*, appartenant au genre *Globorotalia*, sur un intervalle temporel situé à 3.2 Ma (Pliocène moyen). Cette période correspond à un évènement majeur de diversification chez les menardellidés, pendant lequel six espèces homéomorphiques coexistèrent, conduisant à une taxonomie des plus complexes. Nous proposons une nouvelle approche taxonomique reposant sur la reconnaissance de populations de foraminifères planctoniques, combinant analyses de distribution de fréquences de taille, morphométrie géométrique du test et reconstructions ontogénétiques séquentielles. Un total de 7700 spécimens ont été analysés, répartis entre 19 localités en Atlantique, Pacifique et dans l'océan Indien. La collecte des données a été effectuée à l'aide d'un prototype automatisé, le robot AMOR.

L'étude de la distribution des fréquences de taille des menardellidés du Pliocène permet l'identification de six populations différentes, à l'intérieur desquelles un total de huit morphotypes sont définis. Ces morphotypes sont différentiés par la répartition de leur taille, la forme de leur test (représentée par le ratio de la longueur de spire (δX) divisé par le diamètre axial (δY)), par l'aspect de la paroi de leur test et par le nombre de chambres dans la dernière spire. L'abondance relative de ces morphotypes permet la distinction de cinq provinces biogéographiques à 3.2 Ma. Les morphotypes MA et MB sont cosmopolites, alors que les morphotypes MC3, SH1 et SH2 sont restreints à l'océan Atlantique. Le morphotype ME est quant à lui endémique à la *Warm Pool* dans l'océan Pacifique.

Les différents morphotypes sont comparés aux espèces de menardellidés formellement établies. Les morphotypes MA et ME sont tout deux interprétés comme correspondant à l'espèce *Globorotalia menardii*. La distribution des fréquences de taille de ces deux morphotypes suggère l'existence de deux populations différentes, chacune ayant une répartition géographique distincte. Les études

ontogénétiques confirment que les spécimens appartenant au morphotype MA, communément situés dans la gamme de taille <200µm, sont des individus adultes et sexuellement matures ayant un modèle de croissance spécifique. Le morphotype MB est attribué à l'espèce *G. (M.) limbata,* caractérisé par une extension du stade de croissance néanique conduisant à l'établissement de test de grande taille. En comparaison avec le morphotype MA, le morphotype MB montre un développement morphologique précoce pendant la croissance, associé à un retardement de la reproduction (hypermorphose).

Trois différents morphotypes, MC1, MC2 et MC3 sont interprétés comme correspondant à l'espèce *G. (M.) multicamerata*. Les morphotypes MC1 et MC2 appartiennent à la même population; leurs distributions biogéographiques se recoupent de manière significative, bien que le morphotype MC2 soit dominant dans l'Atlantique Ouest et la *Warm Pool* Pacifique. Le morphotype MC1 est quant à lui dominant dans l'océan Indien et dans l'Atlantique Est. Ces deux morphotypes sont interprétés comme étant deux éco-variants de la même espèce. L'étude de leur séquence ontogénétique révèle une extension du stade adulte relativement à la durée ontogénétique totale, ce qui correspond à un comportement de type *stratégie K*, probablement en réponse à l'évolution de leur habitat vers de plus faibles profondeurs. Les morphotypes SH1 et SH2 sont attribués respectivement à *G. (M.) exilis* et *G. (M.) pertenuis*. Ils se distinguent des autres morphotypes par la surface finement perforée de leur test et par une direction allométrique distincte.

Notre nouvelle approche s'avère être un moyen efficace et précis pour accéder aux signaux de diversité spécifique, en particulier en cas de forte intergradation morphologique. La procédure d'identification de population par l'étude de distribution des fréquences de taille est validée par les données ontogénétiques mettant en évidence qu'à chaque distribution de taille correspond un schéma de croissance spécifique.

Mots-clés : morphométrie; biogéographie, ontogénie, foraminifères planctoniques, morphotypes, menardellidés, évolution, diversité, hétérochronie, Pliocène, taxonomie.

Zusammenfassung

Trotz ihrer zentralen Bedeutung in der Biostratigraphie und in der Paläo-Ozeanographie bleibt die Erforschung der planktonischen Foraminiferen eine grosse Herausforderung in der Mikropaläontologie. Im Verlaufe der vergangenen Jahre haben kombinierte Untersuchungen gezeigt, dass bei Foraminiferen die Klassifikation aus rein morphologischen Merkmalen nicht immer mit der genetischen Klassifikation übereinstimmt: Traditionell morphologisch definierte Arten stellen sich immer wieder als ein Konglomerat kryptischer Arten heraus, welche zwar morphologisch scheinbare Identität aufweisen, nach genetischen, biogeographischen und ökologischen Gesichtspunkten jedoch grosse Unterschiede aufweisen. Diese Erkenntnis erfordert ein neues, differenzierteres Herangehen bei der morphologisch gestützten Klassifikation fossiler Vergesellschaftungen.

In der vorliegenden Studie wird innerhalb einer Zeitscheibe bei 3.2 Millionen Jahren vor heute (mittleres Pliozän) die morphologische Variabilität der tropisch-subtropischen planktonischen Foraminifere *Menardella* untersucht, einer Untergattung in der Gattung *Globorotalia*. Zur damaligen Zeit wiesen die Menardellidae eine höhere Diversität auf als in den heutigen Meeren. Im mittleren Pliozän koexistierten mindestens 6 Arten innerhalb der Menardellidae, was wegen ihrer grossen morphologischen Ähnlichkeit eine komplizierte und oft auch verwirrende Taxonomie hervorgebracht hatte.

Eine neue taxonomische Heransgehensweise wird vorgeschlagen, die auf der Erkennung und Rekonstruktion von Populationen planktonischer Foraminiferen beruht. Statistische Verteilungen von Grösse und morphologischen Parametern der Schalen wurden hierzu aus den Sedimenten gewonnen und an ausgewählten Proben mit ontogenetischen Untersuchungen kombiniert. Insgesamt wurden 7700 Exemplare von 19 weltweit verteilten Bohrlochproben des Ocean Drilling Programmes untersucht, welche aus dem Atlantik, Pazifik und dem Indischen Ozean stammten. Die Gewinnung der Daten erfolgte mit Hilfe eines neuartigen Abbildungsautomaten für Mikrofossilien, dem Roboter AMOR.

Die statistische Untersuchung der Verteilungsmuster der Schalengrösse bei den Menardellidae aus dem Pliozän erlaubte die Identifikation von sechs verschiedenen Populationen, innerhalb welcher acht Morphotypen definiert werden konnten. Diese Morphotypen können durch die Verteilung ihrer Grösse sowie mehrerer Formparameter unterschieden werden. Als aussagekräftige Parameter dienten vor allem das Verhältnis von Windungshöhe (δX) geteilt durch den Axialdurchmesser (δY) der Schale in der Profilansicht, sowie die Anzahl der Kammern in der letzten Windung. Die Auskartierung der relativen Häufigkeiten der Morphotypen in den untersuchten Proben führte zur Abgrenzung von fünf geographischen Provinzen vor 3.2 Millionen Jahren. Die Morphotypen MA und MB weisen eine kosmopolitische Verbreitung auf, während die Morphotypen MC3, SH1 und SH2 eng auf den Atlantischen Ozean beschränkt sind. Der Morphotyp ME ist endemisch im Pazifischen "Warm Pool" Gebiet.

Die gefundenen Morphotypen werden mit den formellen gültigen Arten der Menardellidae verglichen. Die Morphotypen MA und ME werden beide als Vertreter der Art *Globorotalia (Menardella) menardii* interpretiert. Ihre Grössenverteilungsmuster lassen die Existenz zweier verschiedener Populationen mit unterschiedlicher geographischer Verbreitung vermuten. Detaillierte ontogenetische Studien am untersuchten Material bestätigen, dass es sich bei den Exemplaren, welche dem Morphotypen MA zugeordnet wurden, um adulte und und geschlechtsreife Formen handelt, trotz ihrer geringen Grösse unterhalb von 200 µm. Diese Erkenntnis wurde aus den Wachstumskurven der Schalen, welche ausserdem artspezifisch sind, abgeleitet. Der Morphotyp MB wird wird der formell bekannten Art *Globorotalia (Menardella) limbata* zugeordnet. In diesem Morphotyp konnte mit Hilfe der ontogenetischen Wachstumskurven der Schalen ein verlängertes neanisches (prä-adultes) Stadium nachgewiesen werden. Damit weist der Morphotyp MB seinem Partner-Morphotypen MA gegenüber eine frühreife morphologische Entwicklung auf, welche, relativ gesehen, eine verzögerte und/oder verkürzte sexuelle Reproduktionsphase (Hypermorphosis) zur Folge hat.

Die drei Morphotypen MC1, MC2 und MC3 werden als morphologisch unterschiedliche Vertreter von *Globorotalia (Menardella) multicamerata* interpretiert. Die Morphotypen MC1 und MC2 gehören derselben Population an: Ihre biogeographischen Verteilungen sind signifikant deckungsgleich, jedoch mit unterschiedlicher Dominanz: Während der Morphotyp MC1 im Indischen Ozean und im östlichen Atlantik vorherrscht, bleibt der Morphotyp MC2 im westlichen Atlantik und im Westpazifik (Warm Pool) die dominierende Form. Diese beiden Morphotypen werden als Ökovarianten derselben Art interpretiert. Die Untersuchung ihrer ontogenetischen Entwicklung der Schalen weist relativ zur gesamten ontogenetischen Dauer gesehen eine Verlängerung des adulten Stadiums auf, welches unter den Foraminiferen typischerweise bei K-Strategen auftritt, und welches vermutlich als evolutive Anpassung an einen Lebensraum in geringerer Tiefe zu betrachten ist. Die Morphotypen SH1 und SH2 entsprechen den formellen Arten *Globorotalia (Menardella) exilis* und *Globorotalia (Menardella) pertenuis*. Sie unterscheiden sich von den übrigen Menardella-Morphotypen durch eine feiner perforierte Oberfläche ihrer Schale und durch eine unterschiedlich allometrische Grössenzunahme ihrer Schalen.

Die Kombination von morphometrischer Populationsstatistik und ontogenetischer Vermessung der Schalen erwies sich als besser geeignet und genauer als die herkömmliche visuelle und qualitative Kennung der Formen, inbesondere wenn man die morphologisch stark überlappenden Schalen der verschiedenen Menardella-Morphotypen betrachtet. Auf diese Weise können biologisch interessante, aussagekräftige und artspezifische Signaturen auch an fossilen Schalen gewonnen werden.

Schlüsselwörter: Morphometrie; Biogeographie, ontogenetisches Wachstum, planktonische Foraminiferen, Morphotypen, Menardellidae, Evolution, Diversität, Heterochronie, Pliozän, Taxonomie.

Riassunto

La definizione rigorosa delle specie di foraminiferi planctonici rimane un'importante sfida scientifica, nonostante il ruolo centrale che essi rivestono in biostratigrafia e paleoceanografia. Durante lo scorso decennio, i risultati combinati di studi molecolari e morfometrici hanno rivelato alcuni aspetti critici della loro classificazione: entro le specie morfologiche riconosciute tradizionalmente, esiste infatti una variazione genotipica che demarca specie "criptiche", biogeograficamente ed ecologicamente distinte. Il riconoscimento delle specie sorelle richiede un nuovo approccio che prenda in considerazione altri parametri oltre che la morfologia del guscio.

Il presente lavoro si occupa della variabilità morfologica nei foraminiferi planctonici del sottogenere *Menardella*, parte del genere *Globorotalia*, in un istante temporale a 3.2 Ma (Pliocene medio). Questo momento corrisponde a un evento principale di diversificazione dei menardellidi, durante il quale esistettero sei specie omeomorfiche, che diede luogo a una tassonomia intricata. Proponiamo un nuovo approccio tassonomico popolazionale, basato sulla combinazione di distribuzione di frequenza di taglia (SFD), morfometria geometrica del guscio e ricostruzione ontogenetica sequenziale. Un totale di 7700 esemplari originari di 19 località tropicali dell'Oceano Atlantico, Pacifico e Indiano è stato studiato in dettaglio in un istante temporale a 3.2 Ma. La raccolta di dati è stata eseguita con l'aiuto di un dispositivo automatico, il robot AMOR.

L'analisi dell'SFD dei menardellidi del Pliocene medio permette di identificare sei popolazioni diverse, nelle quali è presente un totale di otto morfotipi differenti. Questi morfotipi si differenziano per la distribuzione di taglia, la forma del guscio (dato dal rapporto del diametro assiale (δY) rispetto all'altezza della spirale (δX)), l'aspetto della parete e il numero di camere nella voluta finale. L'abbondanza relativa dei morfotipi permette di stabilire cinque distinte province di menardellidi a 3.2 Ma. I morfotipi MA e MB sono cosmopoliti, mentre i morfotipi MC3, SH1 e SH2 sono ristretti all'Oceano Atlantico e il morfotipo ME è ristretto alla Warm Pool dell'Oceano Pacifico. I morfotipi così riconosciuti sono poi stati confrontati con le morfospecie già riconosciute di menardellidi.

I morfotipi MA e ME sono interpretati come *Globorotalia menardii*. La distribuzione SFD di queste forme suggerisce la presenza di due popolazioni separate con un areale biogeografico distinto. Le dimensioni sono il parametro più importante per distinguere questi due morfotipi. Studi ontogenetici confermano che gli esemplari più piccoli (<200μm) del morfotipo MA sono individui adulti che si sono riprodotti con uno schema di crescita specifico. Il morfotipo MB corrisponde a *G. (M.) limbata*. Questo morfotipo mostra uno stadio neanico esteso, con un'alta variabilità intraspecifica,

che porta a un guscio più grande. In confronto al morfotipo MA, il tipo MB esibisce un inizio precoce dell'evoluzione morfologica delle camere durante la crescita, associata a una riproduzione ritardata (ipermorfosi).

Alla morfospecie *G. (M.) multicamerata* corrispondono i tre morfotipi MC1, MC2 e MC3. I tipi MC1 e MC2 appartengono alla stessa popolazione. La loro distribuzione biogeografica si sovrappone significativamente, anche se la dominanza di MC2 è limitata all'Atlantico occidentale e alla Warm Pool del Pacifico. Al contrario, MC1 è tipico dell'Oceano Indiano e domina l'Atlantico orientale. I due morfotipi sono interpretati come ecovarianti della stessa specie. Lo studio della sequenza ontogenetica di questi morfotipi rivela un'estensione dello stadio adulto rispetto all'intera ontogenesi, interpretata quale una strategia K in risposta a un adattamento al loro habitat adulto in acque poco profonde. I morfotipi SH1 e SH2 sono attribuiti a *G. (M.) exilis*, rispettivamente *G. (M.) pertenuis*. Sono separati dal loro aspetto parietale densamente perforato, e da una direzione allometrica distinta.

Il nostro protocollo si è dimostrato un modo accurato ed efficiente per investigare gli schemi di diversità nel complicato plexus morfologico. L'identificazione di popolazione di foraminiferi attraverso l'analisi di frequenza di taglia è confermata dall'evidenza ontogenetica che a ogni distribuzione di taglia corrisponde uno schema di crescita specifico.

Parole chiave : morfometria, biogeografia, ontogenesi, foraminiferi planctonici, morfotipi, menardellidi, evoluzione, diversità, eterocronia, Pliocene, tassonomia.

Thesis overview

The present work is an investigation of the morphological variability of menardellid globorotalids (planktonic foraminifera) during the Mid-Pliocene. The biogeography of morphological variants of this group of marine protists in a 3.2 million years old time-slice (Mid-Pliocene) is studied in a global tropical-subtropical belt including the Atlantic, Pacific and Indian Oceans, and the relationships to the established menardellid species is discussed. The innovative component of this study is the application of a technique to recognize foraminiferal population structures in these ancient sediments. Menardellids commonly present intergraded shell morphologies rendering the recognition of species and subspecies difficult. In this way it is attempted to quantify and better understand the significance of morphological shell variations from the intra-sample to inter-specific levels of differences.

The population-based approach constitutes the red line of this investigation. Methodologically, shell size variation is obtained using advanced techniques of automated image capturing, processing and automated morphometry, which are presented in chapter 2. In chapter 3 the population based taxonomy is worked out in the tropical Atlantic Ocean, where menardellids are known to be abundant, well-preserved, diversified during the Mid-Pliocene. In chapter 4 this analysis is extended to and compared with isochronous samples from selected key locations worldwide. As a confirmation of this approach and results, a sub-group of menardellid morphotypes were further investigated by studying their internal shell structure and developmental sequence, which is treated in chapter 5. This final experiment delivered detailed and unprecedented information about the growth dependent ontogenetic change of shell shape in menardellids, which is important to better understand and interpret the predominantly continuous spectrum of shell morphologies of this particular group of planktonic foraminifera. In the conclusions all findings are summarized and discussed with the perspective to elucidate the biological meaning of morphotypes and morphologically erected species and their implications for morphologically based phylogenetic reconstructions.

CHAPITER 1: Introduction: background and forewords

CHAPITER 2: AMOR: An automated system for orientation and imaging of microfossils

Morphological variability investigations on a global scale are limited by technical constraints. To overcome this situation, a new automated device called AMOR has been constructed, which automatically orientates and images microfossils under a binocular microscope. The present work constitutes the first-time routine application of AMOR to collect a global morphometric dataset of microfossils. In chapter 2 a brief description of AMOR is presented, together with the especially developed scripting procedure, performance tests, methods of morphometric data generation, and partial solutions to some of the persistent problems when working with AMOR.

CHAPTER 3: Morphological variability of tropical Atlantic menardellids in a 3.2 Ma old time-slice

The investigation in the tropical Atlantic Ocean is the first step in the population based morphometric analysis of menardellids. Here, the case concentrates on 5 isochronous samples from a Mid-Pliocene time slice at 3.2 Ma taken from tropical locations in the Atlantic, *e.g.* at ODP Sites 502, 659, 661, 667 and 925. Using this sample set each methodological step is explained leading from the recognition of populations in menardellid frequency distributions by Gaussian fitting to the establishment of morphotypes.

In brief, the results suggest the presence of 7 different morphotypes, which are informally named MA, MB, MC1, MC2, MC3, SH1 and SH2 during the Mid-Pliocene. The transformation from populations A, B, C and D into these morphotypes is discussed in detail, and a comparison of the found morphotypes with formally established morpho-species known in the literature is presented. The biogeographic tendencies of the morphotypes in the Atlantic Ocean are highlighted as well.

CHAPTER 4: Worldwide morphological variability in Mid-Pliocene menardellid globorotalids revealed by population-based taxonomy

The population based taxonomy method proposed in chapter 3 is expanded to a worldwide scale, with samples selected from the 3.2 Ma time-slice in the Indian and Pacific oceans, and 2 additional ones in the western Atlantic. Our results suggest that most of the morphotypes defined in the Atlantic occur worldwide, and that a limited number of morphotypes are restricted to the Atlantic Ocean and or the western Pacific Ocean. The Mid-Pliocene menardellid faunas diversify into 5 different provinces: The western Atlantic, the eastern Atlantic, the Indian Ocean, the western Pacific Warm Pool, and the eastern tropical Pacific.

CHAPTER 5: Ontogenetic and heterochronic patterns in menardellid globorotalids

In Chapter 5, the morphology of selected menardellids is studied at an individual scale, by comparison of the ontogenetic growth of the three most abundant Pliocene morpho-species, *i.e.* Globorotalia menardii, *G. (M.) limbata* and *G. (M.) multicamerata*. In order to obtain a statistically relevant number of specimens, a simple protocol to easily open foraminifera shell was applied using hydrochloric acid, allowing the ontogenetic study of as many as 350 specimens. Growth curves and morphological measurements were further used to distinguish menardellid species from an ontogenetic development point of view. These observations revealed hypermorphic heterochronic changes in the phylogenetic lineage of *G. (M.) menardii - G. (M.) limbata - G. (M.) multicamerata*. In this way, the population derived model for menardiform taxonomy, which is based on size, could be validated.

Chapter 6: conclusion, synopsis and outlook

Chapter 1: Introduction, background and forewords

1.1 Introduction

Planktonic foraminifera are marine heterotrophic protists that build a calcareous shell. They are relatively small organisms, ranging in size from 50 to 1000µm (de Vargas *et al.*, 2004), and show a wide range of shell morphology. While the modern planktonic foraminifera diversity is comparably modest (estimated to include no more than about 50 species according to Hemleben (1989), Kennett and Srinivasan (1983), Kucera (2007), many more extinct taxa existed in the fossil record. Planktonic foraminifera are major contributors to the marine calcareous flux and deep-sea carbonate (Schiebel and Hemleben 2000).

On a global scale, five biogeographic provinces are recognized in both hemispheres of the modern oceans, *i.e.* a tropical, a subtropical, a transitional, a sub-polar and a polar province (Bradshaw, 1959; Bé and Tolderlund, 1971). The diversity of planktonic foraminifera is lowest in polar areas and maximal in sub-tropical areas. It is mainly controlled by temperature and vertical niche partitioning in the water column (Rutherford *et al.*, 1999). The majority of extant planktonic foraminifera are known to be cosmopolitan within these biogeographic provinces, with the exception of three known endemic species in the Indian and Pacific Oceans (*Globigerinella adamsi*, *Globoquadrina conglomerata*, and *Globorotaloides hexagonus*) and another endemic form (pink variety of *Globigerinoides ruber*) in the tropical Atlantic Ocean (Kucera, 2007).

The fossil record of planktonic foraminifera is an exceptionally complete one for fossils in general, and, provided that carbonate preservation is sufficient, allows identification at species level (Bolli and Saunders, 1985). Their high evolutionary rate (de Vargas *et al.*, 1997), their enormous abundance, and their relatively simple "Bauplan" (Berger, 1969), made planktonic foraminifera a very interesting candidate for evolutionary studies. For all these reasons, these organisms have been intensively used for biogeochronology and for paleo-environmental reconstructions. During the last decades, research about planktonic foraminifera has widened to include the development of proxies for paleoceanographic reconstructions, which are based on the improved analysis of trace-elements (Cd, Ba), elemental ratios (Ca/Mg), stable isotope composition of the shells or the faunal composition. A particularly growing and challenging field of research has become the molecular taxonomy with extant foraminifera, which became possible through the development of enhanced PCR

methods to extract and amplify DNA from living cells and the availability of rapid routine DNA sequencing techniques (Stathoplos and Tuross, 1994, Seears 2011). These are essential for finding integrated congruent species concepts, which are a fundamental pre-requisite for reliable paleo-environmental reconstructions.

1.2 Classification and species concept of planktonic foraminifera

Extant and fossil planktonic foraminifera have been traditionally classified by paleontologists on the basis of wall structure and overall external shell morphology. Species of foraminifera are consequently morpho-species, a species concept defined as "the smallest unit that is consistently and persistently distinct and distinguishable by ordinary means" (Cronquist, 1978; Mayden, 1997; McGowran, 2005, see Mallet, 2007 for a review). Explicitly, the diagnosis of the shell is the central concept of this species definition.

Historically, the classification of planktonic foraminifera relies on the establishment of type specimens - holotypes, which are specimens that serve as the typical reference for a particular species. All major classical reference studies and atlases on planktonic foraminifera, such as Stainforth *et al*., (1975), Blow (1979), Kennett and Srinivasan (1983), Bolli and Saunders (1985), Loeblich and Tappan (1988), Pearson (1993), Pearson *et al*., (2006) follow this practice. The creation of type species emerged to become very common for standardizing index forms in industrial biostratigraphy from the early 1910's through the 1970's and later (McGowran, 2005). Problematic with this practice is that a single specimen is used to describe a whole species neglecting the morphological variability at intra- or inter-specific levels (Scott, 2010). It therefore received much criticism (Kucera and Darling, 2002; Darling and Wade, 2008; Scott, 2011), especially because the erection of type specimen remains subjective through the glasses of the investigator who has selected it from an assemblage.

1.2.1 Sibling "cryptic" species in planktonic foraminifera

The advancement of molecular sequencing techniques brought to the light the existence of genetically distinct "cryptic species" within the morphological species (see Darling and Wade, 2008 for a review), which challenged the traditional, morphology-based classification. Investigation of specific morphologies of these cryptic species revealed that the geographic morphological variability, traditionally considered as ecophenotypy, was actually a possible indication for genetic differences (Huber *et al.*, 1997; de Vargas *et al.*, 1997, Morard *et al.,* 2009; Aurahs *et al.,* 2011). Cryptic species are adapted to different ecological niches, and are distributed in distinct biogeographic provinces (Darling and Wade, 2008).The tendency of recent marine pelagic taxa to diverge in ecology, life cycle, or behavior and to form sibling species (*sensu* Steyskal, 1972) is well known (Knowlton, 1993; Verity and Smetacek, 1996), and has important implications to the classification and phylogenetic reconstruction of extant and extinct (micro) fossils.

Cryptic species indicate that the current classification may greatly underestimate the diversity of recent and ancient planktonic foraminifera (Pawlowski and Holtzmann, 2002; Darling and Wade, 2008). The evolutionary pressure induced by competition among sibling species within the same lineage may slow down the apparent rate of evolution (Alizon *et al.*, 2008), which may theoretically explain the picture of gradual evolution in several planktonic foraminiferal lineages. Finally, the idea that planktonic foraminifera are cosmopolitan organisms with capacity of long distance dispersal appears to be a consequence of the broad definition of morphological species (de Vargas *et al.*, 2004). In contrast, biogeographic molecular analyses have revealed a distinct distribution with a narrow geographic dimension between the limiting ecological barriers in a number of extant species (Aurahs *et al.*, 2011; Darling and Wade, 2008, Darling *et al.,* 2006; de Vargas *et al.*, 2004). Therefore, foraminiferal genotypes seem to show considerable endemism (Kucera and Darling, 2002; Kucera *et al.*, 2005). Nevertheless, molecular analyses confirmed that some species of planktonic foraminifera show spectacular dispersal, for example between Arctic and Antarctic populations of *Neogloboquadrina pachyderma*, (Darling *et al,.* 2000; Stewart *et al.*, 2001) or in populations of *Truncorotalia truncatulinoïdes* (Sexton and Norris, 2008).

1.2.2 The debate about species concept in planktonic foraminifera

Conceptually, sibling species constitute a critical limitation to a species concept relying on morphology (*e.g.* Mallet, 2007). Sibling species can only be recognized on the basis of subtle morphological differences, which hitherto have not yet been taken into consideration by taxonomists, or if other observations than morphology are available. Such parameters may include the genetic composition, behavior, reproduction preferences, seasonality, and vicariance, to name a few. Not all of them are recordable in the sediments, but some could indirectly be (using for instance stable isotopes or Ca/Mg ratios).

If some attempts have been successful in predicting the genetic type using morphology with a reasonable error range (Quillévéré *et al.*, 2011), the recognition of biological species based on morphological characters remains largely problematic. There is no constant relationship between morphological characters and genetic diversity. In some case, cryptic species such as *Orbulina universa* are separated by subtle differences in microstructure (Morard *et al.*, 2009), whereas *N. pachyderma* and *N. incompta*, some genetic variants traditionally lumped under *N. pachyderma*, show an important difference in coiling direction (Darling *et al.*, 2006). In contrast, *Globigerinoides sacculifer* shows a wide range of morphologies without any obvious genetic difference (André *et al.*, 2012), which is not yet well understood among taxonomists. However, epigenetic variability and intraspecific variation of genome content is suggested to strongly influence foraminifera phenotype variation (Parfrey *et al.*, 2008).

In an attempt to overcome the difficulty with morpho-species and cryptic genotypes, Darling and Wade (2008) suggested that morpho-species represent genera rather than species-level taxonomical units, while de Vargas *et al.,* (2004) suggested morpho-species to be super-species (*an assemblage of allopatric species of monophyletic origin, often with slight but distinct morphological differences*, definition from de Vargas *et al.*, 2004, following Mayr, 1970). However, none of these two definitions provides indication in how species recognition should be applied in practice, especially in fossil taxa. An integrative concept for species, which satisfies biologists, ecologists, geneticicists, and paleontologists, still remains an unsolved issue at this time.

1.3 The evolution prospection project

If the identification of genetic differences is limited to living assemblages, the fossil record is pivotal for understanding climatic and environmental changes in the past. As suggested by Darling and Wade, (2008), morphological and molecular approaches to recognize species are far from being mutually exclusive, but are rather complementary. A better understanding of planktonic foraminifera diversity could not be accomplished without a new integrative taxonomical protocol that takes into account the significant advances obtained from molecular data. An important issue is that not only local, but global morphological variability ought to be included in the definition of species, on a biogeographic level but also back in geological time (*i.e.* between points of speciation). Also, not only specimens, but populations ought to be characterized (Scott, 2011).

The evolutionary prospection project attempts to integrate these different concepts into taxonomical investigations (Knappertsbusch, 2011; Figure 1.1). The idea is to morphologically map species of planktonic foraminifera at different locations, along well-known ecological gradients or bio-provinces, and during different time-slices in the geological past. If isolated populations can be identified, it could be possible to map the morphological diversity and to unravel environmental parameters that influence morphological variability. Local populations are then compared between successive time-slices with the perspective to visualize morphological evolution within lineages, and understand underlying processes. In this way, speciation events (cladogenesis: the geographic separation of an ancestral lineages into two sister species; anagenesis: phyletic change, *i.e.* evolution of the entire population without branching) should be identifiable and mapped. Quantitative methods of visualizing morphological change through time have been explored in this context in Knappertsbusch and Mary (2012). This approach of geographic investigations through time conceptually is known as chronophenetics (see Dzik, 2005 for a review), but has never been realized in such a rigorous approach.

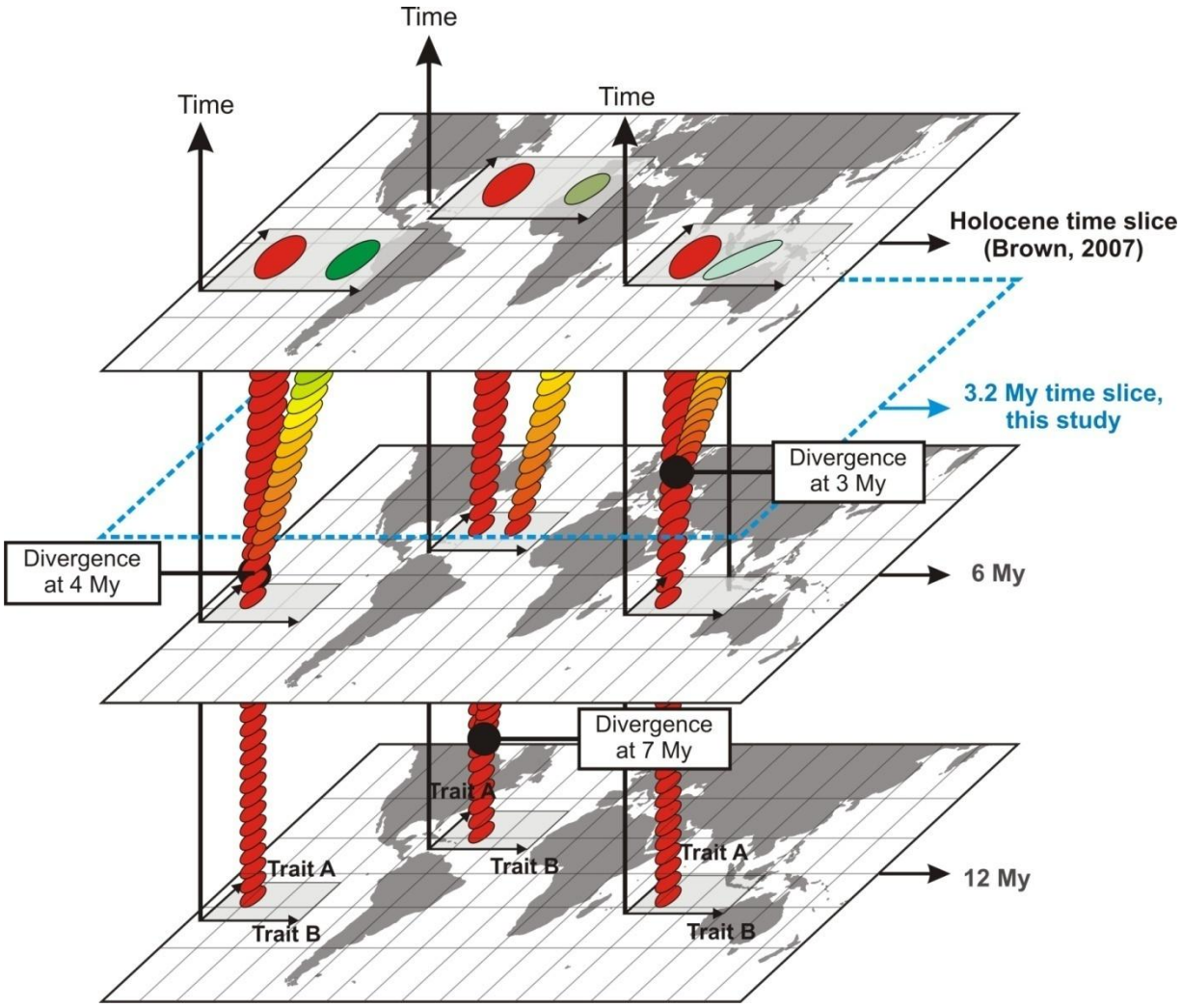

Figure 1.1: Conceptual schema of the evolutionary prospection project (after Knappertsbusch, 2011) . The hypothetical morphological speciation (cladogenesis) is seen in the moments of splitting and divergence of bivariate shell parameters trait A and trait B over a geographically global scale and through time. The youngest time slice represents the Holocene and has been investigated in a study by Brown (2007). The present study takes focus on the time slice at 3.2 Ma.

In this context, menardellids were selected as a model. Menardellids form a subset within the formal genus *Globorotalia*, which are characterized by sharing the global morphology of their extant representative *Globorotalia (Menardella) menardii* (Blow, 1979; Brown, 2007). Menardellids are cosmopolitan in tropical oceans and found in abundance in

sediments. They have a wide stratigraphic range, and have undergone considerable radiation, especially during the Pliocene. In addition, their test is often well preserved in the sediment, and their lenticular morphology is relatively easy to model in two dimensions.

1.3.1 Previous work: the Holocene time-slice

The initial global morphological investigation of menardellids was performed by Brown (2007). This first step into the evolutionary prospection project served as a morphological reference for menardiform variability. Extant menardellids consist, with the exception of *G. (M.) menardii*, of only few menardellid morpho-species. The coexisting plexus of *G. tumida* was also included, because of continuous morphological intergradation (the phylogenetic relationships of the two groups needs still to be clarified).

Brown (2007) worked out the morphological variation of menardellids and tumids from more than 70 surface sediment samples, which are globally distributed in the modern tropical oceans. The analysis of morphological variability of up to 6000 individual shells allowed the identification of two intergrading morphoclines, between the morphological plexus of *G. (M.) menardii and G. tumida*, which consists of a total of six distinct morphotypes *:* the menardellid morphotypes α, β (initially described in Knappertsbusch, 2007), χ and η on one hand, and tumid morphotypes ε and φ on the other hand (Brown, 2007). These morphotypes were shown to have distinct but overlapping biogeographical distributions.

1.3.2 The Mid-Pliocene time-slice

The Mid-Pliocene represents a transitional period, *i.e.* it was the last period of warmth before the onset of climate deteriorations leading to the northern hemisphere glaciations (Haywood *et al.*, 2009). At that time the foraminiferal assemblages were already relatively similar to modern morphospecies, and the distribution of menardellids in the Atlantic is comparable to present distribution (Dowsett and Robinson, 2007). The progressive closure of the Isthmus of Panama, between 4.2 and 3.5 Ma (Jain and Collins, 2007 and reference

therein), has led to a major reorganization of currents in the Atlantic and Pacific Oceans (Steph *et al.*, 2010; Fedorov *et al.,* 2013), and the closure of the Indonesian Seaway (at about 5–3 Ma; *e.g.*, Cane and Molnar, 2001; Karas *et al.*, 2009) strongly affected the global hydrography as well (Karas *et al.*, 2011). Simultaneously, the menardellids underwent a major radiation from middle Miocene to early Pliocene (Kennett and Srinivasan, 1983), and especially in the Atlantic, as a vicarious speciation event induced by the closure of the Panama isthmus (Chaisson, 2003; Knappertsbusch, 2007). Six distinct morpho-species evolved, which were closely related to *G. (M.) menardii*. The strong morphological similarities among Pliocene menardellid morpho-species have led to a very intricate taxonomy. The biogeography and the ecological preferences of these species at that time are only poorly known.

For these reasons, the Mid-Pliocene was considered as a second time-slice that is worth of focussing for evolutionary prospection. For the present investigation, a set of 29 samples around the tropical to subtropical world oceans was identified with the help of Neptune numerical dating tools (NEPTUNE-working group 2000) and the materials were acquired from respective ODP core repositories. Ideally, this period also represents the study target of the Pliocene Research, Interpretation and Synoptic Mapping (PRISM) (*e.g.* Dowsett, 2007 and references therein). A comprehensive database for paleo-environmental reconstructions is available for this period.

Basic questions to solve are:

1) Is it possible to distinguish discrete menardellid populations based on morphological characterization of their shells?

2) What is the best solution for defining morpho-species in case of morphological intergradation?

3) What is the origin of the observed morphological plasticity?

4) Is the menardellid morphological variability congruent with distinct regional or large scale habitat changes?

1.4 Evolution and mechanism of morphological change

1.4.1 Speciation mode and planktonic foraminifera

One of the most fundamental questions that underpin diversity studies is how new species arise. Considering the species as a meta-population, (*i.e. with groups of interconnected populations that form an extended reproductive community and an unevenly distributed but unitary gene pool or field for gene recombination* (citation from de Quieros, 2005)),what defines a new species is then the reproductive isolation of a given population, which opposes gene flow and makes the distinction between permanent populations (Mayr, 1942; Gould, 2002). Consequently, theses two notions (reduction of gene flow and the reproductive isolation) are the central concept in the definition of biological speciation modes. Theoretically, four distinct types of speciation exist, allopatric, peripatric, parapatric and sympatric speciation (Figure 1.2), which constitute a continuum, differing only in the degree to which the initial reduction of gene exchange is generated by a physical barrier external to the organism, or by evolutionary change in the biological characteristics of the organisms themselves.

Allopatric speciation (Figure 1.2A) results from a geographical barrier to gene flow or dispersal between populations, by topography or unfavorable habitat. It is often associated with vicariance (divergence of two large populations). The physical barrier reduces gene flow sufficiently to prevent gene exchange if the geographically isolated populations later come into contact. Allopatry is however not defined by the geographical distance, as populations with a low power of dispersal may be micro-geographically isolated (Futuyama, 2005), especially in pelagic environment, where vertical niche separation can lead to allopatry (de Vargas *et al.*, 2004; Weiner *et al.*, 2012).

Peripatric speciation (Figure 1.2B), also known as the founder effect (Mayr, 1954), is defined as the divergence of a small population from a large widely distributed ancestral form in an adjacent ecological niche located in the periphery of the distribution of the ancestral population.

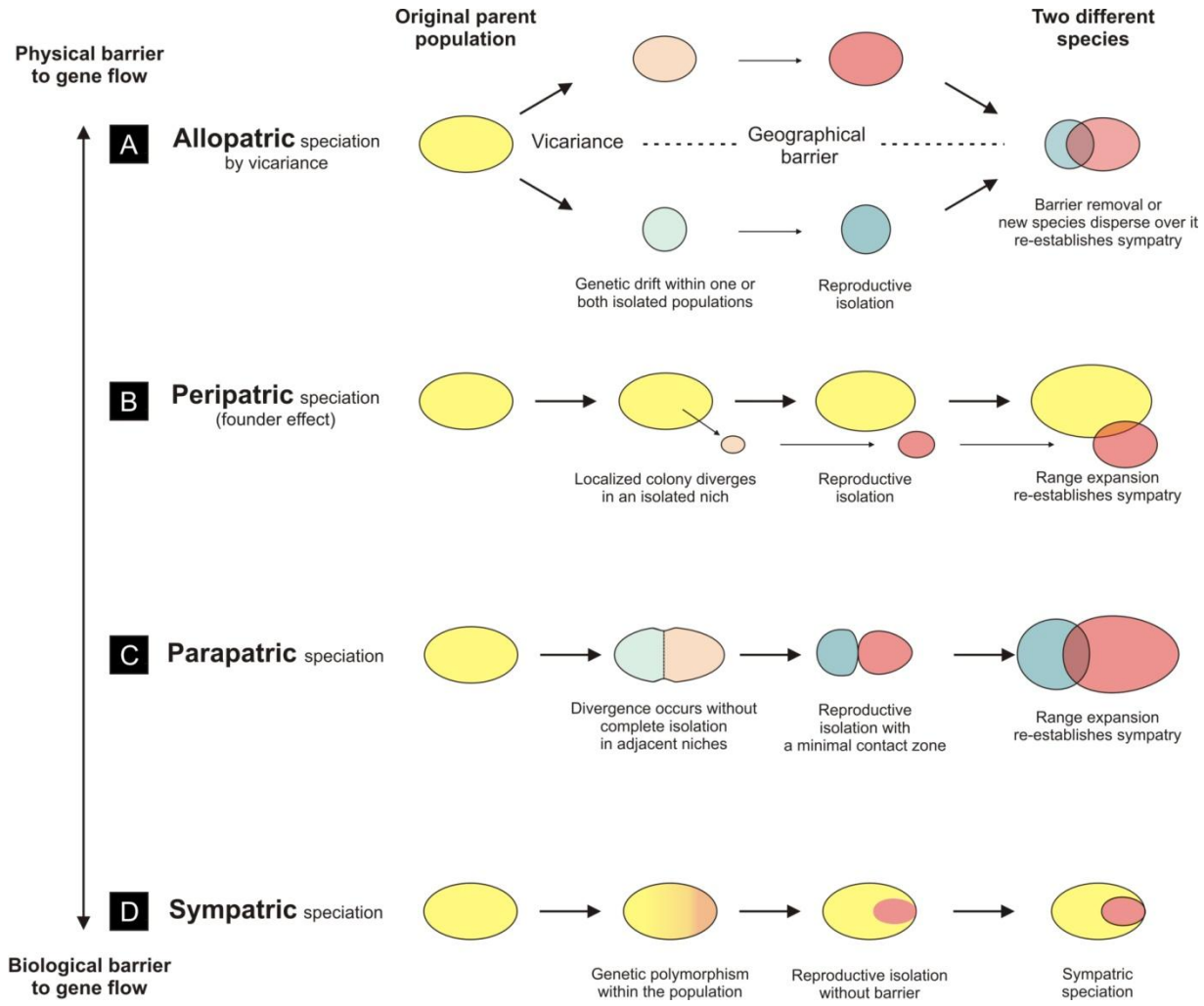

Figure 1.2: Conceptual schema of the four speciation types. Drawn after Futuyama (2009). (A). Allopatric speciation. (B) Peripatric Speciation. (C) Parapatric speciation. (D) Sympatric speciation.

In **parapatric speciation** (Figure 1.2C), adjacent populations diverge and become reproductively isolated without complete geographic isolation. Partial isolation may occur by unequal dispersal, incomplete geographical barrier or any narrow environment discontinuity, resulting in limited gene flow. Parapatric population divergence implies that the distribution of the divergent population remains in the range of the ancestral one. There are consequently only little extrinsic barriers to gene flow. Parapatric mode of speciation is favored in the open oceans, especially in foraminifera (Lazarus, 1986; Sexton and Norris, 2008). Tectonic barriers

and water mass fronts, acting as potent isolating mechanisms, are, in some cases, very weak. (Darling *et al.*, 2000; Sexton and Norris, 2008).

In the **sympatric speciation model** (figure 1.2D), speciation occurs without any geographic barrier, within the same geographic region. The term sympatry refers to organisms whose ranges significantly overlap. In that case there are no physical barriers that oppose gene flow. In planktonic foraminifera, species are naturally vertically distributed in the water column (Schiebel and Hemleben, 2005). The sediment record of foraminifera integrates each above living population in the same sediment interval. Specific co-occurrences in sediment may therefore be misinterpreted as apparent sympatry, although strong vertical niche partitioning could occur (Weiner *et al.*, 2012).

1.4.2 Heterochrony: the evolution of ontogeny

The change of ontogenetic development, relative to the development sequence in the ancestor species, is defined as heterochrony (McKinney and McNamara, 1991). Heterochrony is one of the most important evolutionary pattern part, a major source of morphological variations and evolutionary novelties (*e.g.* Gould 1977; Albrecht *et al.*, 1979; McKinney and McNamara, 1991; Hall, 1992; Webster and Zelditch, 2005). Heterochrony and the evolution of ontogeny in general have already been of great interest among evolutionary biologists (Raff, 1996; McKinney, 1999). Although it is known to be of great importance, for example, in the evolution of morphological characters of larger benthic foraminifera, relevant studies have remained scarce in planktonic foraminifera. During the late 1990's, the concept of heterochrony was extended by developmental biologists to include the entire developmental story of the organism from the earliest stage of ontogeny to maturity (sequential heterochrony: Klingenberg, 1998; Smith, 2001), in contrast to classic allometry studies of heterochrony, which describes the relationship between size and shape. Two distinct modes of heterochrony are defined, which are based on the nature of the developmental modification in the descendent species in comparison to its ancestor.

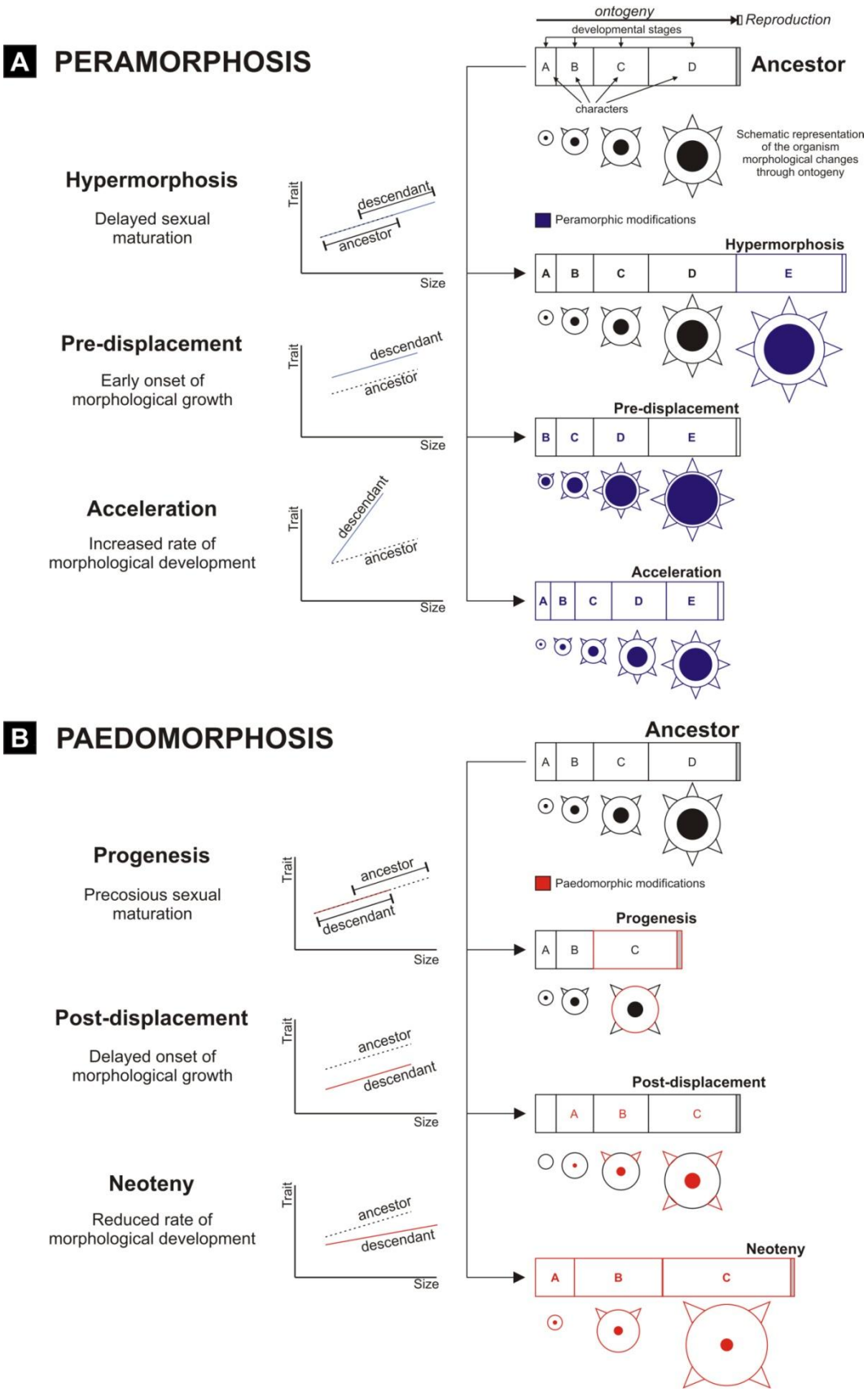
A PERAMORPHOSIS
ontogeny
Reproduction
developmental stages
A B C D
Ancestor
characters
Schematic representation of the organism morphological changes through ontogeny
Peramorphic modifications
Hypermorphosis
Delayed sexual maturation
Trait
descendant
ancestor
Size
A B C D E
Pre-displacement
Early onset of morphological growth
B C D E
Acceleration
Increased rate of morphological development
B PAEDOMORPHOSIS
Paedomorphic modifications
Progenesis
Precosious sexual maturation
A B C
Post-displacement
Delayed onset of morphological growth
Neoteny
Reduced rate of morphological development

Figure 1.3 (on previous page): Conceptual scheme of the six heterochronic modes with respect to ancestral development trends. Allometric relationship (size versus trait) between ancestor and descendant are shown in parallel (from McKinney, 1986) associated with corresponding representation of organism development (from McNamara, 1986). Definitions are according to McNamara(1986). (A) Peramorphic heterochronic modes - hypermorphosis, pre-displacement, acceleration. (B) Paedomorphic heterochronic modes - Progenesis, post-displacement and neoteny.

If the rate of morphological changes is prograding (for example size increase or an extension of the development) during ontogeny, the heterochronic change is called **peramorphosis** (Figure 1.3A). Peramorphic changes can occur by hypermorphosis, which means the delay of sexual maturation, by pre-displacement, which means an earlier onset of growth of particular morphological structures, or by acceleration, which is an increase in the overall rate of morphological development (not only related to a particular structure).

In the opposite, if the ontogenetic development is reduced, or if the developmental sequence is interrupted, the heterochronic change is called **paedomorphosis** (Figure 1. 3B). Also here, three sub-modes of paedomorphic change exist: progenesis means a precocious sexual maturation, which alters the further ontogenetic sequence. The delayed onset of growth of a particular morphological structure is called post-displacement. Finally, the decrease of the rate of development is termed neoteny.

Studies of heterochronic changes in planktonic foraminifera are rare in the literature. They concentrate on allometric heterochrony, depicting chrono-phyletic trends of shell shape and size mirroring of trends during ontogenetic growth. An example is the post-displacement of the onset of the neanic stage in *Globoconella inflata* in comparison to its ancestor *G. puncticulata* (Wei *et al.*, 1992). In the case of Morozovellids, the appearance of the keel from ancestral *Praemurica uncinata* to its descendant *Morozovella angulata* was interpreted as the result of complex paedomorphic changes (Kelly *et al.*, 1996). Morphological changes, which occur shortly before extinction in that lineage was explained by progenesis (Kelly *et al.*, 2001). These examples suggest a prominent role of heterochronic change in the evolutionary history of planktonic foraminifera. However, no direct observation with regard of the onset or termination of such developments in individuals has been done yet.

1.5 Methodological approach

The present study combines three different types of measurements extracted from menardellid shells: size frequency distributions of shell length versus shell width in profile view, density distributions of linear shell parameter measurements, and ontogenetic shell growth measurements (Figure 1.4).

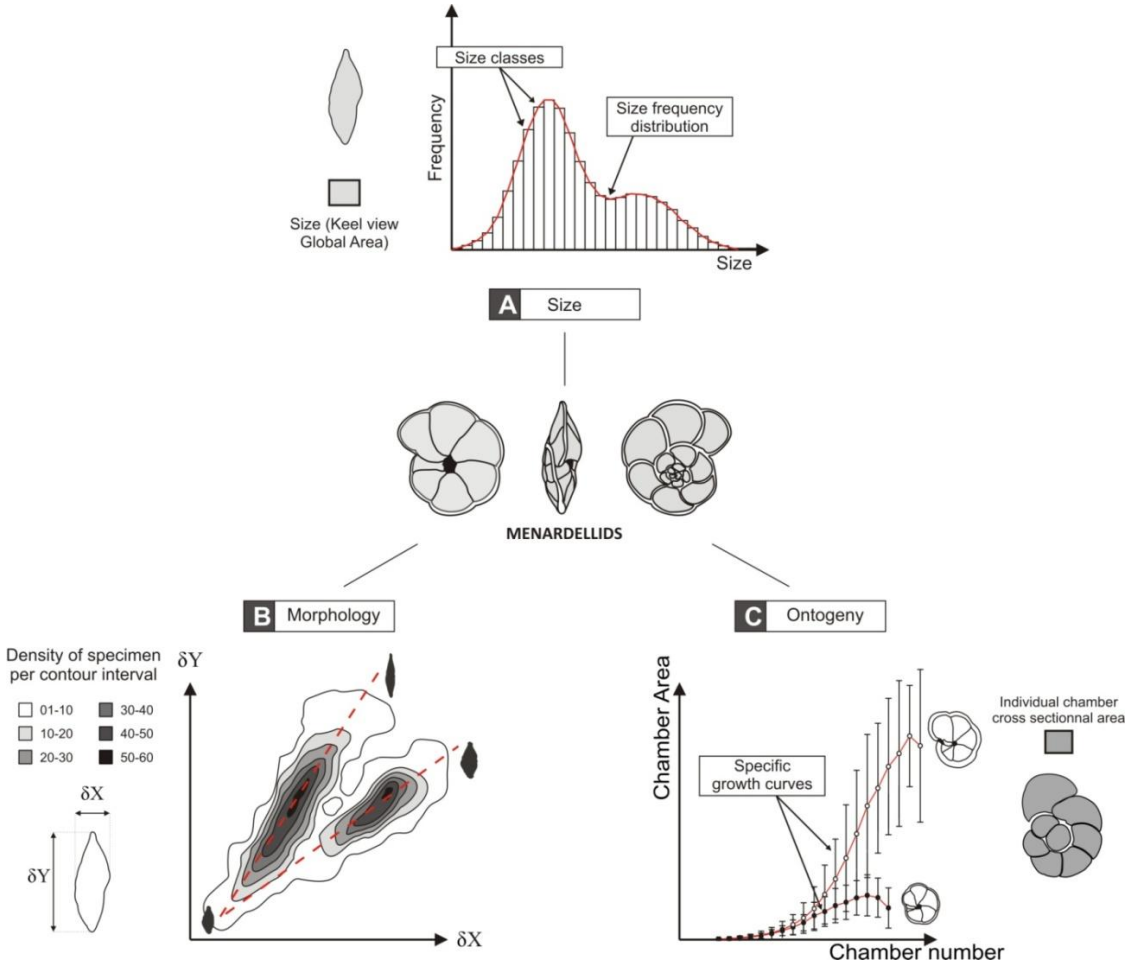

Figure 1.4: Schematic chart of the three types of analyses involved in the present study, and derived from menardellid shells. (A) Size frequency distribution (SFD) of the overall menardellid population in the sediment. Size is represented by keel view (profile view) area. The red line represents the SFD extracted from size distribution histogram. (B) Density distribution of menardellid populations using contoured frequency diagrams of bivariate measurements δX (spiral view) and δY (axial diameter). (C) Specific ontogenetic shell growth curves of two menardellid species.

1.5.1 Size-frequency distribution modeling

Size is a fundamental morphological property to discriminate between planktonic foraminifera. Because the size of the test is linearly correlated with cytoplasmatic mass (Schmidt *et al.*, 2006), it is strongly influenced by the ambient environment (Spero *et al.*, 1991). A foraminiferal species will reach larger size under optimal conditions, which are often species specific (Schmidt *et al.*, 2004; Schmidt *et al.*, 2006), while growing to smaller sizes if stressed (Hecht, 1976; Schmidt *et al.*, 2004, Schmidt *et al.*, 2006). Considering the multi-dimensionality of marine habitats, the size of organisms varies with increasing distance from optimum conditions. The partitioning of oceanic depth into vertically segregated ecological niches strongly influences distribution of organism size (Rutherford *et al.*, 1999; Al-Sabouni *et al.*, 2007) including planktonic foraminifera.

Many parameters describing a shell can be selected as estimators for overall size: shell size (surface or volume) and total weight are usually reasonable proxies to describe planktonic foraminiferal body size (Schmidt *et al.*, 2006, Regenberg et al., 2010). Working with surface, volume or total weight has several advantages, in comparison to single linear measurements taken from the shell. They suffer little from positioning errors while allowing direct inter-specific comparisons. Here, and using digital imagery the overall shell area was taken as the estimator of size, which can easily be derived from outline coordinates. At the population level, histograms of size frequency distributions (SFDs) (Figure 1.4A) show to what extend the size of an individual species may vary between environments.

Empirical measurements have demonstrated that the SFD of a particular foraminiferal population, which settles through the water column, can be approximated by the sum of an exponential distribution, representing juvenile individuals in the smaller size fractions, and a Gaussian distribution representing pre-adult and adult specimens in the larger size fractions (Peeters *et al.*, 1999). In addition, the comparison of planktonic foraminiferal specific SFDs collected in surface water plankton tows, sediment traps, and surface sediments has shown a progressive reduction in abundance of small juveniles towards the sea floor, depending of the species (Peeters *et al.*, 1999).

Such an under-representation of juveniles in the sediment in comparison to the standing stock in the plankton or transient path to the sea-floor is indicated by the absence of the exponential component in the SFD. However, the preservation of juveniles depends on many factors, such as diagenesis, dissolution, season, and population dynamics. To some degree, experiences has shown that the shape of the SFD is also species dependent: for example, the exponential component occurs more frequently in globigerinid species than in others (Peeters *et al.*, 1999). The fraction of small specimens appears to vary also with geography: while larger specimens are major contributors to the $CaCO_3$ flux in the Arabian Sea and the Red Sea (Bijma and Hemleben, 1994), the situation is reversed in the North-East Atlantic, where small specimens are the dominant contributors to the foraminiferal $CaCO_3$ flux (Schiebel and Hemleben, 2005). According to Schmidt *et al.*, (2006), a large size of planktonic foraminiferal test is rather indicative for fast growth than for a prolonged individual growth period, which is opposite to larger benthic foraminifera. Consequently, the residence time of transient juveniles in the water column of comparably large planktonic species tends to be shorter than in the case of small sized planktonic foraminifers. This could serve as an explanation for the observation that in case of the comparably large menardellid juveniles are under-represented in sediments, despite excellent calcite preservation.

Taking the above considerations into account, it is deduced that most menardellids reach their adult stage in size-fractions above 125µm. Consequently, and following the model of Peeters *et al.,* (1999), the sedimentary representation in the size fraction > 100µm of menardellids, which settled from a specific plankton population, can be assumed to follow a Gaussian distribution. Hence, in the present investigation, Gaussian decomposition of mixed size frequency distributions (SFDs) is applied as a discriminative prospection tool to identify ancient menardellid populations.

1.5.2 Density distribution of shell morphology

Shells of menardellid globorotalids can be parameterized with few geometric measurements, ideally in profile view (Knappertsbusch, 2007). Experience has shown that well suited measurements include the spiral height, the axial diameter, the spiral and umbilical side inflation, and the number of chambers.

At the population level morphospaces are defined as geometric mathematical spaces, which describe and relate organismal phenotype configurations (Mitteroecker and Huttegger, 2009), where a single specimen is represented by a point. The geometric arrangement and accumulation of these points among each other suggests an ecological meaning, *i.e.* may induce phenotypy (*e.g.*, Shoval *et al.*, 2011). In this context, (contoured) density diagrams allow fast and precise visualization of clusters of specimens (Figure 1.4B). In a particular location, a single morphotype may be recognized as a stable cluster in the applied morphospace. If the distribution of specimens is multimodal or multidirectional, *i.e.* if several clusters exist and/or superimpose, more than one morphotype is indicated.

Looking on a global scale, key locations must be selected, which may serve as *regio typicae* for a particular oceanic environment. This was done here in the Atlantic, Indian, and Pacific Oceans at the 3.2 Ma time-slice, in order to obtain a global impression of menardellid morphotypes, their end-members and transitions, and to detect their provincial preferences.

1.5.3 Ontogenetic reconstruction

The study of ontogenetic tendencies provides a different insight to better understand the morphological variability of shells, which comes from the fine level on individual scales. The comparison of average specific ontogenetic growth rates is a very promising way to detect meaningful biological differences between species, and is therefore of great use for the classification of planktonic foraminifera (Brummer *et al.*, 1987; Huber, 1994). Menardellid globorotalids are especially well suited for ontogenetic analysis because of their low trochospiral, biconvex morphology showing only little chamber overlap. Micro-dissection of

shells is one way to study shell growth and chamber accretion during the entire life span of the organism.

Ontogenetic studies of menardellid foraminifera are thus carried out using cross-sectional measurements of successive chambers, based on digital imaging of internal shell structure. Chamber area measurements allow the quantification of specific growth curves (Figure 4C). The number of instars is taken as an estimation of biological lifetime of the individual. This allows a comparison of growth among organisms, which share similar allometric behavior (Blackstone, 1987). The absolute "ontogenetic clock" (*i.e.* the absolute span of life-time) cannot yet be derived from fossils, but a relative "ontogenetic clock" can be drawn on the basis of the measured growth rates. In addition, the life-span of an individual is most probably strongly non-linear, influenced by environmental conditions and metabolic states (*e.g.* Blackstone, 1987; Strauss, 1987; Schmidt *et al.*, 2004; Schmidt *et al.*, 2008).

In classical studies the ontogenetic growth of planktonic foraminifera is divided into 5 different stages (Brummer *et al.*, 1987; Wei *et al,.* 1992; Huber, 1994), *i.e.* the embryonic, the juvenile, the neanic, the adult and the terminal stages (Brummer *et al.*, 1987; Wei *et al.*, 1992). During the present investigation, these stages were quantitatively constrained, which was done by measurement of a number of parameters like cross sectional chamber areas. In addition, the shape classification of chambers proposed by Cifelli and Scott (1986) was used to interpret specific habitat adaptations (following Lipps, 1979). Estimation of the porosity of successive chambers from the proloculus (first chamber resulting of the gamete fusion) to the terminal chamber served as an estimator of gaseous or ionic exchange of the cell with the environment, and is therefore an interesting proxy for metabolic activity during growth and maturation (Hemleben, 1989).

References

Al-Sabouni, N., Kucera, M., Schmidt, D.N., 2007. Vertical niche separation control of diversity and size disparity in planktonic foraminifera. Marine Micropaleontology 63, 75–90.

Alizon, S., Kucera, M., Jansen, V.A.A., 2008. Competition between cryptic species explains variations in rates of lineage evolution. PNAS 108 (34), 12382-12386.

André, A., Weiner, A., Quillévéré, F., Aurahs, R., Morard, R., Douady, C., de Garidel-Thoron, T., Escargel, G., de Vargas, C., Kucera, M., 2013. The cryptic and the apparent reversed : lack of genetic differentiation within the morphologically diverse plexus of the planktonic foraminifer *Globigerinoides sacculifer*. Paleobiology 39 (1), 21-39.

Aurahs, R., Treis, Y., Darling, K., Kucera, M., 2011. A revised taxonomic and phylogenetic concept for the planktonic foraminifer species *Globigerinoides ruber* based on molecular and morphometric evidence. Marine Micropaleontology 79, 1–14.

Bé, A. W. H., Tolderlund, D. S. 1971. Distribution and ecology of planktonic foraminifera. In: B. M. Funnell and W. R. Riedel (Eds), The micropaleontology of oceans , 105–150. London: Cambridge University Press.

Berger, W.H., 1969. Planktonic foraminifera: basic morphology and ecologic consideration. Journal of Paleontology, 43(6), 1369-1383.

Bijma, J., Hemleben, Ch., 1994. Population dynamics of the planktic foraminifer *Globigerinoides sacculifer* (Brady) from the central Red Sea. Deep-Sea Research 41 (3), 485-510.

Blackstone, N.W., 1987. Size and Time. Systemic Zoology, 36(2): 211-215.

Blow, W.H., 1979. The Cainozoic *Globigerinida*. E.J. Brill, Leiden (3 vols.), pp 1413

Bolli H.M., Saunders J.B., 1985. Oligocene to Holocene low latitude planktic foraminifera.- In: Bolli H.M., Saunders J.B.. and Perch-Nielsenk. (eds.), Plankton stratigraphy. Cambridge University Press, Cambridge, 155-262.

Bradshaw, J. S., 1959. Ecology of living foraminifera in the North and Equatorial Pacific Ocean. Cushman Foundation for Foraminiferal Research: Contributions, 10, 25–64.

Brown, K., 2007. Biogeographic and morphological variation in late Pleistocene to Holocene globorotalid foraminifera. Dissertation Phil. Nat. Fakultät, Universität Basel, 128 p. pdf file available at http://pages.unibas.ch/diss/2007/DissB_8290.htm.

Brummer, G.J.A., Hemleben C. and Spindler M., 1987. Ontogeny of Extant Spinose Planktonic Foraminifera (Globigerinidae): A Concept Exemplified by *Globigerinoïdes sacculifer* (Brady) and *G. ruber* (d'Orbigny). Marine Micropaleontology 12, 257-381.

Cane, M., Molnar, P., 2001. Closing of the Indonesian seaway as a precursor to east African aridification around 3–4 million years ago. Nature 411, 157–162.

Chaisson, W.P., 2003. Vicarious living: Pliocene menardellids between an isthmus and an ice sheet. Geology 31,1085–1088.

Cifelli, R., Scott, G., 1986. Stratigraphic record of the Neogene globorotalid radiation (planktonic foraminifera). Smithsonian Contributions to Paleobiology 58.

Cronquist, A., 1978. Once again, what is a species? in L. Knutson, ed. BioSystematics in Agriculture. Alleheld Osmun, Montclair, NJ, 3-20.

Darling, K. F., Wade, C. M., Steward, I. A., Kroon, D., Dingle, R., Leigh Brown, A. J., 2000. Molecular evidence for genetic mixing of Arctic and Antarctic subpolar populations of planktonic foraminifers. Nature, 405, 43–47.

Darling, K. F., Kucera, M., Kroon, D., Wade, C. M., 2006. A resolution for the coiling direction paradox in *Neogloboquadrina pachyderma*. Paleoceanography, 21, 1-14.

Darling, K., Wade, C., 2008. The genetic diversity of planktonic foraminifera and the global distribution of ribosomal RNA genotypes. Marine Micropaleontology 67, 216–238.

Dowsett, H. J., 2007. The PRISM palaeoclimate reconstruction and Pliocene sea-surface temperature. In Deep-time perspectives on climate change: marrying the signal from computer models and biological proxies (eds M. Williams, A. M. Haywood, J. Gregory and D. N. Schmidt). Micropalaeontological Society, Special Publication, 459–480. London, UK: Geological Society of London.

Dowsett, H., Robinson, M.M., 2007. Mid-Pliocene planktic foraminifer assemblage of the North Atlantic Ocean. Micropaleontology 53, 105–126.

Dzik, J., 2005. The chronophyletic approach: stratophenetic facing an incomplete fossil record. Special Papers in Palaeontology, 73, 159–183.

Fedorov, A.V., Bierly, C.M., Lawrence, K.T., Liu, Z., Dekens, P.S., and Ravelo, A.C., 2013. Patterns and mechanisms of early Pliocene warmth. Nature 496, 43-49.

Futuyama, D.J., 2005. Evolution. Sinauer Associates, Sunderland, Massachusetts.

Gould, S. J., 1977. Ontogeny and phylogeny. Belknap Press of Harvard University Press, Cambridge.

Gould, S.J., 2002. The structure of evolutionary thought. Harward university press, Cambridge.

McGowran, B., 2005. Biostratigraphy: Microfossils and Geological Time. Cambridge University Press, 479 pp.

Hall, B. K., 1992. Evolutionary Developmental Biology. Chapman and Hall, London, 505 pp.

Haywood, A.M., Dowsett, H.J., Valdes, P.J., Lunt, D.J., Francis, J.E., Sellwood, B.W., 2009. Introduction. Pliocene climate, processes and problems. Philosophical Transactions of the Royal Society A : Mathematical, Physical and Engineering Sciences 367, n°1886, 3–17.

Hemleben, C., Spindler, M., Anderson, O., 1989. Modern Planktonic Foraminifera. Springer, New York.

Hecht, A.D., Bé, A.W., Lott, L., 1976. Ecologic and palaeoclimatic implications of morphologic variation of *Orbulina universa* in the Indian Ocean. Science 194, 422–424.

Huber, B.T., 1994. Ontogenetic Morphometrics of Some Late Cretaceous Trochospiral Planktonic Foraminifera from the Austral Realm Smithsonian Contributions to Paleobiology number 7.

Huber, B. T., Bijma, J., Darling, K. 1997. Cryptic speciation in the living planktonic foraminifer *Globigerinella siphoniphera* (d'Orbigny). Paleobiology, 23, 33–62. Jain, S., Collins, L.S. 2007. Trends in Caribbean paleoproductivity related to the Neogene closure of the Central American Seaway. Marine Micropaleontology, Amsterdam, vol. 63, p. 57-74.

Karas, C., Nürnberg, D., Gupta, A. K., Tiedemann, R., Mohan, K., Bickert, T., 2009. Mid-Pliocene climate change amplified by a switch in Indonesian subsurface throughflow. Nature Geoscience, 2, 434–438.

Karas, C., Nürnberg, D., Tiedemann, R., Garbe-Schönberg, D. 2011: Pliocene climate change of the Southwest Pacific and the impact of ocean gateways. Earth and Planetary Science Letters 301; 117–124.

Kelly, D. C., Arnold, A. J., Parker. W. C., 1996. Paedomorphosis and the origin of the Paleogene planktonic foraminiferal genus *Morozovella*. Paleobiology 22, 266–281.

Kelly, D.C., Bralower, T.J., Zachos, J.C. 2001. On the demise of the early Paleogene *Morozovella velascoensis*: Terminal progenesis in the planktonic foraminifera. Palaios 16, 507-523.

Kennett, J.P., Srinivasan, M.S. 1983. Neogene planktonic foraminifera. A phylogenetic atlas. Hutchinson Ross Publishing Company, Stroudburg, Pennsylvania, 1-265.

McKinney, M. L., 1986. Ecological causation of heterochrony: a test and implications for evolutionary theory. Paleobiology 12, 282-289.

McKinney, M. L., McNamara, K. J. 1991. Heterochrony: the evolution of ontogeny. Plenum Press, New York, 437 pp.

McKinney, M. L., 1999. Heterochrony: beyond words. Paleobiology 25, 149–153.

Klingenberg, C. P., 1998. Heterochrony and allometry: the analysis of evolutionary change in ontogeny. Biological Reviews 73, 79–123

Knappertsbusch, M.W., 2007. Morphological variability of *Globorotalia menardii* (planktonic foraminiferan) in two DSDP cores from the Caribbean Sea and the Eastern Equatorial Pacific. Carnets de Géologie / Notebooks on Geology, Brest, Article 2007/04. URL: http://paleopolis.rediris.es/cg/CG2007_A04/index.html

Knappertsbusch, M. W., 2011. Evolution im marinen Plankton. Mitteilungen der Naturforschenden Gesellschaften beider Basel, 13:3-14.

Knappertsbusch, M. W., Mary, Y., 2012. Mining morphological evolution in microfossils using volume density diagrams. Palaeontologia Electronica, Vol. 15, Issue 3; 7T: 209p. URL: http://palaeo-electronica.org/content/issue-3-2012-technical-articles/282-volume-density-diagrams/

Knowlton, N.,1993 Sibling species in the sea. Annual Review of Ecology and Systematics 24. 189-216.

Kucera, M., Darling, K., 2002. Cryptic species of planktonic foraminifera: their effect on palaeoceaographic reconstruction. Philosophical Transactions of the Royal Society of London 360, 695–718.

Kucera, M., Weinelt, M., Kiefer, T., Pflaumann, U., Hayes, A., Weinelt, M., Chen, M.-T., Mix, A. C., Barrows, T. T., Cortijo, E., Duprat, J., Juggins, S., and Waelbroeck, C., 2005. Reconstruction of sea-surface temperatures from assemblages of planktonic foraminifera: Multi-technique approach based on geographically constrained calibration datasets and its application to glacial Atlantic and Pacific Oceans. Quaternary Science Reviews, 24, 951–998.

Kucera, M., 2007. Planktonic Foraminifera as Tracers of Past Oceanic Environments. In Hilaire-Marcel, C., De Vernal, A. (eds) Developments in Marine Geology, Volume 1, 213-262.

Lazarus, D. (1986). Tempo and mode of morphologic evolution near the origin of the radiolarian lineage Pterocanium prismatium. Paleobiology, 12(2), 175-189.

Lipps; J.H, 1979 Ecology and Paleoecology of Planktonic foraminifera. In Lipps, J.H., Berger, W.H., Buzas, M.A., Douglas, R.G., Ross, C.A. Foraminiferal Ecology and Paleoecology, 62-104. Society of Economic Paleontologists and Mineralogists Short Course Note N°6, Houston, Texas.

Loeblich, A.R., Tappan, H., 1988. Foraminiferal genera and their classifications. N.Y.: Van Noslrand Reinhold. 970, 847.

Mallet, J., 2007. Species, concept of. In Lewin, S. etal. (eds) Encyclopedia of Biodiversity. Volume 5. Academic press, 427-440.

Mayden, R. L., 1997. A hierarchy of species concepts: the denoument in the saga of the species problem. in M. F. Claridge, H. A. Dawah and M. R. Wilson. (eds). Species: The units of diversity. Chapman and Hall, London, 381-423.

Mayr, E., 1942. Systematics and the Origin of Species (Columbia Univ. Press, New York).

Mayr, E., 1970. Populations, Species, and Evolution (Harvard Univ. Press,Cambridge, MA).

Morard, R., Quillevere, F., Escarguel, G., Ujie, Y., de Garidel-Thoron, T., Norris, R., de Vargas, C., 2009. Morphological recognition of cryptic species in the planktonic foraminifer *Orbulina universa*. Marine Micropaleontology 71, 148–165.

Mitteroecker, P., Huttegger, S.M. 2009: The Concept of Morphospaces in Evolutionary and Developmental Biology: Mathematics and Metaphors. Biological Theory 4(1), 54–67.

McNamara, K. J. 1986. A guide to the nomenclature of heterochrony. Journal of Paleontology 60:4–13.

NEPTUNE-working group 2000 (Dave Lazarus, Cinzia Cervato, Michael Knappertsbusch, Milena Pika-Biolzi, Jean-Pierre Beckmann, Katharina von Salis, Heinz Hilbrecht, and Hans Thierstein). NEPTUNE-online II. URL http://micropal-basel.unibas.ch/NEPTUNE/Start.html

Parfrey, L.P., Lahr, D.J.G., Katz, L.A., 2008. The Dynamic Nature of Eukaryotic Genomes. Molecular Biology and Evolution 25 (4), 787-794.

Pawlowski, J., Holzmann, M., 2002. Molecular phylogeny of foraminifera - a review. European Journal of Protistology 38, 1-10.

Pearson, P.N., 1998. Evolutionary concepts in biostratigraphy. In: Doyle, P., Bennett,M.R. (Eds.), Unlocking the Stratigraphic Record. JohnWiley and Sons, Chichester, 124–144.

Pearson, P.N., Olsson, R.K., Huber, B.T., Hemleben, C., Berggren, W.A. (Eds.), 2006. Atlas of Eocene Planktonic Foraminifera: Cushman Foundation for Foraminiferal Research Special Publication, 41, pp. 1–513.

Peeters, F., Ivanova, E., Conan, S., Brummer, G.J., Troelstra, S., Van Hinte, J., 1999. A size analysis of planktic foraminifera from the Arabian Sea. Marine Micropaleontology 36, 31–63.

Quieros de, K. 2005. Ernst Mayr and the modern concept of species. PNAS 102 sup 1, 6600-6607.

Quillévéré, F., Morard, R., Escargel, G., Douady, C. J., Ujiié, U., de Garidel-Thoron, T., de Vargas, C. 2011. Global scale same-specimen morpho-genetic analysis of *Truncorotalia truncatulinoides* : A perspective on the morphological species concept in planktonic foraminifera. Palaeogeography, Palaeoclimatology, Palaeoecology 1-11

Raff, R. A. 1996. The shape of life. University of Chicago, Chicago, 544 pp.

Rutherford, S., D'Hondt, S., Prell, W. 1999. Environmental controls on the geographic distribution of zooplankton diversity. Nature, 400, 749–753.

Regenberg, M., Nielsen, S.N., Kuhnt, W., Holbourn, A., Garbe-Schönberg, D., Andersen, N. 2010. Morphological, geochemical, and ecological differences of the extant menardiform planktonic foraminifera Globorotalia menardii and Globorotalia cultrata. Marine Micropaleontology, 74, 96-107.

Schiebel, R., Hemleben, C. 2005. Extant planktic foraminifera: A brief review. Palaentogische Zeitschrift, 79, 135–148.

Schmidt, D. N., Thierstein, H.R, Bollmann, J. 2004. The evolutionary history of size variation of planktic foraminiferal assemblages in the Cenozoic. Palaeogeography, Palaeoclimatology, Palaeoecology 212 (2004) 159– 180.

Schmidt, D.N., Lazarus, D., Young, J.R., Kucera, M., 2006. Biogeography and evolution of body size in marine plankton. Earth-Science Reviews 78, 239–266.

Scott, G.H. 2011. Holotypes in the taxonomy of planktonic foraminiferal morphospecies. Marine Micropaleontology 78 96–100.

Seears, H. 2011 Biogeography and Phylogenetics of the Planktonic foraminifera. Dissertation, University of Nottingham 395 pp.

Sexton, P.F., Norris, R.D., 2008. Dispersal and biogeography of marine plankton: long-distance dispersal of the foraminifer *Truncorotalia truncatulinoides*. Geology 36, 899-902.

Smith, K. K. 2001. Heterochrony revisted: the evolution of developmental sequences. Biological Journal of the Linnean Society (2001) 73, 169-186.

Spero, H.J., Lerche, I., Williams, D.F., 1991. Opening the carbon isotope "vital effect" box, 2. Quantitative model for interpreting foraminiferal carbon isotope data. Paleoceanography 6 (6), 639–655.

Stainforth, R.M., Lamb, J.L., Luterbacher, H., Beard, H.J., and Jeffords, R.M., 1975. Cenozoic Planktonic Foraminiferal Zonation and characteristics of index forms. Article 62 The University of Kansas Paleontology Institute.

Stathoplos, L., Tuross, N. 1994: Proteins and DNA from modern planktonic foraminifera. Journal of Foraminiferal Research 24, n°1, 49-59

Steph, S., Tiedemann, R., Prange, M., Groeneveld, J., Schulz, M., Timmermann, A., Nürnberg, D., Rühlemann, C., Saukel, C., Haug, G.H. 2010. Early Pliocene increase in thermohaline overturning: A precondition for the development of the modern equatorial Pacific cold tongue. Paleoceanography 25, PA2202.

Stewart, I.A., Darling, K.F., Kroon, D., Wade, C.M., Troelstra, S.R., 2001. Genotypic variability on subarctic Atlantic planktic foraminifera. Mar. Micropaleontol. 43, 143–153.

Steyskal, G.C., 1972. Systematic Zoology Vol. 21, No. 4, December 1972 p. 446.

Vargas, C. de, Zaninetti, L., Hilbrecht, H., and Pawlovski, J., 1997. Phylogeny and rates of molecular evolution of planktonic foraminifera: SSU rDNA sequences compared to the fossil record. Journal of Molecular Evolution, 45, 285–294.

Vargas C., de, Saez A.G., Medlin L.K., Thierstein, H.R., 2004. Superspecies in the calcareous plankton. In: Thierstein HR, Young JR (eds) Coccolithophores: from molecular processes to global impact. Springer, Berlin, 271–298.

Verity, P.G., Smetacek, V. 1996. Organism life cycles predation, and the structure of marine pelagic ecosystems. Marine Ecology Progress Series. 130, 277-293.

Webster M., Zelditch M. L. 2005. Evolutionary modifications of ontogeny: heterochrony and beyond. Paleobiology, 31(3), 354–372

Wei, K.Y., Zhang, Z.W. ,Wray. C.,1992. Shell ontogeny of *Globorotalia inflata* (I): growth dynamics and ontogenetic stages. Journal of Foraminiferal Research 22:318-327

Weiner, A., Auras, R., Kurasawa, A., Kitazato, H., Kucera, M., 2012. Vertical niche partitioning between cryptic sibling species of a cosmopolitan marine planktonic protist. Molecular ecology 21, 4063-4073.

Chapter 2: AMOR, an automated system for orientation and imaging of microfossils.

Yannick Mary[a,b]

a: Natural History Museum Basel, Augustinergasse 2, 4001-Basel, Switzerland

b: Geologisch-Paläontologisches Institut, Universität Basel, Bernoullistrasse 32, CH-4056 Basel, Switzerland

Abstract

Manual orientation and imaging of large datasets of microfossil for morphometrics is difficult and time consuming. For routine application of shell morphology analysis, an automated device that automatically orients foraminifera under light binocular microscope has been made: the robot AMOR. AMOR is capable of imaging foraminifera test in optimal profile "keel view" position, and to automatically capture images of specimens. The performances of the AMOR device are evaluated through the analysis of up to 600 specimens of Indian Ocean menardellids. In this sample, the AMOR failure rate, in the automatic mode was about 21%, which is quite high. Examination of error sources indicates that most of the failure is imputable to specific morphologies that cannot be handled by the positioning protocol. The development of AutoIt scripts, using the AMOR manual mode, is suggested as a possibility to solve AMOR positioning issues and to further increase the autonomy of the device.

2.1 Introduction

Morphometry based on digital images of foraminifera is an increasing field of micropaleontology. The manual collection of a statistically significant number of specimens (Knappertsbusch, 2007; Brown, 2007) includes major and tedious effort to produce sound data. The morphological analysis of extended datasets cannot easily be handled without the help of automated devices.

Planktonic foraminifera are tiny organisms with multifaceted 3D structures. While during the past decade automated image processing systems for the routine measurement of randomly oriented microfossils have become increasingly documented in the literature (Bollmann *et al*., 2004; Schmidt *et al*., 2004; Eynaud *et al*., 2008), the automated orientation of specimens to homologous position remained a major challenge. This is one of the main reasons why traditional morphometry on microfossil shells has remained difficult for routine application.

In order to resolve these difficulties, the automated device AMOR (Automated Measurement system for shell mORphology) was recently realized by Knappertsbusch *et al*., (2009) in a several years lasting collaboration with students and engineers of the University of Applied Sciences (FHNW) in Brugg/Windisch, Switzerland. AMOR has been designed for automatic orientation of microfossils and for imaging of isolated specimens under light binocular microscope. Its development was part of a major effort to study the morphological evolution of the Neogene planktonic foraminiferal plexus *Globorotalia menardii* (Knappertsbusch, 2011a; Knappertsbusch and Mary, 2012). The present chapter describes some aspects and limitations of AMOR and provides ideas for potential further development. Many observations, testing results and traditional morphometric applications in context of the development of AMOR are available in MorphCol, which is a periodically updated compendium of traditional morphometric procedures developed for and used during the evolutionary morphometrics of menardiform globorotalid (Knappertsbusch, 2004-2013: MorphCol). New insight and contributions that resulted particularly during the present PhD thesis include:

1.) The recognition of the influence of microfossil shape on the performance of AMOR has recently led to improvement of AMOR to its current version 3.28 (Knappertsbusch 2004-2013: MorphCol; Schorpp, 2013), see the sections about performance under Results and Discussion further below.

2.) The operation of the graphical user interface (GUI) of AMOR using AutoIt as a scripting bot was an advanced innovation to increase the efficiency of automated microfossil automation (see Discussion).

2.2 Material and methods

2.2.1 Technical description

AMOR consists of a motorized binocular microscope and a four axis motorized stage (Figure 2.1). The microscope is a standard MZ6 from Leica, which is equipped with a motor focus from Leica and a customized motorized zoom for automatic magnification (ranging from 0.63x through 4x). For real-time imaging a 3CCD color videocamera from Sony (DXC390P) with a sufficiently fast image transmission rate has been used. The four-axis motor stage is composed of four Nanotec micro-stepping motors allowing for movement into four degrees of freedom. Two motors drive a pitch and roll tilting movements of the sample holder, which are perpendicular to each other, while two additional motors allow for perpendicular gliding of the sample within the current planes of tilting. The tilting range had to be limited from -30° through +30° in order not to collide with the microscope stand or with the objective of the microscope. The sample holder is a central aluminum plate showing a rectangular cavity, where a standard micro-faunal sample slide from P.A.S.I. s.r.l. Torino can be placed.

All moving components (*e.g.* the four motors of the four-axis stage, the zoom-motor and the focus-motor) and the camera are controlled by the AMOR software, which is installed on a PC running under Windows 2000. The images collected in this investigation were collected using AMOR version 3.17. Meanwhile, AMOR was further improved and extended to version 3.28. The AMOR software was developed under the LabView 8.5 development

system from National Instruments. While all stepping motors driving the tilting- and gliding movements of the stage and the motorzoom are digitally fed by controllers (connected to data acquisition boards DAQmx 8.6 from National Instruments), the Leica motorfocus is controlled using the CAN interface, which is connected to IMAQ 1405 frame-grabber from National Instruments, where also the camera is mounted.

Illumination of the central sample slide is provided by two sources. Two lateral fiber-optic swan-neck lamps located on the right and left side of the motorized stages, produce incident light. In order to reduce reflections from the bottom of the sample slide and to enhance the contrast between the microfossil and its surroundings, the tips of the swan-necks are covered by polarizing filters, which can be twisted. A coaxial ring illumination from Volpi is mounted underneath the objective of the microscope providing homogeneous light. Also this light passes a polarizing filter, which can be adjusted for total extinction of reflections from the bottom of the sample. For optimum contrast between slide and the microfossil, which has in most cases a bright surface, the slide-bottom has been chosen black.

The AMOR software can be operated in two modes: a semi-manual mode, where functions for orientation (gliding, tilting, image rotation, magnification, and image capture) and focusing can be activated my mouse clicks, and a fully automated mode, where a full sequence of auto-orientation, auto-focusing, magnification, and image capture is run from the previously selected array of fields in the multi-cellular slide. In order to make the system flexible enough for microfaunal slides with different field numbers, a slide calibration module was implemented too.

2.2.2 Optimal positioning

In comparison to many other planktonic foraminifera, the menardellid shell morphology is relatively simple. Its compressed, low trochospiral shell is divided in two halves, the umbilical side, where the aperture is located, and the spiral side, where the successive addition of chamber along the spire is visible. Key features of the menardellid shells are the aperture (primary opening of foraminiferal shell), the apex (the initial portion of a trochospiral test) and the keel (peripheral thickening of the shell) (Figure 2.2). For efficient

and accurate comparison of shells, these structures need to be turned into homologous positions as good as possible.

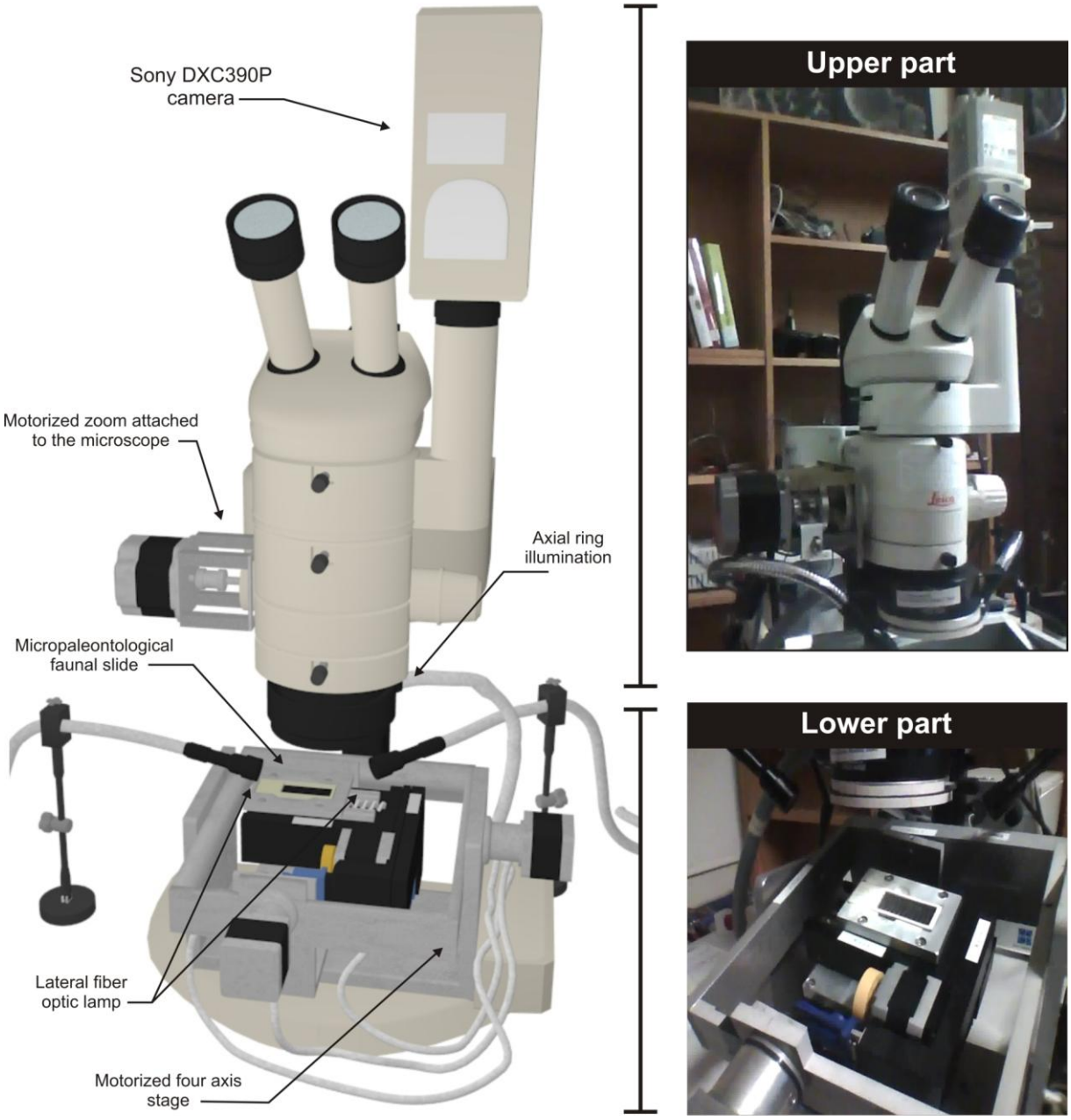

Figure 2.1: 3D model of AMOR device, realized with the free software *Blender*. PC and stepper-boxes are not shown. Close-up photographies of upper part (modified Leica microscope) and lower part (four axis stage) of the AMOR are displayed.

Most of the variation of menardellid shells is best seen in profile "keel" view rather than in umbilical or spiral view. Keel view means that the keel is central in this position, which allows the measurement of two simple parameters, δX (spiral height), and δY (axial diameter). Figure 2.2 illustrates a virtual menardellid specimen in perfect keel view.

For reaching the optimal keel view positionning, several preconditions must be met. The specimen needs to be in upright position, standing on the keel. The spiral side must point to the left side, while the aperture needs to be facing upward in direction to the microscope objective. The aperture should be in the middle of the axial length. The tip of the apex should ideally coincide with the minimum X-coordinate of the shell's outline. Furthermore, the line connecting the uppermost and lowermost Y-coordinates of the outline should be vertical (keel view definition adopted from Knappertsbusch 2007).

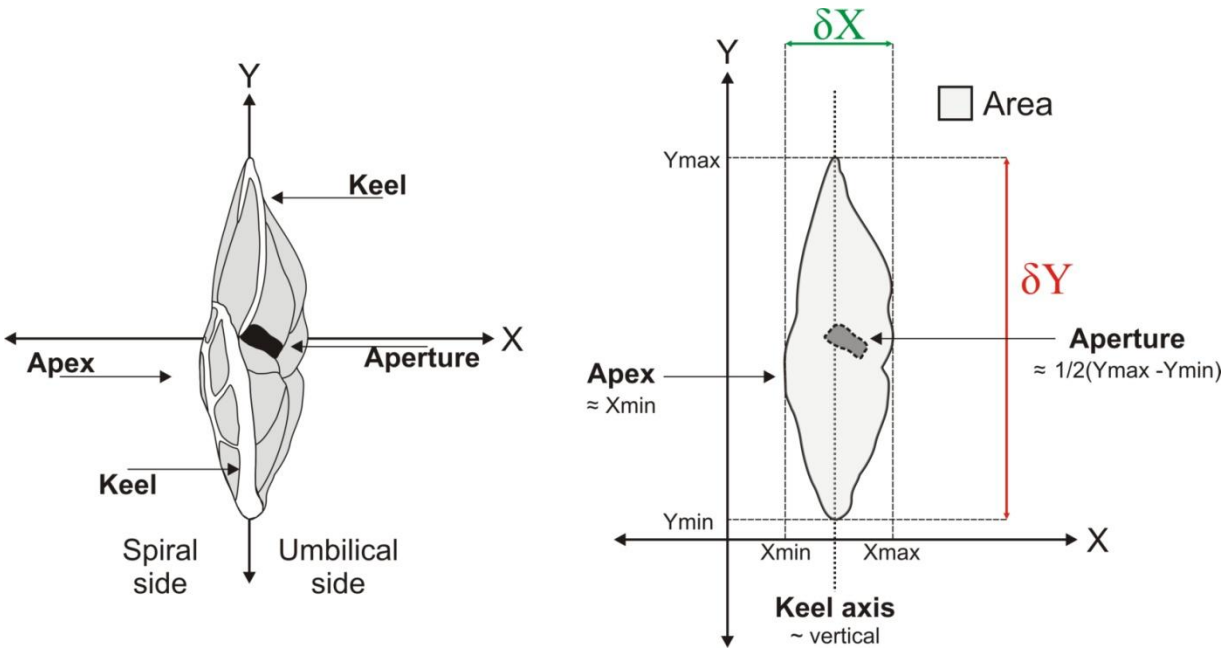

Figure 2.2: Optimal keel view positioning of a hypothetic menardellid specimen (see text for further explanations).

2.2.3 Automated orientation

In order to automatically orientate individual specimens in optimal keel view AMOR mechanically drives the specimen by successively roll- and pitch movements, while holding the specimen within the field of view (which is a function of magnification) by the two gliding motors. Simultaneously the specimen is constantly re-focused after every mechanical change of tilt- and roll condition. In order to satisfy the "vertical line requirement", the specimen on the monitor is soft-rotated (*i.e.* the image is rotated instead of the specimen). Each status of orientation is checked by calculation of the surface area of the foraminiferal particle, its length, and the deviation from verticality from the actual LUT image.

• Roll movement

Roll means the repeated tilting of the mounted specimen from a condition where the foraminiferal equatorial plane is inclined to the right to a condition, where the equatorial plane is inclined to the left, or reverse. Mathematically, this is performed by finding the position, where the enclosing area of the shell is minimal (=Roll condition). After giving the command the robot initializes the Roll procedure by a sequence of Roll movements, while constantly calculating the specimen area at each Roll angle. Using the minimum condition and a sequence of *If case* logics, the optimum "upright" condition is found.

• Pitch movement

Subsequently, the orientation of the specimen continues with a sequence of forward- and backward tilting movements (=Pitch movement). Here, the desired position is reached as soon as the longest axis of the shell in keel view (δY, see Figure 2.2), reaches its maximum value.

• Image rotation

Once the Roll and Pitch conditions are attained, the last step consists in a rotation of the specimen. This is performed by soft-rotation of the image in AMOR (*i.e.* without physical movement of the shell). The best vertical positioning is attained if the momentum of inertia of the grey-level image becomes minimal (this condition works as long as the deviation of the longest axis of the shell does not surpass plus or minus 45°, see Knappertsbusch *et al*., 2009).

The definition of these three conditions, necessary to reach an optimal positioning in keel view, were set and designed through experimentation. They are limited to forms similar to the menardiform shell geometry. Specific morphologies of other microfossil groups involve other positioning constraints that must be evaluated through experimentation before analysis. Next to the keel view positioning AMOR includes also the possibility to orientate shells in spiral and umbilical views as well. Here, the algorithm for shell orientation is simply based on successively maximizing the enclosing shell area.

2.2.4 Working procedure

Before imaging, every single specimen was mounted by hand in keel view as good as possible, on multicellular micropaleontological faunal slides. In order to facilitate operation of AMOR without failure, specimens were glued to the slide in approximate profile position with the spiral apex pointing always to the left. This processing remains unfortunately time consuming: in average, a single slide, including 60 specimens, is mounted in approximately 1h30. The white numerals, which are standard engraved in the faunal cells, were previously blackened out with a pen in order to prevent misinterpretation of drawn numerals with microfossils by AMOR.

In automatic mode AMOR automatically selects the highest possible magnification and automatically focuses on the object under the lense after mechanical movement. If desired, the magnification at which automatic positioning of specimens is performed, can be set interactively, next to other parameters. Alternatively, the automatic zoom can be deactivated too, so that the magnification can be adjusted by hand, which is sometimes useful to accelerate

processing of an entire slide. Once AMOR has been started up, initialized and all parameters are set, the robot scans the multi-cellular slide, field by field until the last specimen is reached. After auto-orientation, focusing, and centering the specimen, the final magnification is set, the image is focused again and a grey-level tiff-image is written to disc. A complete orientation sequence (*i.e.* moving to a particular specimen, auto-centering the specimen, orientation, re-centering, focusing, auto-magnification, imaging, and moving to the next) takes approximately 4 to 8 minutes per specimens.

2.2.5 Post processing

The output of AMOR is a series of tiff files showing oriented specimens in the slide, with one image per specimen, a file containing the magnification at which every specimen was imaged, and a log file with position coordinates and information about errors if automatic positioning of a specimen failed. A visual check of each picture, however, remains necessary in order to survey eventual mal-operation of AMOR due to poor focusing, false-orientation, poor illumination, blending of the camera, a malfunctioning of the auto-magnification unit, etc. If errors occur persistently, specimens can also be oriented using the manual mode of the AMOR, where the diverse functions can be activated manually by mouse-clicks. After collection images are then submitted to a suite of image enhancement operations in the commercial software Adobe Photoshop, which can be scripted for accelerated treatment. This post-processing includes mainly LUT, opening and closing operators and image sharpening or smoothing filters and is necessary to enhance the contrast between particle and the black background before images are further processed to particle outlines. Thereafter, images are converted to binary using the open domain software ImageJ. Extraction of Cartesian outline coordinates and traditional morphometry are then carried out using a suite of programs described in MorphCol (Knappertsbusch 2004), which were adapted to the usage under Windows.

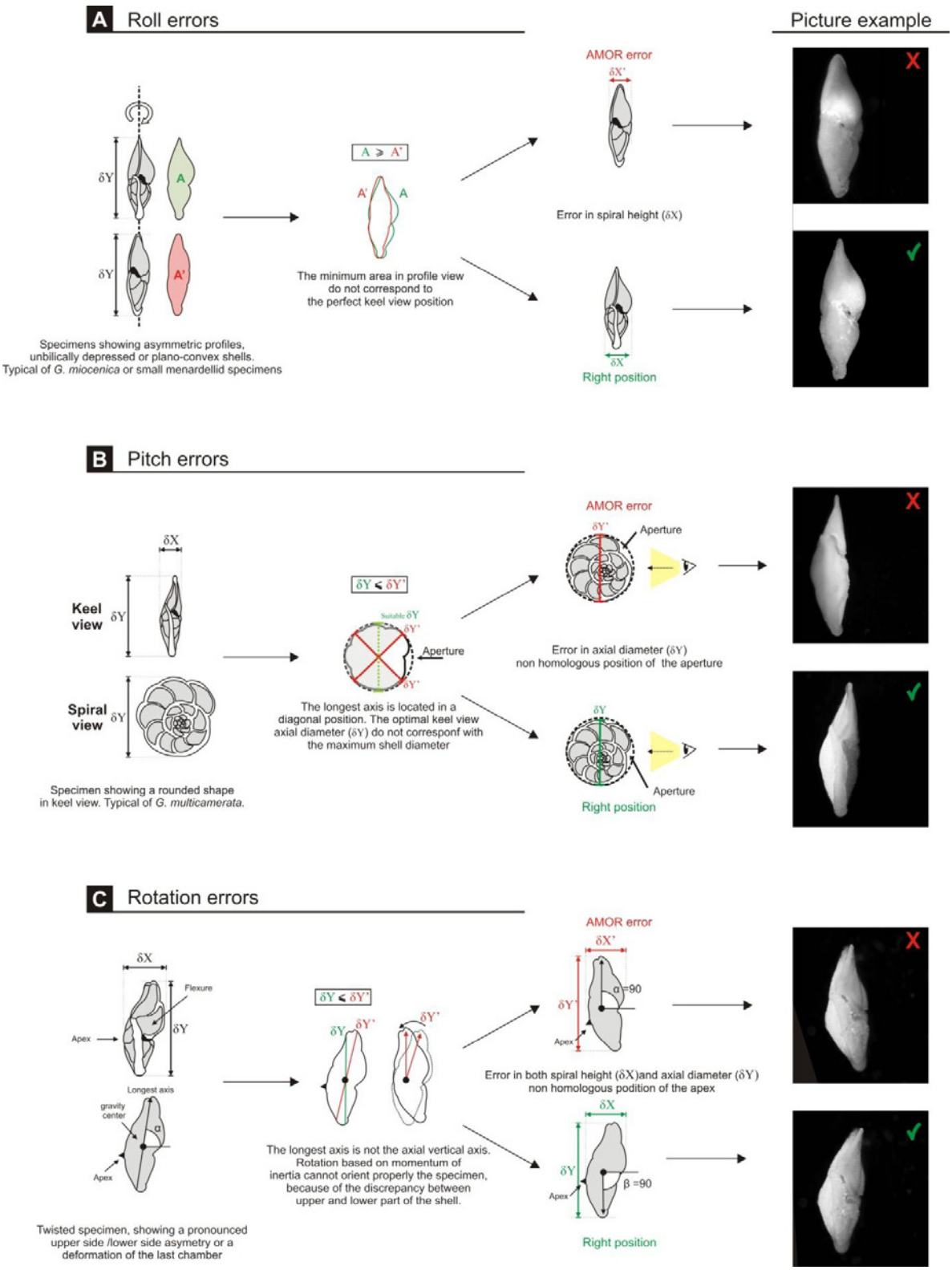

Figure 2.3: Chart showing the three most common orientation errors of AMOR, from the morphological origin of the error to picture example. (A) Roll error (B) Tilt error (C) Rotation error.

2.3 Results

2.3.1 Repeatability

The reproducibility of AMOR imaging was tested in detail before the beginning of this project by Knappertsbusch *et al*. (2009), Knappertsbusch (2004-2013: MorphCol). There, influence of numerous parameter settings has been tested including illumination, thresholds, precision of the X and Y translational and tilting motor, calibration of the camera and calibration of the microscope magnification using always the same specimen. These results will not be repeated here. Test measurements show a reasonable repeatability (refer to results on repeatability tests documented in Knappertsbusch (2004-2013): MorphCol Supplements #3, 5, and 8).

2.3.2 Performance

The performance of AMOR for automated orientation of microfossils can only be evaluated after analysis of an extended dataset. During practical work with AMOR, four types of failure were experienced. The first refers to device failure. This is erroneous behavior during auto-magnification and auto-focusing, sometimes leading to a complete crash of the system. The other three types of failure were observed in combination of an unfavorable orientation of the microfossil.

Roll errors occurred frequently, if the device failed to find a minimum area condition during "rolling", which can be caused by an unfavorable relationship between area enclosed by the microfossil and the tilting (Roll) angle (Figure 2.3A). Such a situation can occur, if the shape of the shell strongly deviates from the typical biconvex menardiform profile. Similarly, Pitch errors occurred, if no maximum of axial length was detected during pitch movement, which may lead to an excessive pitch amplitude and hence mechanical blocking of the stage (Figure 2.3B). Such a situation occurs preferentially, if the periphery of the particle in umbilical or spiral view becomes circular: in that case "pitching" is not capable of finding a major axis.

The third type of failure (rotation error) was observed, if the particle orientation, which is software driven, is unable to set the longest axis vertical on the computer monitor (Figure 2.3C). This situation can occur, if the grey-level distribution over the microfossil is laterally very uneven or asymmetric, so that the computation of the momentum of inertia of the grey-level image returns false rotational angles.

In order to document the performance of AMOR more quantitatively a total of 613 specimens of the Mid-Pliocene (from the 3.2 Ma-time-slice) sample in the Indian Ocean (ODP Site 707) were measured, and the different error messages reported by AMOR in the corresponding Log files were investigated (see Table 2.1). In this sample, the AMOR failure rate in the automatic mode was found to be about 21%, which is relatively high. However, it is interesting to note that the device failure rate is only about 5%, leaving the remainder 16% to the above mentioned Roll-, Pitch- or Rotational or other types of errors.

Table 2.1: Performance of AMOR tested with 613 bulk menardellid specimens form ODP Site 707 (Indian Ocean). The results suggest that the error rate is also susceptible to the size fraction, especially in context with Roll errors. 120 specimens per size fraction where selected where possible.

Slide	Size fraction	Number of specimen	% Error (global)	% Roll error	% Tilt error	% Rotation error	% Device error
1	>600µm	13	15	0	8	8	0
2	500-600µm	60	33	2	17	8	5
3	500-600µm	60	23	5	7	5	7
4	400-500µm	60	15	3	3	5	3
5	400-500µm	60	15	3	3	3	5
6	300-400µm	60	17	3	0	0	12
7	300-400µm	60	18	7	5	3	2
8	200-300µm	60	23	13	0	0	10
9	200-300µm	60	18	10	2	7	0
10	100-200µm	60	20	12	0	2	7
11	100-200µm	60	30	18	5	3	3

2.4 Discussion

2.4.1 Automated positioning as a source of systematic false positioning

Considering Table 2.1, the different types of errors of the AMOR are not randomly distributed. In some cases, there is a size dependent component in the frequency of errors, particularly in case of the Roll error, as seen in Figure 2.4, which displays the size fraction dependent contribution of the three different error types to the global error rate.

Roll errors occur more frequently in the small size range, whereas Pitch and Rotation errors tend to occur more often in the larger size fractions. This information is of particular interest, because it indicates that failures are not an intrinsic or random feature of AMOR version 3.17, but often must be thought in context of the size or shape distributions of the investigated particles.

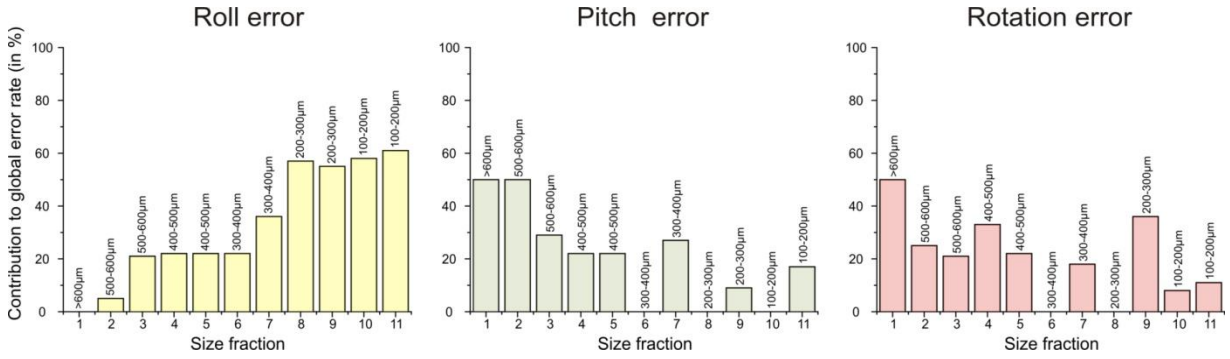

Figure 2.4: Histograms showing the contribution of the three orientation errors to the global error rate (in %), as a function of the size fraction.

This experiment and the inspection of the test sample has led to detect that Tilt and Rotation errors are causally linked with the abundance of circular outlines (in spiral view) and a "twisted" morphology showing aberrant, deformed final chambers in the investigated shells. Such morphologies are known to occur in *Globorotalia multicamerata*, a large menardellid species with a quasi-circular outline abundant in Mid-Pliocene test sample (we coined this particular problem the "circle problem"). Roll errors occur preferentially in cases, where

asymmetric shells with spiro-convex or umbilico-convex profiles prevail, as it commonly occurs with small, immature specimens showing usually a flatter spiral side and a strongly convex umbilical side (this problem is reference to as the "*G. miocenica*-problem", see Knappertsbusch, 2011b and c).

During development of the orientation algorithm, the versions until AMOR 3.17 were tested using the typical biconvex, quasi-symmetric shells of modern *G. (M.) menardii*. Keeping this historical fact in mind, together with the above-mentioned observations, the orientation algorithm needs further adaptation to other types shell profiles. Automatic orientation using versions until AMOR 3.17 thus functions best for morphologies that do not strongly deviate from *G. (M.) menardii*. In all other cases orientation in the manual mode or post-auto-orientation corrections are recommended. Meanwhile, some of these deficiencies (*i.e.* the "*G. miocenica* problem") could be resolved in the current version under development, AMOR 3.28, but testing and application of this new version became beyond scope of this PhD thesis.

2.4.2 Scripting AMOR using AutoIt

The modification of the AMOR code, which is written in Labview, requires special skills from professional engineers. Because of its complexity only simple modifications within the vi's (=virtual instruments) sometimes leads to malfunction, which is difficult to locate in the code. This is an unfavorable situation because other than typical menardiform morphologies are difficult to be automatically oriented with this device. However, the user has the alternative to apply the manual mode, where all necessary functions can be operated interactively by mouse commands. This has led to the idea to "externally" drive the device by automatic scripting all necessary mouse commands, which can be realized using AutoIt scripting language. This has the large advantage that commands of AMOR in manual mode can be combined in any desired combination to a fully automated robot.

AutoIt (version 3) is a free BASIC-like, automation oriented language created for the manipulation of windows and windows related graphic user interfaces (GUIs). Features of this language include several built-in editors, standalone applications and key/mouse/windows

functions that are explicitly designed to automate routine procedures or repetitive software tasks. AutoIt can easily take control over the entire computer, simulate keystrokes, mouse movements, windows control/manipulation, etc. AutoIt compiler and documentation can be downloaded at the official AutoIt website under www.autoitscript.com.

AutoIt is especially designed to create so-called "bots". A bot is a simple computer program made to simulate user decisions, which follow a list of decisional trees created for specialized tasks (such as, in our case the orientation of a microfossil with a specific morphology). It is ideal to perform highly repetitive tasks. Bots are widely used to simple automated tasks, for example over Internet, or in video gaming.

They are different from macros: bots are a sequence of programming instructions that specify how a certain list of functions must be carried out. They have the capacity to execute several programs simultaneously. In contrast, simple macros are usually limited to its "mother-software" and do not show this high degree of flexibility.

Combined with AMOR, an AutoIt-based bot (or any other scripting language capable of controlling mouse commands) can thus easily take control of the entire AMOR GUI and emulate a response from the user. In this way, the Amor Manual Driving Script (AMDS) bot was created in order to circumvent the above mentioned difficulties, The AMDS bot automatically manipulates the manual mode of AMOR: it successively allows to move from one specimen to next in the slide, to orientate and image them using all the built-in routines of AMOR. Even in case of errors, the corresponding error messages and dialogues that are sent to the monitor can be recorded and diverged to a corresponding automated reaction of the AMOR system. With the help of AMDS, AMOR can perform analysis independently, overnight, which is a very welcome gain of time.

The application of the AMDS bot gives most flexibility to the AMOR device and program. AMDS includes routines dealing with occasional AMOR software problems in connection with the auto-magnification module or when auto-zoom failed. In case of a critical situation (strong mechanical blocking of moving elements) AMDS can reboot AMOR operating system, restart, and initialize a new batch. Several version of AMDS are available, each one corresponding to a specific type of analysis. It allows any user to quickly design

procedures adapted to particular microfossil morphology or to variability of sampling quality. For example, AMDS version 9.0 deals with variation of size of microfossil by adjusting the tilting magnification.

The source code of AMDS 9.0 is given in the appendix 1. It must be reminded that some features of AMDS depend on file directories or are coordinated via aliases, which must therefore remain on the desktop.). All these scripting files are thus especially customized to the device, to which they belong for manipulation of the entire system.

2.5 Conclusion

AMOR has convinced to be a very useful device for automated specimen orientation and imaging. Especially, the addition of AutoIt scripting turns AMOR into a fully autonomous robot. Interesting potential is seen in the creation of a portfolio of scripts for all kinds of foraminiferal species and so providing the means for extensive automated morphometric data collection. With this perspective, the proposal of creating a worldwide sample grid including temporal sequences of biogeographic time-slices for mapping the morphological variation of species through time and space may once become a reality to evolutionary research.

References

Bollmann, J., Quinn, P., Vela, M., Brabec, B., Brechner, S., Cortes, M.Y., Hilbrecht, H., Schmidt, D.N., Schiebel, R., Thierstein, H.R., 2004. Automated particle analysis: Calcareous microfossils, p. 229- 252. In Francus, P. (ed.), Image Analysis, Sediments and Paleoenvironments. Kluwer Academic Publishers, Dordrecht, The Netherlands.

Brown, K. 2007. Biogeographic and morphological variation in late Pleistocene to Holocene globorotalid foraminifera. Dissertation Phil. Nat. Fakultät, Universität Basel, 128.

Eynaud, F., Cronin, T.M., Smith, S.A., Zaragosi, S., Mavel, J., Mary, Y., Mas, V., Pujol, C., 2009. Morphological variability of the planktonic foraminifer *Neogloboquadrina pachyderma* from ACEX cores: Implications for Late Pleistocene circulation in the Arctic Ocean. Micropaleontology 55, 101-116.

Knappertsbusch, M.W., 2007. Morphological variability of *Globorotalia menardii* (planktonic foraminiferan) in two DSDP cores from the Caribbean Sea and the Eastern Equatorial Pacific. Carnets de Géologie / Notebooks on Geology, Brest, Article 2007/04.

Knappertsbusch, M., Binggeli, D., Herzig, A., Schmutz, L., Stapfer, S., Schneider, C., Eisenecker, J., and Widmer, L., 2009. AMOR - A new system for automated imaging of microfossils for morphometric analyses. Palaeontologia Electronica 12(2); 2T: 20 p.

Knappertsbusch, M.W., 2011a. Evolution im marinen Plankton. Mitteilungen der Naturforschenden Gesellschaften beider Basel, 13.3-14.

Knappertsbusch, M.W., Mary, Y. 2012. Mining morphological evolution in microfossils using volume density diagrams. Palaeontologia Electronica, Vol. 15, Issue 3; 7T: 209p. URL: http://palaeo-electronica.org/content/issue-3-2012-technical-articles/282-volume-density-diagrams/.

Knappertsbusch, M., 2004 through 2013: MorphCol - A collection of Fortran 77 programs for geometric morphometry. Technical Report. Naturhistorisches Museum Basel, Augustinergasse 2, 4001-Basel, Switzerland, 120 pp. URL: http://micropal-basel.unibas.ch/Research/MORPHCOL/Start.html.

Knappertsbusch, M., 2011b. MorphCol Supplement#19. Lösung des "*G. miocenica* Problems". MorphCol - A collection of Fortran 77 programs for geometric morphometry. Technical Report. Naturhistorisches Museum Basel, Augustinergasse 2, 4001-Basel, Switzerland, 120 pp. URL: http://micropal-basel.unibas.ch/Research/MORPHCOL/SUPPL_19.pdf.

Knappertsbusch, M., 2011c. MorphCol Supplement#20. Tilting (Roll) Experiments in AMOR 3.17. Finding a solution for the "*G. miocenica* problem". MorphCol - A collection of Fortran 77 programs for

geometric morphometry. Technical Report. Naturhistorisches Museum Basel, Augustinergasse 2, 4001-Basel, Switzerland, 120 pp. URL: http://micropal-basel.unibas.ch/Research/MORPHCOL/SUPPL_20.html.

Schmidt, D.N., Renaud, S., Bollmann, J., Schiebel, R., Thierstein, H.R., 2004. Size distribution of Holocene planktic foraminifer assemblages: biogeography, ecology and adaptation. Marine Micropaleontology 50, 319–338.

Schorpp, R., 2013. AMOR Software Beschreibung. Unpublished technical report, Fachhochschule Nordwestschweiz, 65 p. MorphCol Supplement #23, online under http://micropal-basel.unibas.ch/Research/MORPHCOL/SUPPL_23.pdf

Chapter 3: Morphological variability of menardellid globorotalids in the Atlantic Ocean during Mid-Pliocene

---

Yannick Mary[a,b], Michael Knappertsbusch[a]

a: Natural History Museum Basel, Augustinergasse 2, 4001-Basel, Switzerland

b: Geologisch-Paläontologisches Institut, Universität Basel, Bernoullistrasse 32, CH-4056 Basel, Switzerland

This chapter has been accepted for publication
in *Marine Micropaleontology* (in press).
Minor modifications were made from the published version.

Abstract

The morphological variation of the planktonic foraminiferal plexus of *Globorotalia* (*Menardella*) (Bandy, 1972) has been studied in a Pliocene time-slice at 3.2 Ma. Using a combination of size, linear shell measurements and shape analysis, an extended morphological protocol is explored in order to define morphological subgroups within the *Menardella* subgenus. Isochronous samples at 3.2 Ma have been selected at five ODP/IODP Sites in the low latitude Atlantic Ocean, in which up to 600 specimens per sample have been oriented, imaged and analyzed using a new automated prototype for morphological analysis called AMOR. Multimodal size frequency distribution is related to the occurrence of several distinct populations.

Three main ubiquitous populations of such menardellids are isolated, next to two additional biogeographically limited subgroups. These populations strongly differ in abundance and size. Using morphological classifiers, subpopulations are distinguished among these populations, leading to the establishment of seven different morphotypes informally named: MA, MB, MC1, MC2, MC3, SH1 and SH2. These morphotypes are assigned to formal species, *i.e.*, MA corresponds to *Globorotalia (Menardella) menardii*, MB to *G. (M.) limbata*, SH1 to *G. (M.) exilis*, and SH2 to *G. (M.) pertenuis*. In contrast, the species *G. (M.) multicamerata* is interpreted as being composed of three distinct morphotypes, sharing a similar size range, but differing in shell morphology. Morphotype MC1 shows thin and elongated chambers, whereas morphotype MC2 is characterized by a thick and robust test. MC3 is inflated with a distinct flexure in the final chamber. Size differences are linked to variations in habitat temperature and oxygenation, with the exception of *G. (M.) multicamerata* morphotypes, which are probably adapted to a productivity gradient.

3.1 Introduction

Since recent outcomes of combined morphometry and molecular studies have revealed that subtle morphological differences could reflect cryptic genetic diversity (Huber *et al*., 1997; de Vargas *et al*., 2001; Morard *et al*., 2009; Aurahs *et al*., 2011), planktonic foraminifera have been the focus of many biometric investigations (for example: Huber *et al*., 2000; Renaud and Schmidt, 2003; Eynaud *et al*., 2009; Regenberg *et al*., 2010; Moller *et al*., 2011). Traditionally defined morpho-species are actually composed of biogeographically and ecologically distinct populations (Kucera and Darling, 2002; Darling and Wade, 2008). Morphological variability, within these populations, has been inferred as evidence of genetic diversity, thus opening a new field for biometrical investigations.

Only a few studies have tracked morphological variability as possible evidence of species level diversity in ancient forms rather than in living specimens (Kucera, 1998; Kelly *et al*., 2001; Renaud and Schmidt, 2003; Knappertsbusch, 2007; Eynaud *et al*., 2009; Georgescu *et al*, 2009; Hull and Norris, 2009; Rossignol *et al*., 2010). Although the fossil record of planktonic foraminifera contains many examples of morphological gradation that possibly include several cryptic species, the definition of the species boundary within a fossil planktonic population remains problematic. The establishment of significant differences through biometry, without molecular analysis, involves several constraints that must be surmounted. Above all, the tenuous morphological differences between cryptic species make their recognition difficult (de Vargas *et al*., 2001; Morard *et al*., 2009; Aurahs *et al*., 2011), and induce the analysis of hundreds of specimens (Fatela and Taborda, 2002).

Usually, imaging of isolated specimens is carried out manually, which limits sampling size due to technical constraints and efficiency. A few studies have overcome this issue by applying automated techniques for the collection of morphological parameters such as size, area, or roughness (*e.g.* Schmidt *et al*., 2006; Eynaud *et al*., 2009; Moller *et al*., 2011), applied only on randomly oriented tests. Since outline coordinates are sensitive to orientation (Sokal and Rohlf, 1969; Rohlf, 1990), the use of non-oriented tests is not suitable for geometric morphometry. Furthermore, morphometric studies that involve oriented tests are restricted to a limited number of specimen of the >250 μm size fraction per sample (inferior to 500

individuals to less than 100 if several times intervals are analyzed (Kucera and Widmark, 2000; Kelly *et al*., 2001; Renaud and Schmidt, 2003; Hull and Norris, 2009)).

This paper describes a new approach, combining size frequency distributions and morphological measurements of large size samples with the use of an automated imaging robot: the Automated Measurement system for shell mORphology (AMOR) (Knappertsbusch *et al*., 2009). The morphological variability of *Globorotalia (Menardella) menardii*, and related species was investigated through the Pliocene period in the low latitude Atlantic Ocean. This group was chosen because of its high diversity during this period (Bolli and Saunders, 1985). The use of an automated device provides the opportunity to significantly increase the necessary number of individuals. Using contoured frequency distributions allows the identification of clusters within morphological populations. As a biogeographic experiment, shell variation is evaluated by comparing morphological variability from five selected localities corresponding to different environmental settings within the tropical North Atlantic: the Caribbean Sea, the Canary Current, the Equatorial Counter Current, the Mauritanian upwelling, and the Brazilian margin (see Figure 3.1).

3.1.1 Taxonomic considerations

Menardiform globorotalids constitute a subset within the genus *Globorotalia* (Cushman, 1927), in which *G. (M.) menardii* is the best known representative. To express the need to further separate *G. (M.) menardii* and its phylogenetically related forms from the remaining globorotalids, Bandy (1972) suggested the two subgenera *Globorotalia* and *Menardella*, on the basis of the hypothetical phylogenetic relationship. The clade *G. acheomenardii–praemenardii–menardii* and its related species are kept apart from the other globorotalid lineages (*i.e. Fohsella, Jenkinsella, Globoconella, Hirsutella, Truncorotalia, Tenuitella* and *Turborotalia*). This concept was also applied by Kennett and Srinivasan (1983), using the term menardellid to refer to the *G. menardii* clade. Following similar arguments, the terms menardiform globorotalid (Stainforth *et al*., 1975) or menardine (Cifelli and Scott, 1986) were applied to distinguish the *G. menardii* lineage from other globorotalids.

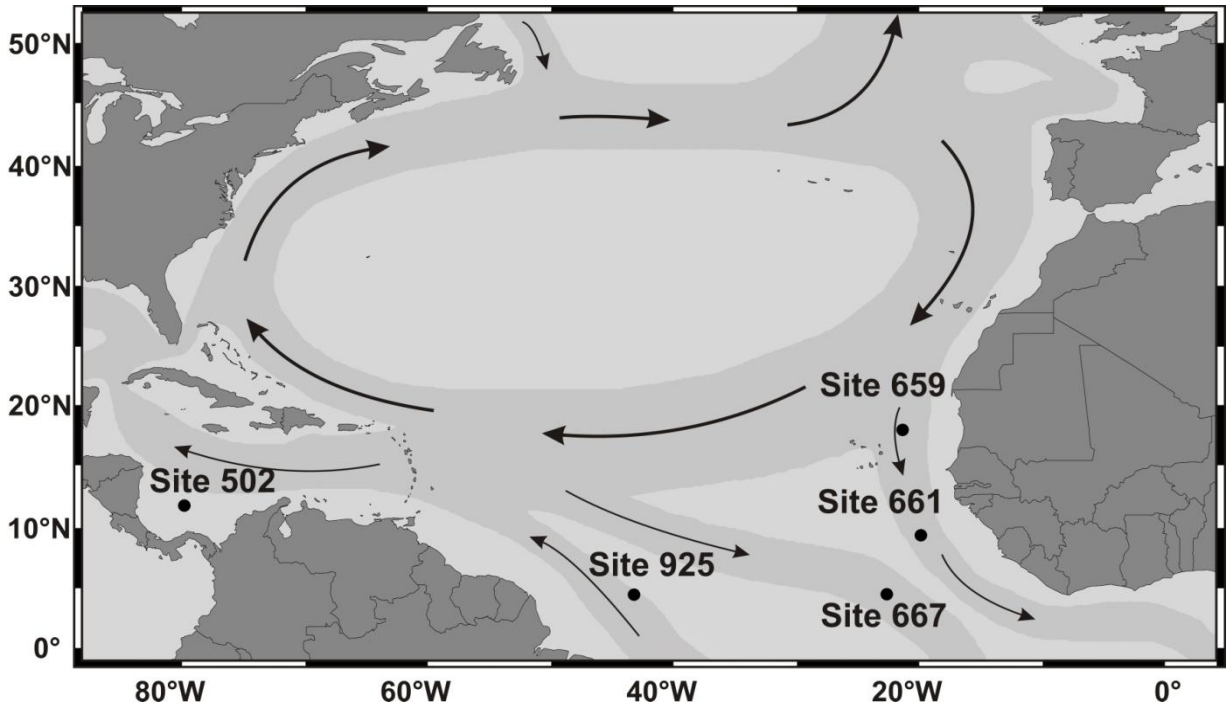

Figure 3.1: Geographic distribution of ODP study Sites 502, 659, 661, 667, and 925. Approximate position of actual currents is shown. Map adapted from Dowsett and Robinson (2007).

The present work follows the generic and specific concept of Bandy (1972) and Kennett and Srinivasan (1983). It takes into consideration the observations of Bolli and Saunders (1985). In synonymy with the term *Globorotalia* (Menardella) sensu Kennett and Srinivasan (1983), we apply the term menardiform of Stainforth *et al*. (1975) for summarizing members of the *G. menardii* lineage.

3.1.2 Test objects: Mid-Pliocene menardellids

We selected menardellid globorotalids as a model because of their ubiquitous occurrence in tropical sediments, their relative large size range, and their wide variety of morphologies. Their lenticular biconvex profile, divided in two sides by a blunt keel, makes them easy objects to model in two dimensions.

The *Globorotalia (Menardella) menardii–Globorotalia (Menardella) multicamerata* lineage originated with the appearance of *G. (M.) menardii* during the middle Miocene zone N12 (between 13.5 and 12 Ma). The species gave rise to *Globorotalia (Menardella) limbata and Globorotalia (Menardella) multicamerata* during the middle Miocene zone N14 and the Late Miocene zone N17b (Kennett and Srinivasan, 1983). A progressive evolution to larger size occurred between 3.11 and 2.29 Ma (Knappertsbusch, 2007). At the end of the Pliocene, all menardellids but *G. (M.) menardii* became extinct.

Extant *G. (M.) menardii* are facultative symbiont bearing species (Hemleben *et al*., 1989) living at the seasonal thermocline depth, but capable to adapt the depth of their habitat depending on temperature (Gasperi and Kennett, 1992). Recently, Sexton and Norris (2011) investigated the ecological preferences of *G. (M.) menardii*. According to these authors, the ventilation of the upper thermocline is the key feature controlling menardellid populations, *G. (M.) menardii* tracking poorly ventilated waters. In contrast, the ecological preferences of *G. (M.) limbata* and *G. (M.) multicamerata* are poorly known. Chaisson and Pearson (1997) and Chaisson (2003) considered them to be thermocline dwellers whereas Pfuhl and Shackleton (2004) interpreted their oxygen isotope ratios to be indicative of shallower habitats. Gasperi and Kenneth (1993) suggested that this group changed its habitat depth from intermediate to shallow during the late Miocene.

G. (M.) menardii, G. (M.) limbata, and *G. (M.) multicamerata* form a phylogenetic lineage, which is expressed as a continuous morphological intergradation from *G. (M.) menardii* to *G. (M.) multicamerata* (Kennett and Srinivasan, 1983; Bolli and Saunders, 1985; Cifelli and Scott, 1986; Chaisson, 2003; Knappertsbusch, 2007). All three species share the typical menardiform test morphology; *i.e.* a low trochospiral circular to oval test surrounded by a prominent keel. Chambers are densely perforated; sutures are straight on the umbilical and curved on the spiral side (Blow, 1969; Kennett and Srinivasan, 1983). They differ by an increase of the number of chambers per whorl (*i.e.* 5 to 6 for *G. (M.) menardii*, 6 to 8 for *G. (M.) limbata* and 8 to 10 for *G. (M.) multicamerata). G. (M.) multicamerata* has a smaller terminal chamber and a wider aperture than its ancestor *G. (M.) limbata* (Pfuhl and Shackleton, 2004), and shows a pronounced keel. Morphological differences are reported to be highly variable with biogeography (Cifelli and Scott, 1986).

The very similar morphology of *G. (M.) menardii* and *G. (M.) limbata* makes their differentiation difficult. Limbation, which is the continuation of the keel over the anterior face of a chamber on the spiral side (sensu Blow, 1969), is often cited as a key taxonomic feature. However, this parameter is not sufficiently diagnostic. Within *G. (M.) limbata* populations, all degrees of limbation can be observed; limbation has been reported to be ontogenetically variable (Kennett and Srinivasan, 1983; Chaisson and Leckie, 1993). In the present study, *G. (M.) limbata* is considered an intermediate form between *G. (M.) menardii and G. (M.) multicamerata,* following Kennett and Srinivasan (1983) and Bolli and Saunders (1985).

Globorotalia (Menardella) exilis and *Globorotalia (Menardella) pertenuis* are separated from the other menardellid species by their delicate, thin, and shiny test, originating from a dense and very fine wall perforation (Blow, 1969; Kennett and Srinivasan, 1983). *G. (M.) exilis* is characterized by a low coiled test, with 5 to 7 chambers in the last whorl and a thin keel. *G. (M.) pertenuis* can be distinguished from *G. (M.) exilis* by its much flatter strongly compressed test, along with its depressed umbilical side. Both species are reported to be endemic in the Atlantic Ocean (Kennett and Srinivasan, 1983; Chaisson and Leckie, 1993).

3.1.3 Settings

The middle Pliocene climate and environmental conditions have become fairly well known due to the climate modeling of the Pliocene Research, Interpretation and Synoptic Mapping (PRISM) Project (see Haywood *et al*., 2009 and references therein). According to the PRISM project, the overall climate at 3.2 Ma ago was on average 3 °C warmer than today (Cronin, 1991; Crowley, 1991; Dowsett and Poore, 1991; Dowsett *et al*., 1996; Dowsett and Robinson, 2009; Dowsett *et al*., 2009). Warming was accentuated at high latitudes whereas tropical temperatures were relatively similar to modern conditions (Chandler *et al*., 2008). Since restriction and closure of the Isthmus of Panama during the early Pliocene (Jain and Collins, 2007), exchanges between the Pacific and Atlantic Oceans were reduced to interrupted. The pattern of the north Atlantic circulation was supposed to be similar to that of the present day, with a subtropical gyre and a western boundary current transporting heat from the equator polewards (Dowsett and Robinson, 2007). Regional upwellings were also reported

similar to those of the present day. Planktonic foraminiferal studies of various sites report remarkably similar assemblages to modern analogs (Chaisson and Pearson, 1997; Cullen and Curry, 1997; Dowsett and Robinson, 2007; Dowsett *et al*., 2009; Lutz, 2011).

Table 3.1: Stratigraphic information of ODP Sites 502, 659, 661, 667, and 925.

ODP Sites	Coordinates	Depth (mbsf)	Age (Reference)
502A	11°29.46 N ; 79°22.74 W	80.91	3.2 Myrs (Keigwin *et al*, 1982; Knappertsbusch, 2007)
659A	18°04.63 N ; 21°01.57 W	99.95	3.2 Myrs (Leg 108 initial report)
661A	09°26.81 N ; 19°23.16 W	45.77	3.2 Myrs (Leg 108 initial report)
667A	04°34.15 N ; 21°54.67 W	44.89	3.2 Myrs (Leg 108 initial report)
925B	04°12.24 N; 43°29.34 W	95.16	3.2 Myrs (Chaisson and Pearson, 1997; Bickert *et al*., 1997)

3.2 Material

Five samples have been selected at a time-slice 3.2 Ma from ODP Sites 502, 659, 661, 667 and 925 (Figure 3.1). These sites were selected for their excellent carbonate preservation and high menardiform globorotalid abundance. Isochronous samples were determined using available range charts and age models reported in the respective volumes of the ODP (see Table 1). The age model for Site 502 follows the one given in Knappertsbusch (2007) which relies on the stratigraphic investigation of Keigwin (1982). The age models for Sites 659, 661, and 667 were derived from planktonic microfossil range charts given in the Neptune database, and are based on initial ODP report for Leg 108. The planktonic foraminiferal assemblages of Chaisson and Pearson (1997) and benthic δO18 ratio of Bickert *et al*. (1997) were used for Site 925. Numerical ages follow the chronology of Berggren Kent (1995). The biogeochronological nomenclature follows that of Gradstein *et al*. (2004).

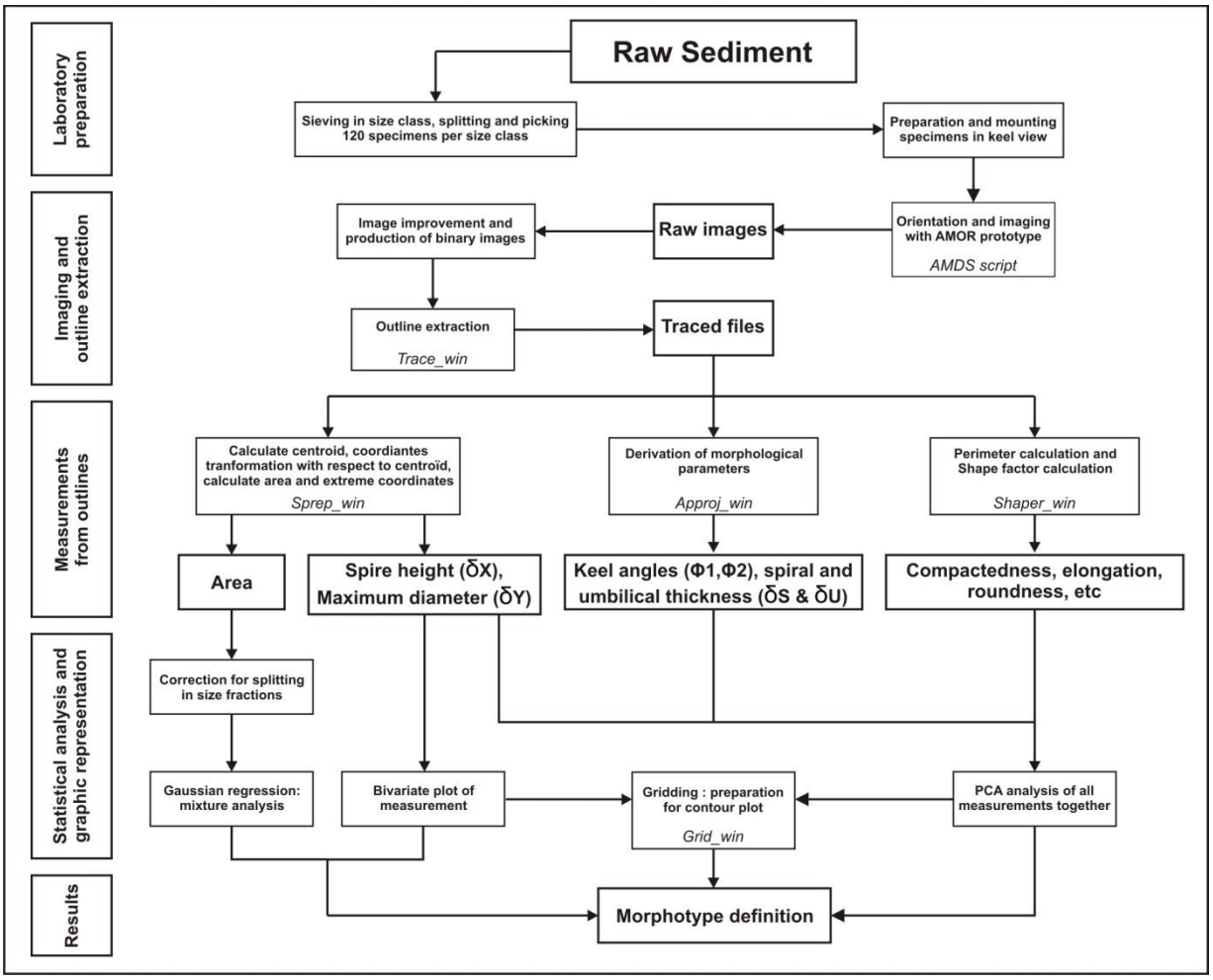

Figure 3.2: Flow chart illustrating the steps of sample and image processing, morphometric measurements and analysis. The names of the programs are shown in italic.

3.2.1 Sampling strategy

Pliocene menardellid shells are not equally distributed within all size fractions (Bolli and Saunders, 1985; Knappertsbusch, 2007): specimens <400 µm occur frequently in Pliocene assemblages, while larger specimens are rare. A random sampling would therefore lead to an underestimation of morphological variation found in the largest specimens. In this study, we select an equal number of specimens from seven successive size fractions (see next section) instead of randomly selecting specimens in the whole size range. The consequence is that

large specimens receive a greater weight to the overall morphological signal while the weight of the dominant smaller specimens is decreased.

In order to analyze the overall menardellid distribution, however, the relative importance of each size class must be corrected. Menardellid specimens are counted before picking and their absolute abundance is determined in each size class of the respective split. Individual frequencies are corrected by statistically weighing each specimen frequency in a size fraction with respect to the absolute abundance of menardellids in that size fraction, using the factor Fc according to the following formula:

$$F_C = N_S / N_p$$

Fc is the correction factor attributed to specimens that belong to size class S, Ns is the absolute number of menardiform specimens within size class S, and Np represents the number of picked specimens in the size fraction S.

3.2.2 Laboratory processing

A complex protocol for laboratory analysis and statistical treatment was applied (see Fig. 2). Sediment samples were weighed and washed through a 63 µm sieve under tap water. The residual fraction was dried for 24 h at 50 °C and weighted again to obtain the dry weight. Each sample was then divided into seven fractions, *i.e.* <100 µm, 100 µm–200 µm, 200 µm–300 µm, 300 µm–400 µm, 400 µm–500 µm, 500 µm–600 µm and >600µm through sieving; the size class <100 µm was not analyzed. After sieving, size fractions were split when needed. Whenever possible, 120 menardiform specimens were randomly picked from each size fraction. Individuals were then mounted in keel view (*i.e.*, the shell stands on the keel with the umbilical side to the right, and the aperture facing upward) on multicellular faunal slides. Only well preserved specimens were collected.

Individuals were then imaged using AMOR, a fully automated device for orientation and digital image acquisition of microfossils (Knappertsbusch *et al*., 2009). The AMOR consists of a motorized four-axis tilting and gliding stage for automatic positioning, under a binocular microscope equipped with a digital video camera. The microscope is driven by

motorized focus and zoom. All components are controlled by software written in Lab View. The AMOR is capable of automatic movements from one specimen to the next, to change the orientation of each specimen, and to capture their images. The AMOR orients menardiform shells into the optimal keel view (see Knappertsbusch, 2007). Optimal position is reached when the apex is visible on the left side of the profile, with the aperture being central (Figure 3.3). The AMOR robot has difficulties to orient deformed, aberrant or highly asymmetric forms, such as variants of *G. (M.) menardii* with a flexuose final chamber. In such cases, manual corrections were applied.

A total of 3132 menardellids were analyzed. All material and prepared slides are deposited in the collections of the Natural History Museum, Basel.

3.3 Measurements and analysis

3.3.1 General aspects of the shell

Specimens are analyzed without any prior taxonomic classification within the menardellid clade. For each shell, coiling direction, number of chamber in the final whorl, test luster, and possible deformation of the last chamber (flexuosa versus normal) were first evaluated under the binocular microscope. The relative abundance of right-coiled and left-coiled specimens is not further discussed. However, dextral specimens dominate strongly the menardellid assemblage (>98%) without showing any significant biogeographic trends. Because many shells display differences in wall structure, tests are categorized into shiny tests (SH) or non shiny tests (NSH). Shiny tests are characterized by a highly reflective chamber surface due to a fine and dense perforation. Specimens are designated as flexuosa variants when the last chamber was strongly flexed.

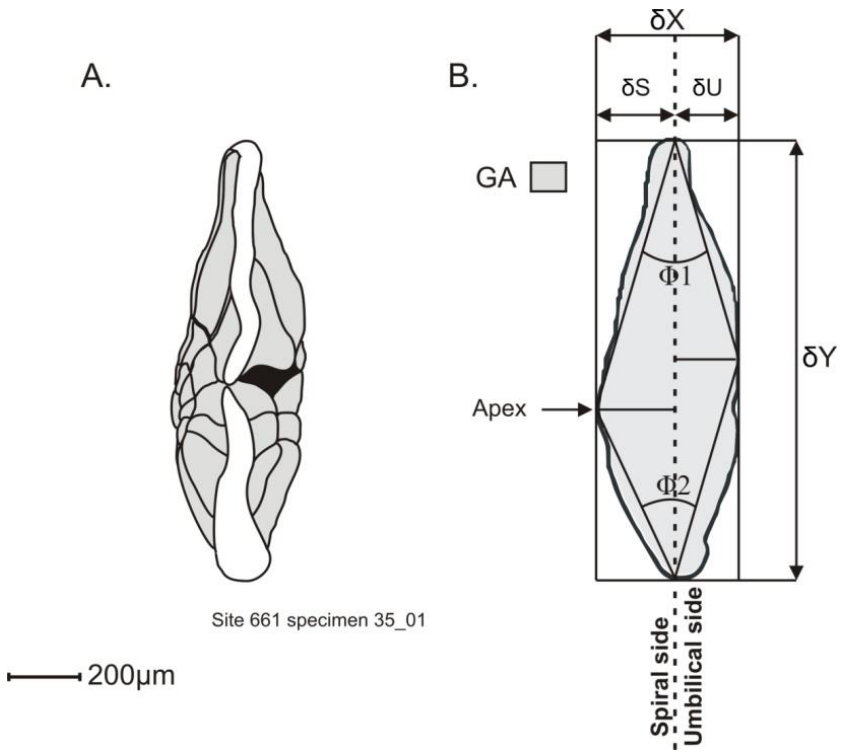

Figure 3.3: Morphometric parameters measured in a menardellid shell. (A) Sketch of a menardellid specimen in keel view. (B) Outline of the same specimen illustrating the morphological parameters measured in this study: spiral height (δX), axial diameter (δY), keel view global area (GA), spiral side inflation (δS), umbilical side inflation (δU), and upper and lower keel angle (φ1 and φ2).

3.3.2 Outline analysis

The outline analysis of the shells in keel view follows the method described in Knappertsbusch (2007). Gray scale pictures are converted to black and white binary images and saved in raw format using ImageJ macros written by the authors. The outline coordinates are extracted from pictures in batch mode using modified versions of the suite of Fortran 77 programs described in Knappertsbusch (2004) and Knappertsbusch (2007). From the outline coordinates, a set of morphological parameters is derived using Windows' versions of the programs Sprep (Knappertsbusch, 2004), Approjwin and Shaperwin (written by the authors). The parameters include: keel view global area (GA) and perimeter length (P), spiral height (δX), maximum axial diameter (δY), spiral and umbilical side inflation (δS and δU respectively), and upper and lower keel angle (φ1 and φ2) (Figure 3.3).

From these measurements four shape factors were calculated, which were adapted from the size invariant morphometrical descriptors of Kucera and Kennett (2002) *i.e.*:

Compactness factor: $F_{co} = P^2 / 4\pi GA$

Elongation factor: $F_{el} = \pi \delta Y2 / 4 GA$

Circularity factor: $F_{ci} = P/2\sqrt{(\pi GA)}$

Symmetry factor: $F_{sy} = \delta S/\delta U$

P (in mm) and GA (in mm^2) represent the perimeter and the area enclosed by the outline of the test in profile view, δY the maximum axial diameter, and δS and δU the spiral and umbilical side maximum width (all in μm). Fco is minimal and equals 1 for a disk, and reaches highest values for elongated objects. Fel becomes 1 for a disk and infinite when the area approaches to zero. Fci represents the difference between the perimeter of the object and he perimeter of a disk with the same area. It equals 1 if the object is perfectly circular. The symmetry factor Fsy becomes 1 for a symmetric test. It is less than1 for an umbilically inflated test and greater than 1 for spirally inflated test.

Bivariate plots of δX versus δY are constructed to describe ontogenetic morphologic differences between specimens and through geography. To represent directions of ontogenetical changes, linear regressions were applied using the least square method implemented in the software Origin.

3.3.3 Frequency analysis

Global test area (GA in mm^2) of the keel view was taken as the main size estimator, representing a proxy for shell volume (Spero *et al*., 1991; Schmidt *et al*., 2006). Values of GA were then converted to size frequency distribution (SFD) in each sample. According to Peeters *et al*. (1999), SFD of living species can be described by superposition of two distributions of which the Gaussian term describes the adult portion while the exponential term describes the juvenile fraction of the ancient population. However, the juvenile part of the population is often subordinate in sediments, due to a greater residence time in the water column of small

specimens, predation, dissolution, and/or population dynamics (Berger, 1971; Peeters *et al*., 1999). For these reasons the exponential term is often not present in sediment, and the fossil population can be approximated by a dominating univariate Gaussian term:

$$Y_C = A/\ W\sqrt{(\pi/2)}\ e(-2\ (X-Xc)^2/w^2)$$

The constant A characterizes the curve amplitude, Xc denotes the mean of the variable and Ws the standard deviation. Differences between SFDs were employed in order to filter out specific frequency trends per locality. For this approach, frequency histograms were established using a bin width of 0.01 mm^2. This numerical common bin value was determined using the square root methods for Site 502:

$$H = Max(x)/\sqrt{N}$$

Where H stands for bin width, N represents the number of data points in the sample, and Max(x) the highest value (Scott and David (1979)). SFDs of menardiform populations were then modeled using the aforementioned Gaussian term.

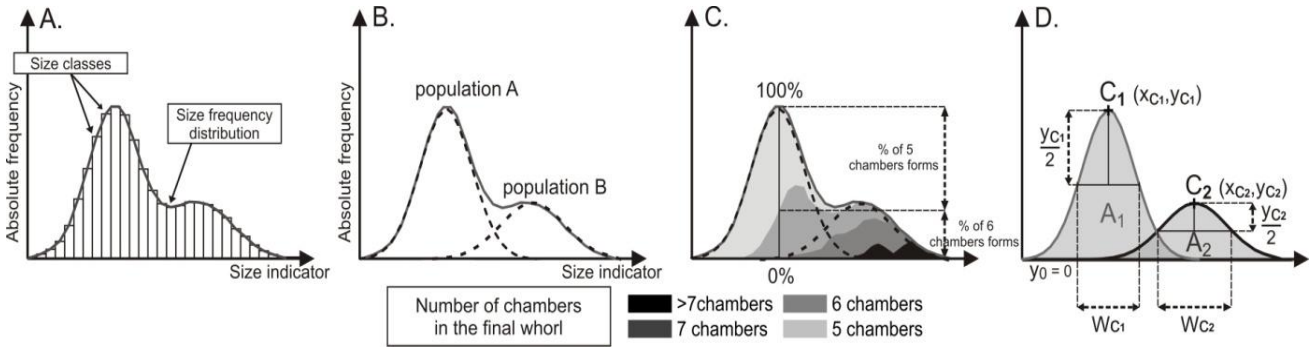

Figure 3.4: Detailed size analysis construction steps of a virtual sample (modified from Peeters *et al*., 1999). Absolute frequencies per size interval are calculated after correction for splitting using the procedure described in part 2.1. (A) Construction of the SFD from size frequency histogram by curve fitting. (B) Construction of individual Gaussian curves by multiple Gaussian curve fitting. (C) For each frequency bin, the proportion of the differently chambered forms is calculated and displayed by an area plot of curve area. Major change in chamber number composition indicates a possible change in species composition. (D) Representation of the different parameter characterizing a Gaussian curve: A represents the area under the curve, C the modal size and W the standard deviation.

Because SFD histograms of Pliocene menardellids are often composed of a mixture of species, a multiple Gaussian curve fitting is used to isolate the different subpopulations. The assumption is that specific menardellid distributions are unimodal about the mean size Xc of particular species (Figure 3.4). The number of Gaussian distributions to investigate was set in order to have the lowest number of components (Goshtasby and O'Neill, 1994).

3.3.4 Multivariate analysis

Principal component analysis (PCA) was applied on the entire set of morphometric measurements from all localities (*i.e.* all measurements and factors except coiling direction and shininess). All variables are previously normalized using a correlation matrix. Values and loadings of the first two PCA axis values are compared in order to describe clusters within menardiform globorotalids.

3.3.5 Contoured frequencies

PCA loadings as well as δX/δY measurements were graphically illustrated using contoured frequency plots. Contour plotting allows the visualization of morphological trends and clusters among large datasets. Such diagrams were constructed by first gridding the raw bivariate series of data into frequencies using the program Grid_extended, modified from Knappertsbusch (2004). A grid-cell size of 10 µm by 20 µm was used, except for the construction of PCA plots that were gridded with a bin interval of 20 µm × 20 µm. These grid-cell dimensions were empirically determined until the most robust frequency modes were obtained. From the frequency matrices, contour plots were generated.

3.3.6 Environmental parameters

The biogeographic distribution of menardellids is discussed in relation to environmental parameters. For this purpose, the PRISM3 annual SST reconstructions database

(Haywood *et al*., 2000; Dowsett and Robinson, 2007; Salzmann *et al*., 2008; Dowsett and Robinson, 2009; Dowsett *et al*., 2009) is compared to the menardiform abundance. The PRISM database relies on microfossil species assemblages, Mg/Ca ratios, and alkenones paleotemperature proxies.

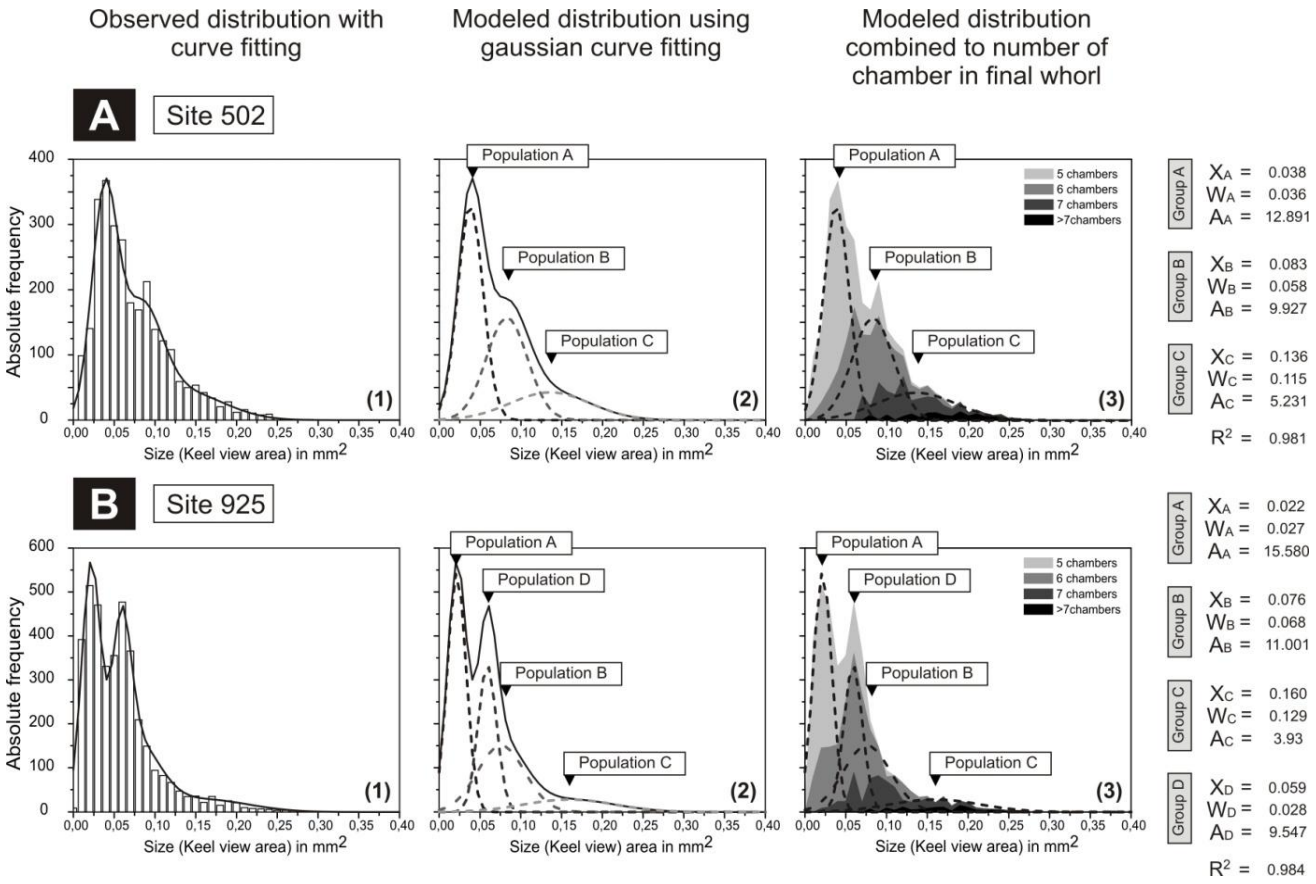

Figure 3.5: Size frequency distributions of the two West Atlantic localities. Absolute frequencies are previously corrected using the procedure described in part 2.1. (A) ODP Site 502 (Caribbean Sea) and (B) ODP Site 925 (Brazilian margin). (1) SFD of menardiform globorotalids obtained by fitting a curve to size distribution histogram. (2) Decomposition of the SFD in multiple Gaussian shaped curves representing the different menardiform populations. (3) Proportion of the different chamber variants per frequency bin shown in the left panels.

3.4 Results

3.4.1 Size analysis

The SFDs of menardellids are considered to represent the sum of the Gaussian distributions from mature populations of the involved species. Multiple Gaussian fits to SFDs leads to the recognition of three majors modes at each locality, to which we assign the three informal designations A (small), B (intermediate) and C (large) (Figures 3.5 and 3.6). Two additional populations are sporadically encountered, which are denominated as C′ and D. Modes of populations A, B and C remain stable in the five locations studied. Changes in populations are reflected by abrupt changes in the distribution of the number of chambers. The rapid increase to six chamber forms delimits the boundary of populations A and B, while the increase to seven chamber forms delimits the boundary between populations B and C. The relative abundances of these three populations allow the recognition of a biogeographic separation into a Western Atlantic province and an Eastern Atlantic province.

3.4.1.1 Western Atlantic province

The Western province covers the Caribbean Site 502 and Site 925 off Brazil (Figure 3.5). These sites share a common abundance pattern regarding populations A, B and C (Figures 3.5A and 3.5B). Menardellid absolute frequencies decrease with size. Small specimens (population A) dominate the overall menardellid composition, while the larger forms (populations B and C) are subordinate.

At ODP Site 502 (Figure 3.5), the mode of population A occurs at 0.038 mm², its size maximum is at 0.098 mm² (Figure 3.5A). The Brazilian Site 925 shows a smaller modal position of population A at 0.022 mm², while its size maximum is at 0.053 mm² (Figure 3.5B). Population B shows a similar trend at the two Western localities. The position of the mode is at 0.076 mm² and 0.083 mm² at Sites 502 and 925, respectively. Size maximum of population B is also similar in the two localities, at 0.18 mm² and 0.20 mm². However, the relative abundance of these individuals is higher in the Caribbean Sea. The geographic distribution of population C is similar to population B. Only slight differences exist in modal size between Sites 502 and 925; the modal size is smaller at Site 502 than at Site 925, 0.136 mm² and 0.160

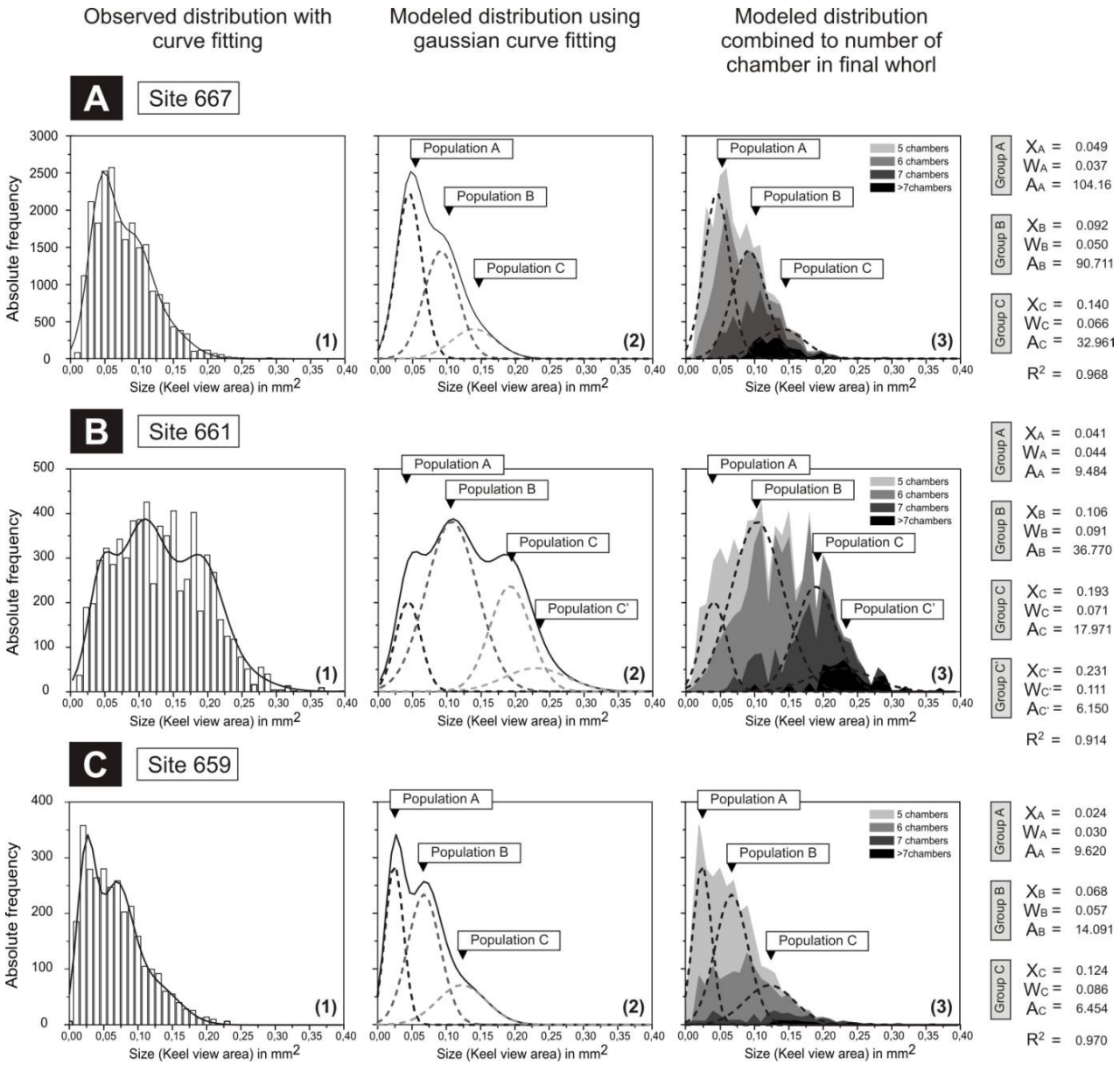

Figure 3.6: Size frequency distributions of the three East Atlantic localities: Absolute frequencies are previously corrected using the procedure described in part 2.1. (A) ODP Site 667 (open ocean), (B) ODP Site 661 (Mauritanian upwelling) and (C) ODP Site 659 (Canary Current). (1) SFD of menardiform globorotalids obtained by fitting a curve to a size distribution histogram. (2) Decomposition of the SFD in multiple Gaussian shaped curves representing the different menardiform populations. (3) Proportion of the different chamber variants per frequency bin shown in the left panels.

mm² respectively. In contrast with populations A and B, population C displays a wider distribution over the size spectrum. At ODP Site 925, a fourth population D is present (Figure 3.5B) which is visible by a peak around 0.05 mm². This peak is marked by a punctual increase of specimens with six and seven chambers in the last whorl.

3.4.1.2 Eastern Atlantic province

The Eastern Atlantic province includes the three ODP Sites 659, 661, and 667. They form a north–south transect extending from the east Atlantic upwelling centers to more open Atlantic areas (cf. Figure 3.1). The three sites share a common trend with respect to abundances of populations A, B, and C: they are characterized by a higher ratio of large specimens in comparison to the Western Atlantic province (Figure 3.6).

The ODP Site 667 represents an intermediate case in between Eastern and Western provinces (Figure 3.6A). There, most menardellids are divided into populations A (mode at 0.049 mm^2) and B (mode at 0.092 mm^2). The abundance of population C is relatively low in comparison (mode at 0.140 mm^2), reaching a maximum of 0.32 mm². Notably, specimens of Site 667 show a higher chamber number per whorl in each size range relative to the other localities (Figure 3.7A). The keel-view area size spectra reach the highest values at Site ODP 661 (Figure 3.6B), where an extra group C′ populates the highest size range. Population A occurs in low abundance in comparison to the other populations B, C, and C′. The modal positions of these populations are 0.041, 0.106, and 0.193 mm² respectively, higher than those at the other locations. ODP Site 659 (Canary Current) exhibits smaller specimens than Site 661 (Figure 3.6C). Population A is characterized by a sharp peak with a mode of 0.024 mm^2. Population B is the dominant one, with a mode at 0.068 mm². The Gaussian modeling suggests the existence of a relatively important proportion of population C, with a smaller mode at 0.124 mm².

3.4.2 Spiral height (δX) versus axial length (δY)

The ratio of spiral height (δX) versus axial length (δY) in profile view (see Fig. 3) was initially employed by Knappertsbusch (2007) to distinguish Pleistocene *G. (M.) menardii*

menardii from *G. (M.) menardii cultrata*. Although profile and spiral view parameters are correlated to each other, the keel view aspect expresses the geometric evolution of shell morphology through ontogeny better than spiral view. δY is a good proxy for the general size of the test, while δX shows a good correlation with shell weight (Regenberg *et al*., 2010). The combination of both δX and δY describes the morphological variation of menardiform shells: the test shape ranges from massive thick and compressed morphologies, located in the middle right part of a bivariate δX versus δY diagram, to delicate and elongated morphologies in the upper left corner. Frequency distributions, within contour plots, are more likely to reflect preferential allometric trends across the entire size range than population structure. We compared morphological change directions using linear regressions (Figure 3.7F). At all localities, the number of chambers per whorl increases with test size.

At Site 502 (Figure 3.7A), menardellid shells show a progressive thickening of the test with size increase, leading to thick and inflated morphologies. All individuals are arranged along an initially narrow, but then successively broadening morphological continuum. To describe this trend, a linear regression is performed on the entire sample, leading to the establishment of the regression line RL1 ($\delta Y=2.6\ \delta X-77$, Figure 3.7A). The line RL1 represents the most common, preferential menardellid allometric growth direction, observed at ODP 502 locality. In order to compare the biogeographic evolution of morphology, this line is taken as a reference trend and then reproduced on other locality diagrams. This locality is chosen as a reference because it shows the lowest morphological variability: all specimens are distributed along a single direction, showing no sign of morphological divergence. Biogeographic differences are therefore visually investigated with respect to RL1. Most of the North Tropical Atlantic specimens follow a very similar line (Figure 3.7B–E). However, morphological variation at ODP Site 661 diverges from Site 502 (RL1, Figure 7D). In the upper part of the diagram (above a δY value of 600 μm) some specimens can be distinguished from other menardellids under the binocular by a distinct flexure of their final chamber. A linear regression performed on specimen presenting a deformed last chamber generates the regression line 2 (RL2) (equation $\delta Y=0.9\ \delta X+522$), which indicates that these specimens follow a different morphological trend. The line RL2 corresponds to a rapid increase of spiral height with size; specimens are characterized by a thick, robust morphology.

Menardellids at ODP Sites 659 and 667 show two distinct directions of morphological changes that converge as size decreases (Figure 3.7C, E). Some specimens are aligned on RL1 while others follow another trend that represents a morphological evolution toward thinner and elongated forms.

The line L1 is drawn visually in order to represent these separated allometric directions (Figure 3.7C, E). The ODP Site 667, moreover, located in the middle of the four other localities (Figure 3.7C), shows the widest morphological distribution. RL1 and RL2, as well as L1 are present in this locality. Specimens with shiny and delicate tests (SH) follow two distinct, different morphological directions. At Site 925, (Figure 3.7B) a linear regression on SH specimens leads to the establishment of regression line SH1 (equation: $\delta Y=2.1\ \delta X+58$). This trend corresponds to a rapid increase of δX value with size. In contrast, linear regression applied to Site 667 shiny specimens (Figure 3.7C) yields the equation $\delta Y=3.8\ \delta X-177$ (regression line SH2). These specimens develop an extremely flat and elongated morphology.

3.4.3 Differential diagnosis

3.4.3.1 Classification concepts

Morphotypes are morphological variants within a single species that share a common morphology. A particular morphotype differs from another by a set of morphological data. The term morphospace defines the space span by all possible, independent morphological descriptors. Within the morphospace, morphotypes may occur as isolated clusters, or as clusters aligned showing a particular trend. Such morphological trends can vary with geography or follow ecological gradients: they are then called morphoclines. The morphological boundaries of a given morphotype may vary with geography.

A morphocline represents a directional trend in morphospace changes, correlated with an ecological gradient. Thus, the succession of morphotypes according to size is considered a morphocline, as size difference reflects difference in ecological niches (Al-Sabouni *et al*., 2007). We investigate the occurrence of morphotypes within the subgroups extracted from the SFD (see Section 4.1). Means (C) and standard-deviations (W) (see Figure 3.4) of each

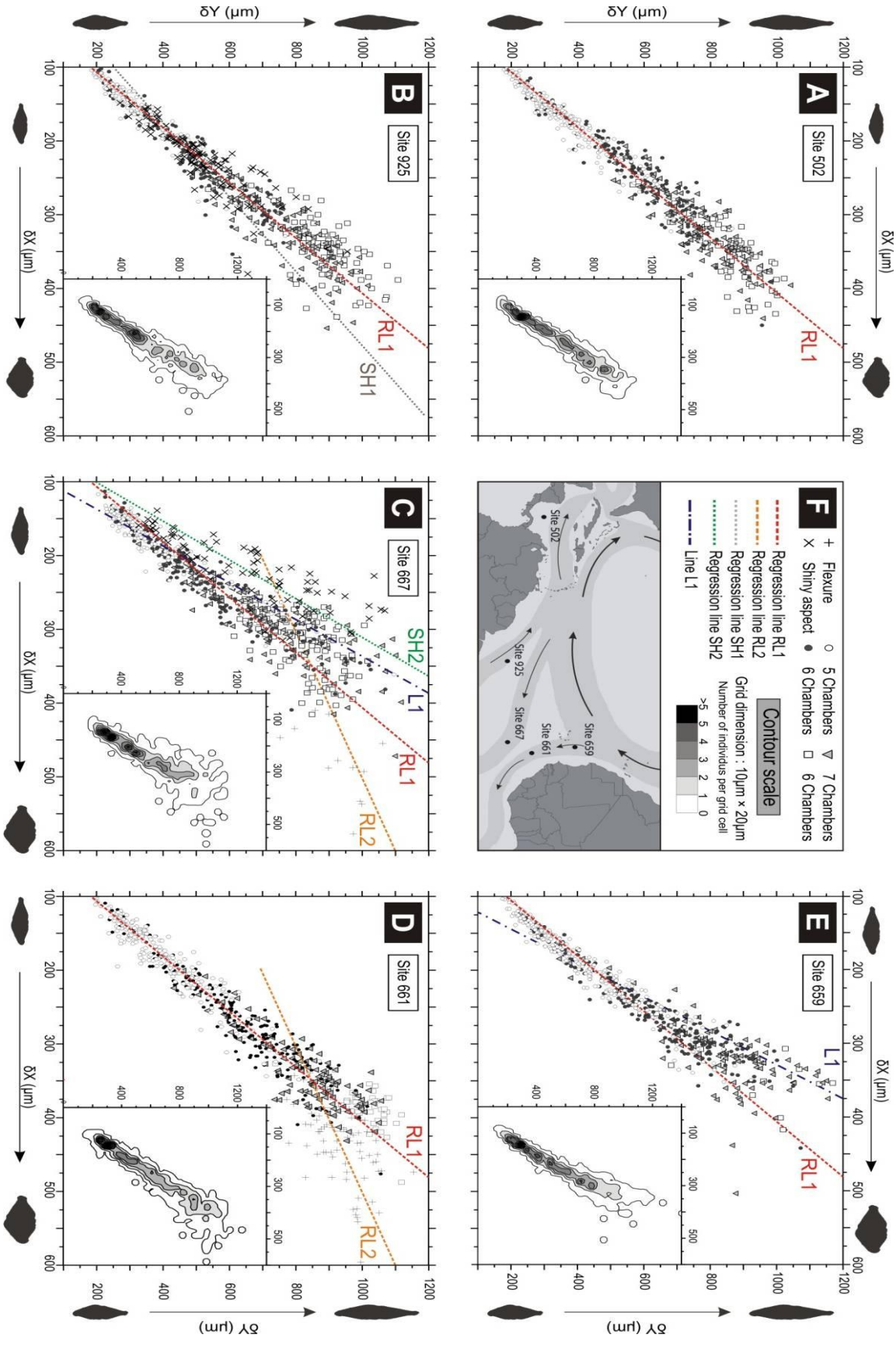
A
Site 502
RL1
B
Site 925
RL1
SH1
C
Site 667
SH2
L1
RL1
RL2
D
Site 661
RL1
RL2
E
Site 659
L1
RL1
F
+ Flexure
× Shiny aspect
5 Chambers
6 Chambers
7 Chambers
6 Chambers
Regression line RL1
Regression line RL2
Regression line SH1
Regression line SH2
Line L1
Contour scale
Grid dimension : 10µm × 20µm
Number of individus per grid cell
>5 5 4 3 2 1 0
Site 502
Site 925
Site 667
Site 661
Site 659
δX (µm)
δY (µm)

Figure 3.7 (on previous page): Biogeographic variation of bivariate measurements: δX (spiral height) versus δY (axial diameter). Graphics are organized following their relative geographic distribution. (A)–(E) For each locality, a number of chamber dependent scatter plot and a contour plot is displayed. Shiny tests are merged together and plotted regardless of chamber number, for clarity reasons. Dotted lines represent the axes of morphological variation. (F) General caption including a map showing the geographic distribution of localities, color scale and scatter plot caption.

population were translated to size versus δY/δX ratio diagram. The boundaries of these subgroups, delimited by two W values, define the morphological boundaries of a morphotype. Contour diagrams facilitate the identification of the different morphotypes and possibly their clinal variation according to δY/δX values. The difficulty is that the frequency distribution in such a diagram may result from a combination of ontogenetic growth trends as well as in test geometry. The limits on y-axis of such a boundary diagram are estimated visually on the basis of minimum overlap of frequency contours.

Figure 3.8 displays an example of the establishment of three morphotypes at the Caribbean Site ODP 502. As a first step, limits of the respective areas are defined by the respective means and standard deviations of each of the subgroup (Figure 3.8A). These values are then projected on the axis of size versus the δY/δX ratio (Figure 3.8B), in order to define three distinct morphotypes and their associated morphospaces (Figure 3.8C).

3.4.3.2 Morphotype extraction

Figure 3.9 illustrates the respective contoured keel view versus δY/δX diagrams, as well as the derived morphological diagrams for the remaining ODP Sites 659, 661, 667 and 925. The test aspect along with the flexure of the last chamber are both used as secondary criteria for morphotype establishment. Seven different morphotypes could be found this way at the studied localities. Among these, three main morphotypes can be separated within menardiforms, corresponding to populations A, B, and C as described in Section 4.1.

Morphotypes MA and MB coincide with the two first Gaussian modes A and B. They occur in relatively high abundances at the five sites (Figures. 3.8, 3.9A, B, C, and D). Morphotype MA is concentrated in the smaller part of the size spectrum and occurs in relative high abundance at all sites. It shows only a few variations in size and morphology through

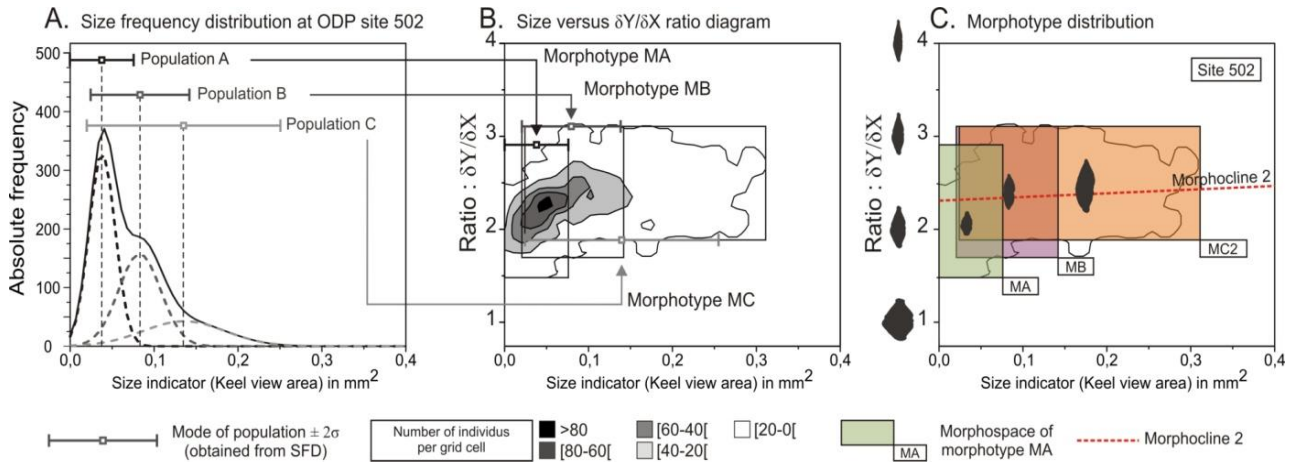

Figure 3.8: Detailed differential diagnosis construction steps at ODP Site 502. (A) Gaussian intervals are extracted from SFD. (B) These intervals are translated to the δY/δX versus size diagrams: The width of a "morphotype box" was taken as plus or minus 2 standard deviations (σ) from the mean Keel view area. The height of a morphotype box was taken as the intersection of the vertical line through the mean keel view area with the drawn base-contour line. Frequencies are corrected before plotting in order to remove the effects of sampling per size fraction. (C) Three morphotypes are established, including their morphological boundaries. δX versus δY regression lines illustrated in Figure 8 are converted and displayed.

geography. It is characterized by a rapid increase of δY/δX with increasing keel view area, which corresponds to a preferential increase of shell diameter with size (Figure 3.9A, B, C, and D). Morphotype MB is characterized by a slower increase of δY/δX ratio and an intermediate size (Figure 3.9A, B, and C, D). Its presence is particularly prominent at ODP Site 661, off Mauritania; it can be seen in the central high frequency contour (Figure 3.9D).

The third Gaussian mode C consists of two distinct morphotypes denominated as MC1 and MC2. Their similar size ranges cause a strong overlap in SFD. Morphotype MC1 (Figure 3.9A, C) is characterized by high values of the δY/δX ratio, which means an elongated and thin shell morphology. MC1 makes up the large menardiforms at Sites 667 and 659; corresponding to specimens distributed along L1 (Figure 3.7C and E). In comparison to MC1, morphotype MC2 shows a slower increase of δY/δX with size. The tests of MC2 are thicker, showing a more robust aspect than MC1. This property is the most common diagnostic feature of the MC morphotypes. At Site 661 and Site 667, morphotype MC3 corresponds to

population C′ (Figure 3.9B, C). It is characterized by a decrease of the δY/δX ratio, which means a preferential increase of shell thickness with size. Specimens that belong to MC3 include strongly flexed forms, which strongly increase the keel view area.

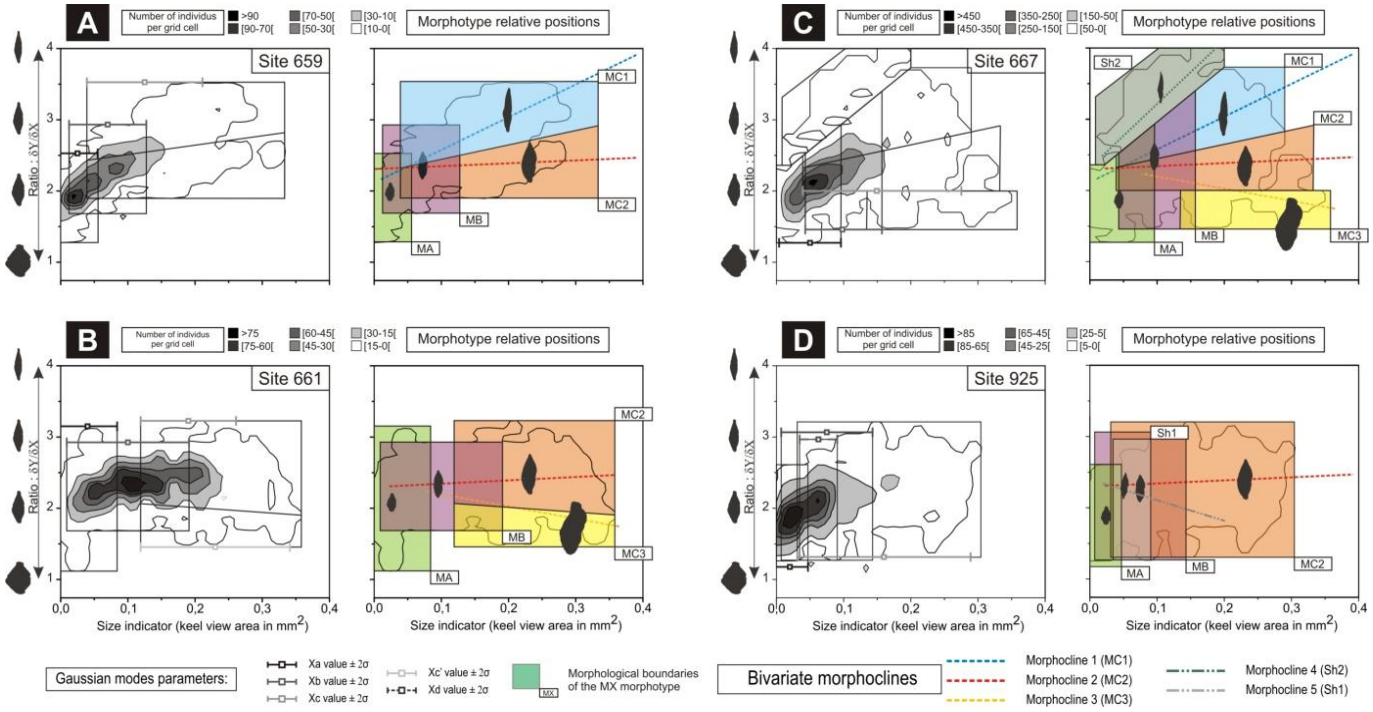

Figure 3.9: Differential diagnosis: area versus δY/δX ratio. Frequencies are corrected before plotting in order to remove the effects of sampling per size fraction. (A) ODP Site 659 frequency distributions, morphotypes and associated boundary distribution (B) Site 661 (C) Site 667 (D) Site 925.

Tests with a shiny surface are classified in two additional morphotypes, SH1 and SH2, in function of their size range and their δY/δX ratio value. They occur in relatively low abundance, only sparsely distributed in the equatorial samples from Sites 925 and 667 (Figure 3.9C, D). Morphotype SH1 represents the most abundant, and the smaller of the two light encrusted morphotypes, corresponding to population D (see Figure 3.5B). SH1 morphospace strongly overlaps MB's, but their δY/ δX ratio decreases with size (Figure 3.9D). Conversely, specimens that belong to morphotype SH2 are characterized by an extremely thin and

elongated shell, which corresponds to a very fast increase of δY/δX with size. As it is only encountered in very low abundance at Site 667, the SFD of SH2 is not visible. However its morphospace is clearly separated, as seen in Figure 3.9C.

3.4.4 Principal component analysis

To further confirm the separation of the morphotypes, a subsequent principal component analysis was carried out. The inputs of the analysis included all measured primary variables including δX, δY, δS, δU, φ1, φ2, GA, and P, as well as shape factors Fco, Fel, Fci, and Fsy (see Section 3.3). All variables were standard-normalized before they were submitted to PCA to make them dimensionless.

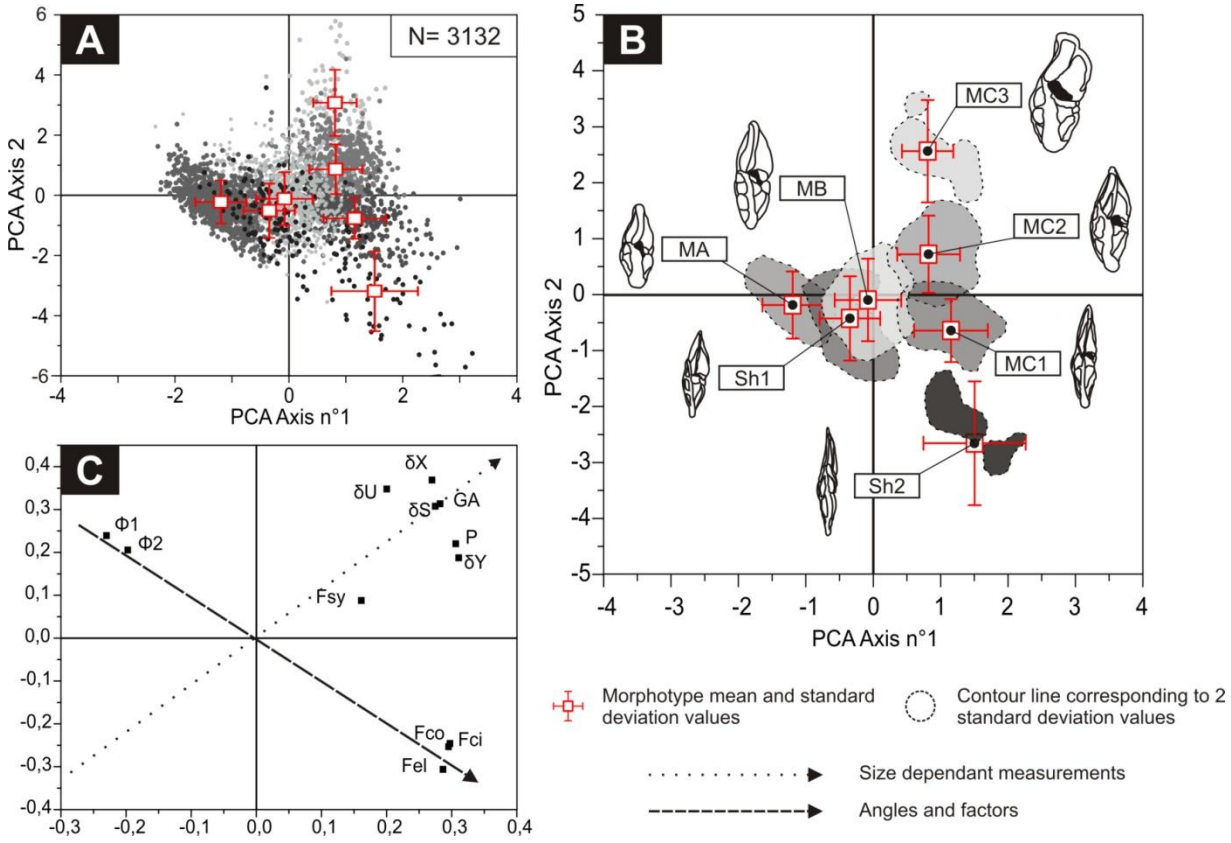

Figure 3.10: Plots of loadings of the first PCA axis against the loading along PCA axis 2. (A) Raw scatter plot of PCA loadings. (B) Contoured distribution of morphotype under consideration. The scaling is

enlarged for better visibility reasons. (C) PCA loadings showing relative distribution of morphological variables.

Figure 3.10A and B shows the position of specimens and morphotypes in the new morphospaces which are spanned by the first and the second principal components axes (PCA1 and PCA2, respectively). These two axes contribute 68% and 16% of the total variance, respectively. In this morphospace, morphotypes MA, MB and MC show the best separation along the first PCA axis whereas the second separates MC1, MC2 and MC3 from the remaining morphotypes (Figure 3.10B). Each morphotype is highlighted as a shaded area in the PCA1 versus PCA2 morphospace. These areas are outlined by a contour that was defined by the scatter data of each morphotype, and which corresponds to 2 standard deviations from the mean.

Signification of these axes with respect to morphological parameters is given in Figure 3.10C. Within this PCA morphospace, two directions of change are identifiable: the first direction combines the variations of size dependant parameters (δX, δY, δS, δU, GA and P). The other axis represents size invariant shape factors (Kucera and Kennett, 2002) and keel angles φ1 and φ2. Size is therefore the most important parameter to distinguish between MA and MB morphotypes. In size values >700 µm (δY value), however, test shapes start diverging into different subgroups. Morphotypes MC1, MC2, and MC3 can be differentiated according to their shape factor values. SH1 and SH2, on the other hand are distributed along axis B because elongation and compactness factors are the most efficient parameters to distinguish them.

3.5 Discussion

3.5.1 Implications for systematics

In order to define the Pliocene menardiforms morphotypes in relation with formal taxonomical units, we attempt to link the analytically found morphotypes to species or sub-species described and illustrated in Stainforth *et al*. (1975), Kennett and Srinivasan (1983), and Bolli and Saunders (1985).

Morphotype MA (Plate 1G1-3) best corresponds to *G. (M.) menardii* (Parker *et al*., 1865). It includes middle Miocene "*menardii A*" of Bolli and Saunders (1985). It is represented in the PCA diagram by the cluster that displays the most negative values along the first PCA axis (Figure 3.10A, B).

Morphotype MB (Plate 1E1-3) (Figure 3.10B) is best represented by *G. (M.) limbata* (Fornasini, 1902), including *menardii B* of Bolli and Saunders (1985). It most commonly holds six to seven chambers in the last whorl, specimens reaching rarely eight chambers in the last whorl. The distinction between morphotypes MA and MB relies essentially on size as they share a similar morphology. A strong continuity between MA and MB morphologies makes the visual distinction difficult.

Morphotype MC2 (Plate 1B1-3) fits best with *G. (M.) multicamerata* (Cushman and Jarvis (1930)) (Figure 3.10B). Morphotype MC1 (Plate 1A1-3) is interpreted as a second variant of *G. (M.) multicamerata* (Cushman and Jarvis (1930)) that developed an elongated test and a decreasing chamber number per whorl in comparison to MC2, similar to *G. pertenuis*. Morphotype MC3 (Plate 1D1-3) is proposed as a third variant of *G. (M.) multicamerata*, including specimens with a flexuous final chamber. It is characterized by a very robust test and a strong keel.

Morphotype SH1 (Plate 1F1-3) is similar to *G. (M.) exilis* (Blow, 1969). It can be distinguished from morphotype MB by its shiny test and from SH2 by its relative thickness in keel view.

Morphotype SH2 (Plate 1C1-3) is tentatively assigned to *G. (M.) pertenuis* (Beard, 1969). In our material, SH2 only occurs in very low abundance (<1%); this morphotype is therefore difficult to characterize accurately. SH2 is morphologically convergent with MC1 but can be distinguished by its position in the lower right quadrant in the PCA diagram. It shares its distinct shiny surface with morphotype SH1.

3.5.2 Atlantic biogeographic distribution of menardellid morphotypes

The present study considered five Tropical Atlantic samples covering different environmental settings: Caribbean Sea ODP Site 502, south–east of the subtropical gyre ODP Site 659, ODP Site 661 in the east African upwelling area, ODP 667 on the western margin of the Sierra Leon Rise and ODP 925 in the North Equatorial Counter Current, close to the Brazilian margin.

In the Caribbean Site 502 and the Brazilian Site 925 the SST range was within 1 °C relative to present day conditions (Cronin and Dowsett, 1996). Studies on planktonic foraminifera in both sites reported similar compositions to modern assemblages (Chaisson and Pearson, 1997; Cullen and Curry, 1997). In contrast, the eastern side of North Atlantic at 3.2 million years ago was warmer than at present day. Enhanced heat transport between warmer waters in the North-East Atlantic induced a warmer Eastern Boundary Current. Consequently, SST at Site 659, located in the South East boundary of the subtropical Atlantic gyre, shows an increase of 2 °C in comparison to present (Raymo *et al*., 1996; Haywood *et al*., 2002).

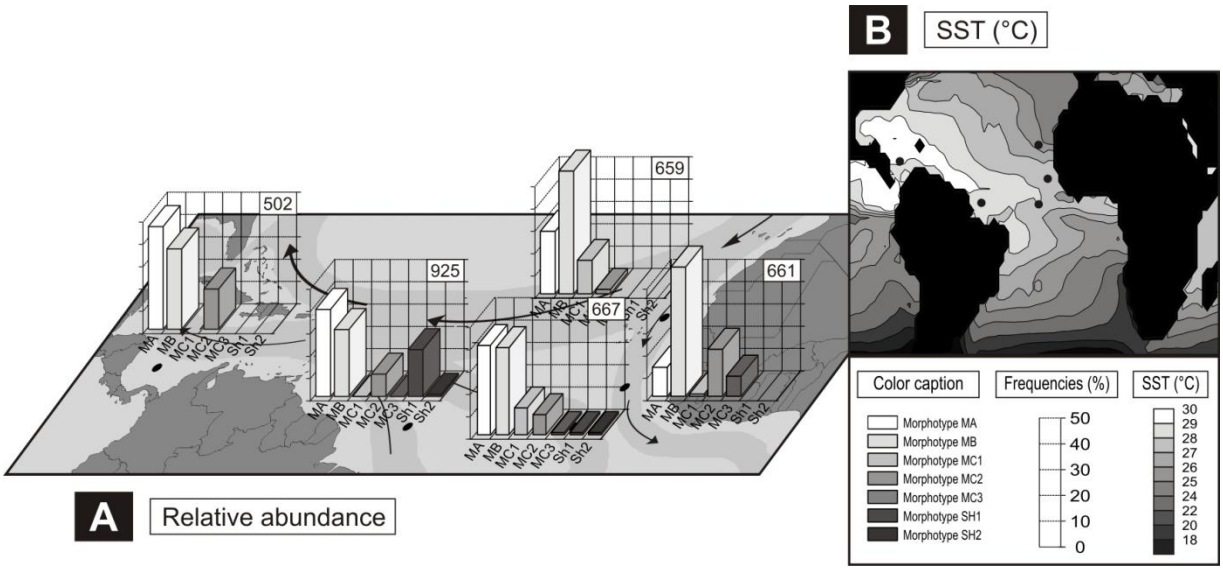

Figure 3.11: Biogeographic distribution of the seven morphotypes under consideration. (A.) Relative abundance of morphotypes MA, MB, MC1, MC2, MC3, SH1, and SH2 in the five localities. (B.) Mid-Pliocene SST reconstruction (in °C), taken from PRISM database (Haywood *et al*., 2000; Dowsett and Robinson, 2007; Salzmann *et al*., 2008; Dowsett and Robinson, 2009; Dowsett *et al*., 2009).

Sites 659, 661, and 667 are aligned along a north–south transect from East Atlantic upwelling zones into an open ocean. A progressive decrease in SST difference between the Mid-Pliocene and the modern occurred to the south. Among the three east Atlantic localities, upwelling conditions occur only at Site 661 (Pradhan *et al*., 2006). The two other eastern locations are documented as being overlain by non-upwelling oligotrophic water in present (Matsuzaki *et al*., 2011). In order to study the biogeographic distribution of menardellid morphotypes, a plot of relative abundance of the seven morphotypes versus absolute temperature reconstructions is carried on (Figure 3.11). Comparison of MC1 through MC3 morphotype distribution suggests a distribution pattern driven by productivity. The abundance of morphotype MC3 suggests a preference for eutrophic upwelling conditions at Site 661. Morphotype MC1 occurs frequently at oligotrophic Sites 659 and 667. Morphotype MC2 is present in all localities in relatively high abundance, except in low productivity zone Sites 659 and 667 where it is dominated by MC1.

Morphotypes MA and MB are distributed among the Tropical Atlantic Ocean along a temperature driven East West trend (Figure 3.11B).Western localities show higher content of MA whereas MB dominates colder eastern assemblages. Both the Caribbean and Brazilian Sites 502 and 925 show similar conditions and foraminiferal assemblages at 3.2 Ma (Dowsett *et al*., 2009). Morphotypes SH1 and SH2 are only encountered in equatorial Sites 925 and 667 suggesting a preference for high SST and eventually strong stratification conditions.

3.6 Conclusion

A Gaussian model was applied for morphological classification of Pliocene menardellid globorotalids. The application of the AMOR robot allows us to overcome the technical limitation in specimen numbers. The multimodality nature of size frequency distributions of menardiform shells reflects the presence of several specific populations in the sediment that overlap each other to a varying degree. Applying a Gaussian best fit method on combined measurements of morphological spiral height (δX) and axial maximal length (δY) ratio led to the identification of seven menardiform morphotypes, MA, MB, MC1, MC2, MC3, SH1 and SH2. Morphotypes MA and MB are assigned *to G. (M.) menardii* and *G. (M.)*

limbata respectively. The three morphotypes MC1, MC2 and MC3 are interpreted as variants of *G. (M.) multicamerata*. The shiny walled morphotypes SH1 and SH2 are suggested to represent *G. (M.) exilis* and *G. (M.) pertenuis*.

The biogeographic distribution of these morphotypes among the five Atlantic localities follows two distinct trends. The distribution of MA, MB, and MC abundances, distinguished by their optimum size, is interpreted as dependent of SST. The abundance of MC1, MC2, MC3, SH1, and SH2 suggests a distribution driven by productivity. A better biogeographic coverage may be needed to further confirm these hypotheses.

Acknowledgments

This study was financed and support by the Swiss National Foundation for Scientific Research (Grant Nos. 200021-121599/1 and 200020_137586/1). This research used samples provided by the Integrated Ocean Drilling Program (IODP). The authors thank Frans Jorissen and two anonymous reviewers for pertinent reviews and comments. We are grateful to Loïc Costeur for useful suggestions and comments on the manuscript and to Benedetto Schiraldi who kindly improved the English language.

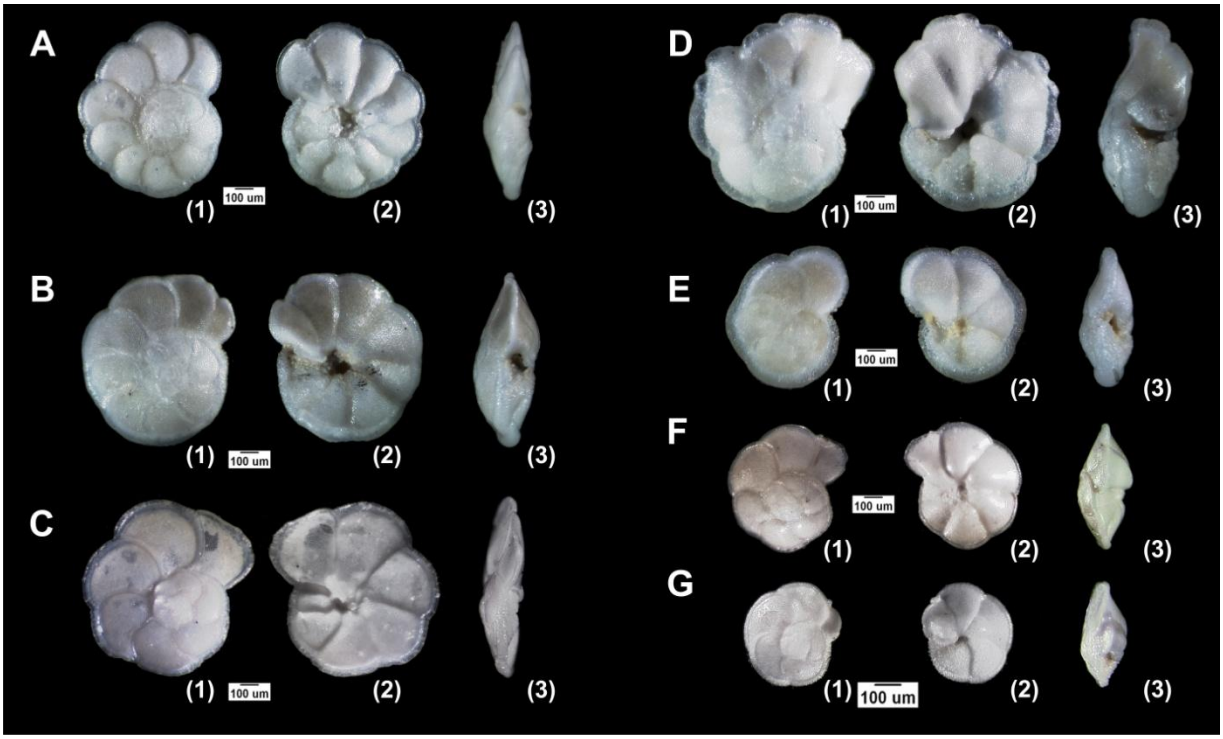

Plate 3.1: Mid-Pliocene menardellid globorotalids. Specimens were imaged using a JC KY-F75U color video camera mounted on the AMOR binocular using with a 1.0× planapochromatic lens.

A). ODP Site 667 morphotype MC1 (*G. (M.) multicamerata*). Size fraction [600–500 µm]. (1) Spiral view, (2) Umbilical view, (3) Keel view.

B). ODP Site 502 morphotype MC2 (*G. (M.) multicamerata*). Size fraction [600–500 µm]. (1) Spiral view, (2) Umbilical view, (3) Keel view.

C). ODP Site 667 morphotype SH2 (*G. (M.) pertenuis*). Size fraction [600–500 µm]. (1) Spiral view, (2) Umbilical view, (3) Keel view.

D). ODP Site 661 morphotype MC3 (*G. (M.) multicamerata*). Size fraction [600–500 µm]. (1) Spiral view, (2) Umbilical view, (3) Keel view.

E). ODP Site 659 morphotype MB (*G. (M.) limbata*). Size fraction [500–400 µm]. (1) Spiral view, (2) Umbilical view, (3) Keel view.

F). ODP Site 925 morphotype SH1 (*G. (M.) exilis*). Size fraction [400–300 µm]. (1) Spiral view, (2) Umbilical view, (3) Keel view.

G). ODP Site 502 morphotype MA (*G. (M.) menardii*). Size fraction [300–200 µm]. (1) Spiral view, (2) Umbilical view, (3) Keel view.

References:

Al-Sabouni, N., Kucera, M., Schmidt, D.N., 2007. Vertical niche separation control of diversity and size disparity in planktonic foraminifera. Marine Micropaleontology 63, 75–90.

Aurahs, R., Treis, Y., Darling, K., Kucera, M., 2011. A revised taxonomic and phylogenetic concept for the planktonic foraminifer species Globigerinoides ruber based on molecular and morphometric evidence. Marine Micropaleontology 79, 1–14.

Beard, J.H., 1969. Pleistocene paleotemperature record based on planktonic foraminifers, Gulf of Mexico: Transactions of the Gulf Coast Association of Geological Societies, 19, p552.

Berger, W.H., 1971. Sedimentation of planktonic foraminifera. Marine Geology 11, 325–358.

Berggren, W.A., Kent, D.V., Swisher, C.C., Aubry, M.P., 1995. A revised Cenozoic geochronology and chronostratigraphy. In: Berggren, W.A., Kent, D.V., Aubry, M.-P., Hardenbol, J. (Eds.), Geochronology, Time Scales and Global Stratigraphic Correlation: Society for Sedimentary Geology, SEPM Special Publication, 54, 129–212.

Bickert, T., Curry, W.B., Wefer, G., 1997. Late Pliocene to Holocene (2.6–0 Ma) Western Equatorial Atlantic deep water circulation: inferences from benthic stable isotopes. Proceedings of the Ocean Drilling Program, Scientific Results 154, 239–253.

Blow, W.H., 1969. Late Middle Eocene to recent planktonic foraminiferal biostratigraphy. Proceedings of the First International Conference on Planktonic Microfossils, Geneva 1967, 1, 199–422.

Bolli, H., Saunders, J.B., 1985. Oligocene to Holocene low latitude planktic foraminifera. In: Bolli, H.M., Saunders, J.B., Perch-Nielsen, K. (Eds.), Plankton Stratigraphy. Cambridge University Press, Cambridge, pp. 155–262.

Cande, S.C., Kent, D.V., 1995. Revised calibration of the geomagnetic polarity timescale for the Late Cretaceous and Cenozoic. Journal of Geophysical Research 100 (B4), 6093–6095.

Chaisson, W.P., 2003. Vicarious living: Pliocene menardellids between an isthmus and an ice sheet. Geology 31, 1085–1088.

Chaisson, W.P., Leckie, R.M., 1993. High resolution Neogene planktonic biostratigraphy of Site 806, Ontong Java Plateau (Western Equatorial Pacific). Proceedings of the Ocean Drilling Program, Scientific Results 130, 137–178.

Chaisson, W.P., Pearson, P.N., 1997. Planktonic foraminifer biostratigraphy at the Site 925: middle Miocene–Pleistocene. Proceedings of the Ocean Drilling Program, Scientific Results 154, 3–31.

Chandler, M., Dowsett, H., Haywood, A., 2008. The PRISM model/data cooperative: mid-Pliocene data-model comparisons. Pages News 16, 24–25.

Cifelli, R., Scott, G., 1986. Stratigraphic record of the Neogene globorotalid radiation (planktonic foraminifera). Smithsonian Contributions to Paleobiology 58.

Cronin, T.M., 1991. Pliocene shallow water paleoceanography of the North Atlantic Ocean based on marine ostracodes. Quaternary Science Reviews 10, 175–188.

Cronin, T.M., Dowsett, H.J., 1996. Biotic and oceanographic response to the Pliocene closing of the Central American Isthmus. In: Jackson, J.B.C., Budd, A.F., Coates, A.G. (Eds.), Evolution and Environment in Tropical America. University of Chicago Press, Chicago, IL, 76–104.

Crowley, T.J., 1991. Modeling Pliocene warmth. Quaternary Science Reviews 10, 275–282.

Cullen, J.L., Curry, W.B., 1997. Variations in planktonic foraminifer faunas and carbonate preservation at Site 927: evidence for changing surface water conditions in the Western Tropical Atlantic Ocean during the Middle Pleistocene. Proceedings of the Ocean Drilling Program, Scientific Results 154, 255–268.

Cushman, J.A., Jarvis, P.W., 1930. Miocene foraminifera from Buff Bay, Jamaica. Journal of Paleontology, Lawrence 4 (4), 353–368.

Darling, K., Wade, C., 2008. The genetic diversity of planktonic foraminifera and the global distribution of ribosomal RNA genotypes. Marine Micropaleontology 67, 216–238.

Dowsett, H., Poore, R., 1991. Pliocene sea surface temperatures of the North Atlantic Ocean at 3.0 Ma. Quaternary Science Reviews 10, 189–204.

Dowsett, H., Robinson, M.M., 2007. Mid-Pliocene planktic foraminifer assemblage of the North Atlantic Ocean. Micropaleontology 53, 105–126.

Dowsett, H., Robinson, M.M., 2009. Mid-Pliocene equatorial Pacific sea surface temperature reconstruction: a multi-proxy perspective. Philosophical Transactions of the Royal Society A 367, 109–126.

Dowsett, H., Barron, J., Poore, R., 1996. Middle Pliocene sea surface temperatures: a global reconstruction. Marine Micropaleontology 27, 13–25.

Dowsett, H.J., Chandler, M.A., Robinson, R.M., 2009. Surface temperatures of the mid- Pliocene North Atlantic Ocean: implications for future climate. Philosophical Transactions of the Royal Society A 367, 69–84.

Eynaud, F., Cronin, T.M., Smith, S.A., Zaragosi, S., Mavel, J., Mary, Y., Mas, V., Pujol, C., 2009. Morphological variability of the planktonic foraminifer *Neogloboquadrina pachyderma* from ACEX cores: implications for Late Pleistocene circulation in the Arctic Ocean. Micropaleontology 55, 101–116.

Fatela, F., Taborda, R., 2002. Confidence limits of species proportions in microfossil assemblages. Marine Micropaleontology 45, 168–174.

Fornasini, C., 1902. Sinossi metodica dei foraminiferi sin qui rinvenuti nella sabbia del Lido di Rimini. Reale Accademia delle Scienze dell'Istituto di Bologna, Memorie di Scienze Naturali, (ser. 5), vol. 10, pp. 1–68 (1902-1904).

Gasperi, J.T., Kenneth, J.P., 1993. Vertical thermal structure evolution of Miocene surface waters: western equatorial Pacific DSDP Site 289. Marine Micropaleontology 22, 117–147.

Gasperi, J.T., Kennett, J.P., 1992. Isotopic evidence for depth stratification and paleoecology of Miocene planktonic foraminifera: western equatorial Pacific DSDP Site 289. In: Tsuchi, R., Ingle, J.C.J. (Eds.), Pacific Neogene Environment, Evolution, and Events. University of Tokyo Press, Tokyo, pp. 117–147.

Georgescu, M.D., Saupe, E.E., Huber, B.T., 2009. Morphometric and stratophenetic basis for phylogeny and taxonomy in the Late Cretaceous gublerinid planktonic foraminifera. Micropaleontology 54 (5), 397–424.

Goshtasby, A., O'Neill, W.D., 1994. Curve fitting by a sum of Gaussians. Graphical Models and Image Processing 56 (4), 281–288.

Gradstein, F., Ogg, J., Smith, A., 2004. A Geologic Time Scale 2004. Cambridge University Press.

Haywood, A.M., Valdes, P.J., Sellwood, B.W., 2000. Global scale paleoclimate reconstruction of the middle Pliocene climate using the UKMO GCM: initial results. Global and Planetary Change 25, 239–256.

Haywood, A.M., Valdes, P.J., Sellwood, B.W., 2002. Magnitude of climate variability during Middle Pliocene warmth: a palaeoclimate modeling study. Palaeogeography, Palaeoclimatology, Palaeoecology 188, 1–24.

Haywood, A.M., Dowsett, H.J., Valdes, P.J., Lunt, D.J., Francis, J.E., Sellwood, B.W., 2009. Introduction. Pliocene climate, processes and problems. Philosophical Transactions of the Royal Society A: Mathematical, Physical and Engineering Sciences 367 (1886), 3–17.

Hemleben, C., Spindler, M., Anderson, O., 1989. Modern Planktonic Foraminifera. Springer, New York.

Huber, B.T., Bijma, J., Darling, K., 1997. Cryptic speciation in the living planktonic foraminifer *Globigerinella siphonifera* (d'Orbigny). Paleobiology 23, 33–62.

Huber, R.,Meggers, H., Baumann, K.-H., Raymo, M.E., Henrich, R., 2000. Shell size variation of the planktonic foraminifer *Neogloboquadrina pachyderma* sin. in the Norwegian-Greenland Sea during the last 1.3 Myrs: implication for paleoceanographic reconstructions. Palaeogeography, Palaeoclimatology, Palaeoecology 160, 193–212.

Hull, P.M., Norris, R., 2009. Evidence for abrupt speciation in a classic case of gradual evolution. Proceedings of the National Academy of Sciences 106, 21224–21229.

Jain, S., Collins, L.S., 2007. Trends in Caribbean paleoproductivity related to the Neogene closure of the Central American Seaway. Marine Micropaleontology 63, 57–74.

Keigwin Jr., L.D., 1982. Neogene planktonic foraminifers from Deep-Sea Drilling Project Sites 502 and 503. Initial Reports of the Deep Sea Drilling Project, College Station, vol 68, pp. 269–288.

Kelly, D.C., Bralower, T.J., Zachos, J.C., 2001. On the demise of the early Paleogene *Morozovella velascoensis*: terminal progenesis in the planktonic foraminifera. Palaios 16, 507–523.

Kennett, J.P., Srinivasan, M.S., 1983. Neogene planktonic foraminifera. A Phylogenetic Atlas. Hutchinson Ross Publishing Company, Stroudburg, Pennsylvania, pp. 1–265.

Knappertsbusch, M.W., 2004. MorphCol — a collection of fortran 77 programs for geometric morphometry. Unpublished technical report. Naturhistorisches Museum Basel, Augustinergasse 2, 4001-Basel, Switzerland.

Knappertsbusch, M. W., 2007. Morphological variability of *Globorotalia menardii* (planktonic foraminiferan) in two DSDP cores from the Caribbean Sea and the Eastern Equatorial Pacific. Carnets de Géologie/Notebooks on Geology, Brest, Article 2007/04.

Knappertsbusch, M. W., Binggeli, D., Herzig, A., Schmutz, L., Stapfer, S., Schneider, C., Eisenecker, J., Widmer, L., 2009. AMOR — a new system for automated imaging of microfossils for morphometric analyses. Palaeontologia Electronica 2T (2) (20 pp. URL: http://palaeo-electronica.org/2009_2/165/index.html).

Kucera, M., 1998. Biochronology of the Mid-Pliocene *Sphaeroidinella* event. Marine Micropaleontology 35, 1–16.

Kucera, M., Darling, K., 2002. Cryptic species of planktonic foraminifera: their effect on palaeoceaographic reconstruction. Philosophical Transactions of the Royal Society of London 360, 695–718.

Kucera, M., Kennett, J.P., 2002. Causes and consequences of a Middle Pleistocene origin of the modern planktonic foraminifer *Neogloboquadrina pachyderma* sinistral. Geology 30, 539–542.

Kucera, M., Widmark, J., 2000. Gradual morphological evolution in a Late Cretaceous deep-sea benthic foraminiferan, *Parkiella*. Historical Biology 14, 205–228.

Lutz, B.P., 2011. Shifts in North Atlantic planktic foraminifer biogeography and subtropical gyre circulation during the Mid-Piacenzian warm period. Marine Micropaleontology 80, 125–149.

Matsuzaki, K.M.R., Eynaud, F., Malaizé, B., Grousset, F.E., Tisserand, A., Rossignol, R., Charlier, K., Jullien, E., 2011. Paleoceanography of the Mauritanian margin during the last two climatic cycles: from planktonic foraminifera to African climate dynamics. Marine Micropaleontology 79, 67–79.

Moller, T., Schultz, H., Kucera, M., 2011. The effect of sea surface properties on shell morphology and size of the planktonic foraminifer *Neogloboquadrina pachyderma* in the North Atlantic. Palaeogeography, Palaeoclimatology, Palaeoecology.

Morard, R., Quillevere, F., Escarguel, G., Ujie, Y., de Garidel-Thoron, T., Norris, R., de Vargas, C., 2009. Morphological recognition of cryptic species in the planktonic foraminifer *Orbulina universa*. Marine Micropaleontology 71, 148–165.

Parker, W.K., Jones, T.R., Brady, H.B., 1865. On the nomenclature of the foraminifera; part XII. The species enumerated by d'ORBIGNY in the Annales des Sciences Naturelles, vol. 7, 1826. Annual Magazine of Natural History London, ser. 3, vol. 16, 15–41.

Peeters, F., Ivanova, E., Conan, S., Brummer, G.J., Troelstra, S., Van Hinte, J., 1999. A size analysis of planktic foraminifera from the Arabian Sea. Marine Micropaleontology 36, 31–63.

Pfuhl, H.A., Shackleton, N.J., 2004. Change in coiling direction, habitat depth and abundance in two menardellid species. Marine Micropaleontology 50, 3–20.

Pradhan, Y., Lavender, S.J., Hardman-Mountford, N.J., Aiken, J., 2006. Seasonal and inter-annual variability of chlorophyll — a concentration in the Mauritanian upwelling: observation of an anomalous event during 1998–1999. Deep-Sea Research II 53, 1548–1559.

Raymo, M.E., Grant, B., Horowitz, M., Rau, G.H., 1996. Mid-Pliocene warmth: stronger greenhouse and stronger conveyor. Marine Micropaleontology 27, 313–326.

Regenberg, M., Nielsen, S.N., Kuhnt,W., Holbourn, A., Garbe-Schonberg, D., Andersen, N., 2010. Morphological, geochemical and ecological differences of the extant menardiform planktonic foraminifera *Globorotalia menardii* and *Globorotalia cultrata*. Marine Micropaleontology 74, 96–107.

Renaud, S., Schmidt, D.N., 2003. Habitat tracking as a response of the planktonic foraminifer *Globorotalia truncatulinoides* to environmental fluctuations during the last 140 kyr. Marine Micropaleontology 49, 97–122.

Rohlf, F.J., 1990. Morphometrics. Annual Review of Ecology and Systematics 12, 299–316.

Rossignol, L., Eynaud, F., Bourget, J., Zaragosi, S., Fontanier, C., Ellouz-Zimmermann, N., Lanfumey, V., 2010. High occurrence of *Orbulina suturalis* and *Praeorbulina-like* specimens in sediments of the northern Arabian Sea during the Last Glacial Maximum. Marine Micropaleontology 79, 100–113.

Salzmann, U., Haywood, A.M., Lunt, D.J., Valdes, P.J., Hill, D.J., 2008. A new global biome reconstruction and data model comparison for the Middle Pliocene. Global Ecology and Biogeography 17 (3), 432–447.

Schmidt, D.N., Lazarus, D., Young, J.R., Kucera, M., 2006. Biogeography and evolution of body size in marine plankton. Earth-Science Reviews 78, 239–266.

Scott, W., David, W., 1979. On optimal and data based histograms. Biometrika 66, 605–610.

Sexton, P.F., Norris, R.D., 2011. High latitude regulation of low latitude thermocline ventilation and planktic foraminifer populations across glacial–interglacial cycles. Earth and Planetary Science Letters 311, 69–81.

Sokal, R.R., Rohlf, F.J., 1969. Biometry: the principles and practice of statistics in biological research. Freeman, San Francisco. (716 pp.).

Spero, H.J., Lerche, I., Williams, D.F., 1991. Opening the carbon isotope vital effect box, 2. quantitative model for interpreting foraminiferal carbon isotope data. Paleoceanography 6, 639–655.

Stainforth, R.M., Lamb, J.L., Luterbacher, H., Beard, H.J., Jeffords, R.M., 1975. Cenozoic planktonic foraminiferal zonation and characteristics of index forms. The University of Kansas Paleontology Contributions 62, 1–425.

de Vargas, C., Renaud, S., Hilbrecht, H., Pawlowski, J., 2001. Pleistocene adaptive radiation in *Globorotalia truncatulinoides*: genetic, morphologic and environmental evidence. Paleobiology 27, 104–125.

Chapter 4: Worldwide morphological variability in Mid-Pliocene menardellid revealed by population-based taxonomy

---

Yannick Mary[a,b], Loïc Costeur, [a] Michael Knappertsbusch[a]

a: Natural History Museum Basel, Augustinergasse 2, 4001-Basel, Switzerland

b: Geologisch-Paläontologisches Institut, Universität Basel, Bernoullistrasse 32, CH-4056 Basel, Switzerland

This chapter has been submitted for publication
to *Palaeogeography Palaeoclimatology Palaeoecology*.
Minor modifications were made.

Abstract

Proper species concepts of planktonic foraminifera are essential for paleo-environmental studies. Although in several cases subtle but key differences indicate the existence of sibling species, the quantitative morphological variability of foraminifera shells remains still poorly documented. We present the morphological analysis of over 7500 oriented specimens of the subgenus *Menardella* (globorotalid foraminifera). Size frequency distributions and linear shell measurements were collected with an automated device, the robot AMOR. Based on the recognition of menardellid populations, morphometric investigations in a total of 19 sampled distributed worldwide and at a time-slice at 3.2 Ma (Mid-Pliocene) were performed. Among formally established menardellid morpho-species, five populations are recognized, associated with eight different morphotypes. Geographic variation in morphotypes abundance allows the recognition of five menardellid provinces among the tropical Atlantic, Indian and Pacific Ocean. The results suggest that the formal morpho-species *Globorotalia (Menardella) menardii* is in fact composed of two distinct populations, which differ in size, morphology and biogeography. Morphological characterization of the morpho-species *G. (Menardella) multicamerata* pointed out a complex polymorphism, interpreted as a potential vertical distribution in the water column.

4.1 Introduction

The recognition of discrete genetic types within formally established morpho-species has challenged our vision of planktonic foraminifera taxonomy (Kucera and Darling, 2002; Darling and Wade, 2008). The occurrence of sibling species overturns the morphology-based species concepts and classification schemes, which are traditionally applied in micropaleontology, biostratigraphy, and phylogenetic reconstructions. In contrast, the recognition of sibling species requires a profound insight of biological and ecological adaptations. Molecular evidence furthermore emphasizes that planktonic foraminifera are geographically variable organisms with parapatric to allopatric distributions, sometimes contrasting with the idea of cosmopolitan planktonic morpho-species (de Vargas *et al*., 2004; Darling and Wade, 2008; Sexton and Norris, 2008). Combined evidences from morphological and molecular analyses have lead to a better understanding of the ecological significance of morphological shell variability (Morard *et al*., 2011; Aurahs *et al*., 2012). These studies have however shown that depending on taxa, a strong morphological variability between specimens may exist, sometimes within the same genetic cluster (André *et al*., 2013; Ujie *et al*., 2010), whereas other cryptic variants could only be kept apart by subtle ultra-structural differences (Morard *et al*., 2009).

As genetic analyses can only be practiced on living faunas, the fossil record remains usually out of reach for molecular studies. Morphological patterns and composition preserved in the fossil planktonic foraminiferal record, however, provide key information about climatic and environment changes through time. Although some studies have tried to recognize cryptic species in sediments (Kucera and Darling, 2002; Quillévéré *et al*., 2011), there is still limited progress to integrate the full morphological variability of a particular taxon into the planktonic foraminiferal species concept. It is still current usage that geographically distinct populations are characterized using the qualitative morphological description raised from a single type specimen (Scott, 2011). Understanding past planktonic morphological diversity on species-level requires, at the opposite, the study of intra- and inter-population morphological variability on a large scale. Scott (2011) further suggested that the traditional singular typological model of holotype description be replaced by a population-based taxonomy. Such approach requires acquisition of large morphological datasets with a broad or global

geographic coverage. Here, it is attempted to arrive at such a perspective by mapping the biogeography of shell variation of a species plexus on a global scale.

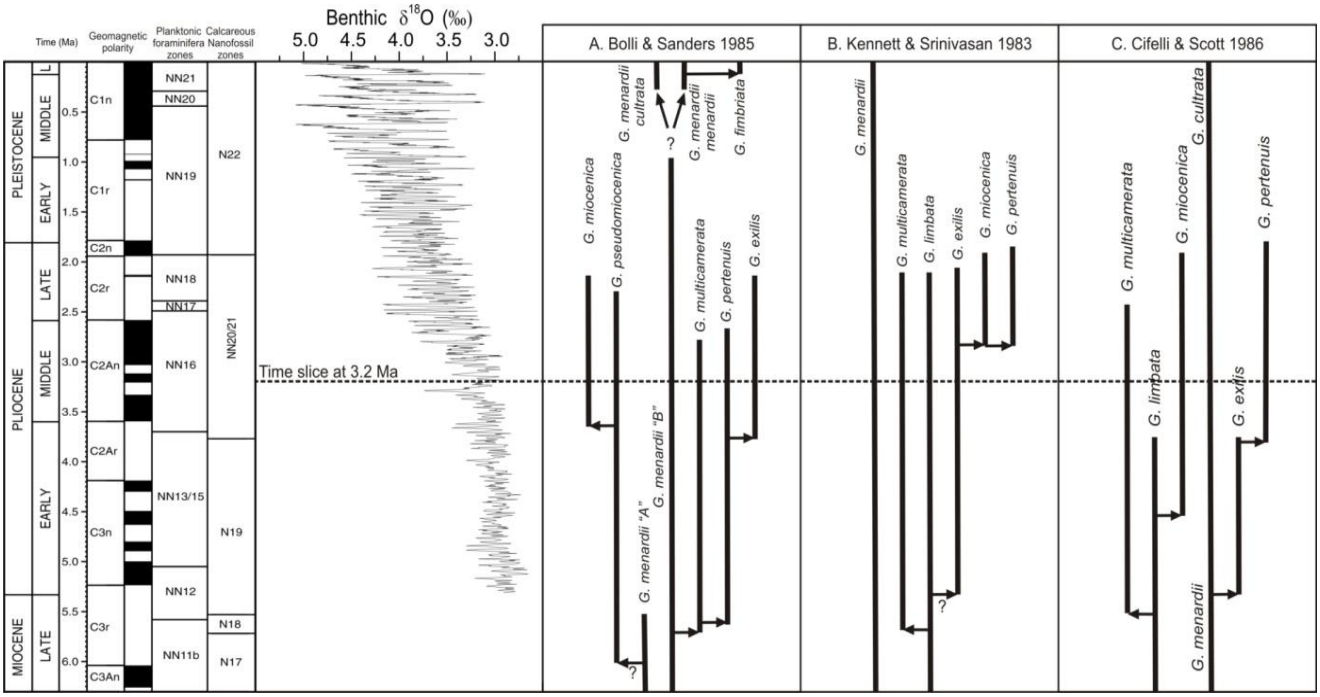

Figure 4.1: Hypotheses about phylogenetic relationships of menardellid globorotalids. (A) As interpreted from the descriptions given in Bolli and Saunders (1985). (B) Modified from Kenneth and Srinivasan (1983). (C) Modified from Cifelli and Scott (1986) and adapted to the biostratigraphic and magnetostratigraphic time scale of Gradstein *et al*., (2004). The benthic δ18O record is from Lisiecki and Raymo (2005). The dashed horizontal line marks the stratigraphic position of the 3.2 Ma times slice investigated in the present work.

For this purpose, menardellid globorotalids are a promising planktonic foraminiferal lineage to investigate. The subgenus *Menardella* forms a subset of the formal genus *Globorotalia*, which includes all species related to the extant *Globorotalia (Menardella) menardii*. Their occurrence is limited to few extant forms in the tropics and subtropics, but the menardellid plexus comprised several lineages in the past. Menardellid species have a strong tendency to homeomorphy: they developed the lenticular trochospiral, disk-like shell with

prominent keel morphology of their supposed ancestor (Kennett and Srinivasan, 1983). They exhibit however considerable size- and shell-morphological plasticity. For these reasons the definition of menardellid morpho-species remained often difficult, leading to an intricate taxonomy. The evolutionary relationships between the different menardellid species are still under debate (Figure 4.1).

In a previous pilot study we have tested the method of population-based morphotype identification using 5 selected key-sites during a Mid-Pliocene time-slice at 3.2 Ma in the Tropical Atlantic (Mary and Knappertsbusch, in press). The present work extends this tropical Atlantic menardiform experiment from the same 3.2 Ma old Mid-Pliocene time-slice to a global scale, including ODP sites from the Atlantic, Pacific and Indian Oceans. This time-slice at 3.2 Ma was selected because most menardellid morpho-species are documented to coexist at that time (Kennett and Srinivasan 1983; Bolli and Saunders 1985; Chaisson, 2003). The recommendations suggested by Scott (2011) are taken as a starting argument, which means that the study relies on a population-level analysis rather than taking single types for identification and derivation of morphotypes. This taxonomical approach is pursued to arrive at a more reliable menardellid taxonomic diagnosis, biogeography, and diversity estimation.

4.2 Settings

4.2.1 Global tropical Mid-Pliocene time-slice

The present work concentrates on a specific time frame at 3.2 Ma, which falls in the last warm Pliocene interval (about 3.3 to 3 Ma) before the onset of the northern hemisphere glacial/interglacial oscillations (Poore, 2007). At that time, the continental paleogeography, ocean basins, and major currents are to some degree similar to modern conditions: atmospheric CO_2 concentrations were comparable to present industrial concentrations (Foster *et al*., 2009; LaRiviere *et al*., 2012), and many extant planktonic foraminifera species already existed at that time (Dowsett and Robinson, 2007; Lutz, 2011). The Mid-Pliocene environment was different, however, in several aspects too. The average temperature was 3°C warmer than present day (Haywood and Valdes, 2004; Jansen *et al*., 2007). The warming was

more accentuated in polar regions (Fedorov *et al*., 2006), and northern hemisphere ice coverage was very limited. The eustatic sea level was approximately 25 m higher than today (Dowsett 2007; Dwyer and Chandler 2009).

In the Pacific Ocean, east-west temperature gradients were strongly reduced (Wara *et al*., 2005; Deckens *et al*., 2007). The tropical Pacific was suggested to be characterized by a permanent el Niño phenomenon (Philander and Fedorov 2003; Wara *et al*., 2005; Fedorov *et al*., 2006; Bonham *et al*., 2009) and the western Pacific Warm Pool was expanded poleward (Brierley *et al*., 2009). Cold water zones were reduced in upwelling zones off the western coast of South and North America until 3 Ma, (Fedorov *et al*., 2006, Fedorov *et al*., 2013). However, recent results suggest that productivity was already high since 3.5 Ma in the East Pacific region (Steph *et al*., 2010), the early cooling of the East Pacific cold tongue beginning between 4.3 Ma and 3.6 Ma (Lawrence *et al*., 2006; Dekens *et al*., 2007).

During the Mid-Pliocene, circulation patterns through tropical gateways, *i.e.* the Indonesian Gateway and Central American Seaway (CAS), were reduced (Srinivasan and Sinha, 1998; Karas *et al*., 2009; Karas *et al*., 2011). The restriction of the Indonesian Gateway between 3.5 and 3 Ma induced a distinct cooling of Indian Ocean surface waters (Karas *et al*., 2009). The closure of the Isthmus of Panama led to an intensification of Atlantic Meridional Overturning Circulation (AMOC) (Haug and Tiedemann, 1998; Lunt *et al*., 2008; Haywood *et al*. 2009). At 3.2 Ma, the water mass exchange was still possible through the CAS, but a critical threshold of communication limitation was reached since 4 Ma (Steph *et al*., 2010).

4.2.2 Mid-Pliocene menardellids

The diversity of menardellids during the Mid Pliocene was high. They are classified into two main lineages: the *G. (M.) menardii* - *G. (M) multicamerata* and *G. (M.) menardii* - *G. (M) pertenuis* lineages. These two branches can be distinguished by the reflectivity of their test surface: Representatives of the *G. (M.) menardii* - *G. (M) pertenuis* lineage display a delicate, reflective surface caused by a fine wall perforation. In contrast, the *G. (M.) menardii* - *G. (M) multicamerata* lineage shows a less reflective surface with a coarse pore density and a

tendency to build stronger calcified tests. However, infilling sediment or poor preservation can easily affect the reflectance of the test.

The phylogeny of menardellid globorotalid remains unclarified. Figure 4.1 illustrates three different phylogenetic hypotheses derived from the descriptions in Bolli and Saunders (1985) (Figure 4.1A), from the Kenneth and Srinivasan (1983) (Figure 4.1B) and from Cifelli and Scott (1986) (Figure 4.1C). These hypotheses are based on qualitative visual classification, without quantitative shell measurements. Among all, the origin of *G. (M). miocenica* is most controversial. Bolli and Saunders (1985) introduced the G. *(M.) menardii* - *G. (M.) pseudomiocenica*- *G. (M.) miocenica* lineage (Figure 4.1A), whereas *G. (M.) pseudomiocenica* is considered synonymous to *G. (M.) exilis* (Figure 4.1B and C) (Kenneth and Srinivasan, 1983; Cifelli and Scott, 1986). The phylogenetic position of *G. (M.) limbata* is also unresolved.

Micropaleontologists working with menardellids are often confronted with the complex morphological intergradation, rendering the classification difficult, even in the presence of statistical morphometric data (Knappertsbusch *et al*. 2007; Regenberg *et al*., 2010). The morphological taxonomic criteria are highly variable between populations and with geography (Bolli and Saunders, 1985; Chaisson, 2003). The number of chambers per final whorl, which is often applied as a diagnostic descriptor (*i.e.* 5-6 in *G. (M.) menardii*, 6-8 in *G. (M.) limbata*, >7 in *G. (M.) multicamerata*) is a strongly allometric feature (Mary and Knappertsbusch, in press). Limbation, which is the extension of the suture over the carina, and which is commonly used to separate *G. (M.) menardii* from *G. (M.) limbata* (Chaisson and Leckie; 1993) is extremely difficult to apply in practical surveys. Ventral or spiral side inflation is a function of ontogenetic maturity of the specimens, and hampers differential diagnosis as well.

Previous work suggests that Mid-Pliocene Atlantic menardellids are composed of seven different morphotypes, based on size frequency distribution and morphometric analyses (Mary and Knappertsbusch, in press). In the latter, morphotypes MA and MB have been assigned to the formal species *G. (M.) menardii* and *G. (M.) limbata* respectively, both mainly separable by size. Within *G. (M.) multicamerata*, three morphotypes were distinguished, informally named MC1, MC2 and MC3. Morphotype MC2 matches best with the traditional

description of *G. (M.) multicamerata* described in Bolli and Saunders (1985) or Kennett and Srinivasan (1983). Morphotype MC1 displays a distinctly thin, elongated morphology, with a reduced number of chambers in the final whorl (7 to 8) in comparison to other morphotypes of *G. (M.) multicamerata* (rather 9-10 in the last whorl). Morphotype MC3 shows a typical robust, thick and multi-chambered shell, with a flexed final chamber. Two additional morphotypes SH1 and SH2 were isolated according to their shiny wall surface, and were respectively attributed to morpho-species *G. (M.) exilis* and *G. (M.) pertenuis*.

4.3 Materials

All morphometric data were raised from 3.2 Ma old samples coming from 29 ODP sites (Figure 4.2 and Table 4.1). Only 19 samples were of reasonable quality, while samples from the remaining 10 ODP sites showed to be barren in menardellid specimens. For core site selection the biogeographic distribution map of modern menardellids of Bé and Tolderlund (1971) was consulted. For proper identification of the 3.2 Ma old time level in each core, reliable stratigraphic datums were taken from the range charts of the respective Initial and Scientific Reports of the ODP. These included magnetic reversals, FADs and LADs of planktonic microfossils (calcareous microfossils, planktonic foraminifers and diatoms), and oxygen isotope datums. In order to maintain inter-comparison to the previously studied cores in Knappertsbusch (2007) all ages were magnetically converted to the Berggren *et al*., (1995) integrated time scale. Numerical age models and calibration of absolute ages from core depth were obtained using the Neptune online tool, the age-depth plot and the *agemaker* software that was developed by Lazarus (1995) and Lazarus *et al*., (1992). Table 4.1 indicates the sources of age models per samples, as well as the number of menardellid specimens analyzed.

In the Atlantic sector, seven sites were selected, extending from the Caribbean Sea to the Tropical East Atlantic (Figure 4.2). In the south Atlantic Sites 532 and 1082, no menardellid was encountered in our samples at 3.2 Ma although menardiforms are known to occur in the area during the Holocene (Brown, 2007; Sexton and Norris, 2011). In contrast, abundant and well preserved menardellids were found during the Pliocene time slice in the tropical North Atlantic. Morphological variability of ODP Sites 502, 659, 661, 667 and 925

ODP Sites	Location	Water Depth	Number of specimen	Coordinates	Age (Reference)
502A	Colombia Basin	3061,5	594	11°29.46 N ; 79°22.74 W	3.2 Ma (Keigwin *et al*, 1982; Knappertsbusch, 2007)
503A	Guatemala Basin	3672	55	4°04,04'N; 95°38,21'W	3.2 Ma (Neptune database; Berggren., 1995; Knappertsbusch, 2007)
532A	Valvis Ridge	1131	Barren in menardellids	19°44,61'S; 10°31,13'E	3.2 Ma (F, N; Neptune database; Berggren *et al*., (1995)
659A	Cape Verde Plateau	99.95	587	18°04.63 N ; 21°01.57 W	3.2 Ma (M, F, N, I; Neptune Database ; Leg 108 Initial Report; Berggren *et al*., (1995)
661A	Sierra Leone Rise	45.77	673	09°26.81 N ; 19°23.16 W	3.2 Ma (M, F, N; Neptune Database ; Leg 108 Initial Report; Berggren *et al*., (1995)
667A	Southern Margin of Sierra Leone Rise	44.89	683	04°34.15 N ; 21°54.67 W	3.2 Ma (F, F, N; Neptune Database ; Leg 108 Initial Report; Berggren *et al*., (1995)
707A	Mascarene Plateau	1552	613	07°32,72'S ; 59°01,01'E	3.2 Ma (F, N, R, D; Neptune database; Berggren *et al*., (1995)
716B	Maldives Ridge	544	526	04°56,0'N ; 73°17,0'E	3.2 Ma (F, N, I; Neptune database; Berggren *et al*., (1995)
721B	Owen Ridge	1944	40	16°40,636'N ; 59°51,879'E	3.2 Ma (M, F, N, R; Neptune database; Berggren *et al*., (1995)
728A	Oman Margin	1428	Barren in menardellids	17°40,790'N ; 57°49,553'E	3.2 Ma (M, F, N, R, I; Neptune database; Berggren *et al*., (1995)
757B	Ninetyeast Ridge	1652	487	17°01,458'S ; 88°10,899'E	3.2 Ma (Leg 121 Initial Report ; F, N; Neptune database; Berggren *et al*., (1995).
758A	Ninetyeast Ridge	2923	199	5°23,049'N ; 90°21,673'E	3.2 Ma (Leg 121 Initial Report ; M, N, D; Neptune database; Berggren *et al*., (1995).
763A	Exmouth Plateau	1368	486	20°35,20' S ; 112°12,50' E	3.2 Ma (Leg 122 Initial Report ; M, F, N; Neptune database; Berggren *et al*., (1995).
806B	Ontong Java Plateau	2519	82	0°19,11' N ; 159°21,69' E	3.2 Ma (Leg 130 Initial Report; Chaisson et Leckie (1993) ; F, N, R, D; Neptune database;
807A	Ontong Java Plateau	2803	255	3°36,42' N ; 156°37,49' E	3.2 Ma (F, N, R, D; Neptune database; Berggren *et al*., (1995)
823B	Queensland Trough	1638	529	16°36,981' S ; 146°47,037' E	3.2 Ma (Leg 133 Initial Report ; F, N; Neptune database; Berggren *et al*., (1995).
834A	Lau Basin	2692	Barren in menardellid	18°34,058' S ; 177°51,735' W	3.2 Ma (M, F, N; Neptune database; Berggren *et al*., (1995)
835B	Lau Basin	2905	Barren in menardellid	18°30,061' S ; 177°18,162' W	3.2 Ma (M, F, N; Neptune database; Berggren *et al*., (1995)
846B	Carnegie Ridge	3296	39	3°5,696' S ; 90°49,078' W	3.2 Ma (F, N, R, D; Neptune database; Berggren *et al*., (1995)
852B	West of the East Pacific Rise	3861	Barren in menardellid	5°17,566' N ; 110°4,579' W	3.2 Ma (M, F, N, R, D, S; Neptune database; Berggren *et al*., (1995)
925B	Ceara Rise	95.16	597	04°12.24' N ; 43°29.34 W	3.2 Ma (Chaisson and Pearson, 1997; Bickert *et al*., 1997)
999A	Kogi Rise, Colombian Basin	2828	368	12°44,639' N ; 78°44,36' W	3.2 Ma (M, F, N; Neptune database; Berggren *et al*., (1995)
1006A	Great Bahama Bank	657	469	24°23,989' N ; 79°27,541' W	3.2 Ma (F, N; Neptune database; Berggren *et al*., (1995)
1082A	Northern Cap Basin	1290	Barren in menardellid	21°5,6373' S ; 11°49,2361' E	3.2 Ma (M, F, N, R, D; Neptune database; Berggren *et al*., (1995)
1143A	South China Sea	2772	462	9° 21,72' N ; 113° 17,11' E	3.2 Ma (M, F, N; Neptune database; Berggren *et al*., (1995; stable isotope model from
1148A	Continental slope of South China Sea	3295	Barren in menardellid	18°50,17' N 116°33,94' E	3.2 Ma (M, F, N; Neptune database; Berggren *et al*., (1995; Su *et al*. 2004)
1236A	Nazca Ridge	1323	Barren in menardellid	21°21,539' S ; 81°26,165' E	3.2 Ma (M, F, N; Neptune database; Berggren *et al*., (1995)
1238A	Carnegie Ridge	2203	Barren in menardellid	1°52,310' S ; 82°46,934' E	3.2 Ma (F, N, D; Neptune database; Berggren *et al*., (1995)
1241A	Cocos Ridge	2027	Barren in menardellid	5° 50,570'N ;8 6° 26,676 W	3.2 Ma (M, F, N, D; Neptune database; Berggren *et al*., (1995)

Table 4.1 (on previous page) : Summary information about investigated ODP samples. Abbreviations to stratigraphic control points used in Neptune age models: M=Magnetic datums, F=planktonic foraminiferal datums, N= calcareous nannoplankton datums, R=radiolarian datums, D= diatom datums, I=oxygen isotope datums, S= silicoflagellate datums. All datums were magnetically converted to the Candy and Kent (1995) magnetic polarity time scale (see Berggren *et al.*, 1995). Most numeric age models are available from http://micropal-basel.unibas.ch/NEPTUNE/Start.html

has previously been studied by Mary and Knappertsbusch (in press). The two locations ODP Site 999 and ODP Site 1006 were included to complete the Atlantic biogeographic coverage.

In the Indian Ocean, seven locations were investigated from the 3.2 million years old tropical time-slice, *e.g.*, from west to east ODP Sites 728, 707, 721, 716, 757, 758, and 763. Of these, Site 728 off the Oman Margin was found to be entirely barren in menardellids and could not be used for our analysis. Concentration of specimens in the adjacent ODP Site 721 was also relatively low. The majority of the remaining sites were devoid in menardellid in the size fractions >500µm.

In the Pacific Ocean, a sample set with a sufficient quality for our analysis was difficult to obtain at 3.2 Ma. Most ODP sites in this ocean are located in the vicinity to the neighboring continents or of mid-Pacific sites, where either the low frequency of carbonate microfossils or poor preservation prevented us from collecting a wide biogeographic area. A total of 13 sites were initially thought to be promising, though, including ODP Sites 1148, 1143, 807, 806, 823, 835 and 834 in the western Pacific, and Sites 1241, 852, 503, 848, 1238 and 1236 on the eastern tropical- to subtropical Pacific. However, only 6 samples remained left after further inspection for our studies after having checked them for content and preservation of menardellids (Figure 4.2). The available Pacific menardellid sample set leaves us therefore with a bimodal coverage: a western Pacific area (including ODP Sites 806, 807, 823 and 1143) showing well preserved and abundant menardellid faunas and an eastern Pacific area, where only the two Sites 503 and 846 contained sufficient amounts of menardiform globorotalids. The remaining localities (ODP Sites 852, 1241, 1238 and 1236) were depleted in these species (Figure 4.2).

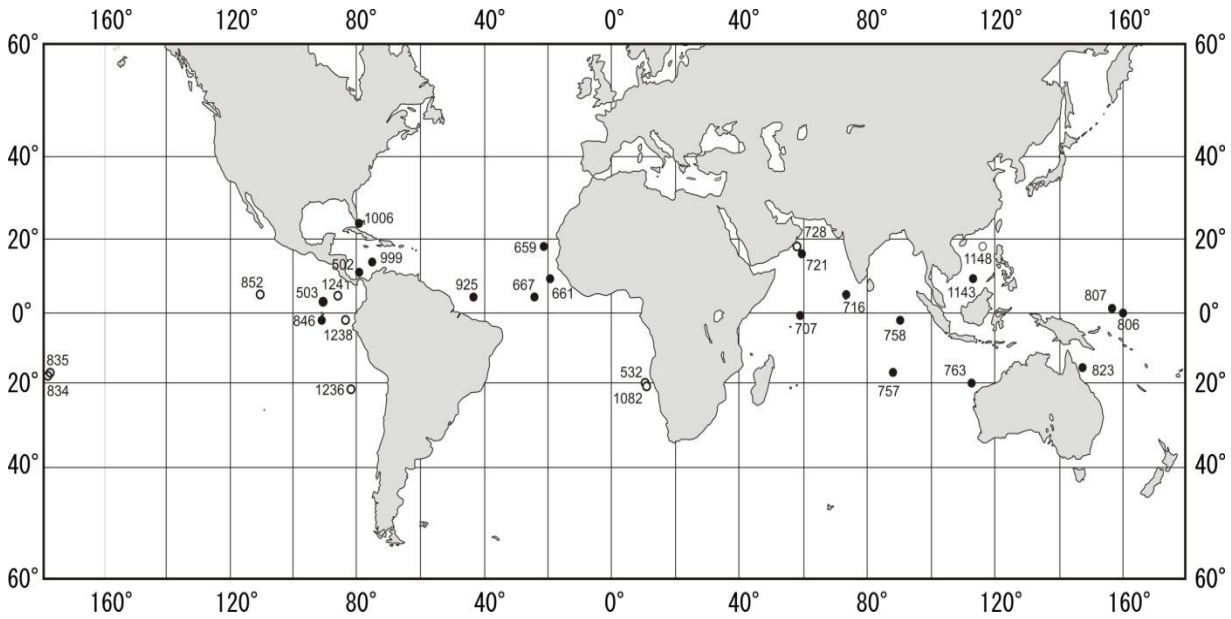

Figure 4.2: Map illustrating the location of ODP Sites from where samples were investigated at 3.2 Ma during this study. Filled circles indicate where menardellid globorotalids were present in the sample. Open circles indicate samples that were checked for menardiform globorotalids but found to be barren and therefore excluded from this study.

4.4 Methods

4.4.1 Laboratory processing

Bulk samples were washed and wet sieved over a 63µm mesh size. The material was then dried at 40°C and weighted. The fraction <63µm was preserved separately but excluded from our studies. For the size fraction >63µm seven sieve sizes were used, *i.e.*, : >600µm; 600µm-500µm; 500µm-400µm; 400µm-300µm; 300µm-200µm; 200µm-100µm; and <100µm. The size fraction <100µm was not used during the morphometric studies. In each size class menardellids were counted without species determination. When necessary, size fractions were down-splitted to manageable aliquots using a binary micro-splitter. If possible, 120 specimens per size class were randomly selected. Under the binocular microscope the number of chambers in the final whorl, the wall aspect, the coiling ratio and the chamber deformations were noted. If less than 120 menardellid specimens were present in the sub-split,

all menardellids were picked. In the ideal case, this protocol produced a total of 720 specimens per sample for morphometric and statistical analyses. Such number of specimen was selected in order to obtain a statistically relevant estimation of morphological variability in each size fraction following the recommendation of Fatela and Taborda (2002).

In order to compensate for a possible artificial size frequency shift due to the selection of 120 specimens per size class, menardellid were counted per size fraction. This allowed to estimate the absolute abundance of individuals per size fraction. Size class weighed frequencies were then calculated using the following formula:

$$Fc = Ns / Np$$

Fc is the correction factor attributed to specimens that belong to size class S, Ns is the absolute number of menardiform specimens within size class S, and Np represents the number of actually picked specimens in the size fraction S. All these methods are detailed in Mary and Knappertsbusch (in press).

4.4.2 Digital image processing and geometric morphometry

Isolated specimens were oriented and imaged in perfect keel position using a device called AMOR, which allows specimens to be automatically oriented in keel view (Knappertsbusch *et al*., 2009). AMOR consists of a motorized Leica MZ6 binocular microscope equipped with a customized motor zoom allowing for continuous magnifications and a tilting motorized stage. It automatically positions, orients, focuses, zooms, and images isolated microfossils mounted in standard multi-cellular micropalaeontological slides. Optimal orientation is reached, when the aperture appears in the middle of the test, the apex is located on the left side outline, and the keel is in the middle of the test.

Basically, this investigation follows a traditional morphometric approach using morphometric measurements sensu Blackith and Reyment (1971); Marcus (1990); Reyment (1991), and Mitteroecker and Huttegger (2009), where measurements are derived from Cartesian outline coordinates. Images were processed following the procedures described in Mary and Knappertsbusch (in press). Primary measurements, which could be extracted in this

way from shell outlines, include the keel view global area (GA), the spiral height (δX), and the maximum axial diameter (δY) (indicated on Figure 4.3). All samples, prepared slides, digital images and numeric data are deposited alongside the collections of the West-European Micropaleontological Reference Center of the DSDP, ODP and IODP, Natural History Museum Basel, Switzerland.

4.4.3 Theoretical ground for population-based taxonomy

In theory, the basic assumption in the present study is that the menardellid assemblage in a bulk sample consists of the superposition of unimodal size frequency distributions (SFD), each one representing a different specific population. In this context it was attempted to isolate discrete clusters from continuous distributions in order to recognize ancient populations. This way the morphological observations fit within a more biological context. Once such clusters were found, morphological criteria can be derived for practical differential diagnoses. Finally, morphotypes can be extracted; a morphotype is considered as a group of individuals sharing a common morphology within a given population.

According to Peeters *et al*., (1999) a living plankton population follows a distribution that is similar to the sum of a Gaussian distribution regarding size, representing the adult and pre-adult specimens, and an exponential component in the juvenile portion. In sediments, the juvenile exponential mode tends to be reduced in comparison with the one in the plankton, because of increasing loss of juveniles with increasing water depth due to fast growth, predation or dissolution. Most of the settling juvenile exponential distribution were moreover observed in the size fraction <125µm (Peeters *et al.,* 1999). Because in the present investigation from ancient sediments the size fractions >100µm were studied, this means that the exponential (juvenile) size spectrum is neglected.

Therefore, and following the model Peeters *et al*. (1999), it is thus reasonable to assume that a specific planktonic foraminiferal population, which is preserved in the sedimentary record, largely appears in form of a normal (Gaussian) distribution. This is the basic tenet that is followed throughout the present investigation. In the case of several coexisting species (including sibling species) the consequence is that the preserved

distribution becomes a multimodal composite of Gaussians. Therefore, fossil menardellids collected from a volume of sediment should be separable into their original, distinct populations when decomposed by multimodal Gaussian best-fitting.

4.4.4 Practical approach: population extraction and morphotype identification

In practice, the analytical approach to find populations in the sediments relies on several steps. First, populations were filtered out from a mixture comprising different menardellid species (Figure 4.3, step 1). These populations were found by Gaussian best fit techniques (Figure 4.3, step 2), and can therefore be described by a set of parameters characterizing the Gaussian distribution, *i.e.* the modal size, the area under the curve, and especially the position of the Gaussian distribution in the size axis (represented by 2 standard deviations) (Figure 4.3, step 3). In parallel, the total intra-sample morphological variability is investigated. Frequency distributions of morphological measurements, together with other observations (number of chambers in the last whorl, wall microstructure and chamber flexure) are plotted in function of shell size per locality (Figure 4.3, step 4). We used the ratio of δY (axial diameter) /δX (Spiral height) to summarize the morphology of menardellid shell shape in keel view (Knappertsbusch 2007). The morphological data are then gridded and represented in a contour frequency diagram (Figure 4.3, step 5).

Corresponding populations from the different samples were combined to morphological diagrams to define morphotypes (Figure 4.3, step 6). Morphospace limits of these morphotypes were found using 2 standard deviations from the distribution mean on the size versus ratios of δX/δY diagram. These contoured frequencies were then used to delimit morphotype boundaries as Boolean disjunction of local morphotype fields. In a final step, these morphotype boundaries are compared to each other from region to region and from ocean to ocean to search for biogeographic provinces or trends (Figure 4.3, step 7).

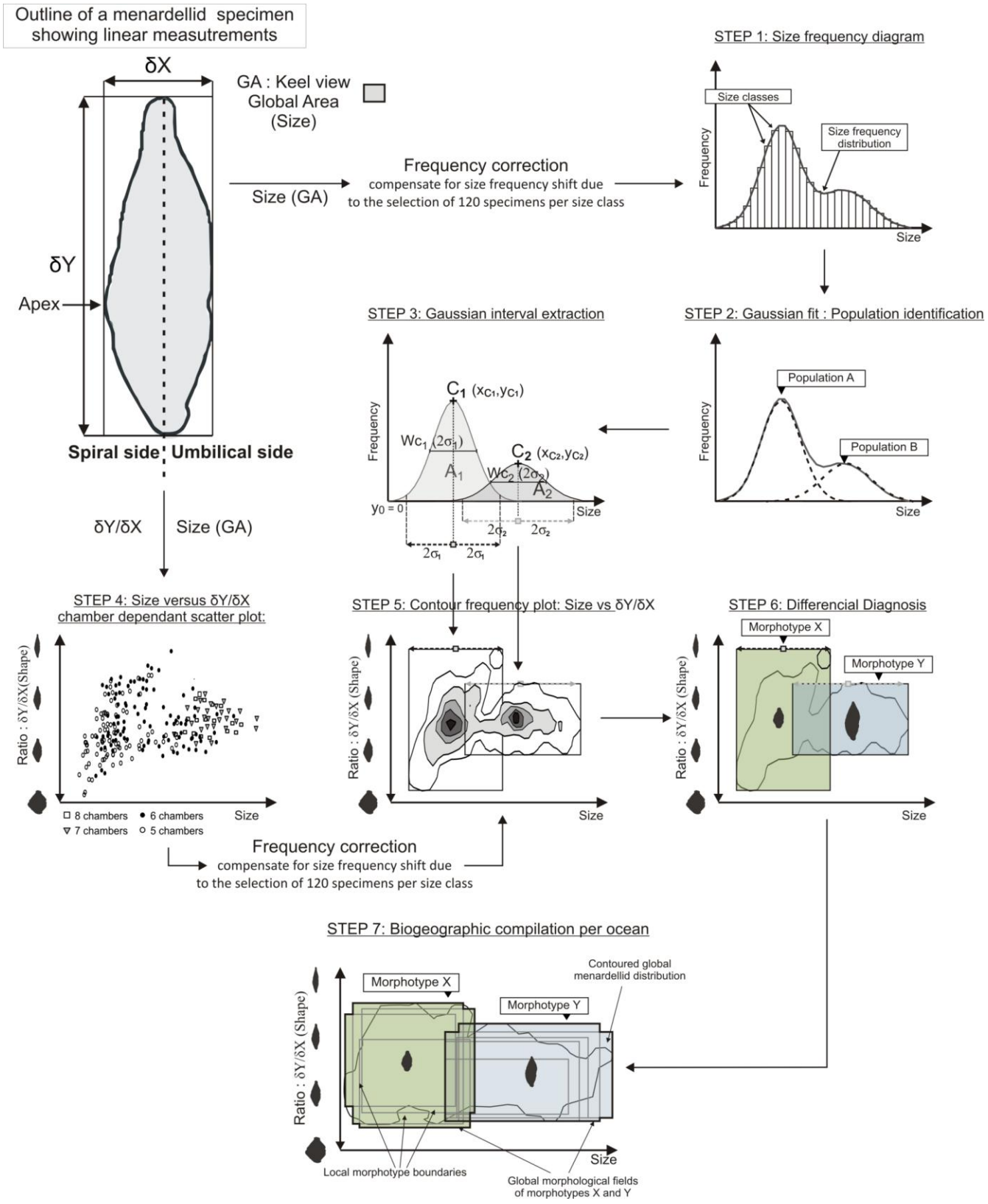
Outline of a menardellid specimen showing linear measutrements
δX
δY
Apex
Spiral side
Umbilical side
GA : Keel view Global Area (Size)
Size (GA)
Frequency correction
compensate for size frequency shift due to the selection of 120 specimens per size class
STEP 1: Size frequency diagram
Size classes
Size frequency distribution
Frequency
Size
STEP 2: Gaussian fit : Population identification
Population A
Population B
STEP 3: Gaussian interval extraction
C1 (xc1,yc1)
C2 (xc2,yc2)
Wc1 (2σ1)
Wc2 (2σ2)
A1
A2
y0 = 0
2σ1
2σ2
δY/δX
Size (GA)
STEP 4: Size versus δY/δX chamber dependant scatter plot:
Ratio : δY/δX(Shape)
8 chambers
6 chambers
7 chambers
5 chambers
STEP 5: Contour frequency plot: Size vs δY/δX
Ratio : δY/δX (Shape)
STEP 6: Differencial Diagnosis
Morphotype X
Morphotype Y
Frequency correction
compensate for size frequency shift due to the selection of 120 specimens per size class
STEP 7: Biogeographic compilation per ocean
Contoured global menardellid distribution
Local morphotype boundaries
Global morphological fields of morphotypes X and Y

Figure 4.3 (on previous page): Linear measurements and explanation of procedures carried out. (Step 1) Total size frequency diagram (SFD) for all menardiform globorotalids per sample, after frequency correction for the division in size class (cf part 4.3.1). (Step 2) Decomposition of total sample split SFD into populations using Gaussian Fitting. (Step 3) Extraction of Gaussian parameters. A_1 and A_2 represent the area under the curve. C_1 and C_2 indicate mode positions along the axis of the keel-view area, σ_1 and σ_2 denote the corresponding standard deviations, and Wc_1 and Wc_2 represent two standard deviations. (Step 4) Scatter plot of size versus $\delta Y/\delta X$ per classes of final chamber numbers. (Step 5) Contoured scatter diagram of size versus $\delta Y/\delta X$. The upper and lower limits of each Gaussians mode (as recognized by basal contour lines) are projected to the $\delta Y/\delta X$ axis. (Step 6) Finding morphotype field limits for differential diagnosis: For each sample the widths of $\pm 2\sigma$ from the mode position are applied to delimit a particular field in horizontal direction. Similarly, the total extension of the $\delta Y/\delta X$ ratio for the respective contour mode was used to find its limit in vertical direction. (Step 7) The respective fields from each individual sample were superposed on top of each other and their outermost boundaries were defined as the resulting morphotype field.

The method was developed and described in Mary and Knappertsbusch (in press) and is, in this manner, applied to investigate the full global variability of menardiform globorotalids. It could eventually be further applied to other groups as well. It does not suffer from taxonomical pre-conceptions, which may vary between specialists. The cost of this method is that it requires a large number of specimens in order to be statistically reliable. A further complication occurs if populations are present at low frequencies and then become masked by the dominant forms. Under-represented populations are often difficult to identify using the Gaussian fitting method.

4.5 Results

In this section, menardellid populations are first identified and described from ocean to ocean. Subsequently, and based on these findings, population specific size frequency distributions for all samples will be divided and proposed as distinctive morphotypes.

4.5.1 Menardellid populations

Menardellid globorotalids display a wide range of shell size, spanning between 0.09 and 0.49 mm² keel view area values. During the Pliocene, they are abundant in the smallest size range (between 100 and 300 µm sieve size), whereas a limited number of specimens occur in the largest size fraction (>500µm), associated with other taxa like *Orbulina universa*, and *Globorotalia tumida*. Results from the Mid-Pliocene time-slice suggest that the majority of menardellids are divided into three cosmopolitan populations, to which the informal names population A, B and C were assigned (Mary and Knappertsbusch, in press). Eventually, endemic populations occur as well, denominated population D and E. Population A comprises the smallest specimens. Their peek for keel view area is centered on 0.05 mm². The peak of the intermediate Population B is located around 0.1 mm^2. Population C is mostly distributed in the larger size range, between 0.1 and 0.2mm². The position of the menardellid SFD in the size spectrum is relatively stable between the oceans. In contrast, biogeographic differences exist in the relative contribution of populations A, B and C.

4.5.1.1 Atlantic Ocean size frequency distribution

In the Atlantic Ocean the menardellid SFD is characterized by typical and representative large specimens, which belong to Population C. They are relatively abundant and well developed in each investigated locality in comparison to the two other oceans (Figure 4.4A). The small population A is the dominant one in all studied sites, except at ODP Site 661, where population B is more abundant. The relative distributions of populations B and C decrease from east to west in counter-direction of the North Atlantic gyre (Figure 4.4A). Eastern Atlantic locations (Sites 659, 661 and 667) contain more of the larger specimens of population B and C than the western ones.

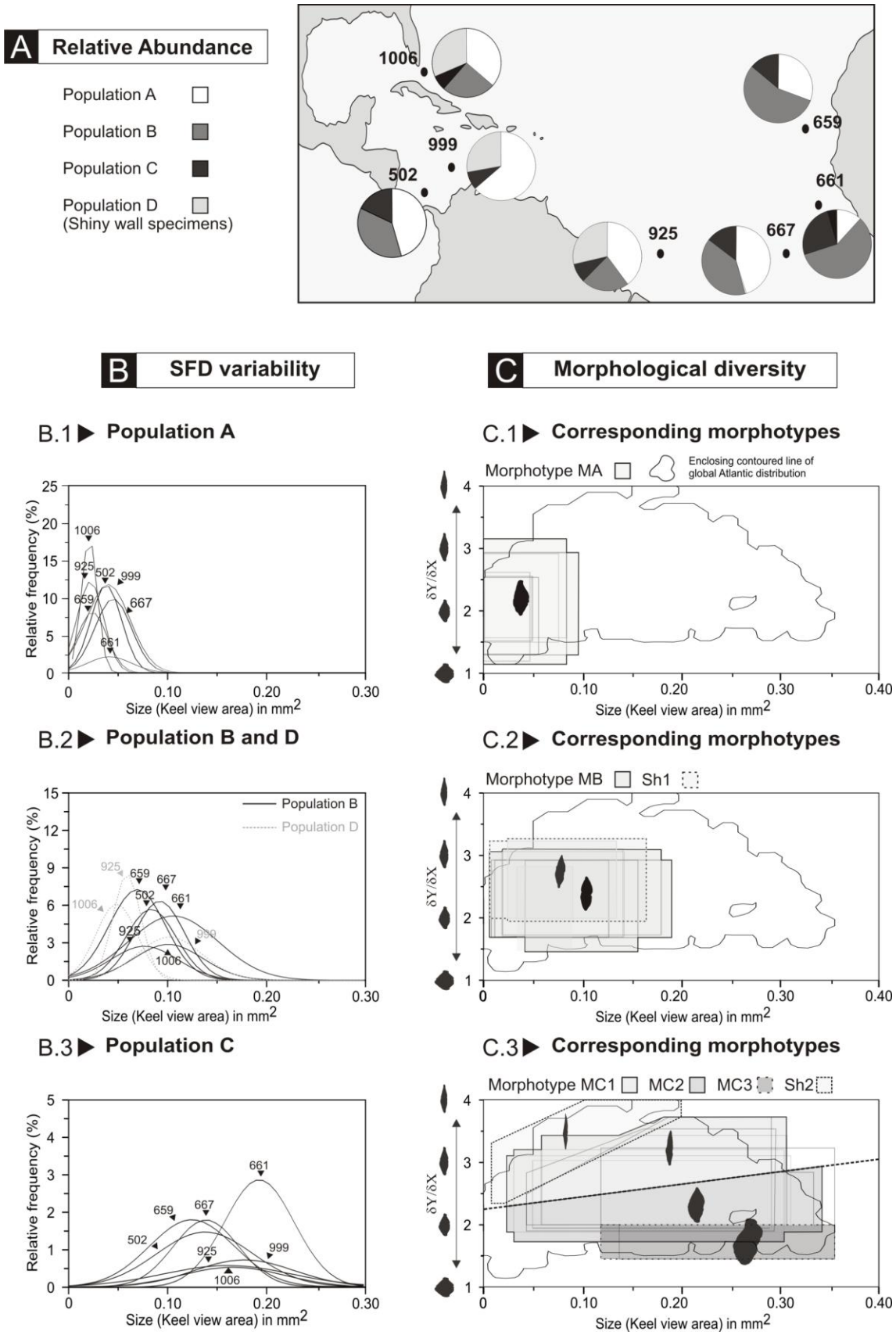
A Relative Abundance
Population A
Population B
Population C
Population D
(Shiny wall specimens)
1006
999
502
925
659
661
667
B SFD variability
B.1 ▶ Population A
Relative frequency (%)
Size (Keel view area) in mm2
B.2 ▶ Population B and D
Population B
Population D
B.3 ▶ Population C
C Morphological diversity
C.1 ▶ Corresponding morphotypes
Morphotype MA
Enclosing contoured line of global Atlantic distribution
δY/δX
C.2 ▶ Corresponding morphotypes
Morphotype MB
Sh1
C.3 ▶ Corresponding morphotypes
Morphotype MC1
MC2
MC3
Sh2

Figure 4.4 (on previous page): Overview of relative abundances, size frequency distributions and morphological variability in the tropical Atlantic Ocean. (A) Map illustrating the relative abundances of populations A, B, C, D. Values are calculated after frequency correction (cf part 3.1). (B) Size-frequency distributions for populations A, B, C and D which were isolated using the Gaussian Fitting method. (C) Diagrams illustrating the differential diagnosis fields for morphotypes MA, MB, SH1, SH2, MC1, MC2 and MC3. Morphotype boundaries are obtained by superposition and combination of the fields drawn from the individual samples (given in appendix 2, see also Figure 3, Step7). Shaded rectangles represent morphological boundaries per sample. The contour lines enclose 100% of menardellid specimens observed in the tropical Atlantic Ocean.

The frequency modes of population A tend to increase when moving southward: The sample from Site 667, for example, contains distinctly larger specimens of population A than the one from Site 1006 (Figure 4.4B1). Population B remains relatively constant over the entire Atlantic dataset (Figure 4.4B2) except at Caribbean Site 999, where it is absent. The SFD of Population C is more variable with biogeography (Figure 4.4B3). Site 661 shows, in comparison to the other locations, a larger modal size, and a higher contribution of population C to the menardellid assemblage. In contrast, Sites 502, 659 and 667 are characterized by a smaller mode.

In the Atlantic Ocean, a fourth population D occurs and is concentrated in the western part of the Atlantic (Figure 4.4B2). Specimens that belong to population D display a finely perforated wall. They are recorded in relatively high abundance at Sites 1006, 999 and 925 but are rare at Site 667. At this locality, the small number of recorded specimens prevented a reasonable interpretation of shiny menardellid SFDs. The SFD of population D overlaps with population B. At Site 999, population B is absent. The SFD at this locality is only composed of populations A, C and D, which may point to special environmental conditions. The SFDs of population D show only little variation along the West Atlantic area (Figure 4.4A). This population is illustrated in more detail at Site 999 in Figure 4.7A.

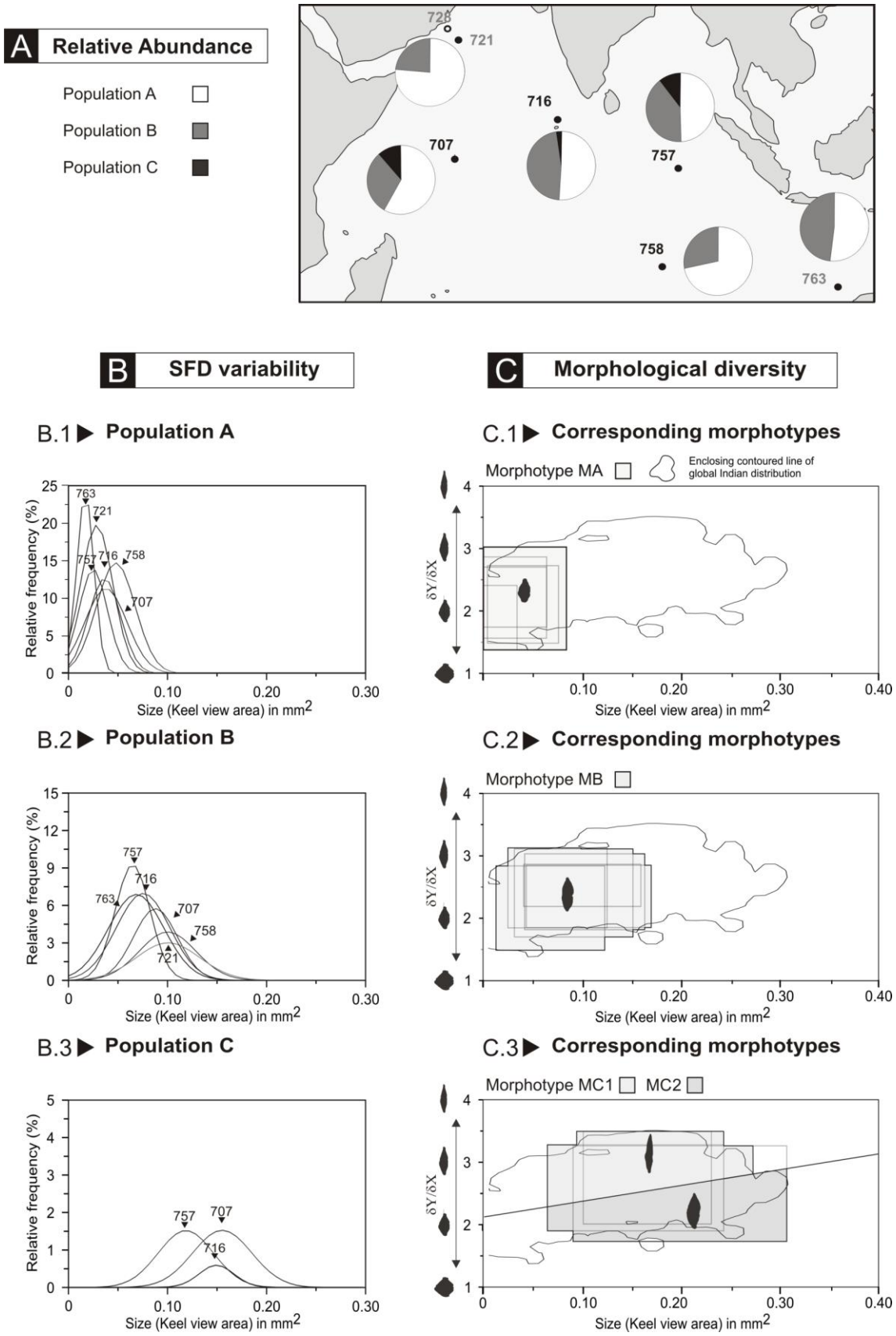
A Relative Abundance
Population A
Population B
Population C
728
721
716
707
757
758
763
B SFD variability
B.1 ▶ Population A
B.2 ▶ Population B
B.3 ▶ Population C
Relative frequency (%)
Size (Keel view area) in mm2
C Morphological diversity
C.1 ▶ Corresponding morphotypes
Morphotype MA
Enclosing contoured line of global Indian distribution
C.2 ▶ Corresponding morphotypes
Morphotype MB
C.3 ▶ Corresponding morphotypes
Morphotype MC1
MC2
δY/δX

Figure 4.5 (on previous page): Overview of relative abundances, size frequency distributions and morphological variability in the tropical Indian Ocean. (A) Map illustrating the relative abundances of Populations A, B and C. Values are calculated after frequency correction (cf part 3.1). (B) Size-frequency distributions for populations A, B and C which were isolated using the Gaussian Fitting method. (C) Diagrams illustrating the differential diagnosis fields for morphotypes MA, MB, MC1 and MC2. Morphotype boundaries are obtained by superposition and combination of the fields drawn from the individual samples (given in appendix, see also caption to Figure 3). Shaded rectangles represent morphological boundaries per locality. The contour lines enclose 100% of menardellid specimens observed in the tropical Indian Ocean.

4.5.1.2 Indian Ocean size frequency distribution

Population D is absent from Indian localities. In the Indian Ocean the population A strongly dominates the menardellid assemblage (Figure 4.5A). The dominance of population A at Oman Margin Site 721 is most probably due to the overall low abundance of menardellids in that sample (the entire sample revealed only 41 specimens). The modal size of population A is shifted to slightly larger values in comparison to the Atlantic (Figure 4.5B1), while smaller modal sizes occur at Sites 763, 721 and 757.

Indian Ocean menardellid faunas are also typically represented by population B, which makes up between 23% at Site 721 and 48% at Site 763 (Figure 4.5A). SFDs of these Indian Ocean populations are fairly similar to those in the Atlantic Ocean, with the exception of Sites 757 and 763, where the modal sizes are smaller (Figure 4.5B2). In these locations, the SFD of population B strongly overlaps with the one of population A.

Population C occurs only in low abundance in the Indian Ocean (Figure 4.5A), with the exception of Sites 707 and 757, where abundance is similar to the Atlantic Ocean (between 10 and 15%). The size range of population C is distinctly narrower than in the other oceans (maximum of 0.20 mm² in the Indian versus commonly 0.30mm² to a maximum of 0.41mm² in the Atlantic), which is explained by fewer large multi-chambered menardellid faunas in the Indian Ocean during the Mid-Pliocene (Figure 4.5B3). The presence of population C at Sites 758 and 763 is manifested in only few representatives (<10 specimens), which did not allow to recognize this population by our Gaussian fitting method.

4.5.1.3 Pacific Ocean size frequency distribution

In comparison to the Atlantic and Indian Oceans, Pacific menardellids are rarely preserved. Only few samples from the 3.2 million years old time-slice were at disposal in the Pacific: from the entire Central Pacific no suitable material could be recovered from that time-slice.

Again, the population A makes up more than 50% of the menardellid populations in both, the western and eastern margins of the Pacific Ocean (Figure 4.6A). Site 846 is particularly intersting, because only specimens of population A were observed. Population B occurs at Sites 823 and 1143 in the western Pacific Warm Pool area, but also at Site 503 on the eastern side (Figure 4.6A), though with only few specimens in the latter case.

The size frequency distributions of population A and B are similar to those of the other Oceans (Figure 4.6B1 and B2). Population C is only rarely encountered in the two western Pacific Warm Pool sites (1143 and 823) and no more than 4 specimens with 7 to 8 chambers were observed at Site 807. Moreover, population C is limited to smaller-sized forms in comparison to Atlantic and Indian relatives (Figure 4.6B3).

Population E is also restricted to the western Pacific (*e.g.*, Sites 806, 807, and 1143, Figure 4.6A), and comprises the largest individuals of the Pacific sample set. They extend over a wide size range up to a keel view area of 0.4 mm^2, which is different to the well defined and narrower size ranges observed for populations A, B and C. The SFD of this population is shown in detail at Site 807 in Figure 4.9A.

Figure 4.6 (on the following page): Overview of relative abundances, size frequency distributions and morphological variability in the tropical Pacific Ocean. (A) Map illustrating the relative abundances of Populations A, B, C and E. Values are calculated after frequency correction (cf part 3.1). (B) Size-frequency distributions for populations A, B, C and E which were isolated using the Gaussian Fitting method. (C) Diagrams illustrating the differential diagnosis fields for morphotypes MA, MB, MC2 and ME. Morphotype boundaries are obtained by superposition and combination of the fields drawn from the individual samples (given in appendix, see also caption to Figure 3). Shaded rectangles represent morphological boundaries per locality. The contour lines enclose 100% of menardellid specimens observed in the tropical Pacific Ocean.

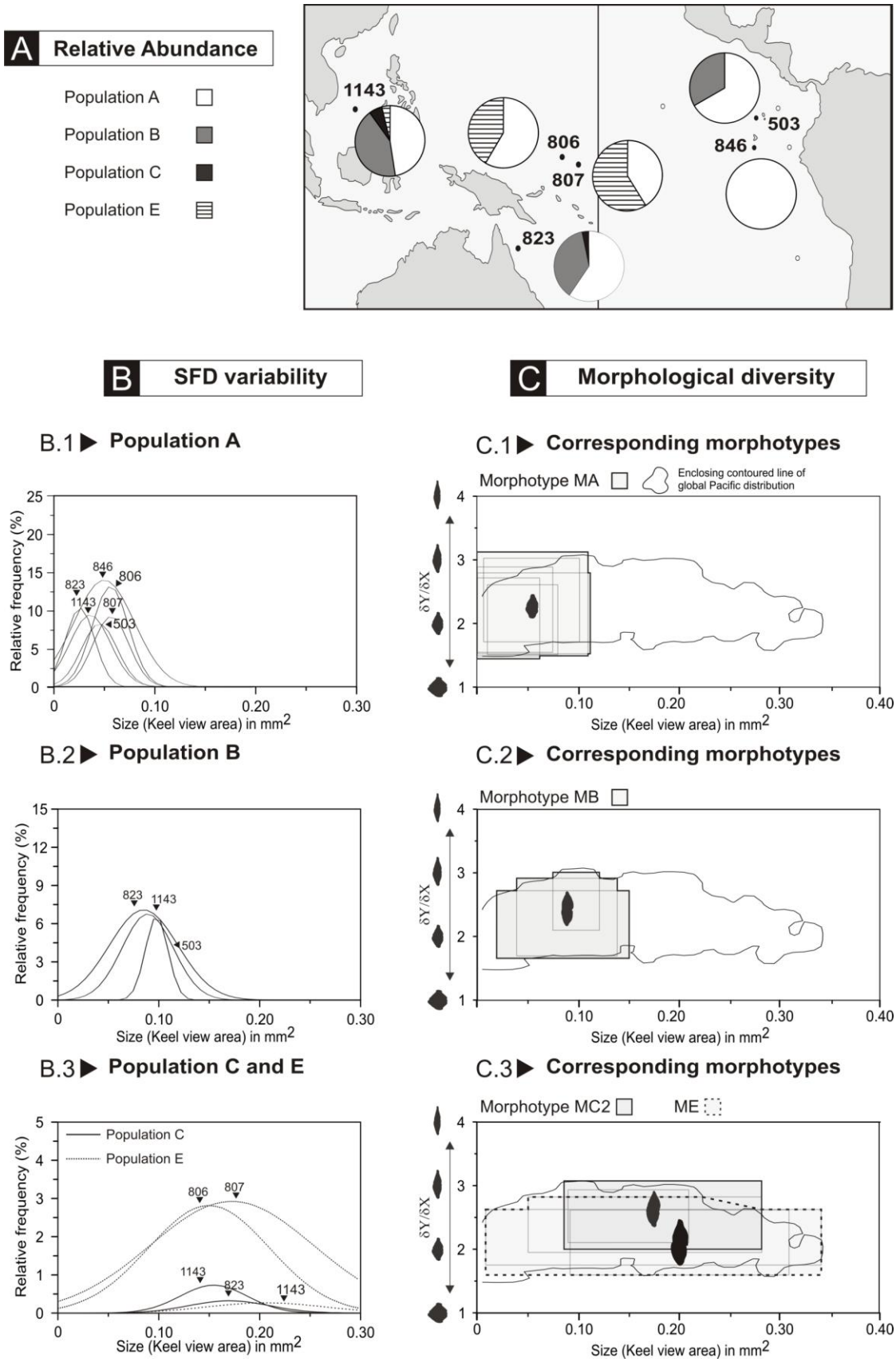
A Relative Abundance
Population A
Population B
Population C
Population E
1143
806
807
823
503
846
B SFD variability
B.1 ▶ Population A
Relative frequency (%)
Size (Keel view area) in mm2
B.2 ▶ Population B
B.3 ▶ Population C and E
Population C
Population E
C Morphological diversity
C.1 ▶ Corresponding morphotypes
Morphotype MA
Enclosing contoured line of global Pacific distribution
C.2 ▶ Corresponding morphotypes
Morphotype MB
C.3 ▶ Corresponding morphotypes
Morphotype MC2
ME
AX3/AX9

4.5.2 Menardellid morphotypes

The SFDs of every population were used in combination to morphological analysis to define menardellid morphotype boundaries per Ocean, following the protocol described in section 4.4. Table 4.2 indicates the populations used for every corresponding morphotype. Morphospace limits of each morphotype are based upon the extremes of all 2σ values for the keel-width area in horizontal direction, and upon the extremes of all δX/δY ratios for the respective populations. Diagrams showing detailed differential diagnosis per locality are given in Appendix 2.

To the two cosmopolitan populations A and B are associated two morphotypes, informally called MA and MB respectively. They are separated from each other by the shape of their test, represented by the ratio of δY/δX, and by their number of chambers in the final whorl. Morphotype MA is characterized by specimens holding 5 to 6 chambers in the last whorl. The larger Morphotype MB comprises specimens with 6 to 8 chambers in the final whorl.

The third population C shows, in general, a higher morphological variability. Most of the population C specimens fall into two different morphotypes, designated as MC1 and MC2, both with more than 7 chambers in the final whorl. These two morphotypes are separated on the basis of their ratio of δY/δX: morphotype MC1 shows ratios larger than 2.5, and morphotype MC2 have ratios less than 2.5, while their morphologies show increasing overlap with decreasing overall test size. The complete descriptions of these morphotypes are given in detail in Mary and Knappertsbusch (2013).

The morphological variability of the encountered morphotypes per ocean is described below in more detail.

4.5.2.1 Atlantic Ocean morphotypes

Seven different menardellid morphotypes are defined in the tropical Atlantic Ocean at the time-slice 3.2 Ma: these are the four cosmopolitan morphotypes MA, MB, MC1, MC2, and three Atlantic endemic morphotypes MC3, Sh1 and Sh2 (Table 4.2). Morphotypes MA and MB show overlap but can be distinguished from each other by the centers of their modes.

The field of morphotype MA is delimited between δY/δX ratios of 1.15 and 3.2 (Figure 4.4C1). These ratios increase rapidly with size. The morphotype MB shows comparable morphological boundaries, spanning between 1.5 and 3.2 (Figure 4.4C2).

Table 4.2: Overview of populations, associated morphotypes, and similarity to literally established species, arranged by ocean.

Atlantic Ocean		Indian Ocean		Pacific Ocean		
Population	**Morphotype**	**Population**	**Morphotype**	**Population**	**Morphotype**	**Taxonomic Interpretation**
Population A	MA	Population A	MA	Population A	MA	*G. (M.) menardii* [1]-"menardii A" [2]
Population B	MB	Population B	MB	Population B	MB	*G. (M.) limbata*[1]
Population C	MC1	Population C	MC1	Population C	-	*G. (M.) multicamerata*[1]
	MC2		MC2		MC2	*G. (M.) multicamerata*[1]
	MC3		-		-	*G. (M.) multicamerata*[1]
Population D	SH1		-		-	*G. (M) exilis*[1]
	SH2		-		-	*G. (M.) pertenuis*[1]
	-		-	Population E	ME	*G. (M.) menardii* [1]-Morphotype α [3]

[1] from Mary and Knappertsbusch, (in press) [2] from Bolli and Saunders, (1985) [3] from Knapperstbusch (2007)

Population C, in contrast, covers a wider morphological range (Figure 4.4C3). The morphotype MC2, characterized by a thick shell, inflated in profile view, with 8 to 12 chambers in the final whorl, is the most common in the Atlantic. Population C in western Atlantic Sites 502, 925, 999 and 1006 are composed exclusively of morphotype MC2. In the East Atlantic Sites 659 and 667 population C morphotypes have shells with elongated chambers and thin shell morphologies (δY/δX above > 2.5) corresponding to morphotype MC1. Morphotypes MC1 and MC2 co-exist with MC1 being the dominant form. A third morphotype MC3 occurs at Site 661 (Figure 4.4C3), spanning in the lowest part of the Size versus δY/δX diagram, which is typical for Atlantic samples. Morphotype MC3 is also characterized by a distinct flexure of the last chamber and a low δY/δX ratio value of less than 2.

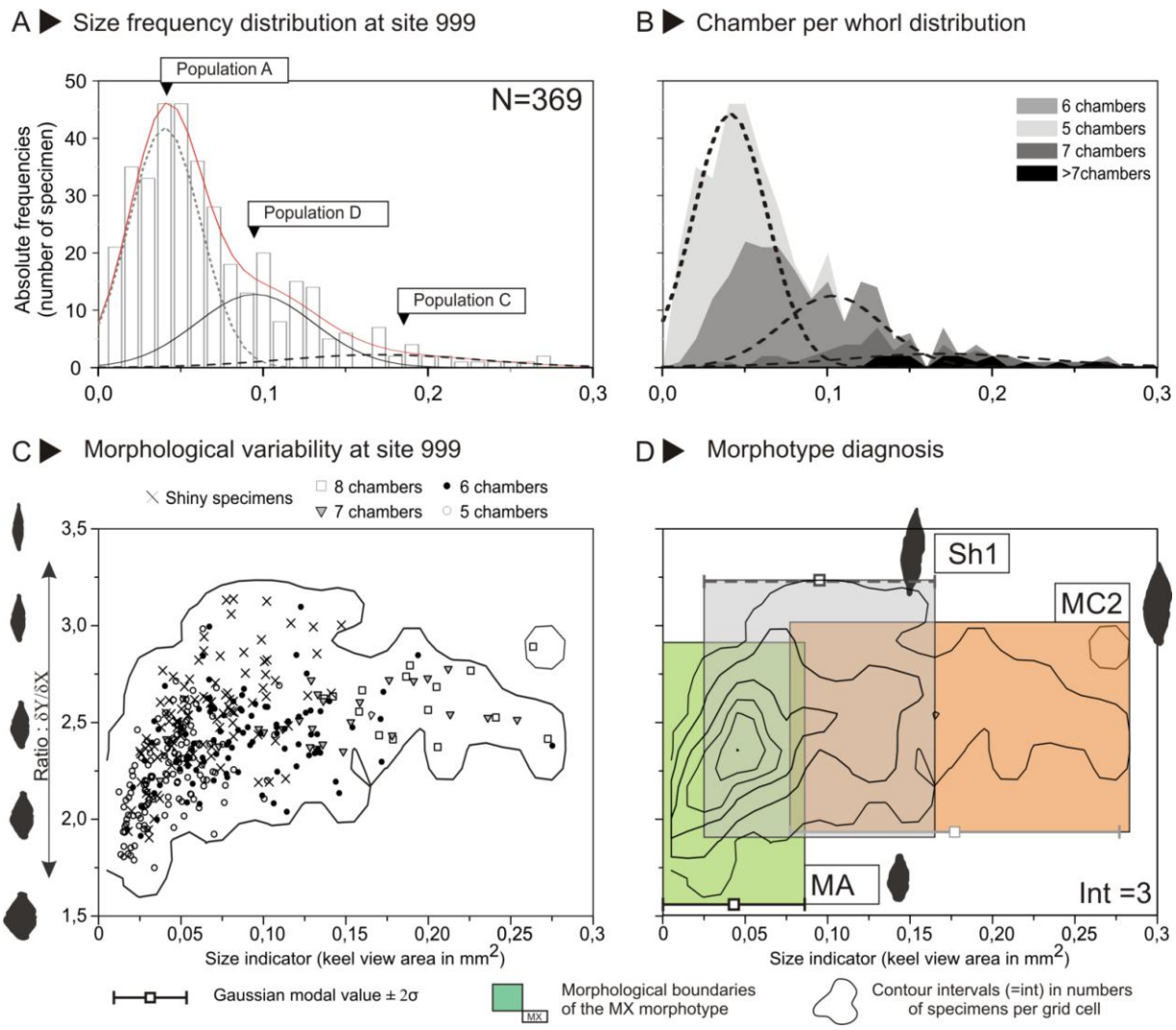

Figure 4.7: SFD and morphological variability at Site 999 (Caribbean Sea). (A) SFD with superposing Gaussian best fitting curves corresponding to populations A, C and D. Population B is absent from this sample. (B) Same sample but showing size frequency distributions separated by number of chambers in the final whorl. (C) Scatter plot of keel view area versus the δY/δX ratio separated by number of chambers in the final whorl. For better visibility, shiny specimens are not plotted in function of their number of chambers. The contour lines enclose 100% of menardellid specimens observed at Site 999. (D) Morphotype fields at Site 999 for morphotypes MA, SH1 and MC2. The Grid cell-size for contouring is 0.01 mm in horizontal direction and 0.05 in vertical direction. The Int number represents the number of specimens per contour interval.

The densely perforated menardellids, belonging to population D, are classified into two separate morphotypes called SH1 and SH2. The morphotype SH1 overlaps in shell morphology with morphotype MB (Figure 4.4C2). It has between 5 and 8 chambers in the last whorl (indicated on Figure 4.7B). The larger specimens of morphotype MA and the smaller morphotype SH1 occupy also the same morphospace, although the latter tends to be larger in size. In Figure 4.7 a complete diagnostic sequence from the SFD to morphotype classification is illustrated for Site 999 because morphotype SH1 occurs here at very high abundances. The population B - and so its morphotype MB – was not observed in this sample and so did not mask other morphotype fields. This special occasion allowed an accurate definition of the field limits of Morphotype SH1 (Figure 4.7D). This morphotype occurs at higher values of the δY/δX ratio than morphotype MA (Figure 4.7C and 4.7D). In conclusion, the addition of sites 999 and 1006 has provided key insights to study in detail the morphological variability of morphotypes SH1 .

The "shiny" morphotype SH2 is characterized by larger size, and by a strongly axially compressed, thin and elongated profile, which is similar to the non-shiny morphotype MC1 (Figure 4.4C3). Morphotype SH2 has a particularly steep slope of the δY/δX ratio versus size. In the 3.2 Ma time slice samples, this morphotype is restricted to the Equatorial Atlantic Site 667 and occurs there in only low abundances.

4.5.2.2 Indian Ocean morphotypes

In the Indian Ocean the morphological diversity in the 3.2 Ma time-slice remains comparably poor and only 4 morphotypes were found. They consist of the morphotypes MA, MB, MC1, MC2 (Table 4.2), also encountered in the Atlantic Ocean. The shiny morphotypes SH1 and SH2, typical for the Atlantic Ocean, do not occur in the Indian Ocean. As in the Atlantic Ocean, the Indian Ocean sedimentary populations A and B were assigned to morphotypes MA and MB, respectively. In the δY/δX ratio versus size diagrams these morphotypes occupy the same morphospace as their Atlantic relatives. Their morphological boundaries are relatively stable worldwide (Figure 4.6C1 and 4.6C2).

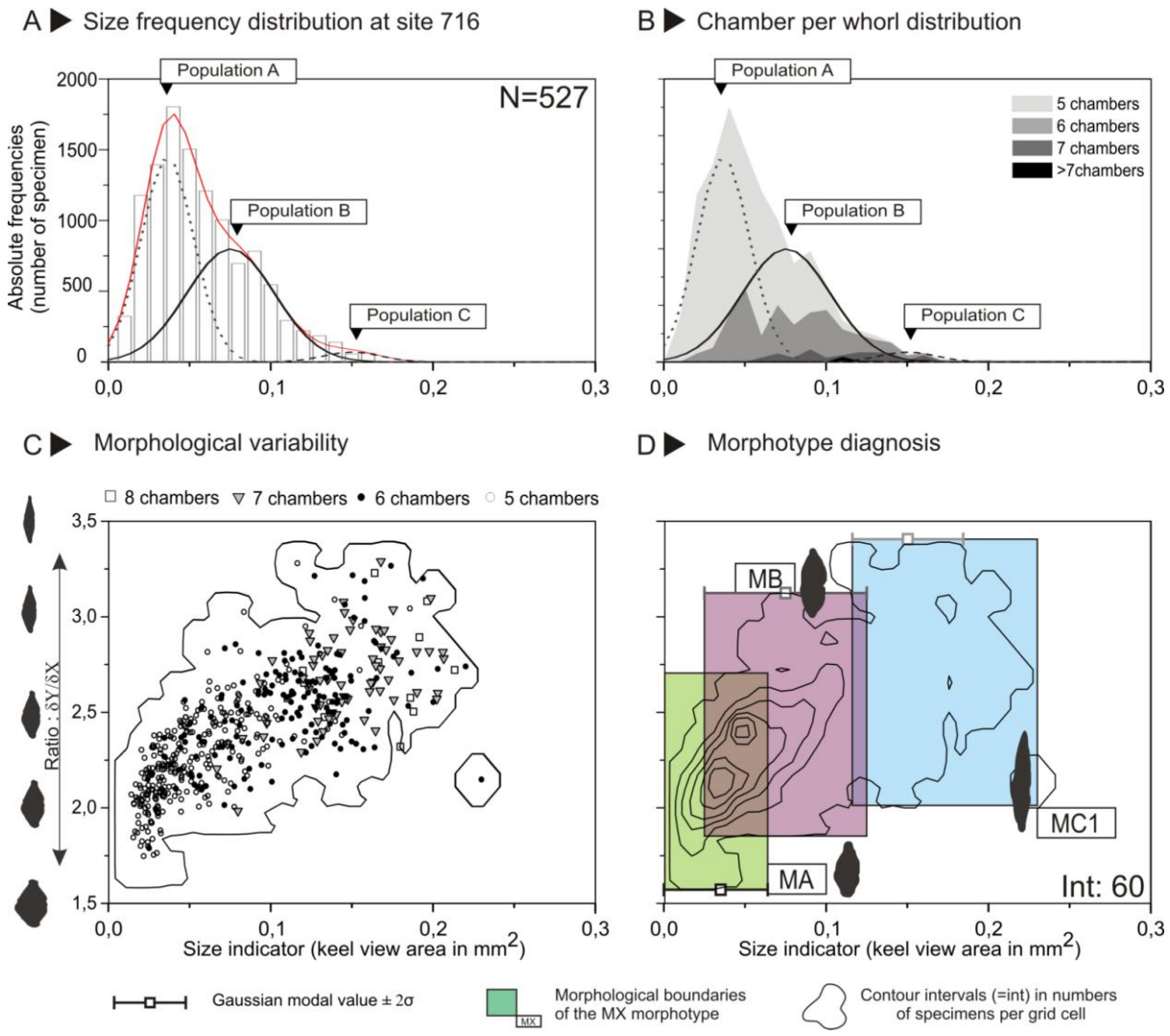

Figure 4.8: SFD and morphological variability at Site 716 (Indian Ocean). (A) SFD with superposed Gaussian best fitting curves corresponding to populations A, B and C. (B) Same sample but showing size frequency distributions separated by number of chambers in the final whorl. (C) Scatter plot of keel view area versus the δY/δX ratio separated by number of chambers in the final whorl. The contour lines enclose 100% of menardellid specimens observed in at site 716. (D) Morphotype fields at Site 716 for morphotypes MA, MB and SH1. The Grid cell-size for contouring is 0.01 mm in horizontal direction and 0.05 in vertical direction. The Int number represents the number of specimens per contour interval.

The Indian Ocean population C consists mainly of morphotype MC1 (Figure 4.5C3). It is characterized by the elongated, thin shell morphology, similar to the eastern Atlantic Sites 667 and 659 (Figure 4.4C). At Sites 716, 758 and 763 only representatives of morphotype MC1 were detected. Morphotype MC2 was only found at the Indian Ocean Sites 757 and 707. The Indian MC2 forms are smaller, and with a more delicate morphology than their Atlantic counterparts (compare Figure 4.4C3 with 4.5C3).

Figure 4.8 summarizes the diagnostic features for morphotypes MA, MB and MC1 at Site 716 in the northern Indian Ocean, where the absence of other morphotypes facilitated the definition of morphospace areas. Individuals with more than seven chambers in the final whorl occur in low abundance at this Site, which is typical of Indian localities (Figure 4.8B).

4.5.2.3 Pacific Ocean morphotypes

In the Pacific Ocean the 4 morphotypes MA, MB, MC2 and ME were observed (Table 4.2). The morphotype ME was found to be endemic to the Pacific Ocean at 3.2 Ma. The remaining morphotypes (MC1, MC3, SH1 and SH2) are all absent from our Pacific samples. A particular difficulty in our Pacific sample set was the limited number of specimens available in the larger size fraction, which made recognition of Pacific morphotypes more difficult. Also in the Pacific Ocean the boundaries for morphotype MA are similar to those from the Atlantic and Indian Oceans, with $\delta Y/\delta X$ ratios ranging from 1.5 to 3.2. The sizes of the Pacific morphotype MA are slightly larger than in the remaining oceans (Figure 4.6C1). The same holds true for morphotype MB, with the exception of Eastern Equatorial Pacific Site 503, where the morphological boundaries are narrowed due to the limited number of specimens available at this locality (Figure 4.6C2).

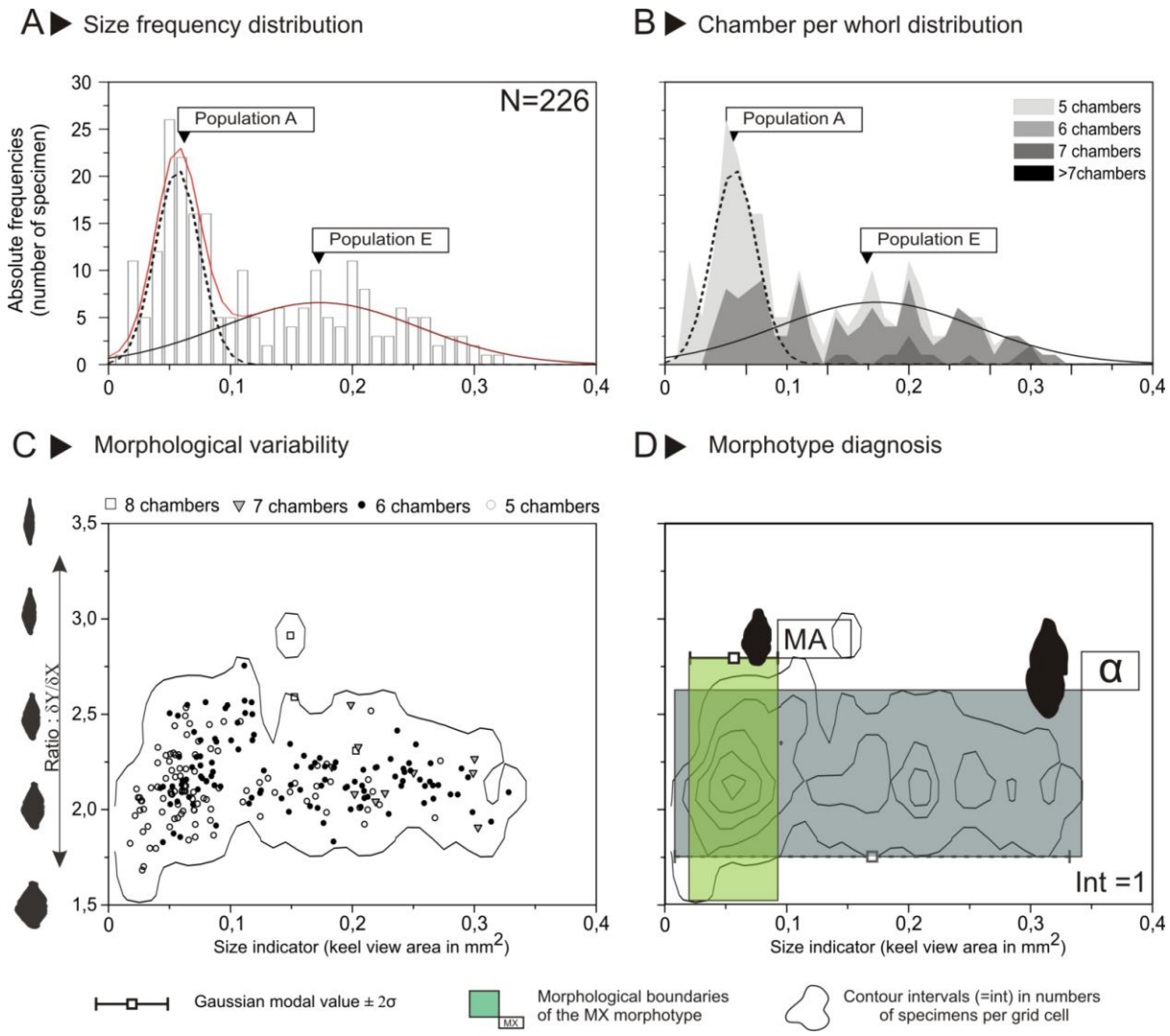

Figure 4.9: SFD and morphological variability at Site 807 (western Pacific Ocean). (A) SFD superposed by Gaussian best fitting curves corresponding to populations A and E. (B) Same sample but showing size frequency distributions separated by number of chambers in the final whorl. (C) Scatter plot of keel view area versus the δY/δX ratio separated by number of chambers in the final whorl. The contour lines enclose 100% of menardellid specimens observed at site 807. (D) Morphotype fields at Site 807 for morphotypes MA an ME. The Grid cell-size for contouring is 0.01 mm in horizontal direction and 0.05 in vertical direction. The Int number represents the number of specimens per contour interval.

In case of morphotype MC2 the δY/δX ratio is narrower than for Atlantic Ocean specimens, but similar to Indian Ocean morphotype MC2 (compare figure 4.5C3 with 4.6C3). The endemic morphotype ME occurs mostly in the western Pacific Sites 806, 807 and at lower proportions also at the South China Sea Site 1143 (Figure 4.6C3). In the δY/δX versus size diagrams there is some overlap of morphotype ME with those of the Atlantic morphotype MC3, but morphotype ME shows always a very low ratio of δY/δX <2 (Figure 4.6C3). The morphotype ME, however, shows a smaller test size, and is characterized by a more inflated umbilical size and a distinct lower number of chambers in the last whorl (5 to 6 versus 8 to 12) (Figure 4.9B). The number of chambers per whorl of morphotype ME is comparable to the number observed in morphotype MA. The morphological variability at site 807, where the morphotype ME is dominating menardellid, shows a clear bimodality between morphotype MA and morphotype ME (Figure 4.9A). The constant number of chambers of menardellid specimens (5 to 6), which is typical for the samples from Sites 806 and 807, can be observed in Figure 8B. The morphotypes MB and MCs are absent.

4.6 Discussion

The application of Gaussian best fitting to size frequency distributions in global tropical to subtropical deposits from 3.2 million years leads to the establishment of 5 different menardiform populations in the sediment: populations A, B and C, which are cosmopolitan, and populations D and E, which are limited to the tropical Atlantic and the Pacific Ocean, respectively. These populations are identifiable by their modal positions of Gaussian frequency distributions. It was found that modal positions remain surprisingly stable from one locality to the next and even more surprisingly show little inter-oceanic variation. This modal stability is generally contrasted by the size range of the distributions and the number of chamber in the last whorl, which are more susceptible to show biogeographic trends.

While menardellid populations are based on the Gaussian components of local intra-oceanic sedimentary size frequency distributions, the proposed morphotypes herein are integrated recognizably units, which show the menardellid variability at an inter-oceanic level of variation. This more global approach resulted in a total of 8 morphotypes with the informal

names MA, MB, MC1, MC2, MC3, SH1, SH2 and ME. They show a high degree of overlap, which makes the classification of individual specimens often difficult. Because of strong similarity in smaller and pre-adult forms, visual classification into discrete morphotypes is practically limited to the more adult tail of the size spectrum, especially in the case of morphotypes MC1, MC2 and MC3 (Figure 4.11).

4.6.1 Biogeographic distribution of menardellids at 3.2 Ma

Mid-Pliocene morphotypes MA and MB where found to show a worldwide geographic distribution, while the occurrence of morphotypes MC1, MC2, SH1, SH2 and ME is indicative of 5 biogeographic provinces: these are 1.) a western Atlantic province, 2.) an eastern Atlantic province, 3.) a western Indian Ocean province, 4.) the Pacific Warm Pool area, and 5.) an eastern equatorial Pacific Ocean province.

The distribution of Mid-Pliocene menardellids in the Atlantic Ocean can be divided in two different areas: the western Atlantic province including ODP Sites 502, 925, 999 and 1006. This province is characterized by abundant morphotypes MA and MB in all studied locations. Site 999 shows also assemblages including frequent morphotypes MC2, and the typical finely perforated and delicate morphotype SH1. Site 502 is the only locality depleted in morphotype SH1 despite the proximity to Site 999, where finely perforated menardellids were abundant. The scattered occurrence of finely perforated menardellids was already noted by Chaisson (2003) for samples older than 3 Ma and prior to their rise to dominance in the Atlantic Ocean. During the Mid-Pliocene, the distribution of morphotype SH1 is restricted to the western Atlantic province suggesting that the surface hydrographic condition in this area favored the occurrence of finely perforated menardellids. In the Caribbean Sea the early formation of a Warm Pool between 4.7–4.6 Ma (Steph *et al*. 2010) has initiated the deepening of the thermocline in that region, in response of the global oceanic changes that occurred during the Pliocene (Groeneveld *et al*., 2008; Steph *et al*. 2010). The distribution of Morphotype SH1 may be driven by such conditions. In contrast, the East Atlantic province is mainly characterized by the larger menardellid morphotype MB, which dominates the other coexisting morphotype MCs.

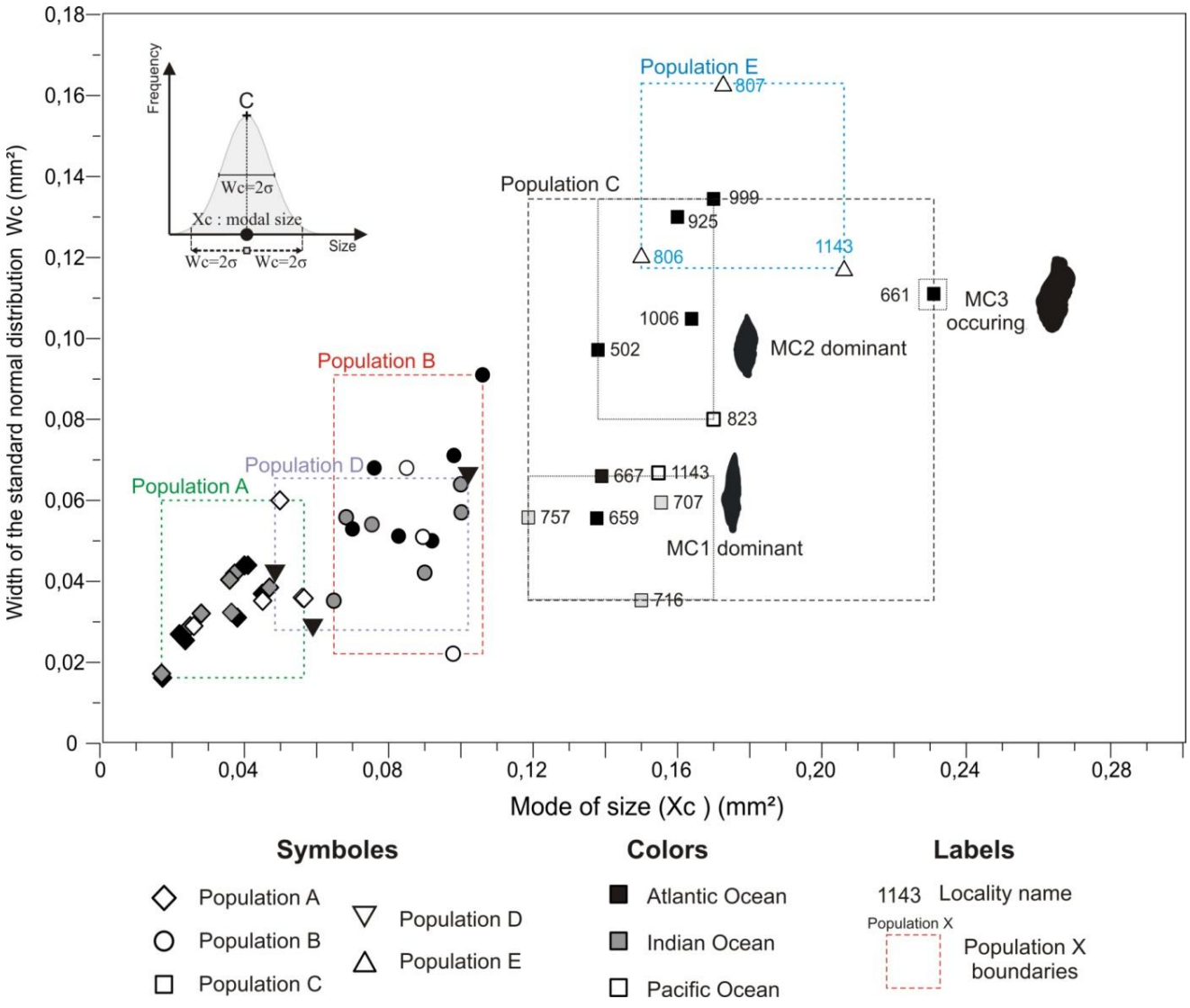

Figure 4.10: Summary plot of modal positions versus widths of all populations found in this study in the three oceans. Modal positions are in units of keel view area (mm2). Population widths are in units of 2 standard deviations of the respective Gaussian best fitting curves. Black symbols are from the Atlantic Ocean, grey ones from the Indian Ocean, and white ones from the Pacific Ocean. Dashed green lines enclose worldwide populations A, dashed purple lines enclose worldwide population D, dashed red lines enclose worldwide population B, dashed black lines enclose worldwide population D, and dashed blue lines enclose worldwide population E.

In the Indian Ocean province, the distribution of menardellids is relatively uniform, as can be seen in the respective 3.2 Ma time-slice samples from Sites 707, 716, 721, 757, 758, 763. This Indian province shows a strong dominance of small morphotype MA, while large menardellids (morphotype MC1) remain generally scarce. Only at Site 707 and 757 the morphotype MC2 was observed in very low abundances.

Similar to the Atlantic Ocean, the Pacific Ocean sample set is subdivided in two menardellid provinces as well: the Pacific Warm Pool province has less multi-chambered menardellids but is characterized by dominant morphotype MC2 (see Sites 823 and 1143). In the eastern part of the Warm Pool area (Sites 1143, 806 and 807) the Pacific endemic morphotype ME occurred while morphotype MC2 in the largest size fraction is rare. The eastern Pacific province is represented, however, only by two samples, where menardellids occur at relatively low abundances and are dominated by morphotype MA. Given the relatively coarse sample density at the 3.2 Ma old time-slice at our disposal for this study, caution must be taken not to over-interpret these findings with the paleo-oceanographic or paleo-current patterns known from that time. In order to obtain a picture about biogeographic tendencies of Mid-Pliocene menardiform morphotypes at higher spatial resolution, further investigations are required.

4.6.2 Contribution to menardellid classification

One of the aims of the present work is to disentangle the intricate menardellid taxonomy with the help of quantitative morphometric analyses of populations. The present data provide key information for hypotheses about a hidden diversity within the otherwise established menardellid classification. Morphotypes MA, MB, MC1 through 3, SH1 and SH2 have previously been tentatively attributed to the formal menardellid species (Mary and Knappertsbusch, in press). A summary of the interpretations of these morphotypes is given in Table 4.2.

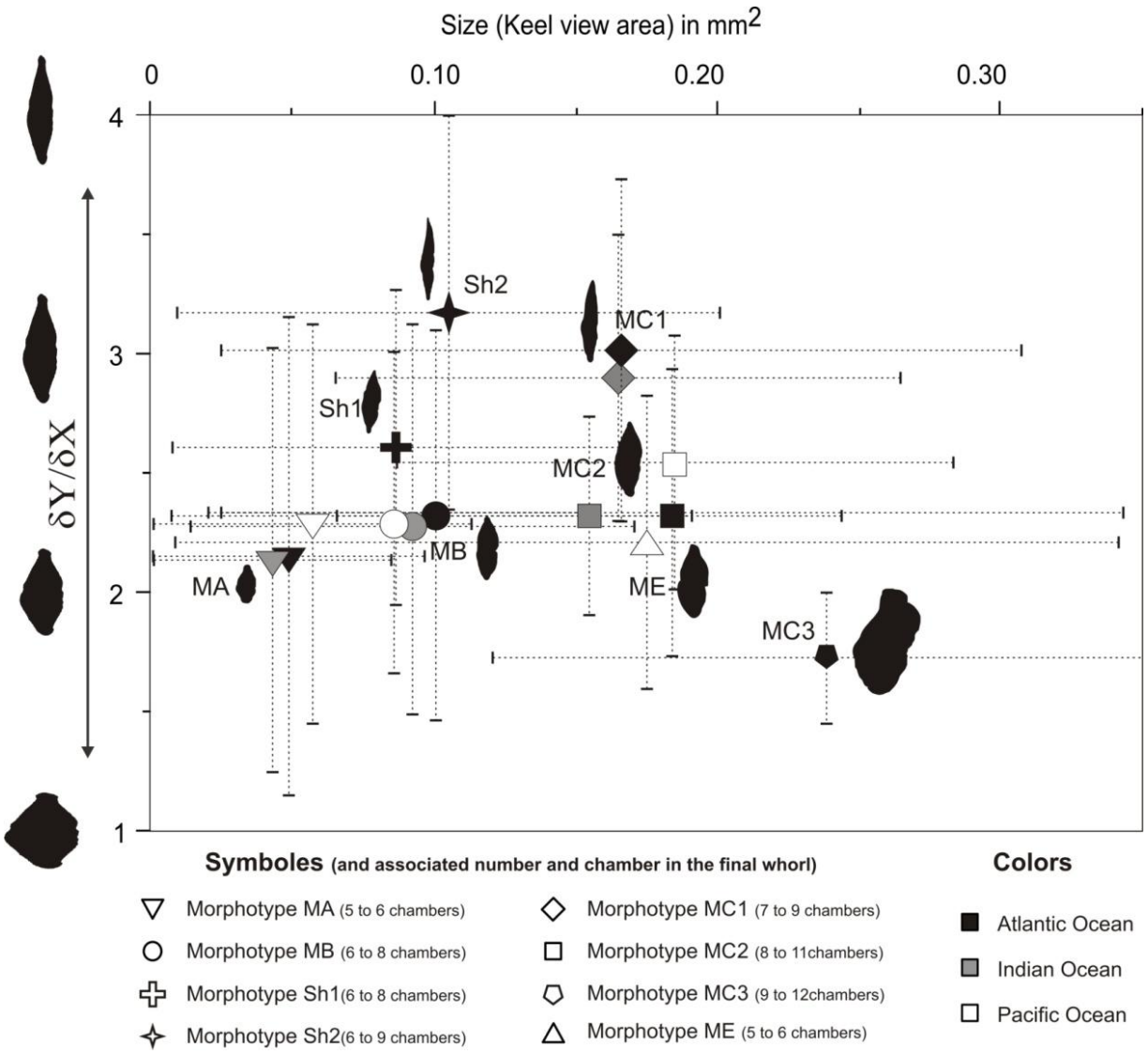

Figure 4.11: Summary of morphotypes proposed in this study in the morphospace of δY/δX ratio versus keel view area (see also Table 2). Symbols represent centers of morphospace fields of respective morphotypes as found in each separate ocean. The error-bars represent the maximum width per morphospace in direction of keel view area (horizontally) and in direction of δY/δX (vertically). Black symbols represent Atlantic locations, grey symbols Indian Ocean locations, and white symbols Pacific locations.

4.6.2.1 The morpho-species concept of *Globorotalia (Menardella) menardii*

Morphotype MA shows several morphological characteristics in common with *Globorotalia (M.) menardii* (Parker *et al*. 1865), to which it has been assigned (Mary and Knappertsbusch, in press). This morphotype was noted to match with the informal *G. (M.)*

menardii "A", which is a small, extinct variant of *G. (M.) menardii* ranging from the Late Miocene to the Early Pliocene (Bolli, 1970). The visual comparison of shell morphology of Morphotype ME with menardellids illustrated in the literature (Kennett and Srinivasan, 1983; Bolli and Saunders, 1985) lets to conclude that this morphotype is a further variant of *Globorotalia menardii* as well. A very similar morphotype (α) was recorded by Knappertsbusch (2007) in the eastern Equatorial Pacific at Site 503 and in the Caribbean Sea Site 502. Both morphotypes, ME and α are virtually identical in shell morphology, number of chambers in the final whorl, and both populate the identical segment in the morphospace spanned by spiral height (δX) versus axial length (δY) (see Figure 4.12).

Morphometric measurements of δX versus δY in the Pacific ODP Site 503 revealed an extended period from Late Miocene through Late Pliocene, during which *G. (M.) menardii* shows a continuous increase of shell size and evolving into shell morphologies representing extant morphotype α (Knappertsbusch, 2007; Brown, 2007). The main morphological expansion did, however, only occur from 2.5 Ma onwards at Site 503, and after 1.7 Ma on the Caribbean side of the Isthmus of Panama, at Site 502. Before this interval, specimens of morphotype α from Knappertsbusch (2007) follow the same morphospace through time as the 3.2 million years old morphotype MA presented herein. During the Mid Pliocene, the Site 503 specimens belong to morphotype MA (Figure 4.12), with the exception of few specimens that coincide with morphotype MB. However, the occurrence of Mid-Pliocene morphotype ME in the western Pacific sample at Site 807 possibly points to an earlier size evolution of Morphotype α towards larger forms in that area than reported at Site 503 by Knappertsbusch (2007).

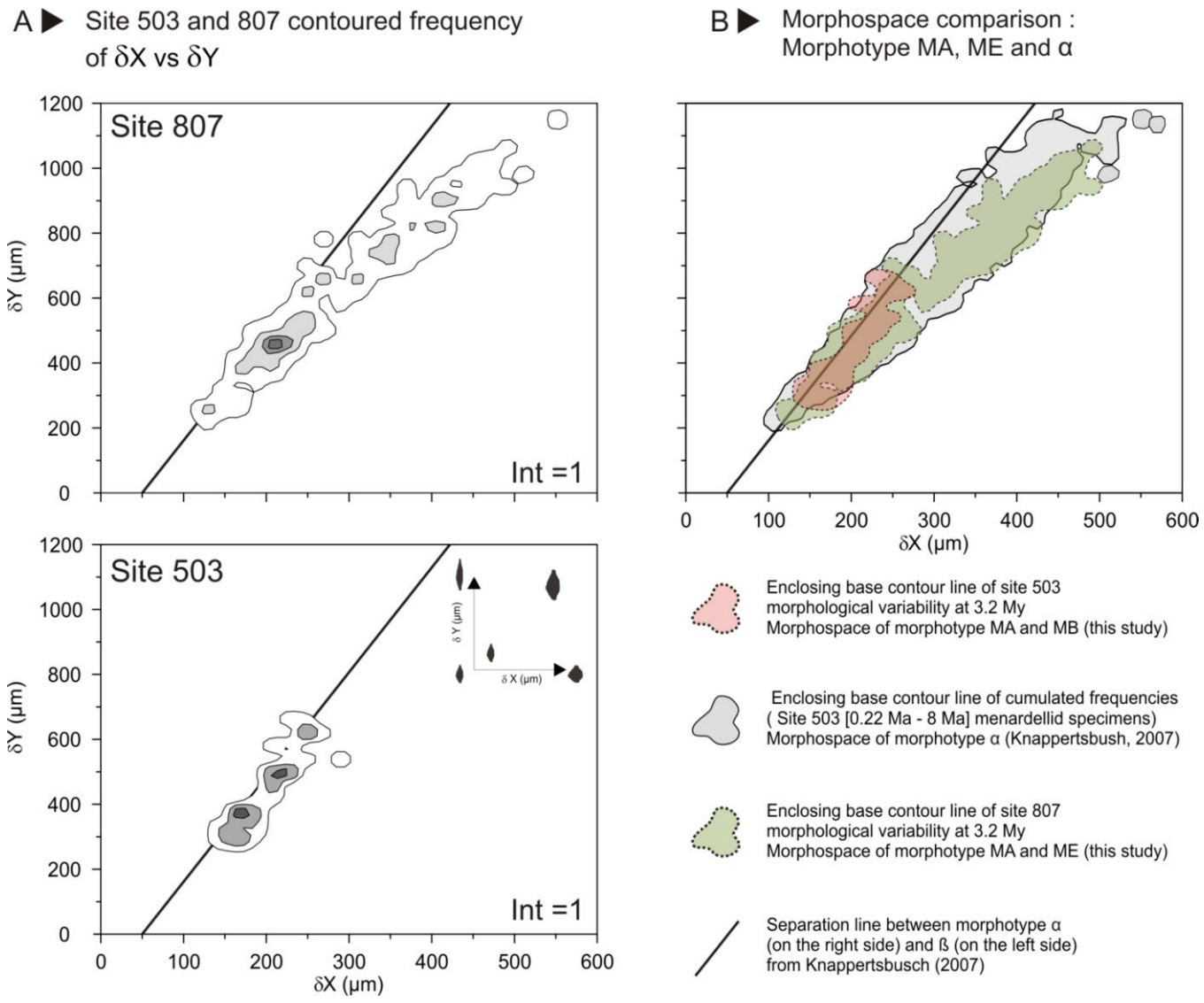

Figure 4.12: Comparison between morphotype MA and morphotype α sensu Knappertsbusch (2007). (A) Bivariate contour plot of δX versus δY measurements at Site 807 (which contains abundant specimens of morphotype MA and α) and at Site 503 (where only morphotype MA is present) (B) A comparison of the base contour line from Site 807 and site 503 during Mid Pliocene with the base contour line including specimens of morphotype alpha younger than 0.22 Ma from Site 503 (eastern Equatorial Pacific) as shown in Knappertsbusch (2007). The Grid cell-size for contouring is 10 µm in horizontal direction and 20 µm in vertical direction.

The presented new time-slice at 3.2 Ma however, indicates that morphotype MA and morphotype α do not belong to the same population (populations A and E respectively, see Figure 4.9). Although there is overlap, both populations differ strongly in modal size (see Figures 4.9 and 10), and their biogeographic distributions are different too (population A shows a worldwide spread during the Mid-Pliocene time-slice whereas population E is limited to the west Pacific). For these reasons we must refrain from the earlier interpretation of Knappertsbusch (2007), *i.e.* that morphotype α includes the small "menardii A" from Bolli (1970). Instead, the new morphometric and biogeographic evidence from the 3.2 time-slice mapping experiment suggests that the small morphotype MA and the large morphotype ME may constitute distinct, albeit strongly homeomorphic or sibling species.

4.6.2.2 Morphotypes of *Globorotalia multicamerata*

Morphotypes MC1 and MC2 have been interpreted as morpho-variants of *Globorotalia multicamerata* Cushman and Jarvis (1930) (Mary and Knappertsbusch, in press). Morphotype MC1 shows a typically thin and elongated shell whereas morphotype MC2 displays a more robust shell. Other shell features let one to distinguish the two morphotypes by the number of chambers in the final whorl, which is less in morphotype MC1, and the average size.

There are, however, no clear indications that the two morphotypes belong to different populations considering their SFDs: both morphotypes are derived from one population C. The variation of the SFDs of population C is high from sample to sample, *i.e.* from place to place (see Figure 4.10). In the western Atlantic the larger morphotype MC2 dominated at 3.2 Ma, whereas in the Indian Ocean morphotype MC1 was the prevailing form at that time. These findings support the view of considerable ecophenotypic variability in Mid-Pliocene *G. (M.) multicamerata*. The larger morphotype MC2 occurred preferentially in the Caribbean Sea and the Pacific Warm Pool area indicating preference for extremely warm and highly stratified waters. The thinner and more elongated morphotype MC1, which corresponds to the forms illustrated in Bolli and Saunders (1985), are interpreted by as being transitional between *G. (M.) multicamerata* and *G. (M.) pertenuis* (cf. Figure 4.1A.).

The morphological investigations confirm the morphological similarity between morphotype SH2 (= *G. (M.) pertenuis*, Mary and Knappertsbusch, in press) and morphotype MC1. The typical thin morphology of *G. (M.) pertenuis* has been interpreted as adaptation to surface water conditions, and is perhaps indicative for hosting symbionts (Chaisson 2003). The depth-habitat of *G. (M.) multicamerata* has been studied in detail by Pfuhl and Shackleton (2001). These authors mentioned a progressive rise of *G. (M.) multicamerata* to shallow water depths from the Late Miocene to Early Pliocene. Keeping this in mind, the thin morphology of morphotype MC1, which is similar to *G. (M.) pertenuis,* may be interpreted as an adaptation to a shallower habitat, in contrast with morphotype MC2, which probably lived deeper in the water column. To further confirm these morphological interpretations, extra tests need to be done in future, for example with the help of stable isotopes.

4.7 Conclusions

Applying the method of Gaussian best fitting to the menardellid SFDs, we identify eight different morphotypes MA, MB, MC1, MC2, MC3, SH1, SH2 and ME in global tropical to subtropical sediments from a 3.2 million years old time-slice. The majority of these morphotypes (MA, MB, MC1, and MC2) shows a worldwide geographic spread, albeit at different degrees of dominance in each ocean. A subset of the menardellids from the 3.2 million years old time-slice shows an endemic spread within a particular ocean. The morphotype ME was found to be limited to the Pacific Ocean. The Morphotypes SH1 and SH2, which show a shiny shell surface, are restricted to the western Atlantic Ocean. Morphotype MC3 was observed at a single locality (ODP Site 661) in the eastern Atlantic.

Our mapping experiment demonstrates the existence of biogeographic provincialism in Mid-Pliocene menardellids: in the Atlantic Ocean a western and an eastern menardellid province were found. Similarly, in the tropical to subtropical Pacific Ocean, menardellid faunas differentiated in a western Pacific margin province and an eastern tropical Pacific margin province. Indian Ocean menardellid faunas did not reveal any obvious biogeographic trends.

The proposed morphotypes show very strong overlap rendering the practical visual identification difficult. Among all morphometric parameters investigated the ratio of δY/δX in keel view proved to be the best combination of characters to separate morphotypes from each other. Size (as expressed by the area enclosed by the profile in keel view) is also a fundamental character, but it may be complicated by the demographic structure of the preserved ancient plankton population: while in a population, adults are usually identifiable without any difficulty, morphotypic differences are frequently hidden by the dominating number of smaller pre-adults with less well differentiated shell morphologies. This masking effect becomes even more pronounced if menardellid faunas are composed of more than one species.

Acknowledgments

We would like to express our gratitude to the financial support of the Swiss National foundation for scientific Research (SNF grant Numbers 200021-121599 (Evolutionary prospection in Neogene planktonic foraminifera) and 200020-137486 (Evolutionary prospection in Neogene planktonic foraminifera-continuation). We are also grateful to IODP center for providing sample materials (IODP sample request # 21438A, B and C). We acknowledge the technical help of Antoine Heitz from Natural History Museum Basel for his assistance in sample preparation.

References

André, A., Weiner, A., Quillévéré, F., Aurahs, R., Morard, R., Douady, C., de Garidel-Thoron, T., Escargel, G., de Vargas, C., Kucera, M., 2013. The cryptic and the apparent reversed : lack of genetic differentiation within the morphologically diverse plexus of the planktonic foraminifer *Globigerinoides sacculifer*. Paleobiology 39(1), 21-39.

Bé, A. W., Tolderlund, D. S., 1971, Distribution and ecology of living planktonic foraminifera in surface waters of the Atlantic and Indian Oceans, in Funnel, B. M., and Riedel, W. R. (eds.), the Micropalaeontology of oceans: London, Cambridge University Press, p. 105-149.

Berggren, W.A., Kent, D.V., Swisher, C.C., Aubry, M.P. 1995. Geochronology, time scales and global stratigraphic correlation. Society of Economic Paleontologists and Mineralogists, Special Publication. Chapter A, revised Cenozoic geochronology and chronostratigraphy. 54, 129–212.

Bickert, T., Curry, W.B., Wefer, G., 1997. Late Pliocene to Holocene (2.6-0 Ma) Western Equatorial Atlantic deep water circulation: Inferences from benthic stable isotopes. Proceedings of the Ocean Drilling Program, Scientific Results 154, 239–253.

Blackith, R.E., Reyment R.A., 1971. Multivariate Morphometrics. London: Academic Press, 412pp.

Bolli, H.M. 1970. The foraminifera of Sites 23-31, Leg 4.- Initial Reports of the Deep Sea Drilling Project, College Station, vol. 4, p. 577-643.

Bolli, H.M., Saunders J.B., 1985. Oligocene to Holocene low latitude planktic foraminifera.- In: Bolli H.M., Saunders J.B.. Perch-Nielsenk. (eds.), Plankton stratigraphy. Cambridge University Press, Cambridge, p. 155-262.

Bonham, S.G., Haywood, A. M., Lunt, D. J., Collins, M., Salzmann U. 2009. El Niño Southern Oscillation, Pliocene climate and equifinality. Philosophical Transactions of the Royal Society. A. 367, 127-156.

Brierley, C.M., Fedorov, V.A., Lieu, Z., Herbert, T. D., Lawrence, K.T., LaRiviere J.P. 2009. Greatly expanded tropical Warm Pool and Weakened Hadley Circulation in the Early Pliocene, Science 27, 323 , 1714-1718.

Brown, K. 2007. Biogeographic and morphological variation in late Pleistocene to Holocene globorotalid foraminifera. Dissertation Phil. Nat. Fakultät, Universität Basel, 128 p. pdf file available at http://pages.unibas.ch/diss/2007/DissB_8290.htm

Chaisson, W.P., Leckie, R.M., 1993. High resolution Neogene planktonic biostratigraphy of site 806, Ontong Java Plateau (western equatorial Pacific). Proceedings of the Ocean Drilling Program, Scientific Results 130, 137–178.

Chaisson, W.P., Pearson, P.N., 1997. Planktonic foraminifer biostratigraphy at the Site 925: Middle Miocene-Pleistocene. Proceedings of the Ocean Drilling Program, Scientific Results 154, 3–31.

Chaisson, W.P., 2003. Vicarious living: Pliocene menardellids between an isthmus and an ice sheet. Geology 31,1085–1088.

Cheng, X., Tian, J., and Wang, P., 2004. Data report: stable isotopes from Site 1143. In Prell, W.L., Wang, P., Blum, P., Rea, D.K., and Clemens, S.C. (Eds.), Proc. ODP, Sci. Results, 184: College Station, TX (Ocean Drilling Program), 1–8. doi:10.2973/odp.proc.sr.184.221.2004

Cifelli, R., Scott, G. 1986. Stratigraphic record of the Neogene globorotalid radiation (planktonic foraminifera). Smithsonian Contributions to Paleobiology 58.

Cushman, J.A., Jarvis, P.W., 1930. Miocene foraminifera from Buff Bay, Jamaica. Journal of Paleontology, Lawrence, vol. 4, n° 4, 353-368.

Darling, K., Wade, C. 2008. The genetic diversity of planktonic foraminifera and the global distribution of ribosomal RNA genotypes. Marine Micropaleontology 67, 216–238.

Dekens, P. S., Ravelo, A. C., McCarthy, M. D., 2007, Warm upwelling regions in the Pliocene warm period. Paleoceanography, 22, PA3211.

Dowsett, H., Robinson, M.M., 2007. Mid-Pliocene planktic foraminifer assemblage of the North Atlantic Ocean. Micropaleontology 53, 105–126.

Dowsett, H. J., 2007. The PRISM palaeoclimate reconstruction and Pliocene sea-surface temperature. In Deep-time perspectives on climate change: marrying the signal from computer models and biological proxies (eds M. Williams, A. M. Haywood, F. J. Gregory , D. N. Schmidt). The Micropalaeontological Society, Special Publication, pp. 459–480. London, UK: The Geological Society.

Dwyer, G. S., Chandler, M. A., 2009 Mid-Pliocene sea level and continental ice volume based on coupled benthic Mg/Ca palaeotemperatures and oxygen isotopes. Philosophical Transactions of the Royal Society of London A 367, 157–168. (doi:10.1098/rsta.2008.0222)

Fatela, F., Taborda, R., 2002.Confidence limits of species proportions in microfossil assemblages. Marine Micropaleontology 45, 168–174.22

Fedorov, A.V., Deckens, P.S., McCarthy, M., Ravelo, A.C.,Menocal, de P.B., Barreiro, M., Philander, R.C.S.G. 2006. The Pliocene Paradox (Mechanisms for a Permanent El Niño) Science 312, 1485-1489.

Fedorov, A.V., Bierly, C.M., Lawrence, K.T., Liu, Z., Dekens, P.S., and Ravelo, A.C. 2013 Patterns and mechanisms of early Pliocene warmth. Nature, 496, 4 April 2013, 43-49.

McGowran B., 2005. Biostratigraphy: microfossils and geological time. Cambridge University Press, Cambridge, 459pp

Groeneveld, J., Nürnberg, D., Tiedemann, R. , Reichart, G.J., Steph, S. , Reuning, L. , Crudeli, D., Mason, P. 2008. Foraminiferal Mg/Ca increase in the Caribbean during the Pliocene: Western Atlantic Warm Pool formation, salinity influence, or diagenetic overprint? Geochem. Geophys. Geosyst., 9(1), Q01P23, doi:10.1029/ 2006GC001564.

Haug, G.H., and Tiedemann, R., 1998. Effect of the formation of the Isthmus of Panama on Atlantic Ocean thermohaline circulation. Nature (London, U. K.), 393-673.

Haywood, A.M., Valdes, P.J, 2004. Modelling Pliocene warmth: contribution of atmosphere, oceans and cryosphere. Earth and Planetary Science Letters 218, 363-377

Haywood, A.M., Dowsett, H.J., Valdes, P.J., Lunt, D.J., Francis, J.E., Sellwood, B.W., 2009. Introduction. Pliocene climate, processes and problems. Phil. Trans. R. Soc 367, 3–17.

Jansen, E. 2007 Palaeoclimate. In Climate change 2007: the physical science basis. Contribution of Working Group I to the Fourth Assessment Report of the Intergovernmental Panel on Climate Change (eds S. Solomon, D. Qin, M. Manning, Z. Chen, M. Marquis, K. B. Averyt, M. Tignor, H. L. Miller). Cambridge, UK: Cambridge University Press.

Karas, C., Nürnberg, D., Gupta, A. K., Tiedemann, R., Mohan, K., Bickert, T. 2009. Mid-Pliocene climate change amplified by a switch in Indonesian subsurface throughflow. Nature Geoscience, 2, 434–438

Karas, C., Nürnberg, D., Tiedemann, R., Garbe-Schönberg , D. 2011. Throughflow and Leeuwin Current dynamics: Implications for Indian Ocean polar heat flux. Paleoceanography 26, PA2217

Keigwin, Jr, L.D., 1982. Neogene planktonic foraminifers from Deep-Sea Drilling Project Sites 502 and 503. Initial Reports of the Deep Sea Drilling Project 68.

Kennett, J.P., Srinivasan, M.S., 1983. Neogene planktonic foraminifera, a phylogenetic atlas. Hutchinson Ross,Stroudburg, Pennsylvania.

Knappertsbusch, M.W., 2007. Morphological variability of *Globorotalia menardii* (planktonic foraminifera) in two DSDP cores from the Caribbean sea and the eastern equatorial pacific. Carnets de Geologie 04.

Knappertsbusch, M.W., Binggeli, D., Herzig, A., Schmutz, L., Stapfer, L., Schneider, C., Eisenecker, J., Widmer, L., 2009. Amor - a new system for automated imaging of microfossils for morphometric analyses. Palaeontologia Electronica 12.

Kucera, M., Darling, K., 2002. Cryptic species of planktonic foraminifera: their effect on palaeoceaographic reconstruction. Philosophical Transactions of the Royal Society of London A 360, 695–718.

LaRiviere J., Ravelo, A.C. , Crimmins, A., Dekens, P.S., Ford, H.L. 2012. Late Miocene decoupling of oceanic warmth and atmospheric carbon dioxide forcing. Nature 486, 97–100 Lawrence, K. T., Liu, Z. , Herbert, T. D. 2006. Evolution of the eastern tropical Pacific through Plio-Pleistocene glaciation, Science, 312, 79–83

Lazarus D. 1992. Age depth plot and age maker: Age modeling of stratigraphic sections on the Macintosh series of computers. Geobyte, vol. 2, p. 7-13.

Lazarus, D., Spencer-Cervato, B.C., Pianka-Biolzi, M., Beckmann J.P., von Salis, K., Hilbrecht, H., Thierstein, H. R. 1995 Revised Chronology of Neogene DSDP holes From the World Ocean. Ocean Drilling Program, Technical Note No. 24.

Lunt, D.J., Valdes, P.J., Haywood, A., Rutt, I.C., 2008. Closure of the Panama Seaway during the Pliocene: implications for climate and Northern Hemisphere glaciation. Climate Dynamics 30, 1–18.

Lutz, B.P., 2011. Shifts in North Atlantic planktic foraminifer biogeography and subtropical gyre circulation during the mid-Piacenzian warm period. Marine Micropaleontology 80, 125-149.

Marcus, LF 1990. Traditional morphometrics. In: Proceedings of the Michigan Morphometrics Workshop (Rohlf F.J., Bookstein F.L., eds), 77–122. Ann Arbor, MI: University of Michigan Museums.

Mary, Y., Knappertsbusch, M.W. In press. Morphological variability of Menardiform Globorotalids in the Atlantic Ocean during Mid-Pliocene. Marine Micropaleontology.

Mitteroecker P., and Huttegger S. M. 2009. The Concept of Morphospaces in Evolutionary and Developmental Biology: Mathematics and Metaphors. Biological Theory 4, 54-67.

Morad R., Quillévéré, F., Douady, C, De Vargas, C, de Garidel-Thoron, T., Escarguel, G., 2011. Worldwide genotyping in the Planktonic foraminifer *Globoconella inflata*: Implications for Life History and Panleoceanography. PLoS ONE 6(10).

Morard, R., Quillevere, F., Escarguel, G., Ujie, Y., de Garidel-Thoron, T., Norris, R., de Vargas, C., 2009. Morphological recognition of cryptic species in the planktonic foraminifer *Orbulina universa*. Marine Micropaleontology 71, 148–165.

NEPTUNE-working group 2000 (Dave Lazarus, Cinzia Cervato, Michael Knappertsbusch, Milena Pika-Biolzi, Jean-Pierre Beckmann, Katharina von Salis, Heinz Hilbrecht, and Hans Thierstein). NEPTUNE-online II. Microfossil datums from drilling holes of the DSDP and ODP. http://micropal-basel.unibas.ch/NEPTUNE/Start.html

Parker, W.K, Jones, T.R, Brady, H.B, 1865. On the nomenclature of the foraminifera; Part XII. The species enumerated by d'ORBIGNY in the Annales des Sciences Naturelles, vol. 7, 1826. Annual Magazine of Natural History London, ser. 3, vol. 16, 15-41.

Peeters, F., Ivanova, E., Conan, S., Brummer, G.-J., Ganssen, G., Troelstra, S., van Hinte, J., 1999. A size analysis of planktonic foraminifera from the Arabian Sea. Marine Micropaleontology 36, 31-63.

Pfuhl, H.A., Shackleton, N.J. 2004. Change in coiling direction, habitat depth and abundance in two menardellid species. Marine Micropaleontology 50, 3–20.

Philander, S. G. , Fedorov, A. V. 2003. Role of tropics in changing the response to Milankovich forcing some three million years ago. Paleoceanography 18, 10–45.

Poore, R.Z. 2007 : Paleoclimate reconstruction.Pliocene Environments. in Encyclopedia of Quaternary Science. Scott A. Elias (eds), Oxford; 2007, 1948-1958.

Quillévéré, F., Morard, R., Escargel, G., Douady, C. J., Ujiié, U., de Garidel-Thoron, T., de Vargas, C. 2011. Global scale same-specimen morpho-genetic analysis of *Truncorotalia truncatulinoides* : A perspective on the morphological species concept in planktonic foraminifera. Palaeogeography, Palaeoclimatology, Palaeoecology 1-11.

Regenberg, M., Nielsen, S.N., Kuhnt, W., Holbourn, A., Garbe-Schonberg, D., Andersen, N., 2010. Morphological, geochimical and ecological differences of the extant menardiform planktonic foraminifera *Globorotalia menardii* and *Globorotalia cultrata*. Marine micropaleontology 74, 96–107.

Reyment RA 1991. Multidimensional Paleobiology. New York: Pergamon Press.

Ujiié, Y., de Garidel-Thoron, Watanabe, S., Wiebe, P., de Vargas, C. 2010. Coiling dimorphism within a genetic type of the planktonic foraminifer *Globorotalia truncatulinoides*. Marine Micropaleontology 77, 145-153.

Scott, G.H. 2011. Holotypes in the taxonomy of planktonic foraminiferal morphospecies. Marine Micropaleontology 78 96–100.

Sexton, P.F., Norris, R.D. 2008. Dispersal and biogeography of marine plankton: long-distance dispersal of the foraminifer *Truncorotalia truncatulinoides*. Geology 36, 899-902.

Sexton, P. F., Norris, R.D. 2011. High latitude regulation of low latitude thermocline ventilation and planktic foraminifer populations across glacial-interglacial cycles. Earth and Planetary Science Letters 311 (2011) 69-81.

Srinivasan, M.S., Sinha, D.K. 1998 : Early Pliocene closing of the Indonesian Seaway : evidence from north-east Indian Ocean and Tropical Pacific deep sea cores. Journal of Asian Earth Sciences 16, 29-44.

Steph, S., Tiedemann, R., Prange, M., Groeneveld, J., Schulz, M., Timmermann, A., Nürnberg, D., Rühlemann, C., Saukel, C., Haug, G.H. 2010. Early Pliocene increase in thermohaline overturning:A precondition for the development of the modern equatorial Pacific cold tongue. Paleoceanography 25, PA2202.

Su, X., Xu, Y., and Tu, Q. 2004. Early Oligocene–Pleistocene calcareous nannofossil biostratigraphy of the northern South China Sea (Leg 184, Sites 1146–1148). In Prell, W.L., Wang, P., Blum, P., Rea, D.K., and Clemens, S.C. (Eds.), Proc. ODP, Sci. Results, 184: College Station, TX (Ocean Drilling Program), 1–24. doi:10.2973/odp.proc.sr.184.224.2004

Vargas de C., Saez A.G., Medlin L.K., Thierstein, H.R. 2004. Superspecies in the calcareous plankton. In: Thierstein HR, Young JR (eds) Coccolithophores: from molecular processes to global impact. Springer, Berlin, 271–298.

Wara, M. W., Ravelo, A. C., Delaney, M. L. 2005 Permanent El Niño-like conditions during the Pliocene warm period. Science 309, 758–761.

Chapter 5: Ontogenetic and heterochronic patterns in menardellid foraminifera

---

Yannick Mary[a,b], Loïc Costeur[a], Daniel Mathys[b], Michael Knappertsbusch[a]

a: Natural History Museum Basel, Augustinergasse 2, 4001-Basel, Switzerland

b: Geologisch-Paläontologisches Institut, Universität Basel, Bernoullistrasse 32, CH-4056 Basel, Switzerland

Abstract

Using micro dissolution of the umbilical side, we invested the morphological development of 350 specimens of the three Pliocene menardellid species composing the phylogenetic lineage of *Globorotalia (Menardella) menardii* - *G. (Menardella) limbata* - *G. (Menardella) multicamerata*. Based on internal shell structure, we measured the cross sectional area of successive chambers to establish growth curves. In addition, the chamber shape, the shell diameter and the pore density were analyzed to quantify morphological changes associated with growth. Our results demonstrate that the ontogenetic model of planktonic foraminifera, defined by Brummer *et al*. (1987) applied to menardellids as well. Growth is associated with 5 successive growth stages.

Although there is common intergradation between the three menardellid species under consideration, adult specimens can be relatively easily distinguished using growth pattern. However, pre-adults or immature forms are virtually impossible to differentiate on the basis of external morphology. Intra-specific variability in growth stages is high, and show species-specific pattern. Our study demonstrates that without a detailed knowledge about growth patterns, size is not a good estimator to ontogenetic stages in menardellid.

The comparison of morphological development associated with growth revealed peramorphic heterochronic patterns between the three species. The phyletic increase in shell size among this lineage is the consequence of gradual hypermorphic extensions of the neanic stage in *G. (M.) limbata* and in the adult in *G. (M.) multicamerata.* This evolutionary change is interpreted as an adaptation to shallower habitat and more K-strategy behavior.

5.1 Introduction

The adult shell morphology of planktonic foraminifera is the basis of their classification, which is an important tool in biostratigraphy and paleoceanography. Intra-specific shell morphological variability is however commonly high. Since the early 2000s, what was traditionally considered as ecophenotypic variations of morphology was associated with fundamental genetic differences (Kucera and Darling, 2002; Darling and Wade, 2008). Combined studies of molecular analysis with morphometric measurements revealed that morphological variation within the same genotypes can be considerable (Ujié *et al*., 2010; André *et al*., 2013) and is commonly explained by differences in habitat (Renaud and Schmidt 2003; Al-Sabouni *et al*., 2007, Regenberg *et al*., 2010).

The morphological plasticity of planktonic foraminifera is strongly controlled by ontogeny (Brummer *et al*., 1986; Hemleben *et al*., 1989). Shell development results in discrete and step-wise chamber addition on the spiral of earlier chambers. The entire ontogeny is consequently recorded within a single specimen. Individual tests therefore provide key information to understand the observed morphological variability in planktonic foraminifera. Investigations of early stages of ontogenetic growth involve, however, very labor-intensive techniques, like micro-radiographic imagery (Hedley, 1957; Bé *et al*., 1966; Leary and hart, 1988 ; Georgescou *et al*., 2009), or novel X-ray computer micro-tomography (*e.g.* Speijer *et al*., 2008; Görög *et al*., 2012). These methods allow the study of foraminifera shell growth at the individual level, but remain time-consuming and not adapted to routine application in significant amounts of specimens.

Consequently, despite their central place in geosciences only few studies exist so far on the developmental sequence in planktonic foraminifera (Brummer *et al*., 1987; Hemleben, 1989; Wei *et al*., 1992, Huber, 1994). External morphological changes related to ontogenetic growth have also been documented for other taxa (Huang, 1981, Bummer *et al*., 1986). In addition, these pioneering studies emphased that the sequential study of ontogenetic growth is a very valuable way to characterize planktonic foraminiferal species, which otherwise are difficult to distinguish from their external shell morphologies (Brummer *et al*., 1987; Huber, 1994). In addition, the comparison of developmental sequences among lineages eventually

allows the recognition of heterochronic patterns, *i.e.* the recognition of evolutionary changes in timing or rate of developmental events, relative to the same events in the ancestor (McKinney and McNamara, 1991). Heterochrony is one of the major phenomenon that causes much morphological variations and is linked to major evolutionary novelties (*e.g.* Gould 1977 ; Albrecht *et al*., 1979; McKinney and McNamara, 1991; Webster and Zelditch, 2005). In biology (foraminifera excluded) heterochrony is often discussed solely by consideration of the external morphology (see Klingenberg 1998), using analysis of shell shape and size as an approximation of ontogenetic stage. In the case of foraminifera, notably in larger benthic foraminifera, there is an exhaustive body of literature describing heterochrony elements (as for example Drooger's "theory of nepionic acceleration") (McGillavry, 1963; Hofker, 1966; Van der Vlerk and Gloor, 1968; O'Herne, 1972; Van der Vlerk, 1973; Drooger, 1993; Hottinger, 2001). In planktonic foraminifera heterochrony becomes meanwhile increasingly investigated as well (Nederbragt, 1989; Nederbragd, 1993; Wei, 1994; Kelly *et al*., 1996; MacLeod *et al*., 2000; Kelly *et al*., 2001; Quillévéré *et al*., 2002).

Among planktonic foraminifera, menardellid globorotalids are a good example of morphological intergradation, especially during the Pliocene. At that time, a wide morphological plexus of poorly defined menardellid morpho-species occurred in tropical regions, encompassing the evolutionary lineage of *Globorotalia menardii* - *G. (M.) limbata* - *G. (M.) multicamerata* (Kennett and Srinivasan, 1983). The shell morphology of these species is characterized by a phylogenetic increase in the number of chambers in the final whorl: *G. (M.) menardii* has preferentially 5 to 6 chambers, versus 6 to 8 for *G. (M.) limbata* and 8 to up to 12 for *G. (M.) multicamerata*. This number of chamber overlap, together with their quite similar morphologies, has led to an intricate taxonomy (Cifelli and Scott, 1986; Bolli and Saunders, 1985).

Menardellids are promising candidates for ontogenetic studies. Their relatively large low trochospiral test, showing only little chamber overlap, makes them a suitable to explore ontogenetic patterns. For these reasons, they have a long history of allometric investigations based on external morphology (Schmid, 1934; Cifelli and Glaçon 1978; Olsson, 1973; Scott, 1973; Hemleben *et al*., 1977; Schweitzer, 1989; Schweizter and Lohmann 1991). Recently, we have experimented an extended worldwide morphometric mapping experiment of

menardellids at a Mid-Pliocene time-slice around 3.2 Ma (Mary and Knappertsbusch, in press; Mary *et al*., submitted).

The present study fits into the extended worldwide morphometric mapping experiment of menardellids at a Mid-Pliocene time-slice around 3.2 Ma (Mary and Knappertsbusch, in press; Mary *et al*., submitted) and now concentrates on the ontogenetic growth of selected, phylogenetically related menardellids: *G. (M.) menardii, G. (M.) limbata,* and *G. (M.) multicamerata*. The first goal is to document their ontogenetic growth, and in this manner to further confirm the validity of geometric morphometric analysis based on external shell morphology in these selected examples. This will finally help to understand the taxonomic significance of the development sequence for the involved species, and to shed light to the evolutionary processes leading to the morphological diversification of the *G. (M.) menardii*-*G. (M.) multicamerata* lineage.

As a significant number of specimens is required to distinguish between intra-specific variation and changes, a special technique was developed for the study of ontogenetic shell growth: the micro-dissection by dissolution of the umbilical side. This proved to be an efficient technique to reconstruct the ontogenetic growth of 350 specimens for the three species.

5.2 The ontogenetic model of planktonic foraminifera

Previous observations of planktonic Foraminifera internal shells have pointed out at similarities in their ontogenetic development. Their growth is subdivided in five different stages (Brummer *et al*., 1987; Wei *et al*., 1992; Huber, 1994): the embryonic, juvenile, neanic, adult and terminal stages. The transitions between these stages are commonly associated with drastic phenotypic changes (Brummer *et al*., 1986, Huang, 1981).

The proloculus, *i.e.*, the first chamber formed after fusion of the gametes, composes the embryonic stage and presents a flattening at the contact with the second chamber. The juvenile stage starts with the deuteroconch (second chamber), and has been documented to encompass 1.5 whorls, with a species-specific number of chambers (Huang, 1981; Brummer *et*

al., 1987). During this stage, the chambers show a uniform rate of growth, the second chamber being usually distinctly smaller than the proloculus (Brummer *et al*., 1987; Wei *et al*., 1992; Huber, 1994).

A pronounced change in growth rate marks the onset of the neanic stage, which corresponds to the transition towards maturity. The amplitude of growth increase depends of the investigated taxa. An abrupt transition associated with drastic morphological changes is documented in globigerinid and globigerinoid species (Brummer *et al*., 1987). In contrast, the beginning of the neanic stage is less pronounced in the globorotalid species *Globoconella inflata* (Wei *et al*., 1992)

Sexual maturity is reached during the adult stage. This stage is usually only composed of 2 to 3 chambers, and is characterized by small changes in external morphology, like for instance the development of secondary apertures in Globigerinoïds (Brummer *et al*., 1987). A fifth stage ends the planktonic foraminifera ontogeny, *i.e.*, the terminal stage, representing the onset of reproduction (Brummer *et al*., 1987). Even if the individual is already mature during its adult stage, the terminal stage has been added because reproduction induces morphological changes that are visible on the external test and are directly related to completion of reproduction (Brummer *et al*., 1987). In many species indeed, the terminal stage is characterized by the addition of aberrant, kummerform chambers related to reproduction rather than normal growth (Hemleben *et al*., 1989). Reproduction ends the life cycle of the foraminiferal individual.

5.3 Material and methods

5.3.1 Material

The single sample of ODP Site 667, which was selected at a time-level of 3.2 Ma (Mid-Pliocene) forms the basis for the present ontogenetic investigation in menardellids. This locality was selected for its high content in menardellids, its excellent carbonate preservation, and because specimens display a very high morphological diversity at this locality (Mary and Knappertsbusch, in press). The age model for Site 667 follows the one of Mary and

Knappertsbusch (in press), based on the combination of the microfossil range chart of the Neptune database and the ODP Initial Report for Leg 108.

A few cubic centimeters of bulk material was first disaggregated in boiling water, and then sieved through a 63µm sieve and gently washed under tap water. The fraction <63µm was retained but was not further used in this study. The sample was oven-dried at 40°C during 24 hours. Dry sediment was then sieved into seven size fractions : <100µm, [100-200µm], [200-300µm], [300-400µm], [400-500µm], [500-600µm] and >600µm. The fraction <100 µm was disregarded for analysis. Approximately 60 menardellid specimens per size class were then randomly selected among undamaged individuals showing no sign of missing chambers, for a total of 350 specimens. Specimens were then visually classified into *G. (M.) menardii, G. (M.) limbata*, and *G. (M.) multicamerata* according to Kennett and Srinivasan (1983) and following morphological criteria statistically identified by Mary and Knappertsbusch (in press). The fraction <100 µm was disregarded for analysis.

5.3.2 Micro-dissolution of the umbilical side

In contrast to the time-consuming serial dissection method of Huber (1994) and Huang (1981), a new protocol was developed, allowing a simple but accurate and more time efficient method, to study the interior geometry of planktonic foraminifera under a binocular microscope. Instead of physically dissecting the shell, the umbilical face was removed using hydrochloric acid (HCl) until juvenile portions of the shell could directly be observed.

Menardellid specimens are first mounted on a standard micro-faunal slide, with umbilical side facing up, using a watery solution of paper glue, in which we add few drops of a solution of sodium hydroxide (NaOH). The volume of this alkaline solution must be sufficient to embrace the entire spiral side, leaving only the keel and the umbilical side above. This solution limits the reaction of HCl with calcite on the spiral side of the shell. The dissection must start immediately after the specimen is put in the glue, before the solution dries.

Removal of the umbilical side was done manually using a fine paintbrush soaked in a concentrated solution of HCl. In every individual whorl the umbilical face of chambers were gently brushed away in the acid microenvironment until the proloculus became visible. When reaching the most juvenile chambers, little extra acid was added by subtly touching them with the paintbrush. Then the reaction was interrupted by addition drops of NaOH. Repeatedly brushing over the chambers leads to selective removal of calcite layers of the chambers.

Once opened, specimens are gently rinsed with tap-water to remove dissolution remnants and infillings, and then placed in a bath of NaOH solution during 48h to neutralize remaining acid. The specimen was rinsed again with water before being stored in standard micro-faunal slides. The entire procedure takes 10 to 15 minutes in average per specimen.

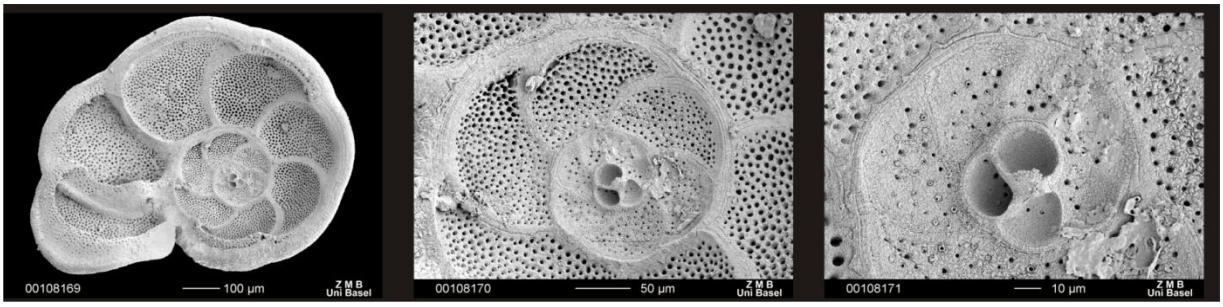

Figure 5.1: Example of a serially dissected specimen using the dissection by dissolution technique.

Serial micro-dissolution is very time- and cost-efficient for accessing the ontogenetic growth pattern of planktonic foraminifera in comparison with classic physical shell dissections. Some limitations, however, arise through the use of acid, which may obviously destroy specimens if treated too long. The rate of loss depends on shell size, but also on geometry, and of course on the investigator's practical experience: small, highly-spired specimens are very difficult to open. For example, in the size fraction 100-200µm 97 specimens were treated to obtain 60 successful preparations (experimental loss of 38%), whereas only 8% of the specimens were lost in the 500-600µm fraction. A total of 450 specimens were selected from sample ODP Site 667, of which 350 specimens could be successfully prepared for our ontogenetic measurements. Another disadvantage is the post

experimental nucleation of salt crystals probably byproducts of the dissolution reaction, after extended exposure of the specimen to air, which eventually may cover and obscure the innermost chambers.

5.3.4 Imaging and measurements

Imaging of opened specimens was carried out using a Philips XL30 FEG ESEM at the microscopy center of the University of Basel. Specimens were mounted on SEM stubs in homologous positions before coating them with gold. Measurements were extracted from the pictures using the software ImageJ, which is in the public domain (http://rsb.info.nih.giv/ij/) and the commercial package Adobe Photoshop. For every specimen, the total number of chambers was determined; the cross sectional area and perimeter of each individual chamber was measured. The number of chambers per whorl was also counted, starting from the deuteroconch. The axial diameter of the shell was manually measured after each whorl. In order to compare with external morphology, the number of chambers in the external final whorl was counted, beginning from the last (adult) chamber.

For every chamber, the Circularity Factor (Fci) (Kucera and Kennett, (2002)) and Growth rate (Gr) were calculated. The Circularity Factor is a shape indicator and represents the difference between the perimeter of an object and the one of a disc with the same area, following the formula:

Circularity Factor: $Fci = P / 2 \sqrt{(\pi A)}$

Where P is the perimeter and A the cross sectional area of a given chamber. It equals 1 if the object is perfectly circular, and decreases for elongated morphologies. In this study, the Circularity Factor is used as a mean to characterize changes of chamber shape through ontogeny. The Growth rate is calculated from neighboring chamber areas: it represents the relative incremental increase from one chamber to the next, following the formula:

Growth rate: Gr = 100*(An -A (n+1))/An

Where An stands for the cross sectional area of the nth chamber and An+1 for the one of the n+1th. Gr is generally negative when the specimen reaches adultness, because of successive reduction in size of the chamber in the adult (Wei *et al*., 1992; Huber, 1994).

The number of pores per surface unit, *i.e.*, pore density, can be accurately estimated per individual chamber from the inner surface of the test. Pores are however fragile structures, susceptible to infilling or secondary calcification during ontogeny (Brummer *et al*., 1987). The use of acid often leads to enlarged pore diameters, preventing precise measurements of pore size or geometry (pers. obs.). The last chambers are more likely to be damaged by the acid than the early whorl: the thicker is the wall, the longer must be the exposure time to the acid to dissolve it, the more the pores are edged by the acid. For all these reasons, a selection of our best preserved specimens was done for our morphometric analyses, and only pore density per chamber was measured.

Two different procedures were involved to calculate pore density. For juvenile whorls, the number of pores is counted visually. When the number of pores per chamber is too high (arbitrarily defined as over 50), the particle analyzer of the software ImageJ was used on the entire chamber. The total number of pores is then divided by chamber area to obtain pore density (pores per μm^2). In case of altered surface or if pores are filled by sediments or dissolution residues, non affected sub-sample areas were taken. The dimension of the sub-sample is chosen to be the closest possible to chamber area.

5.4 Results

5.4.1 Cross sectional area with respect to the total number of chambers

Figure 5.2 summarizes the ontogenetic growth and represents the raw data for all 350 specimens of *G. (M.) menardii*, *G. (M.) limbata* and *G. (M.) multicamerata* together. Figure

5.2A describes the growth of cross-sectional areas of successive chambers, which represents an

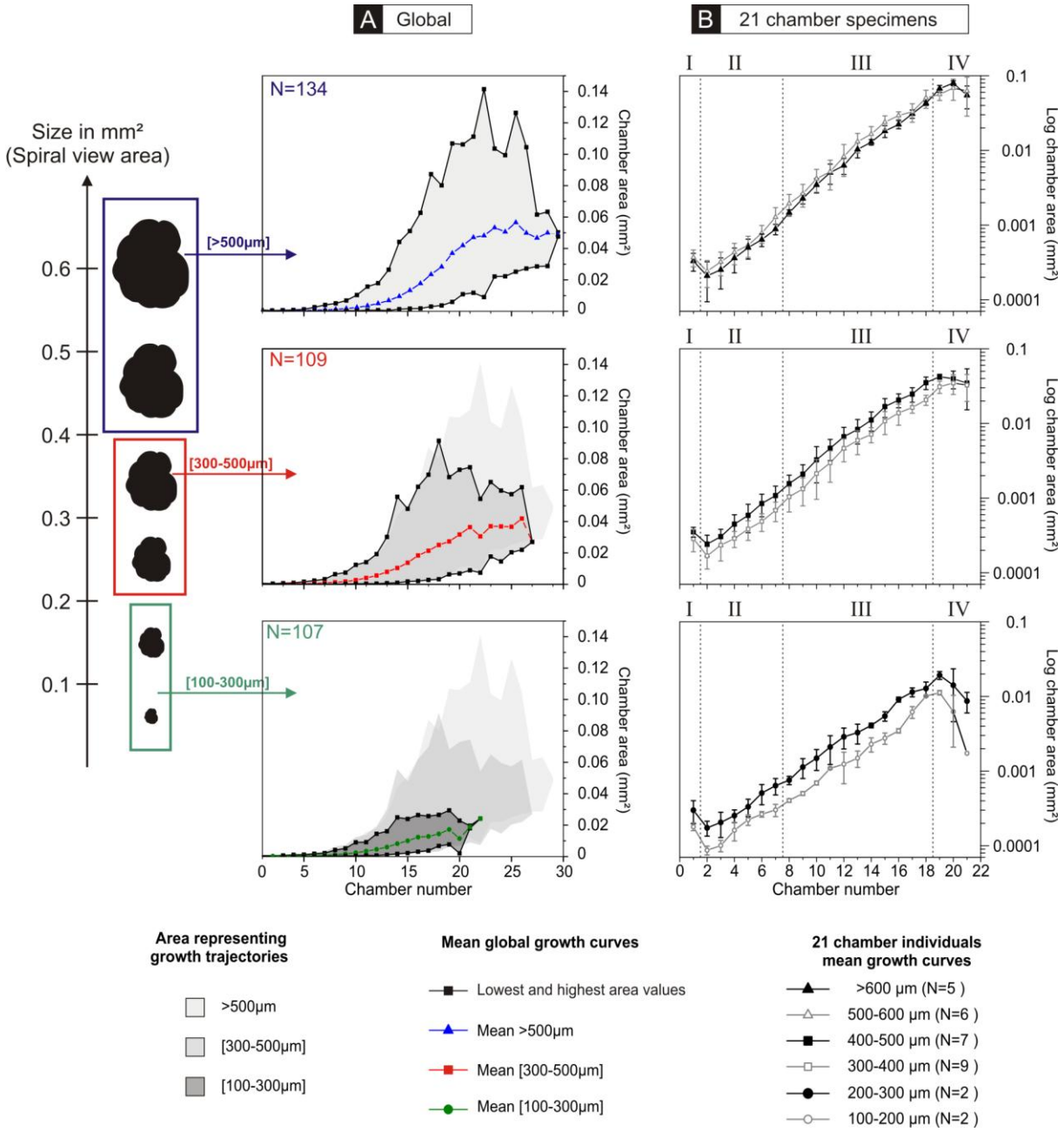

Figure 5.2: Size dependant ontogenetic growth of Pliocene menardellids. (A) cross sectional area of individual chambers in relationship with the total number of chamber. The six analyzed size classes are grouped into three size fractions: 100-300 µm, 300-500 µm and >500 µm. Shaded areas are delimited by maximum and minimum value and represent preferential growth trajectories. (B) Size dependant growth curves at constant number of chambers (21 chambers, which correspond to the average total number of

chambers of all investigated specimens). The six investigated size classes are represented, respectively 500-600 µm and >600 µm (B1), 300-400 µm and 400-500 µm (B2), (B3) 100-200 µm and 200-300 µm. The I to IV intervals represents the different growth stages (I: embryonic II: juvenile III: neanic IV: adult).

accurate mean to describe the rate of chamber increase throughout ontogeny. The growth curves of specimens in the six size classes are first grouped into three diagrams, respectively the large (>500µm), medium (300-500µm) and small fraction (100-300µm). For clarity reasons, only the mean growth curves and the maxima and minima for chamber size increase are shown.

Growth profiles of the three size classes parallel each other and entirely overlap for the first 12 chambers (Figure 5.2A). The variability in chamber area increases thereafter. Specimens reach high chamber area values between chamber 19 and 26. Interestingly, the total number of chambers shows comparatively little variation between the three size classes. On average, the small fraction shows values of total chamber number of 17, versus 21 and 24 for the medium and large fraction, respectively (not shown on Figure 5.2).

Intra-class variability of chamber number is however high (from 12 to 30). In order to remove the effects of chamber number variations, and for better identification of growth stages, specimens with 21 chambers are plotted separately for the six investigated size fractions (Figure 5.2B). The value of 21 chambers was chosen because it represents an average chamber number for the entire sample. Each of these growth curves can be subdivided in 5 different phases, which correspond to the well-known ontogenetic stages identified in planktonic foraminifera (Brummer *et al*., 1987) (Figure 5.2B for mean curves by size-fractions, Figure 5.3 for examples of individual growth curves).

The first ontogenetic stage (I) of menardellid globorotalids consists of the proloculus. Individual growth starts with the juvenile stage (II), which is marked by a distinct decrease of cross-sectional chamber area values at chamber number 2. This stage approximately spans 6 chambers with a constant chamber area increase during the entire stage. On average curves, the transition between the juvenile and the neanic stages is constant, although it can be marked by a pronounced slope break at the end of the juvenile stage in individual growth curves (see Figure 5.3). On average, the neanic stage (III) does not differ significantly from the juvenile (II), although variability exists, which is different in other planktonic foraminiferal species

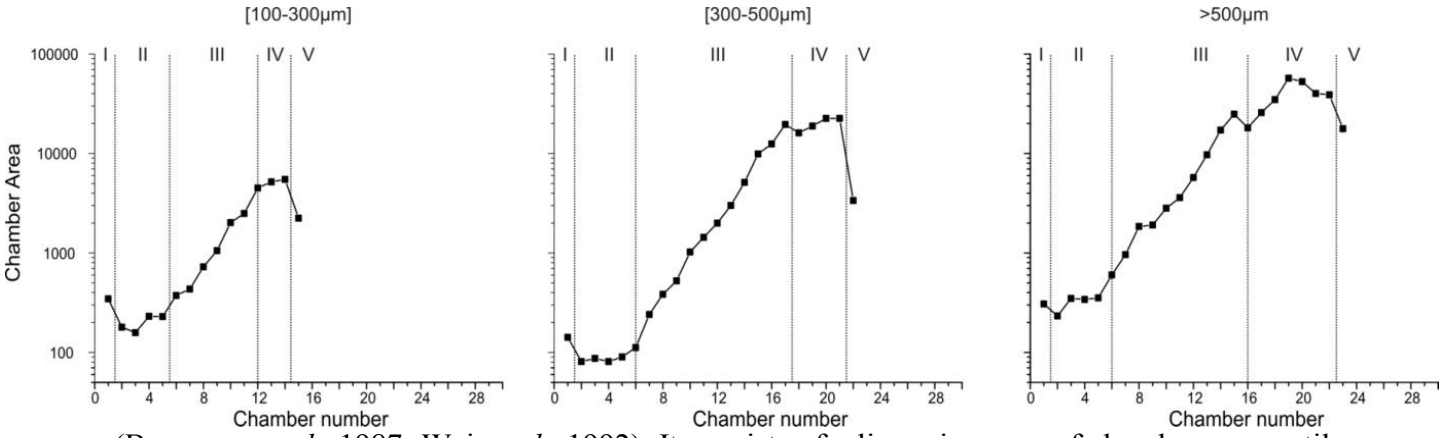

(Brummer *et al*., 1987; Wei *et al*., 1992). It consists of a linear increase of chamber area until adultness. The length of this stage (in chamber number)

Figure 5.3: Example of individual growth curve (chamber cross sectional area versus number of chamber), for three menardellid specimens in the three size fractions. The specimens are selected to illustrate case of well defined transition between growth stages and to have reached reproduction. The I to V intervals represents the different growth stages (I: embryonic II: juvenile III: neanic IV: adult V: terminal).

shows a relatively high variability regardless of the size fraction. Stage IV corresponds to the sexual maturity of the menardellids, and is manifested by a peak or a plateau, after which the growth curve starts to decrease. The length of this stage (in chamber numbers) strongly differs from one individual to the next, *i.e.*, it ranges from 2 to 12 chambers.

The fifth stage, the terminal stage, is not well visible on averaged growth curves, but can well be observed in individual specimens (Figure 5.3). In each size class, specimens with terminal kummerform chambers are observed. Kummerform chambers are associated with gametogenesis (Hemlebem *et al*., 1989) indicating completion of the planktonic foraminiferal maturation (Brummer *et al*., 1987; Wei *et al*., 1992), [not visible in Figure 5.2]. In the pilot ontogenetic study of Brown (2007) similar observations for extant menardellids are described as well. In this context, specimens from the smallest size fraction bearing kummerform chambersrepresent mature individuals, which strongly contradicts the established view that small specimens equal juvenile forms.

5.4.2 Specific ontogenetic trends of Pliocene menardellids

Specific growth curves are calculated by averaging the cross sectional area of individual chambers for all adult specimens of the three chosen species separately. Adults are isolated from immature specimens on the basis of their growth curves: individuals showing a distinct decrease in growth rate at the end of their development are considered mature, following the planktonic foraminiferal ontogenetic model of Brummer *et al*. (1987).

Though it is often difficult to differentiate between menardellids on the basis of their external shell morphology (Knappertsbusch, 2007; Mary and Knappertsbusch, in press), *G. (M.) menardii, G. (M.) limbata* and *G. (M.) multicamerata* are clearly discernible using the ontogenetic growth curves (Figure 5.4A). Although there is overlap in the earlier chambers, growth trajectories show specific patterns after chamber number 7, which corresponds to the onset of the neanic stage. *G. (M.) limbata* is characterized by a sharp increase of growth leading to larger chamber area. *G. (M.) menardii* and *G. (M.) multicamerata* show a lower slope in comparison, the latter is characterized by constant mean chamber area values up to the 20th chamber. *G. (M.) menardii* shows the lowermost values, located in the lowermost part of the diagram (Figure 5.4A).

To further characterize the distribution of menardellid specimens according to their ontogeny, we show the distribution of the cross sectional area of the penultimate chamber with respect to the total number of chambers of adult specimens (Figure 5.4B). A contoured frequency diagram is used to show the density distribution of the individuals. The penultimate chamber is selected to summarize the ontogenetic adultness position on the growth curve, as the variability in the chamber area is higher in the terminal development stage. This chamber was selected instead of the last one because it is less affected by kummerform diminution or flexure of the terminal chamber. The total number of chambers is chosen as a proxy for relative ontogenetic time.

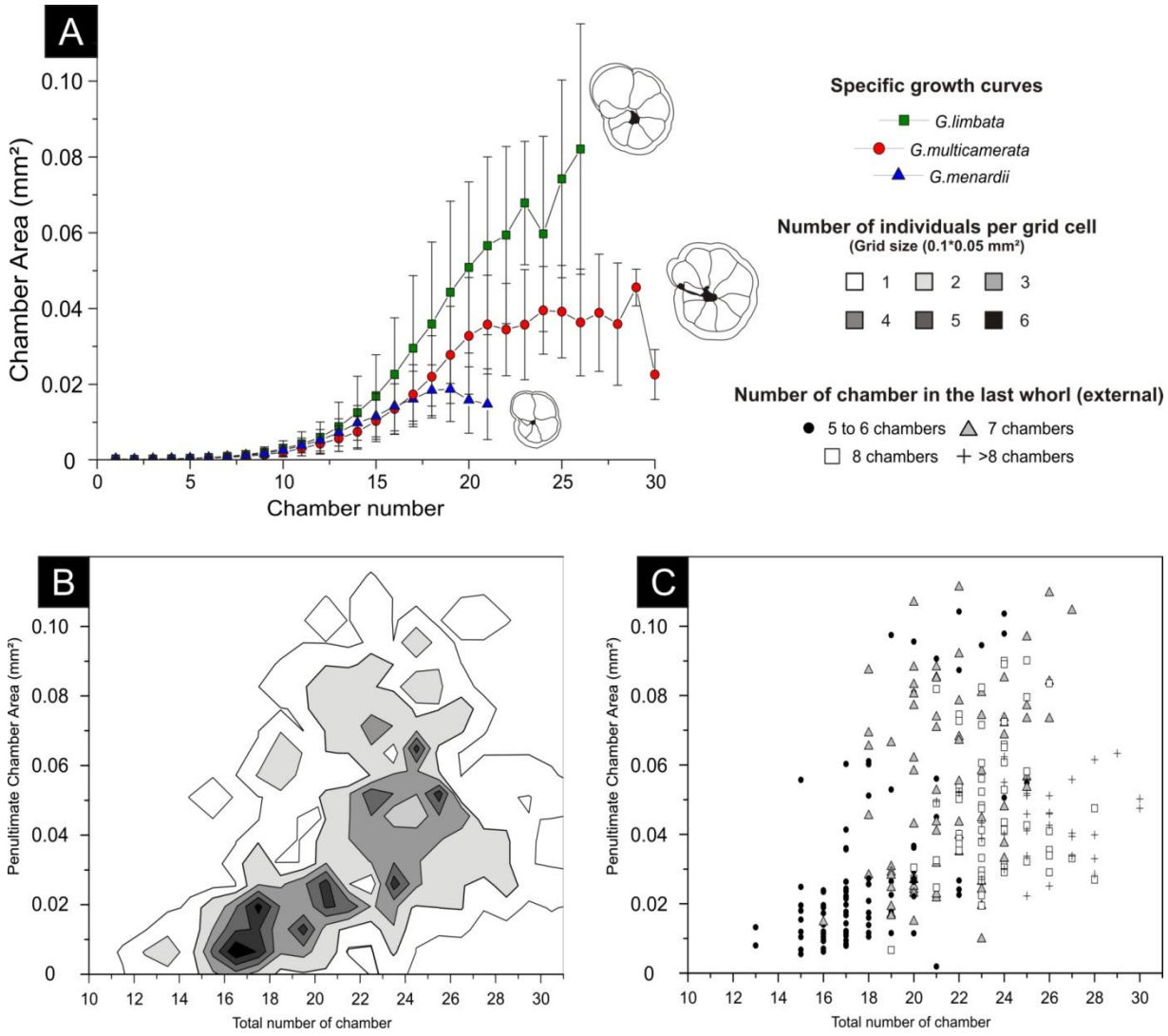

Figure 5.4: Ontogenetic characterization of the three menardellid species *G. (M.) menardii*, *G. (M.) limbata* and *G. (M.) multicamerata.* Only specimens explicitly reaching the adult stage are represented (N= 259) (A) Plot of the average cross sectional area of chambers of adult specimens in respect to the chamber number per menardellid species. (B) Contoured frequency distribution showing density of adult specimen ontogenetic distribution. The penultimate chamber is selected to summarize the ontogenetic trajectory and is plotted versus the total number of chamber. (C). Scatter plot of the penultimate chamber area versus total number of chamber. Specimens are represented according to their number of chamber in the last whorl, showing preferential distribution of chamber number according to the three species.

The distribution of adult specimens clearly shows three clusters, which reflect specific differences in growth curves. As a comparison with traditional taxonomy, the external number of chambers in the final whorl is shown in Figure 5.4C. The result is in agreement with the

formal classification of Pliocene menardellid morpho-species according to their number of chambers (Kennett and Srinivasan 1983; Bolli and Saunders 1985). *G. (M.) menardii* holds commonly 5 to 6 chambers in the last whorl, versus 6 to 8 for *G. (M.) limbata*, and 7 to up to 12 for *G. (M.) multicamerata*.

5.4.3 Ontogenetic variability in number of chambers per whorl

From the external side, menardellids share a near to homeomorphic morphology, differing mostly in number of chambers in the last whorl. This feature is traditionally considered as the most important taxonomic parameter to classify Pliocene menardellid morpho-species (Kennett and Srinivasan 1983; Bolli and Saunders 1985). The number of chambers in the final whorl (external) is a strong allometric feature (Mary and Knappertsbusch, in press): small specimens commonly hold 5 to 6 chambers in the last whorl, whereas the largest ones bear up to 12. Our sample reflects such results (Figure 5.5A). It is therefore interesting to investigate the evolution of chamber number per whorl during the ontogeny. In this purpose, we plot the number of chambers for each whorl in respect to axial diameter frequency distribution, from the proloculus to the fourth (final) whorl (Figure 5.5B-E).

Adult menardellids show between 2 and 4 whorls. Prolocular diameters are comparable for all investigated menardellids, showing a unimodal distribution from 10 to 37 µm (Figure 5.5E). All measured proloculi display a rounded outline with a distinct flattening of the wall at the location where the deuteroconch joins. Cross sectional area of the proloculus shows a unimodal distribution as well, distributed from 88µm² to 744µm².

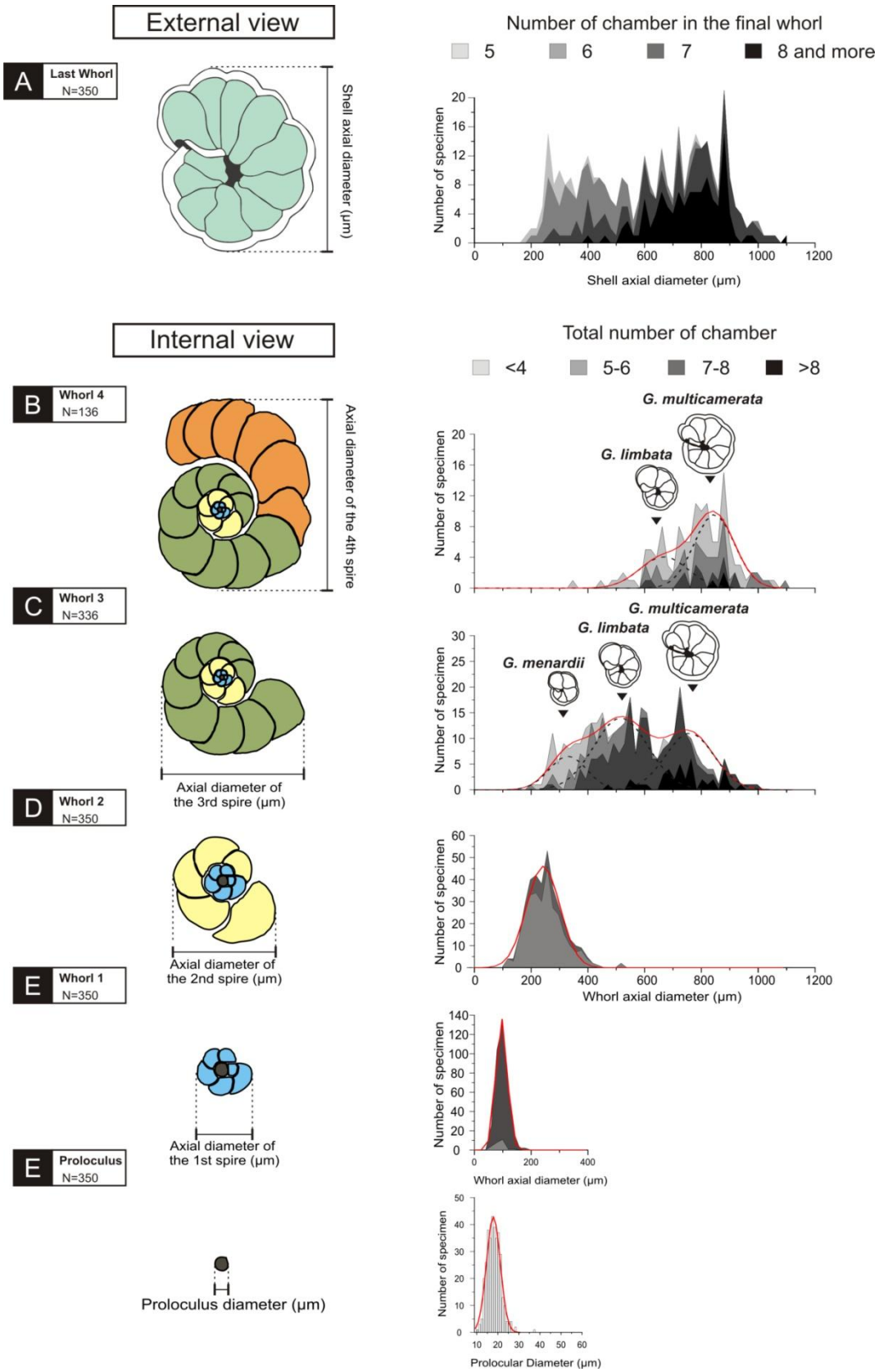
External view
A
Last Whorl
N=350
Shell axial diameter (µm)
Number of chamber in the final whorl
5
6
7
8 and more
Number of specimen
Shell axial diameter (µm)
Internal view
B
Whorl 4
N=136
Axial diameter of the 4th spire
C
Whorl 3
N=336
D
Whorl 2
N=350
Axial diameter of the 3rd spire (µm)
E
Whorl 1
N=350
Axial diameter of the 2nd spire (µm)
E
Proloculus
N=350
Axial diameter of the 1st spire (µm)
Proloculus diameter (µm)
Total number of chamber
<4
5-6
7-8
>8
G. multicamerata
G. limbata
G. menardii
Whorl axial diameter (µm)
Prolocular Diameter (µm)

Figure 5.5 (on previous page): area plot of the evolution of the relative proportion of number of chamber per whorl in comparison with shell diameter frequency distribution. Data is shown for each whorl. The distribution of the three menardellid species, *G. (M.) menardii*, *G. (M.) limbata* and *G. (M.) multicamerata* are represented by Gaussian fitting when possible (B and C). Otherwise, the entire frequency distribution is fitted (D-E-F). (A) composition of chamber number in respect with diameter frequency distribution per last whorl (external).(B-D) distribution of the chamber number in respect with shell diameter frequency distribution in the forth, third and second whorl respectively. Note the drastic reduction of chamber number diversity in the early whorl. (E) proportion of the number of chamber in the first whorl in respect with shell diameter frequency distribution. The frequency distribution of prolocular diameter is shown in addition.

The first whorl, starting with the deuteroconch, displays a remarkably constant number of chambers (Figure 5.5E, in blue), showing preferentially between 6 to 8 chambers with a strong dominance of 7 chambers (81% regardless of the species). Axial diameter shows an unimodal distribution, centered on 100µm. Similarly, the composition of chamber number in the second whorl is also fairly uniform, showing a small reduction of chamber number in comparison to the first whorl, holding rather 6 than 7 chambers (65%, Figure 5.5D). The shell reaches a diameter of 245µm in average.

In the third whorl chamber-per-whorl variability becomes suddenly larger. In comparison to the previous whorls, this number changes in respect to shell diameter values: small specimens reaching three whorls display a lower chamber number, whereas large specimens are characterized by higher values. The axial diameter of the third whorl is characterized by a strong variability as well, spanning between approximately 200 and 1000 µm. The frequency distribution of the axial diameter in the third whorl can be decomposed in three distinct modes, which correspond to the three menardellids, determined by Gaussian best fitting (Figure 5.5C). The first is located at 322 µm and includes forms with 1 to 6 chambers in the third whorl (more commonly 3), the latter being incomplete. Although it could be interpreted as an evidence of immaturity, some of these individuals display a deformed kummerform chamber, which means that they have undergone reproduction. The second mode is situated at 505µm and is composed of 5 to 8 chambers per whorl, and the third has a modal value of 743 µm and displays 8 to up to 12 chambers per whorl.

The frequency curve for specimens having four whorls can be decomposed in two modes with respect to their axial diameter values, corresponding to the second and the third mode of the third whorl. They show slightly larger modal sizes (670 and 858 µm, respectively). The fourth whorl was observed to never be completed in our Mid-Pliocene sample, regardless of the number of chambers it holds. The number of chambers is mostly less than 6 and is comparable for every specimen reaching 4 whorls. There is no apparent correlation between the number of chambers in this 4th final whorl (internal morphology) and the number of chambers in the final whorl (external morphology).

In summary, differences in shell morphology are visible only when at least three whorls are reached. Before that, all menardellid species share the same number of chamber per whorl, independently on the ontogenetic age.

5.4.4 Intra-specific variability of ontogenetic stages

The high number of investigated specimens allows the detailed study of the intra-specific variability. To better visualize this pattern, the relative length of the ontogenetic stages were plotted with respect to the total number of chambers, which is attained until maturity (Figure 5.6). For each of the three species, specimens from the assemblage were re-grouped specifically according to their total number of chambers, *i.e.* 13-21 (*G. (M.) menardii*), 17-25 (*G. (M.) limbata*), and 20-30 (*G. (M.) multicamerata*). These numbers represent the specific minimum and maximum total number of chambers. For each group, the profile of the mean relative growth rate (Gr) was studied for successive chambers. The number of chambers is used as a relative age of the individual.

Gr profile variations allow the separation of the different growth stages. Normalization of variability enhances the transition between the juvenile and the neanic stages in comparison to growth curves (cross sectional chamber area versus chamber number). Such transitions are then marked by a pronounced and stable increase of Gr values. In contrast, individual maturity of the menardellid shell is indicated by a distinct plateau within the falling trend of Gr. This corresponds to a slow-down of growth while becoming adult (Brummer *et al*., 1987; Wei,

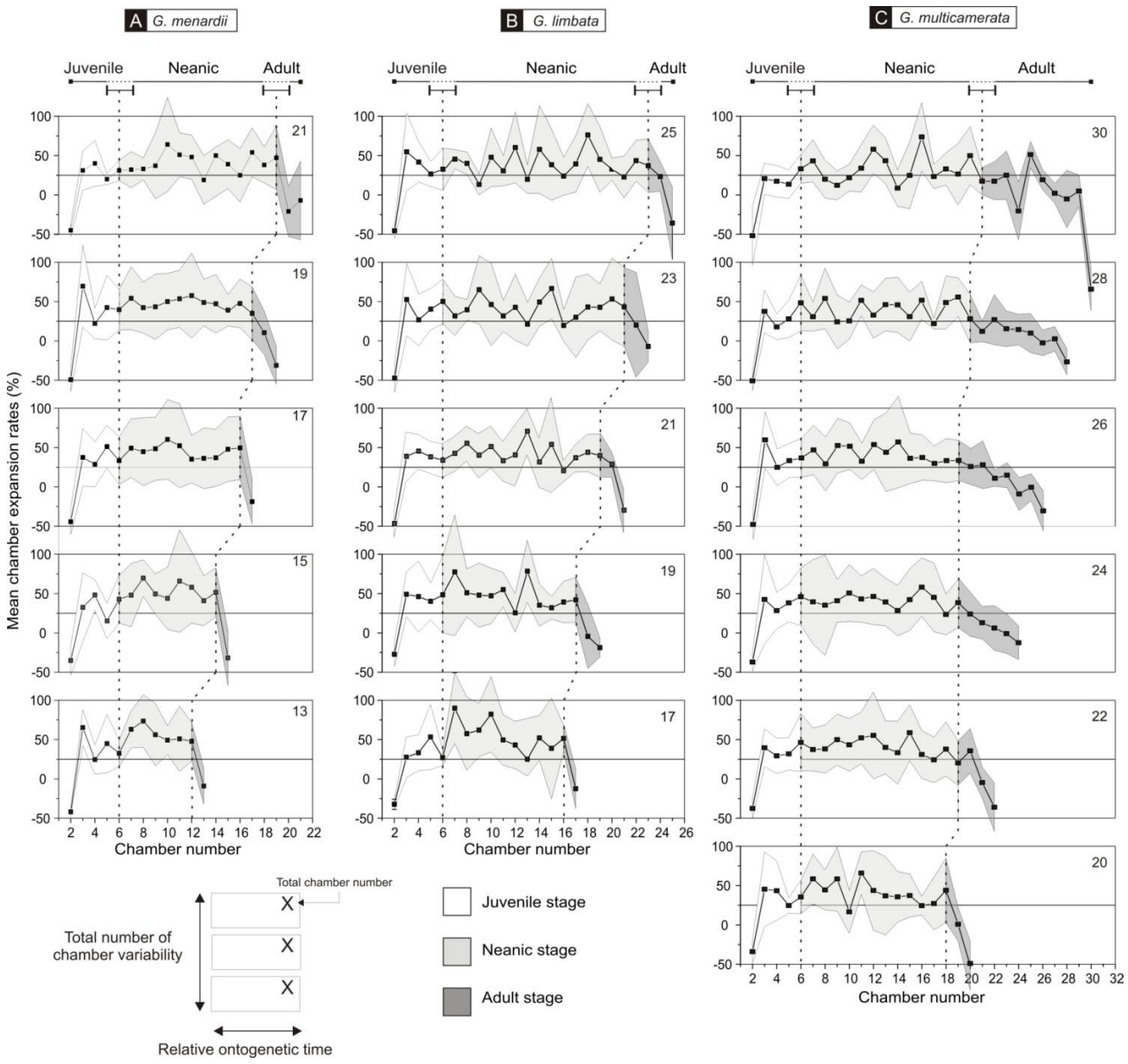

Figure 5.6: intra-specific variability of ontogenetic stages in the three species *G. (M.) menardii, G. (M.) limbata* and *G. (M.) multicamerata*. Specimens are classified according to their total number of chambers, indicated in the up-right corner of each diagrams, from the minimum to the maximum number of chamber. Each individual diagram represents the average relative incremental growth rate (Gr) per chamber for a given total number of chambers. The relative ontogenetic length (in number of chamber) is represented for three growth stages: juvenile (light grey), neanic (grey) and adult (dark grey). Limits of the three growth stages are delimited ± 1 chamber. (A) plots of Gr in function of chamber number for the species *G. (M.) menardii*. (B) plots of Gr in function of chamber number for the species *G. (M.) limbata*. (C) plots of Gr in function of chamber number for the species *G. (M.) multicamerata*.

1992). The comparison of different growth curves suggests that adultness is indicated by a pronounced decrease of Gr by more than about 25% (Figure 5.6). The approximate limits of the so identified growth stages are marked on growth diagrams with a precision of ± 1 chamber. Intra-specific variation is displayed by showing the evolution of the different stages with respect to changing number of chambers (Figure 5.6).

Average Gr values per chamber show only little variation within and between species. *G. (M.) menardii* and *G. (M.) multicamerata* display a rather similar, constant chamber increment by about 50% (Figure 5.6A and 5.6C, respectively). In comparison, the growth rate seen in *G. (M.) limbata* is slightly higher during the neanic stages, rather reaching 75% (Figure 5.6B). The intra-specific neanic variability of Gr is, however, important between specimens. Gr values are higher during the neanic stage when the total chamber number is reduced.

The number of chambers of the juvenile stages (± 1 chamber) is remarkably constant regardless of total chamber number variability. This stage generally lasts until the 6th chamber in all three species. In contrast, the neanic stage shows a broader variability in *G. (M.) menardii* (Figure 6 A). On average, specimens holding 13 chambers show a neanic stage of 6 chambers versus 13 for the individuals with 21 chambers. Similarly, the neanic stage of *G. (M.) limbata* increases with the number of chambers, ranging from 10 to 18 chambers (Figure 5.6B). The adult stages are comparable in both species, occurring only in the last few chambers.

In contrast, the neanic stage of *G. (M.) multicamerata* displays similar values regardless of total chamber number, and is composed of 12 to 15 chambers (Figure 5.6C). Most of the variability in development is explained by variations of number of chambers in the adult stage, which varies from 3 to 9 chambers in average, although higher variability occurs when individual specimens are considered. Specimen maturity is represented by a constant decrease of growth rates below 25% to reach negative values in the terminal chambers. This species shows an extension of the adult stage in comparison to the other species.

5.4.5 Morphological changes associated with growth stages

In order to emphasize the differences in the timing of development of morphological features, the evolution of chamber shape and pore density through ontogeny was investigated (Figure 5.7). Both indicate the transition from one developmental stage to another within individual specimens. In order to better recognize growth stages, the incremental relative growth rate (Gr) is also displayed in Figure 5.7. Pore density is a good indicator of exchange between an organism and its environment, or more generally of trophic behavior (Huber, 1994). It can therefore be interpreted as a proxy for metabolism. Individual chamber shape is known to be a significant parameter in globorotalid taxonomy. Chambers have been classified according to their shape on the spiral side (Cifelli and Glaçon, 1978; Cifelli and Scott, 1986). Among others, three distinct morphologies have been described by the latter authors, based mainly on the angular position of the leading margin and on radial elongation (see Figure 5.7): Type I represents rounded, broadly radial chamber morphologies. A and B-Type morphologies are characterized the degree of elongation in the direction of coiling. Chamber type C is a typical menardellid morphology, which is characterized by radial elongation (see comparison of the different chamber types on Figure 5.7). Variation between types A to C describes the amount of radial rotation of the chamber outline. Chamber shape is quantified by the Circularity factor (Fci, see section on Imaging and measurements under Materials and Methods).

Both pore density and Fci parameters show pronounced variation from juvenile to neanic and from neanic to adult stages. The morphology of individual chambers of *G. (M.) menardii* shows a stepwise change during ontogeny (Figure 5.7A). Fci values are commonly high during the prolocular and juvenile stages (0.8), which correspond to circular, rounded Type I morphologies, associated with immaturity in *G. (M.) menardii*. An abrupt decrease of chamber circularity marks the onset of the neanic stage, to reach an approximate plateau around 0.65 Fci value. Chamber morphology becomes more radially compressed and elongated in the coiling direction, corresponding to type B chamber. Fci increases again at the transition with the adult stage to reach 0.7, developing radial elongated, Type C chambers.

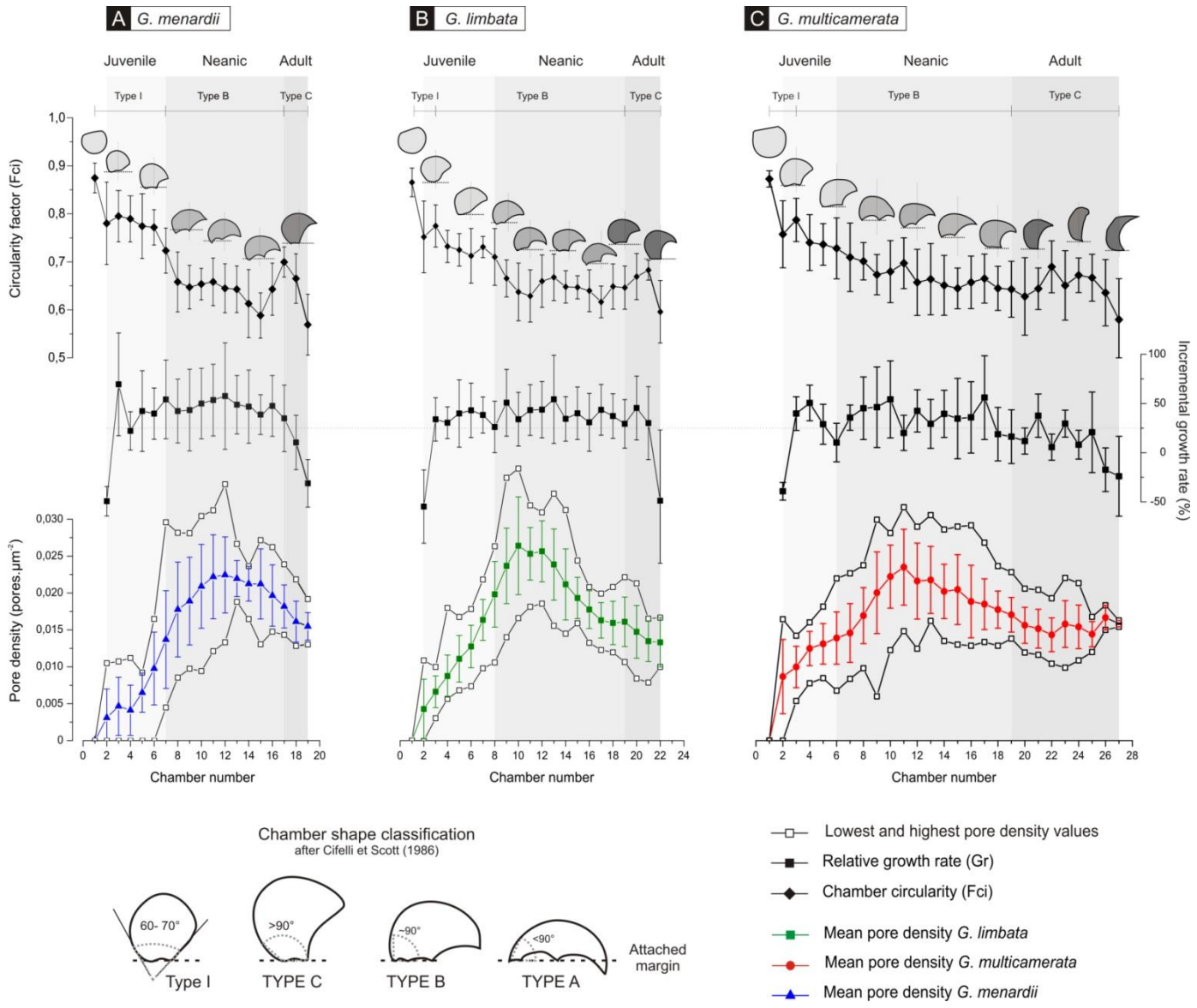

Figure 5.7: specific variability of pore density and chamber shape change in respect to ontogenetic growth. For each species, average pore density, average growth rate and average circularity factors are displayed. To visualize intra specific variability in our sample, minimum and maximum values of pore density are added. Chamber shape changes are represented using schematic drawing of one specimen chamber for each species. This specimen is arbitrarily selected for showing Fci values closed to the specific mean. Chamber type classification is added (after Cifelli and Scott (1986) (A). Fci, Gr and pore density of successive chambers of *G. (M.) menardii*. Juvenile, neanic and adult growth stages are represented. (B). Fci, Gr and pore density of successive chambers of *G. (M.) limbata*. (C). Fci, Gr and pore density of successive chambers of *G. (M.) multicamerata.*

A similar trend is observed in *G. (M.) limbata* (Figure 5.7B), and *G. (M.) multicamerata* (Figure 5.7C) although Fci values are distinctly lower in average during the juvenile stage (0.8 in *G. (M.) menardii* and 0.7 in the two other menardellid species). These two species develop chamber type B earlier in their ontogeny, during the juvenile stage. Transitional chamber shape change in the beginning of the neanic stage is more gradual, especially in *G. (M.) multicamerata*. In this species, Fci remains relatively low during the adult stage as well. This species developed extremely axially elongated Type C chambers with decreasing Fci values (Figure 5.7C).

Likewise, individual chamber pore density shows also three different phases. Values in *G. (M.) menardii* are minimal during the juvenile stage; then strongly increase at the end of the juvenile stage to reach a peak in the middle of the neanic stage. They subsequently decrease around chamber number 14-18, marking the onset of the adult stage. *G. (M.) menardii* chamber pore density (Figure 5.7A) during the juvenile stage is indeed very low in average (0.05 pore.μm^{-2}). Individuals showing no pores in the early chambers are frequent. Pore density values increase strongly to reach an average of 0.022 pore.μm^{-2} towards the middle of their ontogeny, and finally decrease gradually towards the adult stage.

The position of the pore density peak in the neanic stage (around chamber n°11) is similar in the three menardellid species. At the opposite the development of pore density during the juvenile stage is variable. In comparison with *G. (M.) menardii*, the pore density profile of *G. (M.) limbata* shows a more gradual transition from the juvenile to the neanic stage (Figure 5.7B). The number of pore per surface increases constantly from the deuteroconch to maximum values at chamber n°10-12. This species reaches, however, higher values of pore density in comparison to its ancestor *G. (M.) menardii*, which correspond to higher incremental growth rate at the beginning of the neanic stage (between chamber n°9 and chamber n°14). *G. (M.) multicamerata* developed relatively high pore density at the very beginning of the juvenile stage (0.012 pore.μm^{-2}). Pore density values in the early ontogeny are comparable to the situation observed in the adult stage. The latter is longer in *G. (M.) multicamerata* showing an extended plateau at the end of the pore density curve.

5.5 Discussion

5.5.1 Contribution to menardellid classification

The menardellid classification has been a matter of debate for a long time (see Brown, 2007, and Knappertsbusch, 2007 for reviews). Confusion originates from multiple clinal morphological changes, strong convergence in allometry, and from the large individual morphological plasticity (Knappertsbusch, 2007; Regenberg *et al*., 2010; Mary and Knappertsbusch, in press). The taxonomy of Mid-Pliocene menardellid has been recently revised by Mary *et al*., (submitted). They concluded that the classification in use and based solely on the number of chambers in the final whorl may sometimes be misleading. Shell size differences are an at least equally important criterion to differentiate between different menardellid populations.

Ontogenetic data confirm that Pliocene variants of *G. (M.) menardii* are separated from the two other menardellid species by a distinctly smaller test, which corresponds to morphotype MA identified in Mary and Knappertsbusch (in press). In contrast, large 5 and 6-chambered forms, traditionally associated with *G. (M.) menardii*, do not show any significant ontogenetic or developmental differences with 7-chambered forms, which are assigned to *G. (M.) limbata*. Small mature specimens show distinct morphological features and ontogenetic growth pattern (Figure 5.5). A distinction between small and large Miocene *G. (M.) menardii* was already suggested in DSDP Leg 4 by Bolli (1970) in the Pliocene of the Mediterranean Sea. According to these authors, menardellids could be classified into small, 5 to 6 chambers individuals under the informal name "menardii A", whereas the large specimens having 5 to 7 chambers could be designated as "menardii B". Mary and Knappertsbusch (in press) and Mary *et al*., (submitted) demonstrated that a similar pattern existed in the Pliocene time-slice as well. The ontogenetic comparison of our specimens is in agreement with this opinion. Differences in global shell size are therefore a necessary criterion to differentiate Pliocene menardellid species.

In addition, the present observations show that the total number of chambers in adult specimens is an important characteristic to distinguish between *G. (M.) menardii*, *G. (M.) limbata* and *G. (M.) multicamerata*, although this parameter is difficult to obtain from the

external surface of the shell. Menardellid juvenile stages mainly span 6 to 7 chambers (*i.e.* neanic stages starting at the chamber number 7-8), and no specific variation could be observed. The number of chambers per whorl is variable through ontogeny, but is strongly convergent in the early whorl. Juvenile and neanic individuals therefore remain virtually impossible to distinguish from their external morphology: the majority of them has 7 chambers in the first whorl, while the second whorl preferentially shows 6 chambers in the early neanic stage. Consequently, premature specimens of *G. (M.) multicamerata* or *G. (M.) limbata* may easily be misclassified as *G. (M.) menardii*. Nevertheless, the number of chambers in the last whorl can be applied to some degree to identify specimens belonging to *G. (M.) multicamerata*, especially when this number is higher than 8.

5.5.2 Compared development of menardellid species

The present study provides a unique opportunity to compare the developmental sequences of planktonic foraminifera within a phylogenetic lineage, in order to investigate heterochronic patterns. The identification of such processes in planktonic foraminifera has only been based, thus far, on allometric studies (Wei *et al*., 1994, Kelly *et al*., 1996, Kelly *et al*., 2001, Quillévéré *et al*., 2002.) These studies rely on the assumption that size reflects ontogenetic time (the larger the organism is, the longer is the period of maturation). As pointed out by evolutionary biologists, in some cases, this hypothesis may not be true (Klingerberg, 1998; Smith 2001, Schmidt *et al*., 2006). In planktonic foraminifera, instead of reaching premature death in ontogeny, small specimens have been documented to show reproductive structures (Schmidt *et al*., 2008), designated as *micromorph* by Huber (1994). Our study confirms the descriptions of Huber (1994): intra-specific variability of growth stages strongly affects the correlation between size and ontogenetic age.

In our case, we directly compared the ontogenetic sequences of the organisms. We thus put the emphasis on the fundamental dimension of developmental timing in heterochrony, only implicit in allometry studies (Klingerberg, 1998; McKinney 1999). We concentrated on the evolution of size and chamber morphology during the whole ontogeny, which summarizes most of the morphological variability in menardellids (Cifelli and Scott, 1986; Bolli and

Saunders 1985; Mary and Knappertsbusch, in press). We can therefore make solid interpretations of morphological changes between menardellid species in terms of heterochrony.

Our results suggest that the evolutionary trend in the *G. (M.) menardii- G. (M.)-limbata- G. (M.) multicamerata* lineage can be related to fundamental developmental differences. Figure 8 summarizes this evolutionary change and shows the successive delays of maturity together with size increase between *G. (M.) menardii* and *G. (M.) limbata*, and between *G. (M.) limbata* and *G. (M.) multicamerata*. In this context, the morphological differences between the three menardellid species, seen in Figure 5.5, can be interpreted as the result of Peramorphosis. A given descendant is peramorphic if its morphological development expands further than that of its ancestor at the same ontogenetic stage, producing overdeveloped adult traits or morphology (McNamara 1986).

The morphological transition from small, holding a small number of chamber *G. (M.) menardii* morphology (in contrast with extant larger *G. (M.) menardii*, Knappertsbusch, 2007) to the very large shell and multi-chambered morphology of *G. (M.) multicamerata* can be considered as a heterochronocline (directional morphological change among phylogenetic lineage explained by successive heterochronic changes).

5.5.2.1 Peramorphic development of *G. (M.) limbata* with respect to *G. (M.) menardii*

Chambers shape during the juvenile stages of *G. (M.) limbata* is similar to that of the neanic stage of *G. (M.) menardii*. This morphological trait shows an earlier onset of change in the descendant species than in the ancestor, the ontogenetic direction of morphological change remaining unchanged. These are clear evidence of a pre-displacement in chamber shape. The general morphology of the test remains largely similar.

The size difference between the two species is explained by an extended, although variable, neanic stage, but both juvenile and adult stages remain similar in terms of ontogenetic relative time (Figure 5.8). The development of extended neanic stage, where the growth is maximal, without pronounced morphological changes, can be seen as an indication of directional selection of larger size (Cope's rule). *G. (M.) limbata* shows a hypermorphic growth (extension of growth resulting in a delay of sexual maturation), which is followed by a

relatively short adultness, similarly to its ancestor, before reaching reproduction at the end of its life cycle.

Morphologically, the formation of radial elongated (Type B) chambers occurring earlier in ontogeny confers a more rounded shell morphology which allows the species to pack more chambers in the latest (adult) whorl. *G. (M.) limbata* therefore develops multi-chambered morphology holding up to 8 chambers in the final whorl. Such a change could easily be a secondary by-product of size increase related to allometric growth.

5.5.2.2 Peramorphic development of *G. (M.) multicamerata* with respect to *G. (M.) limbata*

The ontogeny of *G. (M.) multicamerata* shows evidence of peramorphic change in comparison to its ancestor *G. (M.) limbata*. Albeit differences between *G. (M.) menardii* and *G. (M.) limbata* are concentrated in the neanic stage, *G. (M.) multicamerata* shows modifications in the latest part of its life cycle. Juvenile and neanic stages of *G. (M.) multicamerata* and *G. (M.) limbata* are comparable, either in their length or in the chamber morphology. In terms of development, the ontogenetic sequence remains mostly unchanged, but is prolonged during the adult stage.

Maturity in *G. (M.) multicamerata* is morphologically characterized by the addition of axially elongated Type C chambers, similarly to *G. (M.) limbata*. The prolongation of the adult stage induces an augmentation of the number of Type C chambers in the terminal whorl: 9 chambers versus 4 in *G. (M.) limbata* (Figure 5.5). The onset of the terminal stage is delayed in comparison to its ancestor, and the general size of the test increases (Figure 5.8). These observations are clear evidences of hypermorphosis. Morphologically, the development of large, elongated shell together with the increment of more radial oriented Type C chambers have been interpreted by Scott (1973) to compensate the hydromechanical disadvantage of large size by developing an elongated, axially compressed shell morphology, augmenting shell buoyancy. The consequence is that *G. (M.) multicamerata*, in comparison to *G. (M.) limbata*, reaches larger size during the Pliocene (Figure 5.8).

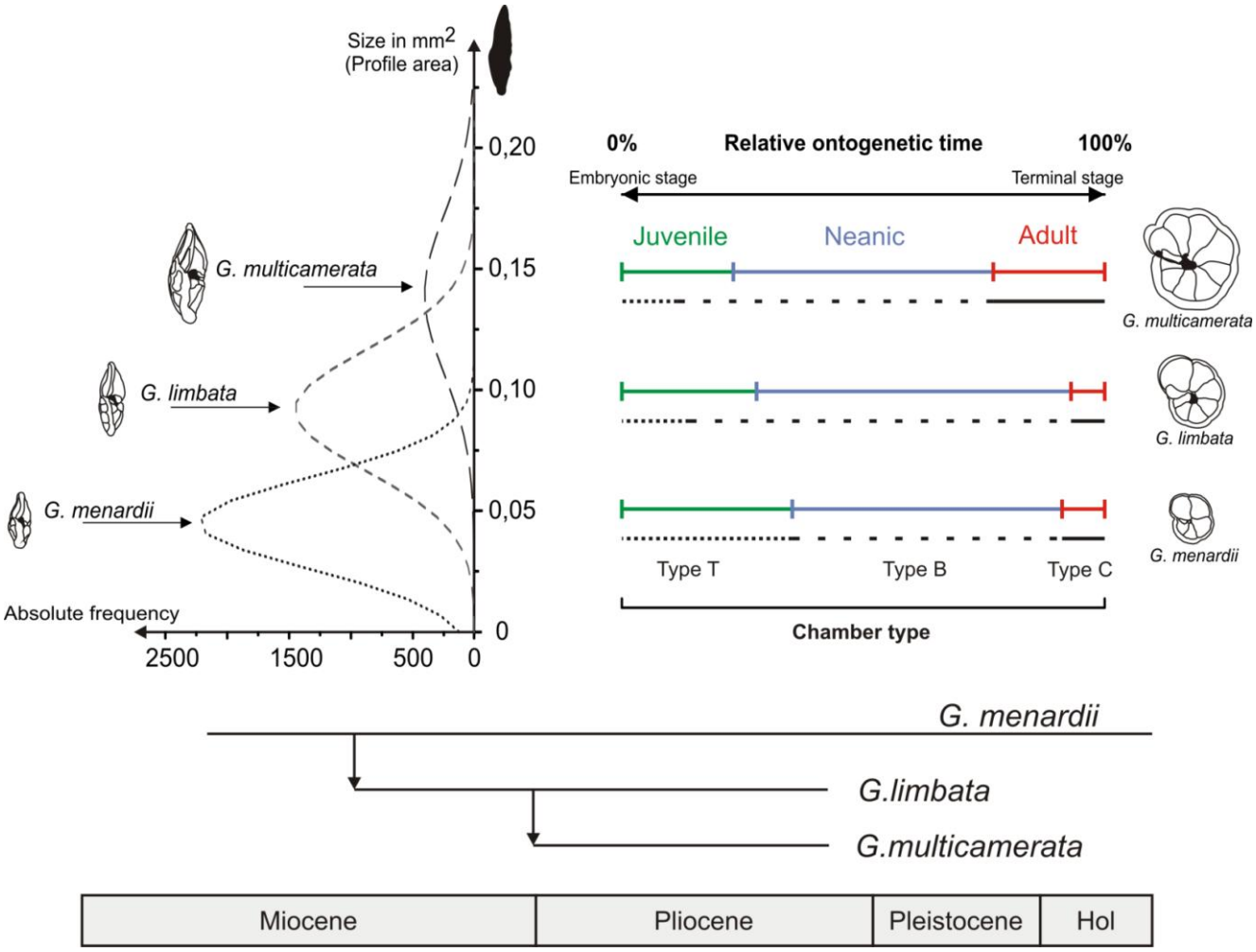

Figure 5.8: inter-specific comparison of relative ontogenetic length and associated change in chamber morphology, compared to size frequency distribution of the three menardellid species at site ODP 667 (after Mary and Knappertsbusch, in press). Gaussian distribution represents the distribution of *G. (M.) multicamerata, G. (M.) limbata* and *G. (M.) menardii*. The average length of the all adult specimens is compared for the three species. The phylogenetic scheme is from Kennett and Srinivasan (1983).

5.5.3 The ecological meaning of heterochrony in Pliocene menardellid

Independent geochemical evidences exist for ecological adaptations of menardellids during the Pliocene. The comparison of Atlantic *G. (M.) limbata* with *G. (M.) multicamerata* $\delta^{18}O$ (adult shells, >250µm) indicates a gradual occupation into different niches of the two

species, the latter rising to shallower habitats from the late Miocene to early Pliocene (Pfuhl and Shackleton, 2004). Considering Mid-Pliocene growth of *G. (M.) multicamerata*, such an adaptation would be consistent with the observed prolonged adult mode of this species. Pfuhl and Shackleton (2004) further interpreted this displacement to a new ecological niche as a response to mixed layer destabilization after 5.77Ma.

The evolutionary change of the ontogenetic sequence of *G. (M.) multicamerata* are corroborating indications of ecological separation between this species and its ancestor *G. (M.) limbata*. The extension of especially the adult stage, together with the pre-displacement of chamber morphological characters, point out to a prolonged stay of *G. (M.) multicamerata* in its adult habitat. This is in contrast to *G. (M.) menardii* and *G. (M.) limbata*, which stay most of their lifetime in the neanic stages but have a less extended adult phase.

Living planktonic foraminifera are known to change their depth of life in the water column during their life cycle. Extant menardellids are shallow thermocline dwellers. According to the model of Hemleben *et al*., (1989) they reproduce in relatively shallow waters to settle down in the water column while getting more mature. They reproduce again in shallower water. In this context, the extension of the adult stage relatively to ontogenetic time (Figure 5.8) can be interpreted as an adaptation to a shallower habitat. Theoretically, morphological modifications allow the peramorphic phenotype to cross an adaptative threshold and to colonize a new environment (McNamara, 1982, McKinney, 1986). Especially in larger benthic foraminifera the development of large shells associated with the prolongation of the adult stage is known as an adaptation to special niches (extreme K-type strategists, Hottinger, 1997, 2000a,b, 2001, McGowran, 2012), in contrast to a prolonged period of rapid growth but short adultness in R-type strategists. Eventually, a similar switch in life strategy, albeit to a less extreme degree, is seen in the planktonic menardellids, whereby *G. (M.) multicamerata* attains a tendency towards K-type strategists, while *G. (M.) menardii* and *G. (M.) limbata* remained in their rather R-type mode of behaviour.

Parapatric diversification by vertical niche partitioning has been recently suggested to be a driven mechanism of planktonic speciation (Weiner *et al*., 2012). Alteration of ontogenetic sequences, in this context, provides an efficient way for planktonic organisms, which vertically migrate in the water column, to colonize a new habitat. Such an idea was

previously proposed by Wei *et al*., (1994), to explain the Pliocene evolution of their *Globoconella* clade.

5.6 Conclusions

The ontogenetic growth of 350 Mid-Pliocene menardellid individuals was studied, distributed in 6 different size classes, and using a new, faster micro-dissection by dissolution protocol. Menardellids show a large variability of ontogenetic growth. Most of this variability can be explained by differences in number of chambers or differences in growth rate between individuals.

1. While menardellid species are often difficult to distinguish on the basis of their external morphology, they show a well distinctive growth pattern. Ontogeny has proved to be an important way to discriminate between foraminiferal species. External shell taxonomic features, like the commonly used number of chambers per whorl, are quite variable through ontogeny. The distinction in number of chambers per whorl between *G. (M.) limbata, G. (M.) menardii* and *G. (M.) multicamerata* is only possible in the adult segment, which begins about in the third whorl.

2- There exist specific differences in the variability of growth curves. In *G. (M.) menardii* and *G. (M.) limbata* most of the ontogenetic variation is seen during the neanic stage, whereas in *G. (M.) multicamerata*, important variation is seen towards the adult stage.

3- Morphological changes in the *G. (M.) menardii* - *G. (M.) multicamerata* lineage are successive heterochronic adaptations. The increase in number of chambers per whorl results in a pre-displacement of chamber morphology. The size increase in this lineage is the consequence of progressive hypermorphic extensions during the neanic stage in *G. (M.) limbata* and during the adult stage in *G. (M.) multicamerata*.

4- Ecologically, the heterochronocline of Pliocene menardellids can be interpreted as a progressive shoaling of their life habitat, leading to a tendencially more K-selective behavior in *G. (M.) multicamerata*.

Acknowledgements

This investigation would not have been possible without the financial support of the Swiss National Foundation for Scientific Research (SNF grant Numbers 200021-121599 (Evolutionary prospection in Neogene planktonic foraminifera) and 200020-137486 (Evolutionary prospection in Neogene planktonic foraminifera-continuation). The authors are particularly grateful to Antoine Heitz for assistance and discussion during the development of the microdissolution protocol. The kind assistance for using the SEM facilities by Marcel Düggelin (Zentrum für Mikroskopie at the University of Basel is greatly appreciated.

Plate 5.1: (on next page): illustrative plate showing three dissolved specimens per Pliocene menardellid species. For each specimen, an overview of the opened shell (A) and a picture of the first whorl (B) are displays.

Specimen 1-2-a/b *Globorotalia menardii* (Size fraction 200-300µm) showing kummerform last chamber. Specimen 3-a/b*: Globorotalia menardii* (Size fraction 100-200µm) showing kummerform last chamber.

Specimen 4-5 - *Globorotalia limbata* (Size fraction 500-600µm).

Specimen 6 - *Globorotalia limbata* (Size fraction 400-500µm), showing kummerform last chamber.

Specimen 7-8 - *Globorotalia multicamerata* (Size fraction 500-600µm).

Specimen 9 - *Globorotalia multicamerata* (Size fraction 400-500µm.

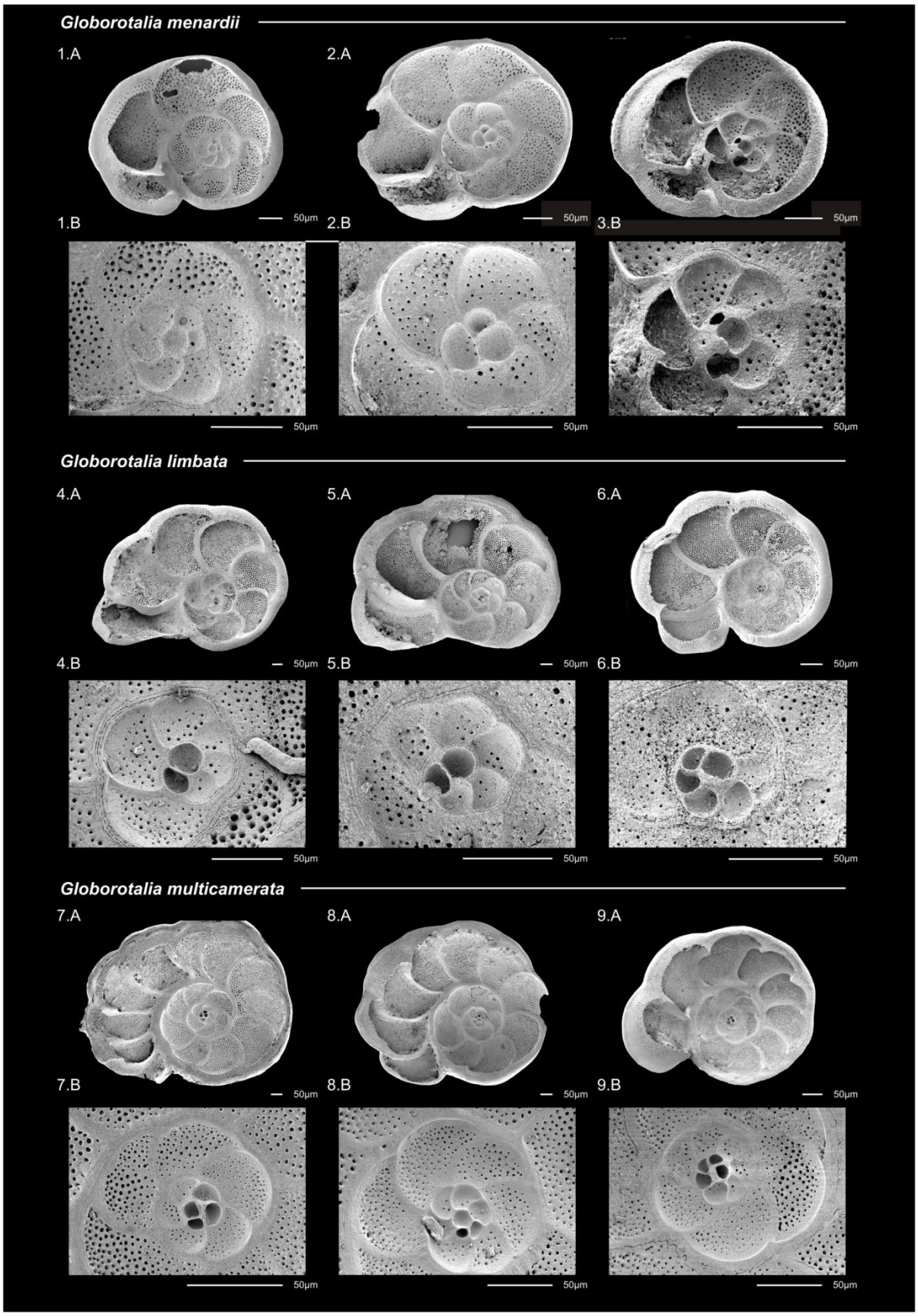
Globorotalia menardii
1.A
2.A
1.B
2.B
3.B
50µm
Globorotalia limbata
4.A
5.A
6.A
4.B
5.B
6.B
Globorotalia multicamerata
7.A
8.A
9.A
7.B
8.B
9.B

References

Al-Sabouni, N., Kucera, M., Schmidt, D.N., 2007. Vertical niche separation control of diversity and size disparity in planktonic foraminifera. Marine Micropaleontology 63, 75-90.

Alberch, P., Gould, S. J., Oster, G. F. , Wake D. B. , 1979. Size and shape in ontogeny and phylogeny. Paleobiology 5, 296–317.

André, A., Weiner, A., Quillévéré, F., Aurahs, R., Morard, R., Douady, C., de Garidel-Thoron, T., Escargel, G., de Vargas, C., Kucera, M. , 2013. The cryptic and the apparent reversed : lack of genetic differentiation within the morphologically diverse plexus of the planktonic foraminifer *Globigerinoides sacculifer*. Paleobiology 39(1), 21-39.

Aurahs, R., Treis, Y., Darling, K., Kucera, M. , 2011. A revised taxonomic and phylogenetic concept for the planktonic foraminifer species *Globigerinoides ruber* based on molecular and morphometric evidence. Marine Micropaleontology 79, 1–14.

Berggren, W.A., Kent, D.V., Swisher, C.C., Aubry, M.P. , 1995. A revised Cenozoic geochronology and chronostratigraphy. In: Berggren, W.A., Kent, D.V., Aubry, M.-P., and Hardenbol, J. (Eds.), Geochronology, time scales and global stratigraphic correlation. Society for Sedimentary Geology, SEPM Special Publication. # 54, 129–212.

Bolli H.M. , 1970. The foraminifera of Sites 23-31, Leg 4.- Initial Reports of the Deep Sea Drilling Project, College Station, vol. 4, 577-643.

Bolli, H., Saunders, J.B. , 1985. Oligocene to Holocene low latitude planktic foraminifera. In: Bolli, H.M., Saunders, J.B. and Perch-Nielsen, K. (Eds.), Plankton Stratigraphy. Cambridge University Press, Cambridge, 155-262.

Brown, K., 2007. Biogeographic and morphological variation in late Pleistocene to Holocene globorotalid foraminifera. Dissertation Phil. Nat. Fakultät, Universität Basel, 128 p. pdf file available at http://pages.unibas.ch/diss/2007/DissB_8290.htm

Brummer, G. J. A., Hemleben, C., Spindlern M., 1986. Planktonic foraminiferal ontogeny and new perspectives for micropaleontology. Nature 319, 50-52.

Brummer G. J.A., Hemleben C. and Spindler M., 1987. Ontogeny of Extant Spinose Planktonic Foraminifera (*Globigerinidae*): A Concept Exemplified by *Globigerinoïdes sacculifer* (Brady) and *G. ruber* (d'Orbigny). Marine Micropaleontology 12, 257-381.

Chaisson, W.P., 2003. Vicarious living: Pliocene menardellids between an isthmus and an ice sheet. Geology 31,1085–1088.

Cifelli, R. and Glaçon, G., 1978. Récapitulation ontogénétique des charactères ancestraux chez *Globorotalia* (Foraminifère). Compte Rendu Acad. Sc. Paris, t. 286 (12 Juin 1978), Série D,. 1665-1667.

Cifelli, R., Scott, G. 1986. Stratigraphic record of the Neogene globorotalid radiation (planktonic foraminifera). Smithsonian Contributions to Paleobiology 58.

Darling, K., Wade, C. , 2008. The genetic diversity of planktonic foraminifera and the global distribution of ribosomal RNA genotypes. Marine Micropaleontology 67, 216–238.

Drooger, C.W., 1993. Radial foraminifera; morphometrics and evolution. Verhandelingen der Koninklijke Nederlandse Akademie van Wetenschappen, Afd. Natuurkunde, Eerste Reeks, deel 41, 242.

Gradstein, F., Ogg, J., Smith, A., 2004. A Geologic Time Scale 2004. Cambridge University Press.

Georgescu, M.D., Saupe, E.E., Huber, B. T., 2009. Morphometric and stratophenetic basis for phylogeny and taxonomy in the Late Cretaceous gublerinid planktonic foraminifera. Micropaleontology 54, n°5, 397-424.

Görög, A., Szinger, B., Toth, E., Viszkok, J. , 2012. Methodology of the micro-computer tomography on foraminifera. Palaeontologia Electronica 15(3), 15p.

McGillavry, H.J., 1963. Phylomorphogenesis and evolutionary trends of Cretaceous orbitoidal foraminifera. Pages 139-196 in: Koenigswald, G.H.R., Emeis, J.D., Buning, W.L., Wagner, C.W. (eds.). Evolutionary trends in foraminifera. A collection of papers dedicated to I.M. Van der Vlerk on the occasion of his 70'th birthday. Elsevier Publishing Company, Amsterdam.

Gould, S. J. , 1966. Allometry and size in ontogeny and phylogeny. Biological Review 41, 587-640.

Gould, S. J. , 1977. Ontogeny and phylogeny. Belknap Press of Harvard University Press, Cambridge.

McGowran, B. , 2012. Cenozoic environmental shifts and foraminiferal evolution. In: Talent, J.A. (ed.): Earth and Life. Global biodiversity, Extinction intervals and biogeographic perturbations through time. Springer Dordrecht, Heidelberg, London, New York, pp. 937-965.

Hall, B. K., 1992. Evolutionary Developmental Biology. Chapman and Hall, London.

Huang, C.Y., 1981, Observations on the interior of some late Neogene planktonic foraminifera. Journal of foraminiferal Research 11, 173-190.

Hedley, R.H., 1957. Microradiography applied to the study of foraminifera : Micropaleontology 3, v1, 19-28

Hemleben, C., Spindler, M., Anderson, O., 1989. Modern Planktonic Foraminifera. Springer, New York.

Hemleben, C., Bé, A.W.H., Anderson, O.R., Tuntivate, S., 1977. Test morphology, organic layers and chamber foramtion of the Planktonic foraminifer *Globorotalia menardii* (D'Orbigny). Journal of foraminiferal Research 7, n°1, 1-25

Hofker, J. jr. , 1966. Zur Evolution der Cenoman-Orbitolinen. N. Jb. Geol. Paläont. Mh., vol. 4, pp. 193-207.

Hottinger, L. , 1997. Shallow benthic foraminiferal assemblages as signals for depth of their deposition and their limitations. Bull. Soc. géol. France, t. 168, 4, 491-505.

Hottinger, L. , 2000a. Adaptations of the foraminiferal cell to life in shallow carbonate environments. Accad. Nac. Sci. Lett. di Modena, Collana di Studi, 21, 135-140.

Hottinger, L., 2000b. Functional morphology of benthic foraminiferal shells, envelopes of cells beyond measure. Micropaleontology, vol. 46, supplementum No. 1, 57-86.

Hottinger, L. , 2001. Learning from the Past ? In: Levi-Montalcini (ed.): Frontiers of Life, vol. 4, part 2: Discovery and spoliation of the biosphere, 449-477. Academic Press (London and San Diego).

Huber, B.T., 1994. Ontogenetic Morphometrics of Some Late Cretaceous Trochospiral Planktonic Foraminifera from the Austral Realm Smithsonian Contributions to Paleobiology number 7. 85pp

Kelly, D. C., Arnold, A.J., Parker, W.C., 1996. Paedomorphosis and the origin of the Paleogene planktonic foraminiferal genus *Morozovella*. Paleobiology 22, 266–281.

Kelly, D.C., Bralower, T.J., Zachos, J.C., 2001. On the demise of the early Paleogene *Morozovella velascoensis*: Terminal progenesis in the planktonic foraminifera. Palaios 16, 507-523.

Kennett, J.P., Srinivasan, M.S., 1983. Neogene planktonic foraminifera. A phylogenetic atlas. Hutchinson Ross Publishing Company, Stroudburg, Pennsylvania, 1-265.

McKinney, M.L., 1988 Heterochrony in evolution: A multi-disciplinary approach. Plenum press, New York. 348 pp.

McKinney, M. L., McNamara, K. J., 1991. Heterochrony: the evolution of ontogeny. Plenum, New York. 437 pp.

McKinney, M. L., 1999. Heterochrony: beyond words. Paleobiology 25, 149–153.

Klingenberg, C. P. , 1998. Heterochrony and allometry: the analysis of evolutionary change in ontogeny. Biological Reviews 73, 79–123

Knappertsbusch, M.W., 2007. Morphological variability of *Globorotalia menardii* (planktonic foraminiferan) in two DSDP cores from the Caribbean Sea and the Eastern Equatorial Pacific. Carnets de Géologie / Notebooks on Geology, Brest, Article 2007/04.

Knappertsbusch, M.W., Mary, Y. , 2012. Mining morphological evolution in microfossils using volume density diagrams. Paleontologia Electronica 15(3); 7T 29p.

Kucera, M., Darling, K., 2002. Cryptic species of planktonic foraminifera: their effect on palaeoceaographic reconstruction. Philosophical Transactions of the Royal Society of London 360, 695–718.

Kucera, M., Kennett, J.P., 2002. Causes and consequences of a Middle Pleistocene origin of the modern planktonic foraminifer *Neogloboquadrina pachyderma* sinistral. Geology 30, 539–542.

Leary, P.N, Hart, M.B., 1988: X-raying planktonic foraminifera. Journal of Micropaleontology 7, 43-44.

McLeod, N., Ortiz, N., Fefferman, N., Clyde, W., Schulter, C., MacLean, J., 2000. Phenotypic response of foraminifera to episodes of global environmental change. In: Culver, S.J. and Rawson, P.F. (eds.). Biotic response to global change, the last 145 million years. Cambridge University Press, U.K., 51-78.

Lombard, F., Labeyrie, L., Michel, E., Spero, H.J., Lea, D. W. , 2009. Modelling temperature dependant growth of planktonic foraminifera. Marine Micropaleontology 70, 1-7.

Pfuhl, H.A., Shackleton, N.J. , 2004. Change in coiling direction, habitat depth and abundance in two menardellid species. Marine Micropaleontology 50, 3–20.

Mary, Y., Knappertsbusch, M.W. , In press. Morphological variability of Menardiform Globorotalids in the Atlantic Ocean during Mid-Pliocene. Marine Micropaleontology.

Mary, Y. Costeur, L. Knappertbusch, M.W. , Submitted. Worldwide morphological variability in Mid-Pliocene menardellid globorotalids revealed by population-based taxonomy. Paleoceanography, Paleoclimatology, Paleoecology.

Morad R., Quillévéré, F., Douady, C, De Vargas, C, de Garidel-Thoron, T., Escarguel, G., 2011. Worldwide genotyping in the Planktonic foraminifer *Globoconella inflata*: Implications for Life History and Paleoceanography. PLoS ONE 6(10):

McNamara, K. J., 1982. Heterochrony and phylogenetic trends. Paleobiology 8, 130–142.

McNamara, K. J., 1986. A guide to the nomenclature of heterochrony. Journal of Paleontology 60,4–13.

Nederbragt, A.J., 1989. Chamber proliferation in the Cretaceous planktonic foraminifera *Heterohelicidae*. Journal of Foraminiferal Research, vol. 19, No. 2, 105-114.

Nederbragt, A.J., 1993. Biometric analysis of multiserial chamber proliferation in Santonian *Heterohelicidae* (planktonic foraminifera). Journal of Foraminiferal Research, vol. 23, No. 3, 192-200.

Olson, R. K., 1973. Growth studies on *Globorotalia exilis* (Blow) and *Globorotalia pertenuis* (Beard) in the Hole 154A Section, LEG 15, Deep Sea Drilling Project. In. Initial Reports of the Deep Sea Drilling Project,15:617-624, Washington, D.C..

O'Herne, L. 1972. Secondary chamberlets in *Cyclclypeus*. Scripta Geologica, vol. 7, 35p.

Quillévéré, F., Debat V., Auffray, J-C., 2002. Ontogenetic and evolutionary patterns of shape differentiation during the initial diversification of Paleocene acarininids (planktonic foraminifera). Paleobiology, 28, 435–448.

Raff, R. A., 1996. The shape of life. University of Chicago, Chicago.544pp.

Regenberg, M., Nielsen, S.N., Kuhnt, W., Holbourn, A., Garbe-Schonberg, D., Andersen, N. 2010. Morphological, geochemical and ecological differences of the extant menardiform planktonic foraminifera *Globorotalia menardii* and *Globorotalia cultrata*. Marine Micropaleontology 74, 96–107.

Renaud, S., Schmidt, S.N., 2003. Habitat tracking as a response of the planktic foraminifer *Globorotalia truncatulinoides* to environmental fluctuations during the last 140 kyr. Marine Micropaleontology 49, 97-122

Scott, G., 1973. Ontogeny and shape in *Globorotalia menardii*. Journal of Foraminiferal Research 3, 142–146.

Schmid, K., (1934). Biometrische Untersuchungen an Foraminiferen (*Globorotalia menardii* (d'Orb.) – *Globorotalia tumida* (Brady) und *Truncatulina margaritifera* Brady – *Truncatulina margaritifera granulosa* Fischer) aus dem Pliocaen von Ceram (Niederl.-Indien). Eclogae geol. Helv. vol. 27, no. 1, 45-134.

Schmidt, D.N., Lazarus, D., Young, J.R., Kucera, M., 2006. Biogeography and evolution of body size in marine plankton. Earth-Science Reviews 78, 239–266.

Schmidt, D. N., Elliot, T., Kasemann, S.A. 2008. The influence of growth rates on planktic foraminifers as proxies for palaeostudies - a review. Geological Society, London, Special Publications 2008; 303, 73-85.

Schweitzer, P.N., 1989. Inference of ecology from the ontogeny of microfossils. PhD Dissertation. Massachusetts Institute of Technology, Dept. of Earth, Atmospheric and Planetary Science. 190 p.

Schweitzer, P N., Lohmann, G.P., 1991, Ontogeny and habitat of modern menardiiform planktonic foraminifera: Journal of foraminiferal Research 21, 332-346.

Smith, K. K., 2001. Heterochrony revisited: the evolution of developmental sequences. Biological Journal of the Linnean Society (2001) 73, 169-186.

Speijer, R.P., Van Loo, D., Masschaele, B., Vlassenbroeck, J., Cnudde, V., Jacobs, P. ,2008. Quantifying foraminiferal growth with high resolution X-ray computed tomography: New opportunities in foraminiferal ontogeny, phylogeny and paleoceanographic applications. Geosphere, 4: 760-763.

Ujiié, Y., de Garidel-Thoron, Watanabe, S., Wiebe, P., de Vargas, C., 2010. Coiling dimorphism within a genetic type of the planktonic foraminifer *Globorotalia truncatulinoides*. Marine Micropaleontology 77, 145-153.

Van der Vlerk, I.M. and Gloor, H., 1968. Evolution of an embryo. Genetica. Nederlands Tijdschrift voor Erfelijkheids- en Afstammingsleer, vol. 39, 45-63.

Van der Vlerk, I.M., 1973. An improved method of biometrical research. Proceedings of the Koninklijke Nederlandse Akademie van Wetenschappen, Amsterdam. Series B, 76(4), 245-259.

Webster M., Zelditch M. L., 2005. Evolutionary modifications of ontogeny: heterochrony and beyond. Paleobiology, 31(3), 354–372

Wei, K.Y., 1994. Allometric heterochrony in the Pliocene-Pleistocene planktic foraminiferal clade *Globoconella*. Paleobiology 20:66–84.

Wei, K.Y., Zhang, Z.W. ,Wray. C., 1992. Shell ontogeny of *Globorotalia inflata* (I): growth dynamics and ontogenetic stages. Journal of Foraminiferal Research 22:318-327

Weiner, A., Auras, R., Kurasawa, A., Kitazato, H., Kucera, M., 2012. Vertical niche partitioning between cryptic sibling species of a cosmopolitan marine planktonic portist. Molecular ecology 21, 4063-4073.

Chapter 6: Synopsis, conclusion, and outlook

6.1 Synopsis

6.1.1 Morphological diversity of Mid-Pliocene menardellids

Using the population-based approach, a total of 8 different but intergrading morphotypes were defined, which were informally denominated morphotypes MA, MB, MC1, MC2, MC3, SH1, SH2 and ME. Morphological overlap between all these forms are systematically observed. The comparison of these 8 morphotypes with formal morpho-species calls for an extended definition of the currently known species.

Two different morphotypes MA and ME correspond to the morpho-species *G. (M.) menardii.* They significantly differ in size, but are very similar in shell morphology. Furthermore, the morphotype ME is interpreted to be equivalent to morphotype α from Knappertsbusch, (2007) and Brown, (2007). Size frequency distributions of these morphotypes indicate however that they do not belong to the same population, and their biogeographic distribution is different as well. Morphotypes MA and ME may therefore belong to different species.

The morphotypes MC1, MC2 and MC3 are assigned to *G. (M.) multicamerata*. They significantly diverge from each other by the morphology of their shells. In profile view, the morphotype MC1 shows a flat shell with an elongated outline, and preferentially 7 to 8 chambers. The morphotype MC2 is characterized by a thicker and more robust shell morphology, reaching commonly 9 chambers in the last whorl. Morphotype MC3 reaches the largest size and is defined by its typical flexure in the last chamber. Morphotypes MC1 and MC2 often co-exist at a single location, and their size frequency distribution cannot be kept apart from each other suggesting that they belong to the same population. Therefore, morphotypes MC1 and MC2 are interpreted here as two ecophenotypic variants of the same species

The morphotype MB coincides best with the morpho-species *G. (M.) limbata*. The morphological boundaries of this morphotype are relatively stable worldwide. However, in contrast to the morphological descriptions given in taxonomical indices (Kennett and

Srinivasan, 1983; Bolli and Saunders 1985), our results suggest that most of the specimens with 5 chambers per whorl in the large size fraction belong to morphotype MB as well.

The morphotypes SH1 and SH2 correspond to *G. (M.) exilis* and *G. (M.) pertenuis*, respectively. They differ from the other morphotypes by their delicate and densely perforated wall structure, as well as by their shell morphology. In the investigated material no evidence for morphotypes were found that would correspond to *G. (M.) miocenica.*

6.1.2 Biogeography of menardellid morphotypes at 3.2 Ma

The biogeographic dataset of this study comprises 19 samples coming from the tropical Atlantic, Pacific and Indian Ocean. They constitute a set of key locations within the distribution of Pliocene menardellids. The sample coverage is better in the Atlantic and is reduced close to the continental border in the Pacific, because of the poor availability of material in that area. A number of 720 menardellid specimens were analyzed in almost every sample, which garantees a solid estimation of the menardellid diversity at the 3.2 Ma time-slice. The menardellid biogeography could be subdivided into 5 distinct oceanic provinces.

In the Atlantic Ocean, 2 provinces could be defined: a Western Atlantic province, where morphotype MA dominates and subordinate occurrences of morphotypes MB, MC2 and SH1. An Eastern Atlantic province, which contains higher abundance of larger menardellids, and which is composed mainly of Morphotypes MA, MB and MC1 and with occasional occurrences of morphotypes SH2 and MC3.

The Pacific Ocean can be subdivided in two provinces as well: The Eastern Pacific area was found to be mostly depleted in menardellids at the 3.2 Ma time-slice; the investigated locations contained dominantly morphotype MA. The diversity of menardellid forms is higher in the Pacific Warm pool. Here, in the Western Pacific, the menardellid assemblage is characterized by the presence of the endemic morphotype ME and the co-existence of abundant morphotypes MA and MB. The morphotype MC2 occurs here only in low abundance.

All Indian Ocean locations show a homogeneous composition of menardellid morphotypes. Here, morphotype MA is the most abundant one, co-occurring with morphotypes MB and MC1.

6.1.3 Ontogenetic development of Mid-Pliocene menardellids

Microdissolution and dissection experiments from more than 350 specimens of *G. (M.) menardii, G. (M.) limbata* and *G. (M.) multicamerata* allowed to recognize 5 distinct growth stages, which correspond to the classical ontogenetic growth model for planktonic foraminifera of Brummer *et al*., (1987). Specific differences in growth stages were observed between the three species. *G. (M.) menardii* and *G. (M.) limbata* show a prolonged neanic stage (relatively to their entire ontogenetic life span). In contrast, *G. (M.) multicamerata* displays an extended adult stage.

The analysis of ontogenetic development confirms that size is an important parameter to taxonomically distinguish menardellid globorotalids. Small specimens located in the lowermost size fraction are recognized to also represent adults of *G. (M.) menardii*, which is unexpected. In contrast, no strong differences were observed between variants of *G. (M.) menardii* at the large end of the size spectrum for forms, holding 5 to 7 chambers in the final whorl.

The morphological evolution and size increase in the menardellid lineage of *G. (M.) menardii* - *G. (M.) limbata* - *G. (M.) multicamerata* are interpreted as the consequences of successive hypermorphic changes. It implies a phyletic delay of the onset of reproductive maturity and an extension of the adult stage in individuals. Such changes may be interpreted as a progressive adaptive response in direction of a K-like behavioral strategy, which is accompanied by habitat changes into a shallower depths in the case of *G. (M.) multicamerata*.

6.2 General conclusion

The main contribution to foraminiferal taxonomy of the present work is the experimentation of a methodological approach that combines geometric morphometry, size frequency distribution modeling and ontogenetic reconstructions to define clusters within the menardellid morphological plexus. The used of SFD's proved to be a possibility to establish differences between morphological clusters, which then permitted an interpretation of the morphological variability in a biological and ecological context. The investigation of the ontogenetic variability within the Gaussian SFD modes has corroborated that these modes may correspond to species. This finding validates the initial assumption that the populations can be deconvolved from mixed sedimentary morphotype assemblages.

Using this population-based approach, a total of 8 morphotypes were defined within the five formal menardellid morpho-species. These morphotypes shows specific biogeographic distribution. Morphotypes MA and MB, which correspond to *G. (M.) menardii* and *G. (M.) limbata*, are cosmopolitans, whereas morphotypes SH1 and SH2 (*G. (M.) exilis* and *G. (M.) pertenuis*) are endemic to the Atlantic Ocean, while morphotype ME is restricted to the Pacific Warm Pool. Morphotypes MC1 and MC2 are abundant in the Atlantic, and rare in the Pacific and Indian Oceans. The relative abundance of these two morphotype varies with geography: MC2 dominates the Atlantic and Pacific Warm pool, whereas MC1 occurs preferentially in the eastern Atlantic and Indian Ocean. The distribution and the similar SFDs suggest that morphotypes MC1 and MC2 represent eco-variants of the same species. The assignement of these two morphotypes to particular ecological niches in the water column is unfortunately out of range of this thesis, and would require additional geochemical investigations.

Nevertheless, the ontogenetic observations make a vertical partitioning of the habitat of the various menardellid morphotypes likely. The shift of maturation onset and the extension in adultness from *G. (M.) menardii* (Morphotype MA), *G. (M.) limbata* (Morphotype MB) to *G. (M.) multicamerata* (Morphotype MC1) suggest a progressive shallowing of the menardellid habitat, indicating a preferential turn to a K-like strategy of life. The limited sample coverage

prevented a more detailed investigation of ontogenetic differences between morphotypes MC1 and MC2, and a biogeographically improved ontogenetic dataset is needed for this. Nevertheless, the present investigation about the menardellid ontogeny shows the high value and need of growth studies for a sound understanding of the taxonomy, biology, and ecology of planktonic foraminifera. Considering the fundamental role of planktonic foraminifera in geosciences, it is surprising to notice that , as pointed out by Scott (2011), ontogenetic data are largely absent in species descriptions and taxonomic studies. More such ontogenetic descriptions, combined with morphological analyses of populations, would certainly lead to a better understanding of fossil planktonic foraminifera at species-level.

This study of menardellid morphological variability also highlights the restricted value of too much simplified classification schemes (*i.e.* drawing lines to separate species) because between species' biogeographic and habitat variability through time there are more than simple linear discriminators. However, simple models serve as zero-order approximations to become able to quantify biological variations, especially when dealing with extinct fossils.

6.3 Suggestions for further developments

The evolutionary prospection project (cf. section 1.3) consists, in part, in successive investigations of different times-slices, which logically calls for another time interval to be investigated, in order to fill the gap between the present study and the previous Holocene menardellid mapping. Considering the large investment of effort and taking into account the collapse of Atlantic populations of *G. (M.) menardii* during glacial event (Sexton and Norris, 2008 and reference therein), a further time slice should be selected very carefully. An interesting project would certainly be the investigation of the beginning of the menardellid lineage during the middle Miocene, in order to frame the evolutionary history of menardellid.

Concerning menardellid diversity, one of the most important issues to solve would be to further concentrate on the apparent bimodal diversity of *G. (M.) menardii* morphotypes MA and ME. Does this bimodality exist in extant sediments as well? To answer this question, the original Holocene dataset from Brown, 2007 could be submitted to a similar size frequency

distribution analysis as was done here. The present study suggests that the Pacific Ocean and especially the Warm Pool in the western Pacific are of great interest to unravel the history of menardellids. A similar evolutionary morphometry study like the one from Knappertsbusch and Mary (2012) could be realized for ODP Site 807 on the Ontong Java Plateau.

The present ontogenetic studies concentrates on only of 3 of the 8 recognized Pliocene menardellid morphotypes. Investigation of the other menardellid variants would provide interesting evidences to understand the evolutionary relationship between the different menardellid species. Is there any biogeographic variability in ontogenetic signal ?

References:

Brown, K. 2007. Biogeographic and morphological variation in late Pleistocene to Holocene globorotalid foraminifera. Dissertation Phil. Nat. Fakultät, Universität Basel, 128 p. pdf file available at http://pages.unibas.ch/diss/2007/DissB_8290.htm

Kennett, J.P., Srinivasan, M.S. 1983. Neogene planktonic foraminifera. A phylogenetic atlas. Hutchinson Ross Publishing Company, Stroudburg, Pennsylvania, 1-265.

Knappertsbusch, M.W. 2007. Morphological variability of *Globorotalia menardii* (planktonic foraminiferan) in two DSDP cores from the Caribbean Sea and the Eastern Equatorial Pacific. Carnets de Géologie / Notebooks on Geology, Brest, Article 2007/04.

Knappertsbusch, M. W. and Mary, Y. 2012. Mining morphological evolution in microfossils using volume density diagrams. Palaeontologia Electronica, Vol. 15, Issue 3; 7T: 209p. URL: http://palaeo-electronica.org/content/issue-3-2012-technical-articles/282-volume-density-diagrams/

Sexton, P.F., Norris, R.D., 2011. High latitude regulation of low latitude thermocline ventilation and planktic foraminifer populations across glacial–interglacial cycles. Earth and Planetary Science Letters 311, 69–81.

Appendix

Appendix 1 : AMDS source code

This appendix give the source code of AMDS version9. It is customized for the computer that run AMOR and cannot be adapted for other application.

```
#cs ----------------------------------------------------------------------------
                AutoIt Version: 3.3.6.0
                Author:  Yannick MARY
                Script Function: Correct AMOR device failure dur to automagnification and autozoom. Interrupt the run in case of roll or pitch error.
                Template AutoIt script.
        #ce ----------------------------------------------------------------------------

        #include <GuiConstants.au3>
        ; Under Vista the  Windows API "SetSystemTime" may be rejected due to system security

        ;NOTE: AMOR parameters
        ;      Average tilting time : 7 minutes
        ;  ...;note : this version has been created for Amor 3.17

        ;Coortinates of AMOR's onglets  (if upleft corner is [0;0])
        ;Initialization
        Global $detailuser[2] = [425, 326]
        Global $adjustlight[2] = [425, 368]
        Global $OkgotoAmor[2] = [497, 465]
        Global $Okmanuelmode[2] = [878, 173]

        ;Title:Settings singlemode
        Global $Loadcustom[2] = [90, 518]
        Global $entermanuel[2] = [93, 558]
        ;Field zone
        Global $fieldinit[2] = [277, 172]
        Global $fieldlast[2] = [243, 172]
```

```
;Magnification zone
Global $zoombutton[2] = [583,163]
Global $zoominit[2] = [677, 172]
Global $zoomlast[2] = [643, 172]
Global $abortmagnification[2] =[656, 96]

;Autocenter
Global $autocenter[2] = [906, 325]

;Autofocus
Global $autofocus[2] = [906, 373]

;Autotilt
Global $autotilt[2] = [906, 419]

;Automagnificate
Global $automag[2] = [906, 462]

;Autorotate
Global $autorotate[2] = [906, 506]

;Capture
Global $autocapture[2] = [906, 691]

;Exit
Global $autoExit[2] = [906, 743]

;Saving dialog parameter
Global $Saveunder[2] = [405, 65]
Global $save[2] = [458, 108]

;windows parameters
Global $windows[2] = [29, 1007]
Global $winquit[2] = [148, 971]
```

```
;Global Variables for functions

Global $Time

Global $Hour[9]

Global $Minutes[9]

Global $Second[9]

Global $Heure

Global $Dim

Global $Pas


;handle variables

Global $Handle_AMOR

Global $Handle_Pad

Global $Handle_rep

Global $handle_Error


;Other variables

Dim $check

Dim $Exitchoice

Dim $file, $answer

Dim $Sample

Dim $send

Dim $Slide

Dim $Specimen

Dim $timeout

Dim $timeout2

Dim $titlepad = "Dokument - WordPad"

Dim $titlepad_name

Dim $titletcheck

Dim $path

Dim $case


;set the emergency and soft exits

HotKeySet("!^q", "MyExit")

HotKeySet("!^s", "softexit")
```

```
; Prompt the user to run the script - use a Yes/cancel prompt

$answer = MsgBox(1, "AMDS", "You are about to run Amor Manual Driving Script (AMDS)" & @CRLF & "This AutoIt made script will allow you to let Amor work alone, in manual mode." & @CRLF & "" & @CRLF & "" & @CRLF & "Version 1.4 By Yannick Mary and Michael Knappertsbusch")

; If "No" was clicked (7) then exit the script

If $answer = 2 Then

        MsgBox(0, "AMDS", "You are about to leave Amor Manual Driving, have a nice day")

        Exit

EndIf


; information prompts

MsgBox(0, "AMDS", "IMPORTANT ---------- IMPORTANT" & @CRLF & "" & @CRLF & "" & @CRLF & "To interrupt AMDS while it is running, press simultaneously Alt+Ctrl+Q keys")

MsgBox(0, "AMDS", "IMPORTANT ---------- IMPORTANT" & @CRLF & "" & @CRLF & "" & @CRLF & "The list of files file would be located on the desktop ")


$Exitchoice = MsgBox(4, "AMDS", "Do you want to shut AMOR at the end of the run ?")

$Sample = InputBox("AMDS", "Please enter sample code" & @CRLF & "" & @CRLF & "" & @CRLF & "The sample code will be written in picture names. Example:" & @CRLF & "503A202105K")

$Slide = InputBox("AMDS", "Please enter the Slide number")

$path = InputBox("AMDS", "Please enter the path to the Amor Slide Calibration file" & @CRLF & "NB: The full path is written on the properties of the file")

MsgBox(0, "AMDS", "NB: The pictures will be saved in folder where the calibration file is located")


; let the user the possibility to escape the script

$answer = MsgBox(1, "AMDS", "Be sure Amor is open, than do the calibration and enter the manual mode")

If $answer = 2 Then

        MsgBox(0, "AMDS", "You are about to leave Amor Manual Driving, have a nice day")

        Exit

EndIf


;Creation of GUI for selection of specimens.

GUICreate("AMDS - Specimen choice", 675, 300)

;Ligne 1

$specimen1 = GUICtrlCreateCheckbox("Spe 1", 5, 5, 80, 17)

GUICtrlSetState(-1, $GUI_CHECKED)
```

```
$specimen2 = GUICtrlCreateCheckbox("Spe 2", 5, 25, 80, 17)
GUICtrlSetState(-1, $GUI_CHECKED)
$specimen3 = GUICtrlCreateCheckbox("Spe 3", 5, 45, 80, 17)
GUICtrlSetState(-1, $GUI_CHECKED)
$specimen4 = GUICtrlCreateCheckbox("Spe 4", 5, 65, 80, 17)
GUICtrlSetState(-1, $GUI_CHECKED)
$specimen5 = GUICtrlCreateCheckbox("Spe 5", 5, 85, 80, 17)
GUICtrlSetState(-1, $GUI_CHECKED)
$specimen6 = GUICtrlCreateCheckbox("Spe 6", 5, 105, 80, 17)
GUICtrlSetState(-1, $GUI_CHECKED)
$specimen7 = GUICtrlCreateCheckbox("Spe 7", 5, 125, 80, 17)
GUICtrlSetState(-1, $GUI_CHECKED)
$specimen8 = GUICtrlCreateCheckbox("Spe 8", 5, 145, 80, 17)
GUICtrlSetState(-1, $GUI_CHECKED)
$specimen9 = GUICtrlCreateCheckbox("Spec 9", 5, 165, 80, 17)
GUICtrlSetState(-1, $GUI_CHECKED)
$specimen10 = GUICtrlCreateCheckbox("Spec 10", 5, 185, 80, 17)
GUICtrlSetState(-1, $GUI_CHECKED)
$specimen11 = GUICtrlCreateCheckbox("Spe 11", 5, 205, 80, 17)
GUICtrlSetState(-1, $GUI_CHECKED)
$specimen12 = GUICtrlCreateCheckbox("Spe 12", 5, 225, 80, 17)
GUICtrlSetState(-1, $GUI_CHECKED)

;Ligne 2
$specimen13 = GUICtrlCreateCheckbox("Spe 13", 135, 5, 80, 17)
GUICtrlSetState(-1, $GUI_CHECKED)
$specimen14 = GUICtrlCreateCheckbox("Spe 14", 135, 25, 80, 17)
GUICtrlSetState(-1, $GUI_CHECKED)
$specimen15 = GUICtrlCreateCheckbox("Spe 15", 135, 45, 80, 17)
GUICtrlSetState(-1, $GUI_CHECKED)
$specimen16 = GUICtrlCreateCheckbox("Spe 16", 135, 65, 80, 17)
GUICtrlSetState(-1, $GUI_CHECKED)
$specimen17 = GUICtrlCreateCheckbox("Spe 17", 135, 85, 80, 17)
GUICtrlSetState(-1, $GUI_CHECKED)
$specimen18 = GUICtrlCreateCheckbox("Spe 18", 135, 105, 80, 17)
```

```
GUICtrlSetState(-1, $GUI_CHECKED)
$specimen19 = GUICtrlCreateCheckbox("Spe 19", 135, 125, 80, 17)
GUICtrlSetState(-1, $GUI_CHECKED)
$specimen20 = GUICtrlCreateCheckbox("Spe 20", 135, 145, 80, 17)
GUICtrlSetState(-1, $GUI_CHECKED)
$specimen21 = GUICtrlCreateCheckbox("Spe 21", 135, 165, 80, 17)
GUICtrlSetState(-1, $GUI_CHECKED)
$specimen22 = GUICtrlCreateCheckbox("Spe 22", 135, 185, 80, 17)
GUICtrlSetState(-1, $GUI_CHECKED)
$specimen23 = GUICtrlCreateCheckbox("Spe 23", 135, 205, 80, 17)
GUICtrlSetState(-1, $GUI_CHECKED)
$specimen24 = GUICtrlCreateCheckbox("Spec 24", 135, 225, 80, 17)
GUICtrlSetState(-1, $GUI_CHECKED)

;Ligne 3
$specimen25 = GUICtrlCreateCheckbox("Spe 25", 265, 5, 80, 17)
GUICtrlSetState(-1, $GUI_CHECKED)
$specimen26 = GUICtrlCreateCheckbox("Spe 26", 265, 25, 80, 17)
GUICtrlSetState(-1, $GUI_CHECKED)
$specimen27 = GUICtrlCreateCheckbox("Spe 27", 265, 45, 80, 17)
GUICtrlSetState(-1, $GUI_CHECKED)
$specimen28 = GUICtrlCreateCheckbox("Spe 28", 265, 65, 80, 17)
GUICtrlSetState(-1, $GUI_CHECKED)
$specimen29 = GUICtrlCreateCheckbox("Spe 29", 265, 85, 80, 17)
GUICtrlSetState(-1, $GUI_CHECKED)
$specimen30 = GUICtrlCreateCheckbox("Spe 30", 265, 105, 80, 17)
GUICtrlSetState(-1, $GUI_CHECKED)
$specimen31 = GUICtrlCreateCheckbox("Spe 31", 265, 125, 80, 17)
GUICtrlSetState(-1, $GUI_CHECKED)
$specimen32 = GUICtrlCreateCheckbox("Spe 32", 265, 145, 80, 17)
GUICtrlSetState(-1, $GUI_CHECKED)
$specimen33 = GUICtrlCreateCheckbox("Spe 33", 265, 165, 80, 17)
GUICtrlSetState(-1, $GUI_CHECKED)
$specimen34 = GUICtrlCreateCheckbox("Spe 34", 265, 185, 80, 17)
GUICtrlSetState(-1, $GUI_CHECKED)
```

```
$specimen35 = GUICtrlCreateCheckbox("Spe 35", 265, 205, 80, 17)
GUICtrlSetState(-1, $GUI_CHECKED)
$specimen36 = GUICtrlCreateCheckbox("Spe 36", 265, 225, 80, 17)
GUICtrlSetState(-1, $GUI_CHECKED)

;Ligne 4
$specimen37 = GUICtrlCreateCheckbox("Spe 37", 395, 5, 80, 17)
GUICtrlSetState(-1, $GUI_CHECKED)
$specimen38 = GUICtrlCreateCheckbox("Spe 38", 395, 25, 80, 17)
GUICtrlSetState(-1, $GUI_CHECKED)
$specimen39 = GUICtrlCreateCheckbox("Spe 39", 395, 45, 80, 17)
GUICtrlSetState(-1, $GUI_CHECKED)
$specimen40 = GUICtrlCreateCheckbox("Spe 40", 395, 65, 80, 17)
GUICtrlSetState(-1, $GUI_CHECKED)
$specimen41 = GUICtrlCreateCheckbox("Spe 41", 395, 85, 80, 17)
GUICtrlSetState(-1, $GUI_CHECKED)
$specimen42 = GUICtrlCreateCheckbox("Spe 42", 395, 105, 80, 17)
GUICtrlSetState(-1, $GUI_CHECKED)
$specimen43 = GUICtrlCreateCheckbox("Spe 43", 395, 125, 80, 17)
GUICtrlSetState(-1, $GUI_CHECKED)
$specimen44 = GUICtrlCreateCheckbox("Spe 44", 395, 145, 80, 17)
GUICtrlSetState(-1, $GUI_CHECKED)
$specimen45 = GUICtrlCreateCheckbox("Spe 45", 395, 165, 80, 17)
GUICtrlSetState(-1, $GUI_CHECKED)
$specimen46 = GUICtrlCreateCheckbox("Spe 46", 395, 185, 80, 17)
GUICtrlSetState(-1, $GUI_CHECKED)
$specimen47 = GUICtrlCreateCheckbox("Spe 47", 395, 205, 80, 17)
GUICtrlSetState(-1, $GUI_CHECKED)
$specimen48 = GUICtrlCreateCheckbox("Spe 48", 395, 225, 80, 17)
GUICtrlSetState(-1, $GUI_CHECKED)

;Ligne 5
$specimen49 = GUICtrlCreateCheckbox("Spe 49", 525, 5, 80, 17)
GUICtrlSetState(-1, $GUI_CHECKED)
$specimen50 = GUICtrlCreateCheckbox("Spe 50", 525, 25, 80, 17)
```

```
GUICtrlSetState(-1, $GUI_CHECKED)
$specimen51 = GUICtrlCreateCheckbox("Spe 51", 525, 45, 80, 17)
GUICtrlSetState(-1, $GUI_CHECKED)
$specimen52 = GUICtrlCreateCheckbox("Spe 52", 525, 65, 80, 17)
GUICtrlSetState(-1, $GUI_CHECKED)
$specimen53 = GUICtrlCreateCheckbox("Spe 53", 525, 85, 80, 17)
GUICtrlSetState(-1, $GUI_CHECKED)
$specimen54 = GUICtrlCreateCheckbox("Spe 54", 525, 105, 80, 17)
GUICtrlSetState(-1, $GUI_CHECKED)
$specimen55 = GUICtrlCreateCheckbox("Spe 55", 525, 125, 80, 17)
GUICtrlSetState(-1, $GUI_CHECKED)
$specimen56 = GUICtrlCreateCheckbox("Spe 56", 525, 145, 80, 17)
GUICtrlSetState(-1, $GUI_CHECKED)
$specimen57 = GUICtrlCreateCheckbox("Spe 57", 525, 165, 80, 17)
GUICtrlSetState(-1, $GUI_CHECKED)
$specimen58 = GUICtrlCreateCheckbox("Spe 58", 525, 185, 80, 17)
GUICtrlSetState(-1, $GUI_CHECKED)
$specimen59 = GUICtrlCreateCheckbox("Spe 59", 525, 205, 80, 17)
GUICtrlSetState(-1, $GUI_CHECKED)
$specimen60 = GUICtrlCreateCheckbox("Spe 60", 525, 225, 80, 17)
GUICtrlSetState(-1, $GUI_CHECKED)


;Fin de creation du Gui
$verif = GUICtrlCreateButton("RUN AMDS", 250, 265, 80, 30)
GUISetState(@SW_SHOW)
While 1
        $msg = GUIGetMsg()
        Select
                Case $msg = $GUI_EVENT_CLOSE
                        Exit
                Case $msg = $verif
                        ExitLoop
        EndSelect
WEnd
GUISetState(@SW_HIDE)
```

```
Sleep(2000)


; Open wordpad ! WORDPAD GERMAN ONLY
Run("C:\Programme\Windows NT\Zubehör\wordpad.exe")
WinWaitActive($titlepad)
$Handle_Pad = WinGetHandle($titlepad)
WinMove("Dokument - WordPad", "", 0, 0)
Sleep(100)
Send("^s")
$titlepad_name = "List_of_files"
;verifie la presence d un fichier list_of_files:txt
$titletcheck = FileExists("C:\Dokumente und Einstellungen\snmmic\Desktop\List_of_files.txt")
If $titletcheck = 1 Then
        MsgBox(0, "AMDS", "The List_of_files file already exists. Please remove it and restart the Script")
        Exit
EndIf


;saving the file
Send($titlepad_name)
Send("{ENTER}")
Sleep(150)
Send("{ENTER}")
Sleep(150)
;moving the position of the wordpad prompt to perform further manipulations
WinMove($Handle_Pad, "", 0, 0)
Sleep(150)
;and good night word pad
WinMinimizeAll()
Sleep(250)
;creating the report file
Run("C:\Programme\Windows NT\Zubehör\wordpad.exe")
WinWaitActive($titlepad)
$Handle_rep = WinGetHandle($titlepad)
WinMove($titlepad, "", 0, 0)
Sleep(100)
```

```
Send("^s")

;saving the file

$titlepad_name = "Report_run"

Send($titlepad_name)

Send("{ENTER}")

Sleep(150)

Send("{ENTER}")

Sleep(150)

Call("Time")

Send($Heure)

$send = "    Début du Run"

Send($send)

Send("{ENTER}")

Send("^s")

Sleep(1000)

Send("{ENTER}")

Sleep(1000)

Send("{ENTER}")

Sleep(1000)


;minimizing again

WinMinimizeAll()

Sleep(250)


;AMOR

WinActivate("AMOR")

$Handle_AMOR = WinGetHandle("AMOR")

Sleep(1500)


;Focus on AMOR, search for any "ERROR" prompt


;---------------------------------main loop for picture and orientation----------------------------------


WinMove($Handle_AMOR, "", 0, 0)

$Specimen = 0
```

```
AdlibRegister("Errors")
For $i = $specimen1 To $specimen60
	$Specimen = $Specimen + 1
	If GUICtrlRead($i) = $GUI_CHECKED Then
		sleep(1000)
		WinActivate($Handle_rep)
		WinWaitActive($Handle_rep)
		Call("Time")
		Send($Heure & " ")
		$send = "Specimen n°" & $Specimen & "_____ "
		Send($send)
		Sleep(1000)
		Send("^s")
		Sleep(1000)
		Send("{ENTER}")
		Sleep(1000)
		Send("{ENTER}")
		Sleep(1000)
		WinSetState($Handle_rep, "", @SW_MINIMIZE)

		;Give focus to Amor
		Do
			$Pas = 0
			WinActivate($Handle_AMOR)
			Sleep(1000)
		Until $Pas = 0

		;Specimen Selection
		Do
			$Pas = 0
			WinActivate($Handle_AMOR)
			Sleep(1500)
			MouseClickDrag("left", $fieldinit[0], $fieldinit[1], $fieldlast[0], $fieldlast[1], 1)
			Sleep(1000)
```

```
		Send($Specimen)
		Sleep(1000)
		Send("{ENTER}")
		Sleep(25000)
Until $Pas = 0

;Autocenter (just in case)
Do
		$Pas = 0
		WinActivate($Handle_AMOR)
		Sleep(1500)
		MouseClick("left", $autocenter[0], $autocenter[1])
		Sleep(2000)
		MouseClick("left", $autocenter[0], $autocenter[1])
		Sleep(2000)
Until $Pas = 0

;Automagnificate
Do
		$Pas = 0
		WinActivate($Handle_AMOR)
		Sleep(1500)
		MouseClick("left", $automag[0], $automag[1])
		Sleep(1000)
		$timeout = WinWaitClose("Automagnificate", "", 90)

		;Include a magnification abort Statement and a reboot Amor Statement
		If $timeout = 0 Then
			winactivate("Automagnificate")
			Winmove("Automagnificate","",0,0)
			Mouseclick("left",$abortmagnification[0],$abortmagnification[1])
			sleep(10000)
			;Check for an automagnification crash
			$timeout2 = winexists("Automagnificate")
```

```
If $timeout2 = 0 then
        WinActivate($Handle_rep)
        WinWaitActive($Handle_rep)
        Call("Time")
        Send($Heure & " ")
        $send = $Specimen & " Automagnificate aborted."
        Send($send)
        Sleep(1000)
        Send("^s")
        Sleep(1000)
        Send("{ENTER}")
        Sleep(1000)
        Send("{ENTER}")
        Sleep(1000)
        WinSetState($Handle_rep, "", @SW_MINIMIZE)
        sleep(5000)
        $case = 1
        call("failure")
endif

If $timeout2 = 1 then
        WinActivate($Handle_rep)
        WinWaitActive($Handle_rep)
        Call("Time")
        Send($Heure & " ")
        $send = $Specimen & " Automagnificate timeout. Amor rebooted"
        Send($send)
        Sleep(1000)
        Send("^s")
        Sleep(1000)
        Send("{ENTER}")
        Sleep(1000)
        Send("{ENTER}")
        Sleep(1000)
        WinSetState($Handle_rep, "", @SW_MINIMIZE)
```

```
                                        Sleep(500)
                                        $case = 1
                                        Call("Reload")
                                EndIf

                        sleep(500)
                        EndIf

Sleep(500)
Until $Pas = 0

;Autotilt
Do
                        $Pas = 0
                        Sleep(500)
                        WinActivate($Handle_AMOR)
                        Sleep(1500)
                        MouseClick("left",$autotilt[0],$autotilt[1])
                        Sleep(1000)
                        $timeout=WinWaitClose("Autotilt","",1800)
                        ;Include reboot Amor Statement

                        if $timeout= 0 then
                                Winactivate($handle_rep)
                                WinWaitActive($handle_rep)
                                Call("Time")
                                send($heure&" ")
                                $send=$specimen&" Autotilt timeout. Amor rebooted"
                                send($send)
                                sleep(1000)
                                Send("^s")
                                sleep(1000)
                                send("{ENTER}")
                                sleep(1000)
                                send("{ENTER}")
```

```
                    sleep(1000)
                    WinSetState($handle_rep, "", @SW_MINIMIZE)
                    sleep(500)
                    $case=2
                    call("Reload")
            EndIf
            Sleep(2000)
Until $Pas = 0

;Automagnificate again
Do
            $Pas = 0
            WinActivate($Handle_AMOR)
            Sleep(1500)
            MouseClick("left", $automag[0], $automag[1])
            Sleep(1000)
            $timeout = WinWaitClose("Automagnificate", "", 90)

            ;Include a magnification abort Statement and a reboot Amor Statement
            If $timeout = 0 Then
                    winactivate("Automagnificate")
                    Winmove("Automagnificate","",0,0)
                    Mouseclick("left",$abortmagnification[0],$abortmagnification[1])
                    sleep(10000)
                    ;Check for an automagnification crash
                    $timeout2 = winexists("Automagnificate")

                    If $timeout2 = 0 then
                            WinActivate($Handle_rep)
                            WinWaitActive($Handle_rep)
                            Call("Time")
                            Send($Heure & " ")
                            $send = $Specimen & " Automagnificate aborted."
                            Send($send)
                            Sleep(1000)
```

```
                    Send("^s")
                    Sleep(1000)
                    Send("{ENTER}")
                    Sleep(1000)
                    Send("{ENTER}")
                    Sleep(1000)
                    WinSetState($Handle_rep, "", @SW_MINIMIZE)
                    sleep(5000)
                    $case = 3
                    call("failure")
                endif

                If $timeout2 = 1 then
                    WinActivate($Handle_rep)
                    WinWaitActive($Handle_rep)
                    Call("Time")
                    Send($Heure & " ")
                    $send = $Specimen & " Automagnificate timeout. Amor rebooted"
                    Send($send)
                    Sleep(1000)
                    Send("^s")
                    Sleep(1000)
                    Send("{ENTER}")
                    Sleep(1000)
                    Send("{ENTER}")
                    Sleep(1000)
                    WinSetState($Handle_rep, "", @SW_MINIMIZE)
                    Sleep(500)
                    $case = 3
                    Call("Reload")
                EndIf

            sleep(500)
            EndIf
```

```
Sleep(500)
Until $Pas = 0

;Autocenter again
Do
	$Pas = 0
	WinActivate($Handle_AMOR)
	Sleep(1500)
	MouseClick("left", $autocenter[0], $autocenter[1])
	Sleep(2000)
	MouseClick("left", $autocenter[0], $autocenter[1])
	Sleep(2000)
Until $Pas = 0

;Autofocus again
Do
	$Pas = 0
	WinActivate($Handle_AMOR)
	Sleep(1500)
	MouseClick("left", $autofocus[0], $autofocus[1])
	Sleep(1000)
	$timeout = WinWaitClose("Autofocus", "", 600)
	If $timeout = 0 Then
		WinActivate($Handle_rep)
		WinWaitActive($Handle_rep)
		Call("Time")
		Send($Heure & " ")
		$send = $Specimen & " Autofocus timeout. Amor rebooted"
		Send($send)
		Sleep(1000)
		Send("^s")
		Sleep(1000)
		Send("{ENTER}")
		Sleep(1000)
		Send("{ENTER}")
```

```
                    Sleep(1000)
                    WinSetState($Handle_rep, "", @SW_MINIMIZE)
                    Sleep(500)
                    $case = 4
                    Call("Reload")
            EndIf
            Sleep(500)
Until $Pas = 0

;Rotating
Do
            $Pas = 0
            WinActivate($Handle_AMOR)
            Sleep(1500)
            Sleep(500)
            MouseClick("left", $autorotate[0], $autorotate[1])
            Sleep(2500)
Until $Pas = 0

;Capture statements
Do
            $Pas = 0
            WinActivate($Handle_AMOR)
            Sleep(1500)
            MouseClick("left", $autocapture[0], $autocapture[1])
            WinWaitActive("Save...")
            WinMove("Save...", "", 0, 0)
            Sleep(1000)
            MouseClick("left", $Saveunder[0], $Saveunder[1])
            WinWaitActive("Datei speichern unter")
            Sleep(1000)
            Send($Sample)
            Sleep(100)

            If $Specimen < 10 Then
```

```
                    Send("0")
                EndIf

                Send($Specimen)
                Sleep(100)
                Send($Slide)
                Sleep(100)

                If $check = 1 Then
                    $send = "_rollerror"
                    Send($send)
                    $check = 0
                EndIf

                Send("{ENTER}")
                Sleep(1000)
                WinActivate("Save...")
                Sleep(1000)
                MouseClick("left", $save[0], $save[1])
                Sleep(2000)
                WinActivate("AMOR")
                Sleep(1500)
Until $Pas = 0

;writing report
WinActivate($Handle_rep)
WinWaitActive($Handle_rep)
Call("Time")
Send($Heure & "     ")
Send($Specimen)
$send = "------ Specimen finished"
Send($send)
Send("^s")
Sleep(1000)
Send("{ENTER}")
```

```
                    Sleep(1000)
                    Send("{ENTER}")
                    Sleep(1000)
                    Send("{ENTER}")
                    Sleep(1000)
                    WinSetState($Handle_rep, "", @SW_MINIMIZE)

                    ;Writing the Magnification in the "list of file" file
                    WinActivate($Handle_AMOR)
                    MouseClickDrag("left", $zoominit[0], $zoominit[1], $zoomlast[0], $zoomlast[1])
                    Send("^c")
                    Sleep(500)
                    WinActivate($Handle_Pad)
                    Sleep(1500)

                    If $Specimen < 10 Then
                            Send("0")
                    EndIf

                    Send($Specimen)
                    Send($Slide)
                    Send("r")
                    Send(",")
                    Send("^v")
                    Send("{ENTER}")
                    Send("^s")
                    Sleep(1000)
                    Send("{ENTER}")
                    Sleep(1000)
            EndIf
    Next

    WinMinimizeAll()
    Sleep(1000)
    WinActivate($Handle_Pad)
```

```
Send("^s")
Sleep(500)
Send("{ENTER}")
Sleep(1000)
Send("{ENTER}")
Sleep(1000)
Send("{ENTER}")
Sleep(1000)

;writing report
WinActivate($Handle_rep)
WinWaitActive($Handle_rep)
Call("Time")
Send($Heure & "     ")
Send($Specimen)
$send = "------ RUN finished ---------------------------------------"
Send($send)
Send("^s")
Sleep(1000)
Send("{ENTER}")
Sleep(1000)
Send("{ENTER}")
Sleep(1000)
Send("{ENTER}")
Sleep(1000)

If $Exitchoice = 6 Then
        Call("softexit")
EndIf

While 1
        Sleep(500)
        MsgBox(0, "AMDS", "Job finished !")
WEnd
```

```
;Error detection function

Func Errors()

	$Dim = WinExists("[W:338;H:324]", "")

	If $Dim = 1 Then

		$handle_Error = WinGetHandle("[W:338;H:324]", "")

		WinActivate($handle_Error)

		Send("{ENTER}")

		Send("{ENTER}")

		WinMinimizeAll()

		Sleep(500)

		WinActivate($Handle_rep)

		WinWaitActive($Handle_rep)


		Call("Time")

		Send($Heure & "     ")

		Send($Specimen)

		$send = "----------Imaq Error----------"

		Send($send)

		Send("^s")

		Sleep(1000)

		Send("{ENTER}")

		Sleep(1000)

		Send("{ENTER}")

		Sleep(1000)

		WinMinimizeAll()

		Sleep(500)

		WinActivate($Handle_AMOR)

		$Pas = 20

	EndIf


	$Dim = WinExists("[W:670;H:162]", "")

	If $Dim = 1 Then

		$handle_Error = WinGetHandle("[W:338;H:324]", "")

		WinActivate($handle_Error)

		Send("{ENTER}")
```

```
                Send("{ENTER}")
                WinMinimizeAll()
                Sleep(500)
                WinActivate($Handle_rep)
                WinWaitActive($Handle_rep)
                Call("Time")
                Send($Heure & "     ")
                Send($Specimen)
                $send = "----------ROLL Error----------"
                Send($send)
                Send("^s")
                Sleep(1000)
                Send("{ENTER}")
                Sleep(1000)
                Send("{ENTER}")
                Sleep(1000)
                WinMinimizeAll()
                Sleep(500)
                WinActivate($Handle_AMOR)
                $check = 1
        EndIf
EndFunc


;function reload
Func Reload()
        Sleep(500)
        ProcessClose("amor3.12.exe")
        Sleep(1500)
        WinActivate($Handle_rep)
        WinWaitActive($Handle_rep)
        Call("Time")
        Send($Heure & "     ")
        Send($Specimen)
        $send = "----------AMOR RELOADED----------"
        Send($send)
```

```
Send("^s")
Sleep(1000)
Send("{ENTER}")
Sleep(1000)
Send("{ENTER}")
Sleep(1000)
WinSetState($Handle_rep, "", @SW_MINIMIZE)
Sleep(3500)
Run("C:\Programme\AMOR3.17\Amor3.17.exe", "", @SW_MAXIMIZE)
WinWaitActive("AMOR")
Sleep(500)
WinActivate("AMOR")
Sleep(1500)
$Handle_AMOR = WinGetHandle("AMOR")
Sleep(1500)
WinMove("AMOR", "", 0, 0)
Sleep(500)
MouseClick("left", $detailuser[0], $detailuser[1])
Sleep(1500)
MouseClick("left", $adjustlight[0], $adjustlight[1])
Sleep(1500)
MouseClick("left", $OkgotoAmor[0], $OkgotoAmor[1])
Sleep(3500)
Send("{ENTER}")
Sleep(120000)
WinActivate("AMOR")
Sleep(500)
WinMove("AMOR", "", 0, 0)
Sleep(1000)
MouseClick("left", $Okmanuelmode[0], $Okmanuelmode[1])
Sleep(2000)
WinMove("Settings singlemode", "", 0, 0)
Sleep(1500)
MouseClick("left", $Loadcustom[0], $Loadcustom[1])
Sleep(1500)
```

```
                Send($path)
                Sleep(1000)
                Send("{ENTER}")
                Sleep(1500)
                Send("{ENTER}")
                Sleep(1500)
                MouseClick("left", $entermanuel[0], $entermanuel[1])
                Sleep(15000)
                WinActivate("AMOR")
                Sleep(500)
                WinMove("AMOR", "", 0, 0)
                WinActivate($Handle_rep)
                WinWaitActive($Handle_rep)
                Call("Time")
                Send($Heure & "     ")
                Send($Specimen)
                $send = "----------AMOR RELOADED OK----------"
                Send($send)
                Send("^s")
                Sleep(1000)
                Send("{ENTER}")
                Sleep(1000)
                Send("{ENTER}")
                Sleep(1000)
call ("Failure")
EndFunc

;function failure
Func Failure()

                ; first Automagnification failure
                If $case >= 1 Then
                        ;Specimen Selection
                        Do
                                $Pas = 0
```

```
		WinActivate($Handle_AMOR)
		Sleep(1500)
		MouseClickDrag("left", $fieldinit[0], $fieldinit[1], $fieldlast[0], $fieldlast[1], 1)
		Sleep(1000)
		Send($Specimen)
		Sleep(1000)
		Send("{ENTER}")
		Sleep(25000)
		mouseclick("left",$zoombutton[0],$zoombutton[1])
		sleep(4000)
Until $Pas = 0

;Autocenter (just in case)
Do
		$Pas = 0
		WinActivate($Handle_AMOR)
		Sleep(1500)
		MouseClick("left", $autocenter[0], $autocenter[1])
		Sleep(2000)
		MouseClick("left", $autocenter[0], $autocenter[1])
		Sleep(2000)
Until $Pas = 0

;Automagnificate
Do
		$Pas = 0
		WinActivate($Handle_AMOR)
		Sleep(1500)
		MouseClick("left", $automag[0], $automag[1])
		Sleep(1000)
		$timeout = WinWaitClose("Automagnificate", "", 300)

		;Include reboot Amor Statement
		If $timeout = 0 Then
			WinActivate($Handle_rep)
```

```
                                        WinWaitActive($Handle_rep)
                                        Call("Time")
                                        Send($Heure & " ")
                                        $send = $Specimen & " Automagnificate timeout. Amor rebooted"
                                        Send($send)
                                        Sleep(1000)
                                        Send("^s")
                                        Sleep(1000)
                                        Send("{ENTER}")
                                        Sleep(1000)
                                        Send("{ENTER}")
                                        Sleep(1000)
                                        WinSetState($Handle_rep, "", @SW_MINIMIZE)
                                        Sleep(500)
                                        $case = 1
                                        Call("Reload")
                                EndIf
                                Sleep(500)

                        Until $Pas = 0
        EndIf

        ; Autotilt Failure
        If $case >= 2 Then
                        ;Autotilt
                        Do
                                $Pas = 0
                                Sleep(500)
                                WinActivate($Handle_AMOR)
                                Sleep(1500)
                                MouseClick("left", $autotilt[0], $autotilt[1])
                                Sleep(1000)
                                $timeout = WinWaitClose("Autotilt", "", 3200)
                                ;Include reboot Amor Statement
```

```
                    If $timeout = 0 Then
                        WinActivate($Handle_rep)
                        WinWaitActive($Handle_rep)
                        Call("Time")
                        Send($Heure & " ")
                        $send = $Specimen & " Autotilt timeout. Amor rebooted"
                        Send($send)
                        Sleep(1000)
                        Send("^s")
                        Sleep(1000)
                        Send("{ENTER}")
                        Sleep(1000)
                        Send("{ENTER}")
                        Sleep(1000)
                        WinSetState($Handle_rep, "", @SW_MINIMIZE)
                        Sleep(500)
                        $case = 2
                        Call("Reload")
                    EndIf
                    Sleep(2000)
                Until $Pas = 0
EndIf

; Second Automagnification failure
If $case >= 3 Then
                ;Automagnificate again
                Do
                    $Pas = 0
                    WinActivate($Handle_AMOR)
                    Sleep(1500)
                    MouseClick("left", $automag[0], $automag[1])
                    Sleep(1000)
                    $timeout = WinWaitClose("Automagnificate", "", 300)
                    ;Include reboot Amor Statement
                    If $timeout = 0 Then
```

```
                                        WinActivate($Handle_rep)
                                        WinWaitActive($Handle_rep)
                                        Call("Time")
                                        Send($Heure & " ")
                                        $send = $Specimen & " Automagnificate timeout. Amor rebooted"
                                        Send($send)
                                        Sleep(1000)
                                        Send("^s")
                                        Sleep(1000)
                                        Send("{ENTER}")
                                        Sleep(1000)
                                        Send("{ENTER}")
                                        Sleep(1000)
                                        WinSetState($Handle_rep, "", @SW_MINIMIZE)
                                        Sleep(500)
                                        $case = 3
                                        Call("Reload")
                                EndIf

                                Sleep(500)
                        Until $Pas = 0
        EndIf

        ;Autofocus failure
        If $case >= 4 Then
                        ;Autofocus again
                        Do
                                $Pas = 0
                                WinActivate($Handle_AMOR)
                                Sleep(1500)
                                MouseClick("left", $autofocus[0], $autofocus[1])
                                Sleep(1000)
                                $timeout = WinWaitClose("Autofocus", "", 1800)
                                If $timeout = 0 Then
                                        WinActivate($Handle_rep)
```

```
                                        WinWaitActive($Handle_rep)
                                        Call("Time")
                                        Send($Heure & " ")
                                        $send = $Specimen & " Autofocus timeout. Amor rebooted"
                                        Send($send)
                                        Sleep(1000)
                                        Send("^s")
                                        Sleep(1000)
                                        Send("{ENTER}")
                                        Sleep(1000)
                                        Send("{ENTER}")
                                        Sleep(1000)
                                        WinSetState($Handle_rep, "", @SW_MINIMIZE)
                                        Sleep(500)
                                        $case = 4
                                        Call("Reload")
                                EndIf
                                Sleep(500)
                        Until $Pas = 0
        EndIf


        $case = 0
EndFunc


;function to get the time from the system, usefull to write the report file
Func Time()
        $Hour = @HOUR
        $Minutes = @MIN
        $Second = @SEC
        $Heure = $Hour & ":" & $Minutes & ":" & $Second
EndFunc


;Function to Stop the Script
Func MyExit()
        Exit
```

```
EndFunc


Func softexit()
        Sleep(20000)
        WinActivate($Handle_Pad)
        Send("^s")
        Sleep(1500)
        Send("{ENTER}")
        Sleep(500)
        Send("{ENTER}")
        Sleep(500)
        WinActivate($Handle_AMOR)
        WinActivate($Handle_AMOR)
        WinWaitClose("Autotilt")
        WinWaitClose("Automagnificate")
        Sleep(500)
        MouseClick("left", $autoExit[0], $autoExit[1])
        Sleep(9000)
        Send("{ENTER}")
        Sleep(20000)
        $Handle_AMOR = WinGetHandle("AMOR")
        Sleep(1500)
        WinMove("AMOR", "", 0, 0)
        Sleep(500)
        MouseClick("left", 883, 615)
        Sleep(2000)
        Send("{ENTER}")
        Sleep(8000)
        Send("{ENTER}")
        Sleep(60000)
        $Dim = 0
        $Dim = WinExists("AMOR")


Select
        case $Dim =1
```

```
                    WinActivate($Handle_rep)
                    $send = "AMOR CLOSING PROBLEME"
                    Send($send)
                    Send("^s")
                    Sleep(1000)
                    Send("{ENTER}")
                    Sleep(1000)
                    Send("{ENTER}")

            Case $Dim = 0
                    WinActivate($Handle_rep)
                    $send = "AMOR CLOSING OK"
                    Send($send)
                    Send("^s")
                    Sleep(1000)
                    Send("{ENTER}")
                    Sleep(1000)
                    Send("{ENTER}")
                    Sleep(1000)
            EndSelect

sleep(1500)
WinActivate($Handle_rep)
sleep(1500)
send("!{F4}")
sleep(1500)
send("{enter}")
sleep(1500)
send("{enter}")
WinActivate($Handle_Pad)
sleep(1500)
send("!{F4}")
sleep(1500)
send("{enter}")
sleep(1500)
```

```
send("{enter}")

sleep(50000)


MouseClick("left",$windows[0],$windows[1])

sleep(500)

MouseClick("left", $winquit[0], $winquit[1])

sleep(1500)

send("{ENTER}")

sleep(1500)

send("{ENTER}")


Exit


EndFunc
```

Appendix 2 : Details diagnosis for each localities.

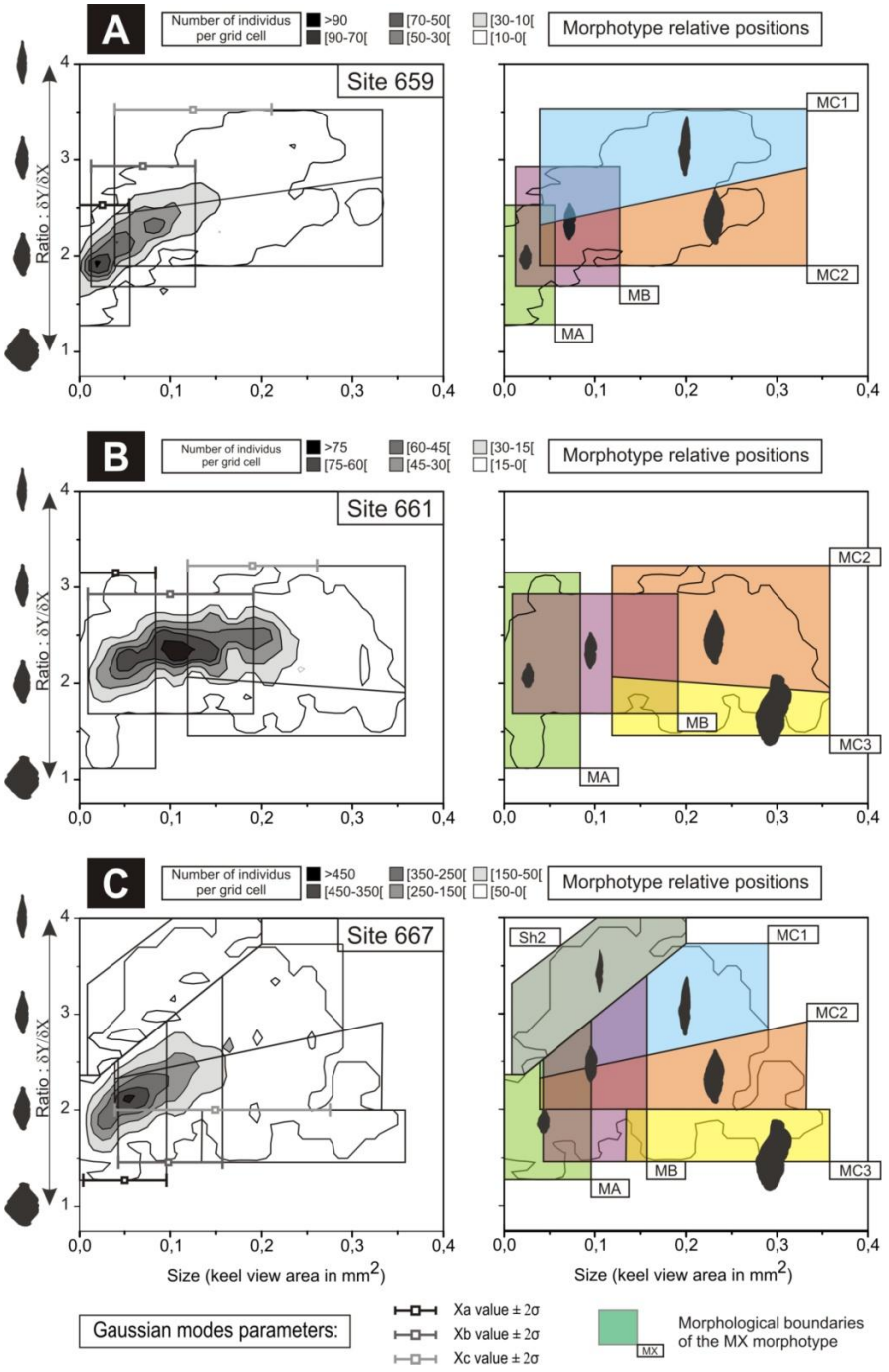

Appendix 2.1: Eastern Atlantic Differential diagnosis: area versus δY/δX ratio. Frequencies are corrected before plotting in order to remove the effects of sampling per size fraction. (A) ODP Site 659 frequency distributions, morphotypes and associated boundary distribution (B) Site 661 (C) Site 667.

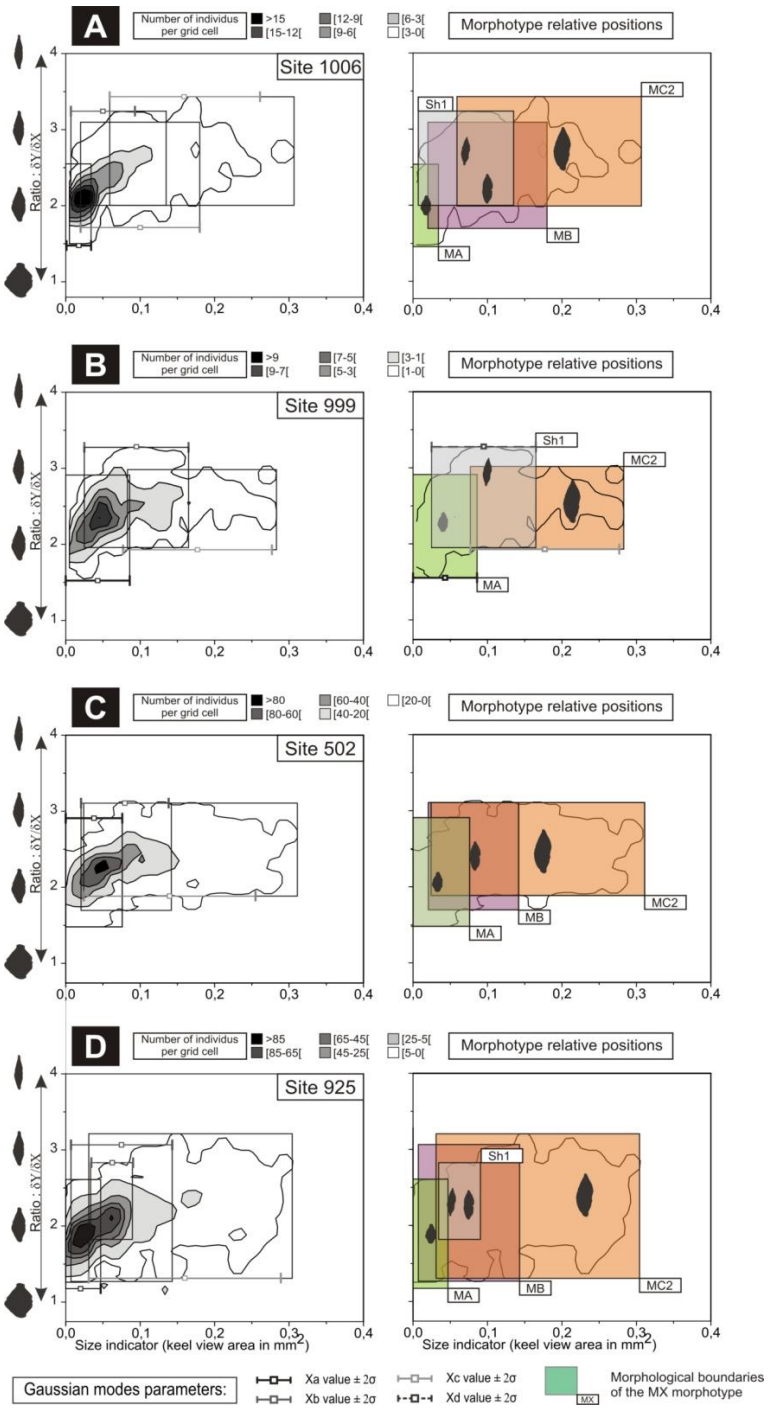

Appendix 2.2: Western Atlantic differential diagnosis: area versus δY/δX ratio. Frequencies are corrected before plotting in order to remove the effects of sampling per size fraction. (A) ODP Site 1006 frequency distributions, morphotypes and associated boundary distribution (B) Site 999 (C) Site 502 (D) Site 925.

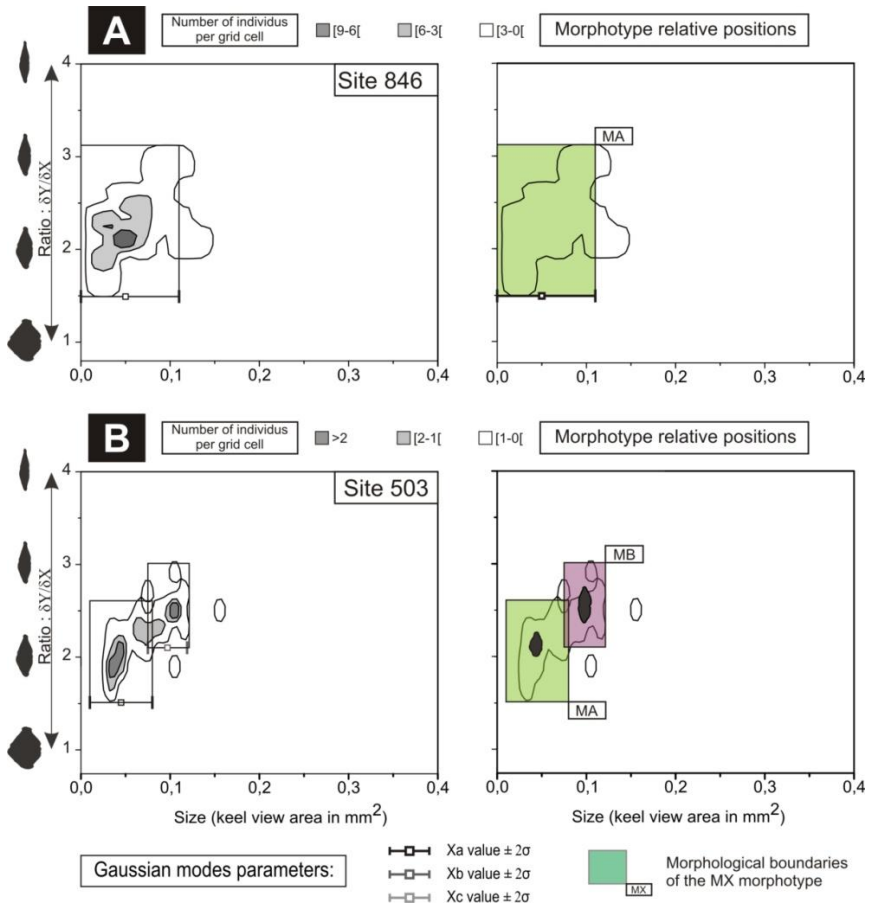

Appendix 2.3: Eastern Pacific differential diagnosis: area versus δY/δX ratio. Frequencies are corrected before plotting in order to remove the effects of sampling per size fraction. (A) ODP Site 846 frequency distributions, morphotypes and associated boundary distribution (B) Site 503.

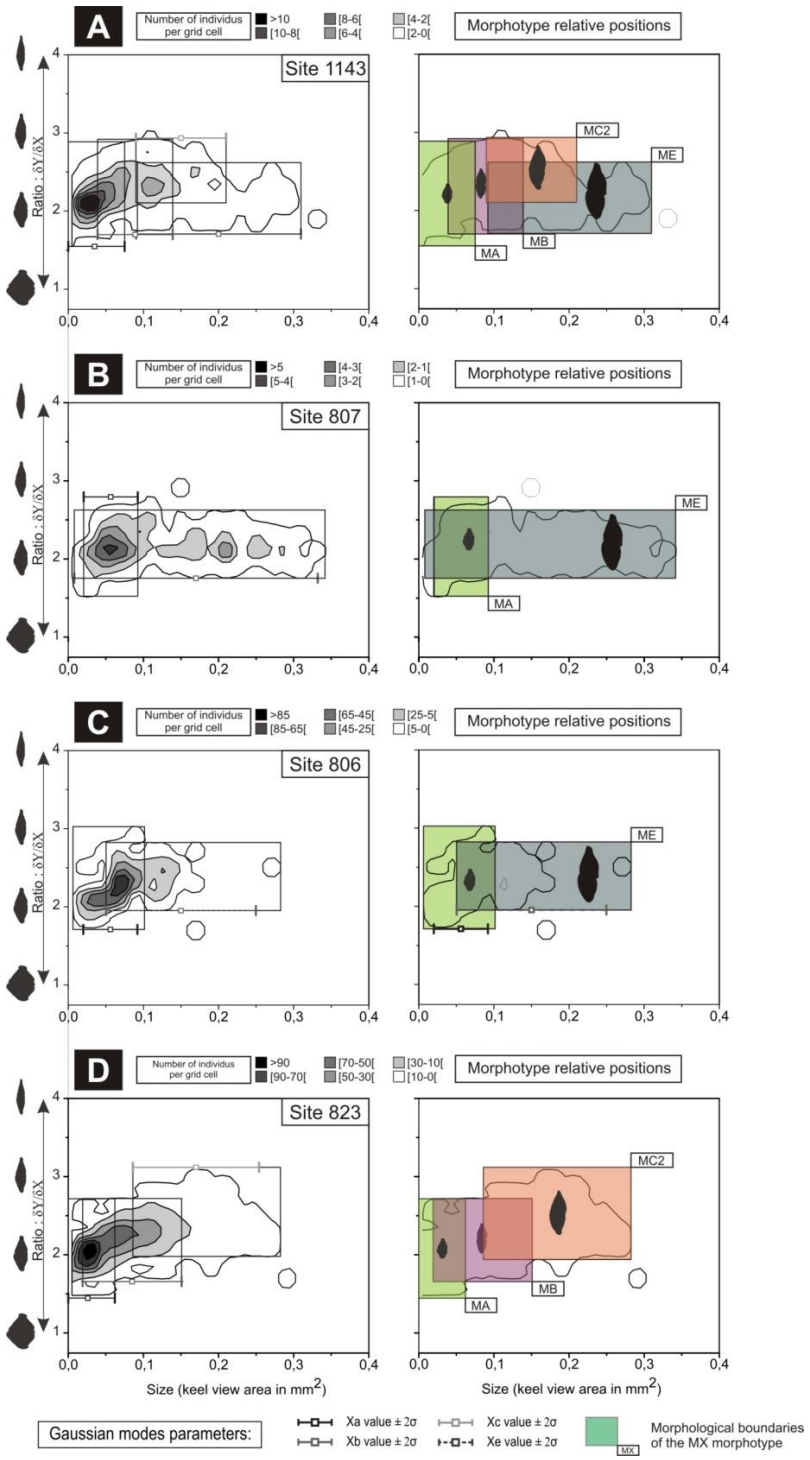

Appendix 2.4: Western Pacific differential diagnosis: area versus δY/δX ratio. Frequencies are corrected before plotting in order to remove the effects of sampling per size fraction. (A) ODP Site 1143 frequency distributions, morphotypes and associated boundary distribution (B) Site 807 (C) Site 806 (D) Site 823

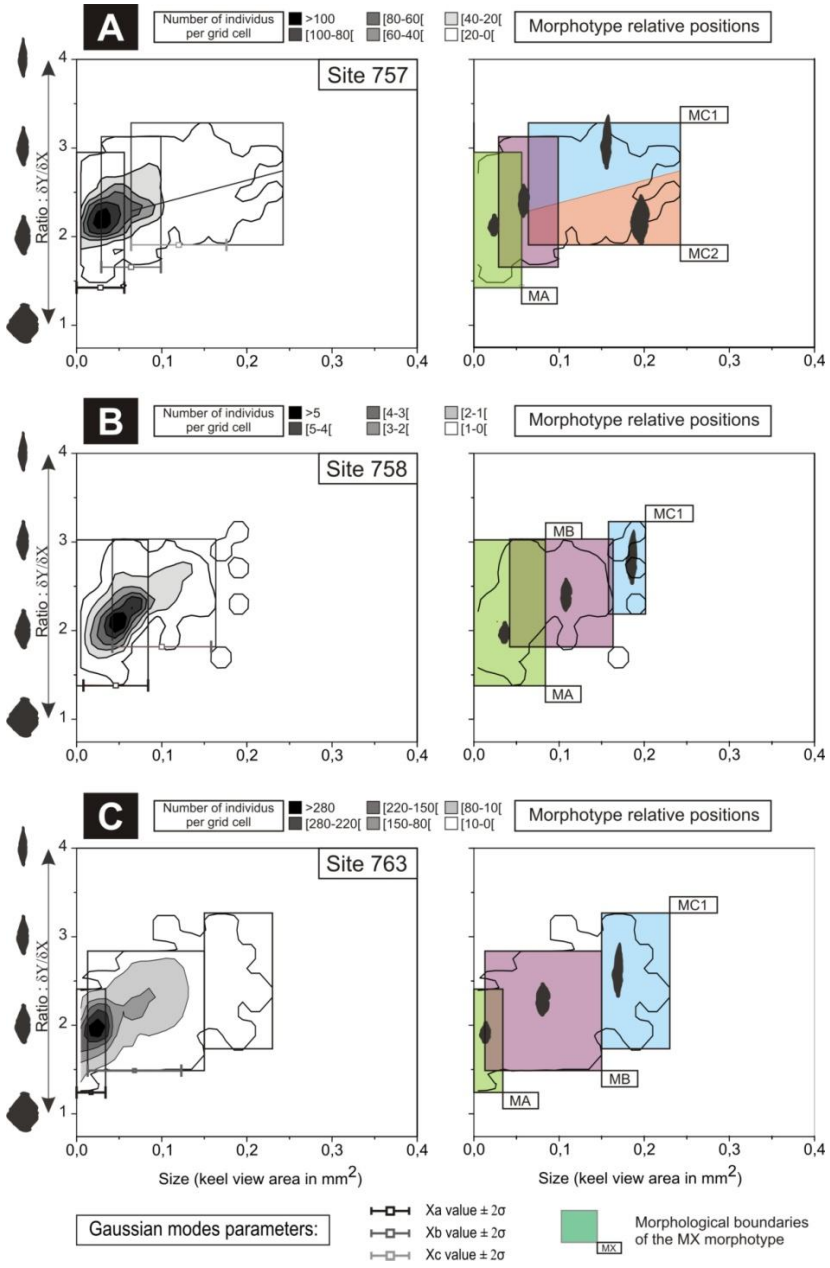

Appendix 2.5: Easter Indian Ocean differential diagnosis: area versus δY/δX ratio. Frequencies are corrected before plotting in order to remove the effects of sampling per size fraction. (A) ODP Site757 frequency distributions, morphotypes and associated boundary distribution (B) Site 758 (C) Site 763.

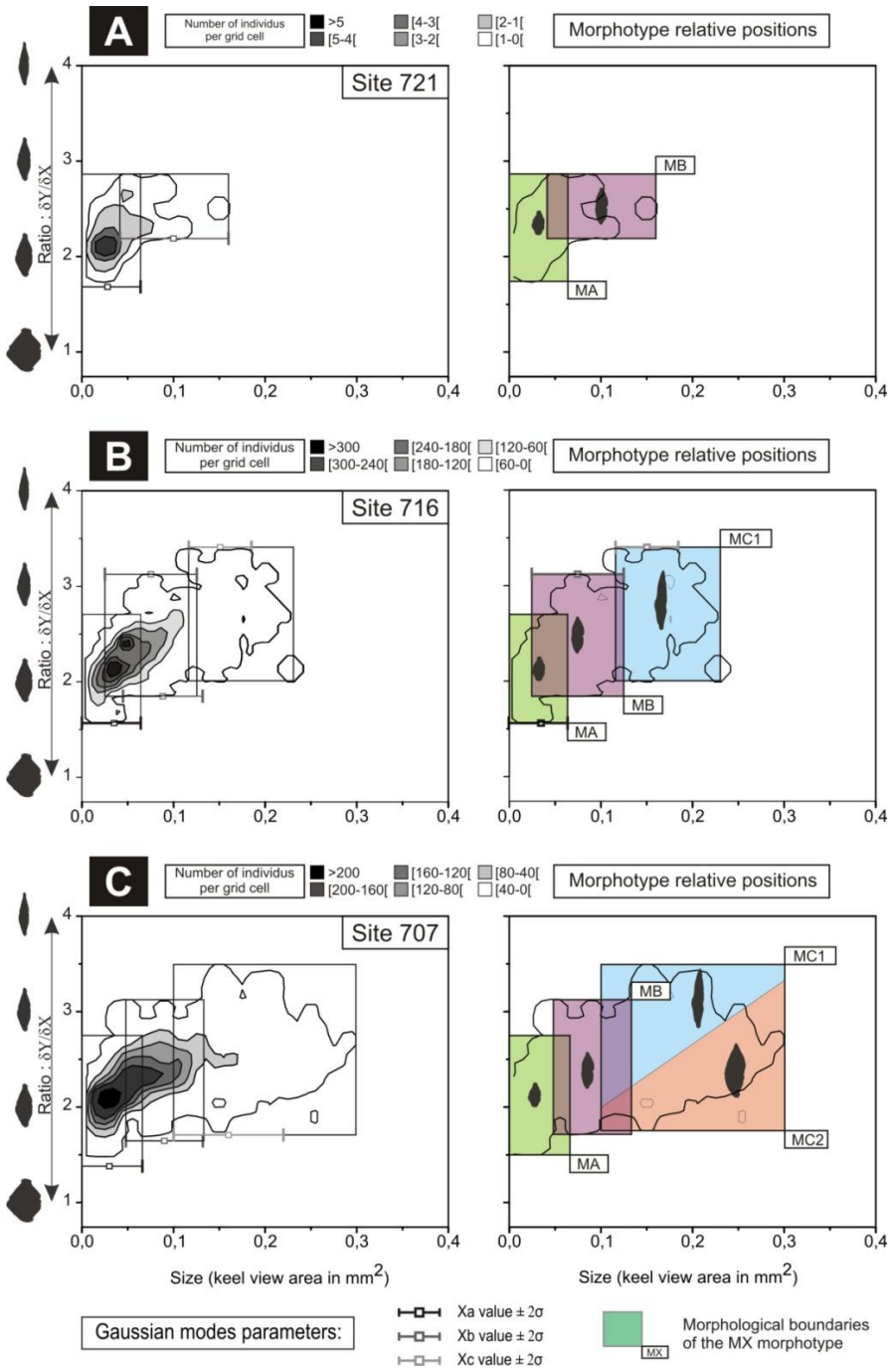

Appendix 2.6: Western Indian Ocean differential diagnosis: area versus δY/δX ratio. Frequencies are corrected before plotting in order to remove the effects of sampling per size fraction. (A) ODP Site721 frequency distributions, morphotypes and associated boundary distribution (B) Site 716 (C) Site 707.